RATE STUDIES OF ORGANOLITHIUM-MEDIATED REACTIONS: REACTION OF LITHIUM DIISOPROPYLAMIDE WITH FLUOROPYRIDINES AND REACTION OF LITHIUM DIETHYLAMIDE WITH AN ALKYL BROMIDE AND AN ALKYL SULFONATE

by Lekha Gupta

RATE STUDIES OF ORGANOLITHIUM-MEDIATED REACTIONS: REACTION OF LITHIUM DIISOPROPYLAMIDE WITH FLUOROPYRIDINES AND REACTION OF LITHIUM DIETHYLAMIDE WITH AN ALKYL BROMIDE AND AN ALKYL SULFONATE

A Dissertation
Presented to the Faculty of the Graduate School
of Cornell University
In Partial Fulfillment of the Requirements for the Degree of
Doctor of Philosophy

by
Lekha Gupta
August 2010

RATE STUDIES OF ORGANOLITHIUM-MEDIATED REACTIONS: REACTION OF LITHIUM DIISOPROPYLAMIDE WITH FLUOROPYRIDINES AND REACTION OF LITHIUM DIETHYLAMIDE WITH AN ALKYL BROMIDE AND AN ALKYL SULFONATE

Lekha Gupta, Ph. D.
Cornell University 2010

Mechanistic studies of the lithium diisopropylamide (LDA)-mediated ortholithiation and subsequent aromatic nucleophilic substitution of fluoropyridines are described. ^{6}Li, ^{15}N, ^{13}C and ^{19}F NMR spectroscopic studies reveal the formation of monomeric aryllithium in THF solution at -78 ^{o}C. Computational studies support trisolvation state of the monomer. A combination of in situ IR and ^{19}F NMR spectroscopic investigations provide the details of the rate-limiting step of the reaction. The dominant reaction pathway in ortholithiation involves substrate-assisted, rate-limiting deaggregation of LDA dimer. Standard and competitive isotope effects confirm post-rate-limiting proton transfer. Rate studies show a direct deaggregation of LDA dimer occurs parallel with an unprecedented tetramer-based pathway. Autocatalysis that emerges as the reaction proceeds originates from ArLi-catalyzed deaggregation of LDA that, paradoxically, proceeds through 2:2 LDA-ArLi mixed tetramers. A hypersensitivity of the ortholithiation rates to traces of LiCl derives from lithium chloride-catalyzed dimer-monomer exchange and a subsequent monomer-based ortholithiation.

Once again, 2:2 LDA-LiCl mixed tetramers are suggested to be key intermediates. Ortholithiations of a range of other arenes mediated by lithium diisopropylamide (LDA) in THF at -78 °C also reveal substantial accelerations by as little as 0.5 mol % LiCl (relative to LDA). Warming the lithiated fluoropyridine solution to 0 °C converts the aryllithium to 2-fluoro-6-(diisopropylamino)pyridine. Rate studies reveal evidence of a reversal of the ortholithiation and a subsequent 1,2-addition via two monomer-based pathways. Computational studies fill in the structural details and provide evidence of a direct substitution without the intermediacy of Meisenheimer complex.

The last chapter describes the rate studies aimed at understanding the principles governing the selectivities in competing N-alkylation, elimination and sulfonation pathways, in the reactions of lithium diethylamide (Et_2NLi) with *n*-dodecyl bromide and *n*-octyl benzenesulfonate. The alkyl bromide undergoes competitive S_N2 substitution and E2 elimination via trisolvated-monomer-based transition structures, in proportions that are insensitive to all concentrations except for a minor medium effect. The *n*-alkyl sulfonate undergoes competitive S_N2 substitution (minor) and N-sulfonation (major). The S_N2 substitution is shown to proceed via a disolvated monomer whereas; the dominant N-sulfonation follows a disolvated-dimer-based transition structure. The differential THF and Et_2NLi orders explain the observed concentration-dependent chemoselectivities.

BIOGRAPHICAL SKETCH

Lekha Gupta was born on June 17, 1982 in the city of Delhi, India. She went to four schools in different parts of Delhi and passed the C.B.S.E (Central Board of Secondary Examination) with distinction in 1999. She joined as an undergraduate student in St. Stephen's College, University of Delhi (India) and earned the Bachelor of Science degree, with Honors specialization in Chemistry in 2002. Later that year, she was admitted to the Masters program in Chemistry in I.I.T. (Indian Institute of Technology) Delhi, India. At I.I.T., she conducted research on the synthesis and characterization of dibutyltin esters of heterocyclic carboxylic acids under the supervision of Prof. Ravi Shankar. After earning her M.Sc. degree in Chemistry, Lekha began her graduate career at Cornell University in Ithaca, NY in July of 2004, where she joined Prof. David Collum's laboratory. Lekha graduated with a doctoral degree in July 2010 and plans to start her industrial career at NLC Nalco in Pune, India.

Dedicated to my Parents,

Mr. Prem Nath Gupta and Mrs. Shukla Gupta

ACKNOWLEDGMENTS

First and foremost, I would like to thank my Ph.D. advisor, Professor David B. Collum for his invaluable support, guidance and encouragement through the years. I consider myself very fortunate to be a part of his group. It has been a pleasure to work with such an understanding, practical and inspiring person. I express my sincere gratitude to him for having faith in me during some of the testing times in the lab. He made my stay at Cornell, a wonderful learning and pleasant experience.

I do not have sufficient words to express my gratitude toward Dr. Antonio Ramirez, without whose support and encouragement, I would not have reached this stage. I am deeply indebted to him, for his time and patience while training me in my first year in the lab and replying to my incessant queries after he moved to Bristol-Myers Squibb. My learning curve increased exponentially while he was a part of the group. I always wished we overlapped for more than a year as lab-mates.

I express my gratitude toward Professor Jón T. Njarðarson, Professor William Dichtel and Professor Tyler McQuade for serving on my special committee.

I would like to thank past and present members of the Collum group for all the fun and discussions in the lab and during group meetings: Dr. Kanwaljit Singh, Dr. Jason Riggs, Sean Breslin, Dr. Peter Godenschwager, Dr. Lara Liou, Dr. Mihai Viciu, Dr. Yun Ma, Dr. Timothy De Vries, Jocelyn Gruver, Alexander Hoepker, Anandarup Goswami, Hariharaputhiran Subramanian, Laura Tomasevich and Angela Bruneau.

I am thankful to Dr. Ivan Kerestzes and Anthony Condo for assistance

with the NMR studies.

I am extremely grateful to all my friends in Ithaca, especially Abhinav Rastogi, Deepti Gadi and Kalyanaraman Krishnamoorthy who were always there for me during all the highs and lows of my stay in Ithaca. Thanks to this Ithaca family for making this seemingly never-ending journey, such a smooth and joyous ride. All the time that we spent together will forever be etched in my mind as some of the most pleasant memories of my stay at Cornell. A special thanks to Anand Teertha Vaidya, Aritro Sinha Roy and Hariharaputhiran Subramanian for making the last year of my Ph.D. much less stressful and much more fun, providing me with continuous support and camaraderie, when some of my dear friends had already left Ithaca. They turned a year I was dreading into a year that I will cherish forever. I would also like to acknowledge Kuldeep Wadhwa (Iowa State University), Payal Mehta (Ohio State University), and Vandana Shahi (I.I.T.D.) for always being there for me. I wish all of them all the very best in life and wish that we would always stay in touch. I also thank Debamita Paul and Jaya Bhatnagar for sticking with me for more than five years as housemates. My time at Cornell was made enjoyable in large part due to many friends that became a part of my life. I am grateful for time spent with Sridhar Bale, Sudhamsu Jawahar, Anandarup Goswami, Amit Singhai, Anupam Chakravarty, Siddharth Chandrasekaran and Tanushree Ghosh.

Finally, I would like to thank my family without whose support and love, I would not have accomplished anything in life. Thanks to my parents for sharing all the trials and tribulations of graduate school with me and for always keeping me in their thoughts. My special thanks goes to my eldest brother, Rohan Gupta, who was the sole motivation behind my Ph.D. dream.

This degree belongs to him as much as it belongs to me. I am also grateful to my elder brother, Puneet Gupta, for his love and support. I would like to thank my two sister-in-laws, Deepti Gupta and Anju Gupta, for bringing joy and happiness to my family. My love goes to my two sweet and cute nieces, Rupashi Gupta and Sashi Gupta, who were born in 2008 and have been a source of unbound happiness in my family. I would also like to thank my family members, especially Anu bhabhi, Babu bhaiya, my cousin Trinka, Kusum didi, Jijaji and, my cousin Nidhi, for their constant love, support and blessing.

This work would not have been possible without the support and love of all these people.

TABLE OF CONTENTS

LIST OF FIGURES

LIST OF TABLES

CHAPTER I

Mechanism of Lithium Diisopropylamide-Mediated Substitution of 2,6-Difluoropyridine*

*Reprinted with permission from Viciu, M. S.; Gupta, L.; Collum, D. B. *J. Am. Chem. Soc.* **2010**, *132*, 6361. Copyright 2010 American Chemical Society.

Mechanism of Lithium Diisopropylamide-Mediated
Substitution of 2,6-Difluoropyridine

Abstract

Treatment of 2,6-difluoropyridine with lithium diisopropylamide in THF solution at -78 °C effects ortholithiation quantitatively. Warming the solution to 0 °C converts the aryllithium to 2-fluoro-6-(diisopropylamino)-pyridine. Rate studies reveal evidence of a reversal of the ortholithiation and a subsequent 1,2-addition via two monomer-based pathways of stoichiometries [ArH•*i*-$Pr_2NLi(THF)$]‡ and [ArH•*i*-$Pr_2NLi(THF)_3$]‡. Computational studies fill in the structural details and provide evidence of a direct substitution without the intermediacy of Meisenheimer complex.

Introduction

During mechanistic studies of lithium diisopropylamide (LDA)-mediated ortholithiations of 2-fluoropyridines we discovered the nucleophilic aromatic substitution depicted in Scheme I.1. This substitution is similar to less hindered examples reported by Singaram and coworkers.[1,2] The yield is exceptional for such a hindered nucleophile, and heteroaromatic aminations are of great importance in the pharmaceutical industry.[3,4] Our interest, however, was piqued by the apparent intermediacy of 3-pyridyllithium[5] **3**, which forms rapidly and quantitatively at -78 °C.

We considered the following mechanisms for the substitution in Scheme I.1.

Mechanism 1. Reversal of the metalation[5d,6] is followed by a product-determining nucleophilic attack by LDA (eq 1). Although the LDA order

Scheme I.1

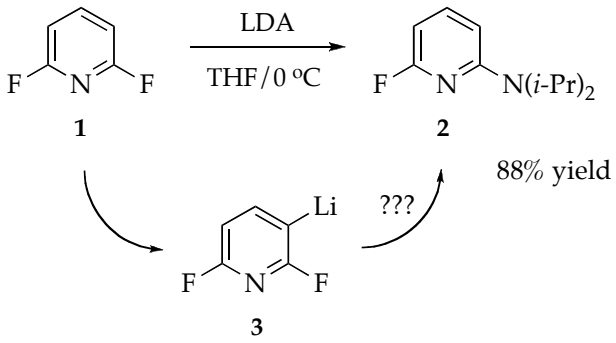

would depend on the aggregation state of the nucleophilic form, a first-order dependence on the diisopropylamine concentration would be a hallmark of this mechanism.[7]

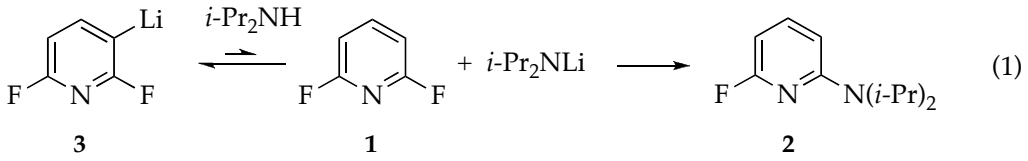

Mechanism 2. Rate-limiting elimination of LiF affords pyridyne **4**,[8] which undergoes a post-rate-limiting trap by LDA (eq 2).[9] In addition to the zeroth orders expected for LDA and diisopropylamine, an inverse dependence on THF concentration might be expected based on analogous LiF eliminations to form benzynes.[10]

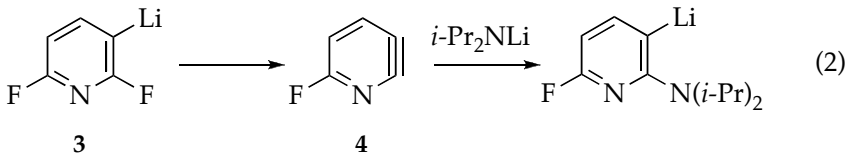

Mechanism 3. Direct substitution of the fluoro moiety of aryllithium **3** by a nucleophilic LDA fragment must be considered, although the electrophilicity of a heteroaryllithium seems somewhat odd. A mixed dimer-based pathway

involving the intraaggregate transfer depicted in eq 3 is one (admittedly somewhat fanciful) possibility.[11] Dependencies on both ArLi and LDA concentration would be characteristic.

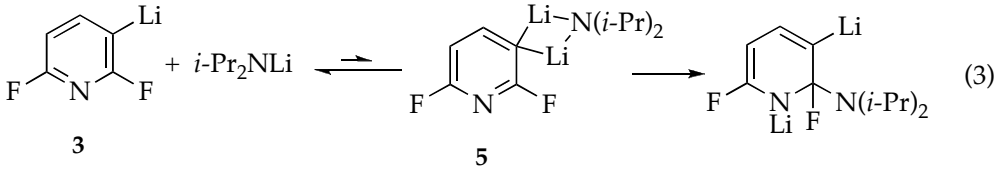

3 **5** (3)

We describe herein mechanistic studies of the substitution in Scheme I.1. Rate data support two competing variants of mechanism 1 that differ only in solvation number in the transition structures. Computational data fill in experimentally elusive details. The discussion includes a detailed description of how the rate law leads to the mechanistic hypothesis.

Results

Solution structures. Assessing the solution structures of LDA and ArLi is essential to interpret the rate data (vide infra). Previous studies of [^{6}Li,^{15}N]LDA using ^{6}Li and ^{15}N NMR spectroscopy revealed exclusively disolvated dimer **6**.[12] Aryllithium **3** is exclusively monomeric as evidenced by C-3 as a doublet of triplets (1:1:1 triplet) owing to ^{13}C-^{19}F and ^{13}C-^{6}Li coupling.[13,14] A solution containing [^{6}Li,^{15}N]LDA and aryllithium **3** shows no ^{6}Li-^{15}N coupling in the ^{6}Li resonance of **3**. An especially large $^{2}J_{C\text{-}F}$ of 122 Hz is emblematic of 2-fluoroaryllithiums.[10,15,16] (By comparison, the distal fluoro moiety displays $^{2}J_{C\text{-}F}$ = 38 Hz.) Density functional theory (DFT) computations of **3** optimized at the B3LYP/6-31G(d) level[17] (supporting information) with single point calculations at the MP2 level of theory indicates that trisolvated monomer **3b** is favored relative to disolvated monomer **3a** at 0 °C, consistent

with previous studies of aryllithiums.[10,18] (The result without MP2 correction is shown in parenthesis.) Moreover, alternative assignment of the monomer as disolvate **3a**, in conjunction with the rate studies, would force on us seemingly untenable mechanistic hypotheses (vide infra).

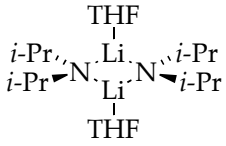

6

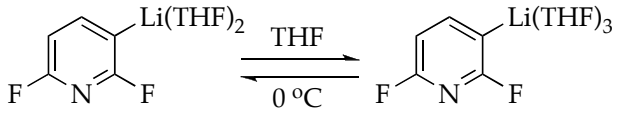

3a **3b**

ΔG = -2.4 kcal / mol (4.0)

Pseudo-first-order conditions were established with LDA (recrystallized)[12] at normal concentrations (0.05-0.50 M) by restricting the substrate concentration to 0.005 M.[19] Diisopropylamine is maintained at 0.10 M unless stated otherwise. In situ IR spectroscopy showed that the disappearance of aryllithium **3** (1576 cm^{-1}) and appearance of arene **2** (1617 cm^{-1}) are first order (Figure I.1). Analogous results were obtained by monitoring the ^{19}F resonances of **3** (-44.8 and -82.0 ppm) and **2** (-68.2 ppm). The resulting pseudo-first-order rate constants (k_{obsd}) are independent of substrate concentration (0.004-0.04 M). Zeroing the IR baseline and monitoring a second injection of substrate affords no significant change in k_{obsd} ($\pm$ 10%), which shows that autocatalysis, autoinhibition, and other conversion-dependent effects are unimportant under pseudo-first-order conditions.

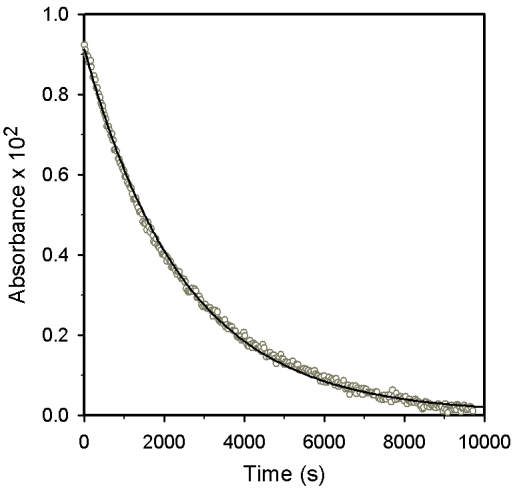

Figure I.1. Plot of IR absorbance (1576 cm^{-1}) vs time for the substitution of **1** (0.005 M) with LDA (0.10 M) in the presence of 0.10 M diisopropylamine in 2.5 M THF at 0 °C. The curve depicts an unweighted least-squares fit to $y = ae^{-bx}$.

A plot of k_{obsd} versus THF concentration shows an inverse-second-order dependence at low THF concentrations and a zeroth-order dependence—a nonzero asymptote—dominating at high THF concentrations (Figure I.2), consistent with two parallel pathways. Plots of k_{obsd} versus LDA concentration (Figure I.3) and k_{obsd} versus diisopropylamine concentration (Figure I.4) show nearly zeroth- and first-order dependencies, respectively. These orders persist at low and high THF concentrations.

The resulting two-term rate law described by eq 5 is consistent with two monomer-based reaction pathways differing in the number of coordinated THFs (eqs 6-9) representing variants of mechanism 1 (eq 1). One pathway (labelled pathway 1 in eq 5) manifests a zeroth-order dependence on THF concentration. Pathway 2 is distinguished by an inverse-second- order dependence on THF concentration. (The solvation number of **9** is not meant to imply the resting state of LDA monomer[20] but simply reflects the eventual loss

of two THFs.) Comparing the rates using *i*- Pr_2NH versus *i*-Pr_2ND[21] affords $k_H/k_D = 1.2$, confirming the reversibility of the proton transfer.[6]

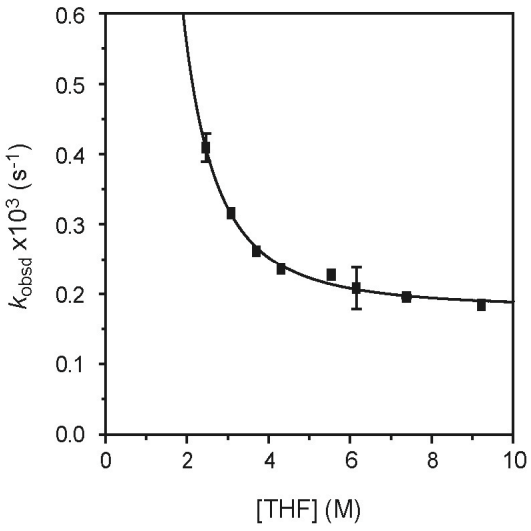

Figure I.2. Plot of k_{obsd} vs [THF] in hexane cosolvent for the nucleophilic substitution of 2,6-difluoropyridine (0.005 M) with LDA (0.10 M) and diisopropylamine (0.10 M) at 0 °C. The curve depicts an unweighted least-squares fit to $k_{obsd} = k[THF]^n + k'$ such that $k = (1.9 \pm 0.7) \times 10^{-3}$ and $n = -2.4 \pm 0.4$, $k' = (1.8 \pm 0.1) \times 10^{-4}$.

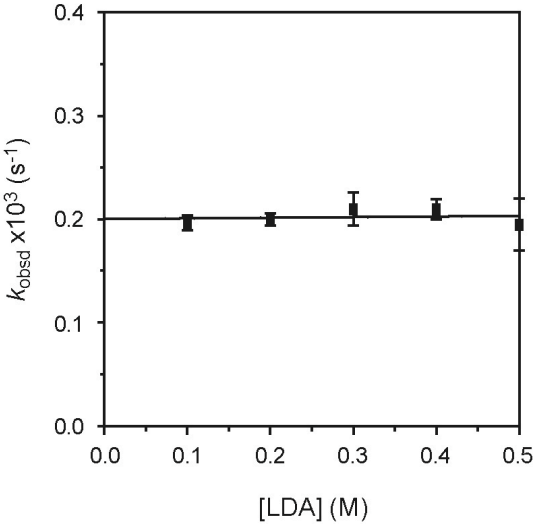

Figure I.3. Plot of k_{obsd} vs [LDA] in 7.4 M THF/hexane and 0.10 M diisopropylamine for the nucleophilic substitution of 2,6-difluoropyridine (0.005 M) at 0 °C. The curve depicts an unweighted least-squares fit to $k_{obsd} = k[LDA] + k'$ such that $k = (0.9 \pm 3.0) \times 10^{-5}$, $k' = (1.9 \pm 0.1) \times 10^{-4}$.

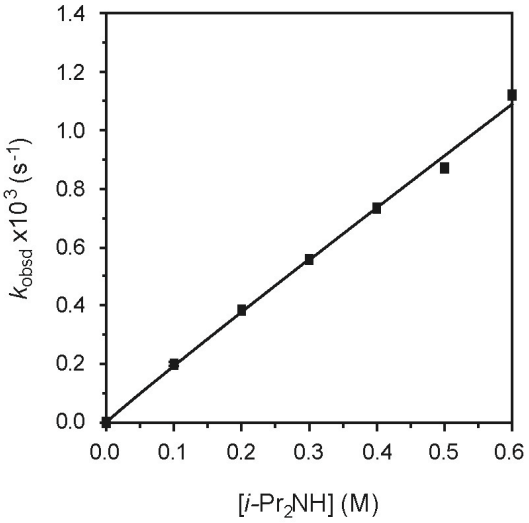

Figure I.4. Plot of k_{obsd} vs [i-Pr$_2$NH] in 7.4 M THF/hexane for the nucleophilic substitution of 2,6-difluoropyridine (0.005 M) with LDA (0.10 M) at 0 °C. The curve depicts an unweighted least-squares fit to $k_{obsd} = k[i\text{-Pr}_2\text{NH}]^n$ such that $k = (1.78 \pm 0.05) \times 10^{-3}$, $n = 0.97 \pm 0.03$.

$$-d[\text{ArLi}]/dt = k'[\text{ArLi}][i\text{-Pr}_2\text{NH}] + k''[\text{ArLi}][i\text{-Pr}_2\text{NH}][\text{THF}]^{-2} \quad (5)$$
(*pathway 1*) (*pathway 2*)

Pathway 1:

$$\underset{\textbf{3b}}{\text{ArLi(THF)}_3} + i\text{-Pr}_2\text{NH} \rightleftharpoons \underset{\textbf{1}}{\text{ArH}} + \underset{\textbf{7}}{i\text{-Pr}_2\text{NLi(THF)}_3} \quad (6)$$

$$\underset{\textbf{1}}{\text{ArH}} + \underset{\textbf{7}}{i\text{-Pr}_2\text{NLi(THF)}_3} \longrightarrow \underset{\textbf{8}}{[\text{ArH}\bullet i\text{-Pr}_2\text{NLi(THF)}_3]^{\ddagger}} \quad (7)$$

Pathway 2:

$$\underset{\textbf{3b}}{\text{ArLi(THF)}_3} + i\text{-Pr}_2\text{NH} \rightleftharpoons \underset{\textbf{1}}{\text{ArH}} + \underset{\textbf{9}}{i\text{-Pr}_2\text{NLi(THF)}} + 2\text{THF} \quad (8)$$

$$\underset{\textbf{1}}{\text{ArH}} + \underset{\textbf{9}}{i\text{-Pr}_2\text{NLi(THF)}} \longrightarrow \underset{\textbf{10}}{[\text{ArH}\bullet i\text{-Pr}_2\text{NLi(THF)}]^{\ddagger}} \quad (9)$$

The results from DFT calculations of monomer-based transition structures bearing 0-3 THF ligands are summarized in Figure I.5. Values

include single point MP2 calculations. The values without the single point energy calculations are shown in parentheses. Detailed analysis is deferred to the discussion section.

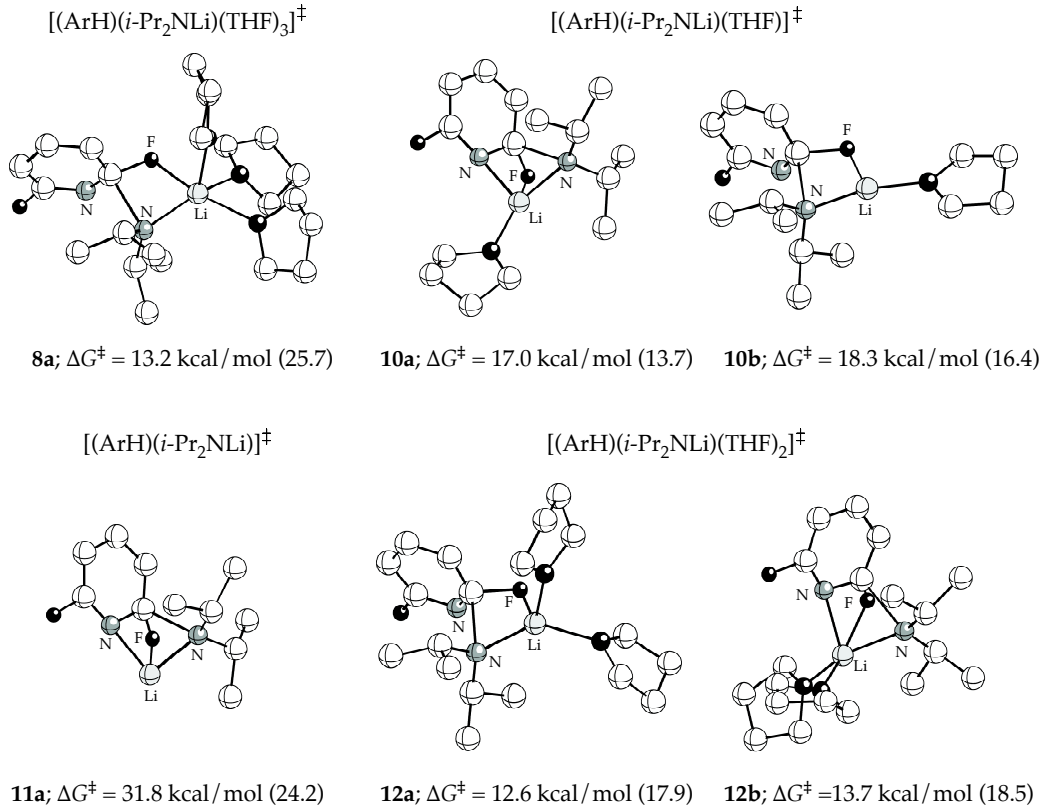

Figure I.5. Calculated monomer-based transition structures at 0 °C. Energies are calculated according to eq 10. Values in parentheses correspond to calculations without single point MP2 corrections.

$$ArLi(THF)_3 + i\text{-}Pr_2NH \longrightarrow [(ArH)(i\text{-}Pr_2NLi)(THF)_n] + (3\text{-}n)THF \qquad (10)$$

Discussion

LDA quantitatively ortholithiates 2,6-difluoropyridine (**1**) in THF at -78 °C to form aryllithium **3**. Warming the solution to 0 °C affords aminopyridine **2** (Scheme I.1). At the outset, we considered three mechanisms for the conversion of aryllithium **3** to adduct **2**: (1) Reversible lithiation with

nucleophilic attack by LDA on unlithiated pyridine **1** (eq 1); (2) LiF elimination to form 2-pyridyne **4** with subsequent trapping by LDA (eq 2); and (3) direct nucleophilic attack of LDA on aryllithium **3**, possibly via a mixed aggregate (eq 3). The rate data described herein support the reversible lithiation described by eq 1. As is often the case, however, a more complex picture emerges (Scheme I.2).

Scheme I.2

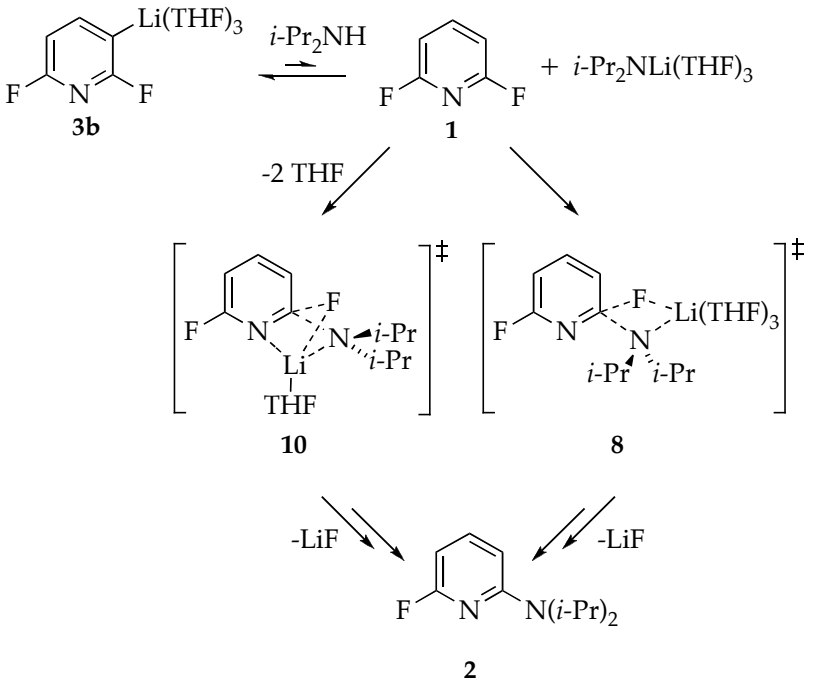

A first-order dependence on diisopropylamine distinguishes the mechanism in eq 1 from the other two. Orders in THF and LDA fill in the details. Recognizing, however, that the nonspecialist may find this example somewhat baffling because of the resting state as aryllithium **3**, we take this opportunity to walk through the process of how one extracts mechanistic insights from the rate law described by eq 5.

We begin by stating a simple yet powerful maxim: *The rate law provides the stoichiometry of the rate-limiting transition structure(s) relative to the reactants.*[7,22] Assigning the reactant structures is critical to assessing the *absolute* stoichiometries of transition structures. LDA is a disolvated dimer **6**, and aryllithium **3** is shown spectroscopically to be a monomer and computationally to be trisolvate **3b**.

First orders in both ArLi and *i*-Pr_2NH at low and high THF concentrations suggest [ArH•*i*-Pr_2NLi]‡, implying a rate-limiting addition. A stoichiometrically equivalent formulation such as [ArLi•*i*-Pr_2NH]‡, reflecting a rate-limiting proton transfer, is excluded by the reversibility of the proton transfer and an isotopically insensitive rate for *i*-Pr_2ND. The affiliation of a zeroth-order LDA dependence with an LDA-monomer-based mechanism is a counterintuitive consequence of the resting state being ArLi/*i*-Pr_2NH rather than ArH/LDA. We note in passing that, had an LDA-*dimer*-based transition structure been operative, a half-order dependence on LDA would have been observed.[7]

A plot of k_{obsd} versus THF concentration (Figure I.2) provides key insights into the role of THF. An inverse second-order dependence—a marked acceleration with *decreasing* THF concentration—shows that *two* THFs are necessarily lost from the reactants en route to the rate-limiting transition structure, which we can now complete as [ArH•*i*-$Pr_2NLi(THF)$]‡. The approach to a nonzero asymptotic limit at high THF concentration points to a zeroth-order dependence, showing that THF is neither lost nor gained as part of a parallel mechanistic pathway en route to [ArH•*i*-$Pr_2NLi(THF)_3$]‡.

We must confess that we are uncomfortable using theory alone to explore organolithium reaction mechanism—there are simply too many

possibilities. Given the stoichiometric constraints imposed by the rate studies, however, we are positioned to consider the DFT computations described by Figure I.5. We hasten to add that the quality of the calculations and the discussion were materially improved by the gentle prodding of a referee.

Monomer-based transition structures bearing one, two, and three coordinated THFs (eq 10, Figure I.5) are all plausible within a liberal definition. Potentially stabilizing Li-F are prominent and Li-N interactions at the pyridyl nitrogen are prevalent at lower solvation numbers. The prominent Li-F interactions add to mounting evidence that Li-F contacts are key determinants of organolithium reaction mechanisms.[10,23,24] Li-N contacts are absent in the sterically congested trisolvate **8a**.

Transition structures **8a** and **10a** or **10b** computed at the B3LYP level of theory are fully compatible with the rate data and offer visually appealing, intimate details of the substitution. We must, however, underscore the quantitative disagreement of theory and experiment. Detecting trisolvated monomer-based transition structure **8a** appeared to be a pyrrhic victory. The rate studies indicate that **8a** and **10a** should be of roughly equal stability whereas computations indicate **8a** is 12 kcal/mol less stable. Although the unprotected charge developing on the pyridyl nitrogen is likely to be the source of some computational problems,[25] 12 kcal/mol is a *large* discrepancy. Computations using diffuse orbitals (supporting information) generally increase all barriers by a few kcal/mol, but preclude detecting trisolvate **8a** altogether. Single point calculations adding MP2 correction reversed the relative energies, rendering **8a** the preferred transition structure by a somewhat smaller (4 kcal/mol) margin.

IRC calculations proved very interesting. The stable minima preceding and following transition structure **10a** correspond to pyridine precomplex **13** and direct substitution product **14**, respectively (eq 11); the substitution proceeds directly without the intermediacy of a stable Meisenheimer complex. IRC calculations on the trisolvate reveal a direct substitution and the complete absence of substrate-lithium complexation prior to or following rate limiting transition structure **8a** (eq 12). Those specializing in early transition metal chemistry would likely refer to these substitutions as sigma bond metathesis.[26] We have always been baffled by the facility of nucleophilic substitutions of arylfluorides;[1] this result seems to shed some light on why aryl fluorides are easily substituted.

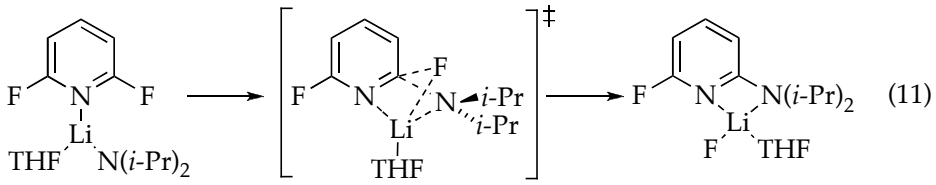

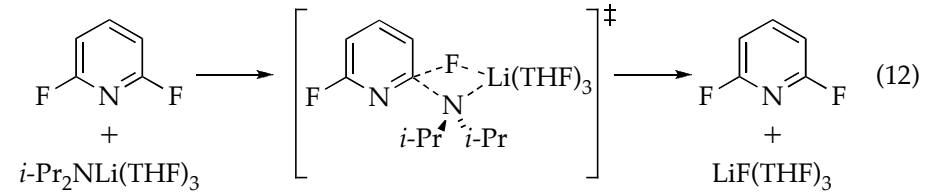

Conclusion

Mechanistic studies offer potentially practical insights for those interested in functionalizing pyridines.[3] The nucleophilic substitution of a 2-fluoropyridine by LDA is remarkably efficient given the exceptional steric demand. If one's goal is to achieve the substitution—if ortholithiation is an unwanted side equilibrium—then low THF concentration and high

diisopropylamine concentration are advised. (Donor solvent *concentration* is an often overlooked variable during optimizations.) If, by contrast, the goal is to achieve ortholithiation and the nucleophilic substitution is an unwanted side reaction—a problem likely to be observed with more electrophilic heteroaromatics than with **1**— then the opposite logic may hold true. In fact, scavenging the free amine with an additional equivalent of *n*-BuLi[27] or using a more hindered lithium amide base should eliminate the unwanted addition altogether.

Experimental Section

Reagents and Solvents. THF and hexane were distilled from blue or purple solutions containing sodium benzophenone ketyl. The hexane contained 1% tetraglyme to dissolve the ketyl. Both LDA[12] and *n*-BuLi[28] used to prepare LDA were recrystallized. Solutions of LDA were titrated using a literature method.[29]

1,2-Addition: Preparative Scale. A 1.6 M solution of *n*-butyllithium (6.9 mL, 11.0 mmol) in hexanes was added via syringe to a solution of dry diisopropylamine (5.0 mL, 3.61 g, 35.6 mmol) in dry hexanes at 0 °C under Ar. After the solution was stirred for 10 minutes, 2,6-difluoropyridine (500 μL, 634 mg, 5.5 mmol) was added to the LDA solution. After being stirred at 0 °C for 2 h, the reaction was quenched with wet THF. The organic layer was washed with aqueous NaCl (3 x 10 mL), dried over Na_2SO_4, filtered, and evaporated to dryness under reduced pressure. Flash chromatography (50% ethyl acetate/hexanes) afforded 2-fluoro-6-(diisopropylamino)pyridine (**2**) as a brown liquid (949 mg, 4.84 mmol) in 88% yield: ^{1}H NMR ($CDCl_3$) *d* 7.39 (q, *J* = 8.4 Hz, 1H), 6.30 (dd, *J* = 8.3 Hz, 2.9 Hz, 1H), 5.99 (dd, *J* = 7.6 Hz, 3.2 Hz, 1H),

4.17 (sept, J = 6.8 Hz, 2H), 1.29 (d, J = 6.5 Hz, 12H); ^{13}C NMR ($CDCl_3$) δ 162.6 (d, J = 232.5 Hz), 157.0 (d, J = 16.7 Hz), 140.8 (d, J = 8.5 Hz), 104.4 (d, J = 4.0 Hz), 93.5 (d, J = 38.4 Hz), 46.1 (s), 20.6 (s); ^{19}F NMR (THF-d_8) δ -68.2 ; HRMS [$C_{11}H_{17}N_2F$] requires m/z 196.1376, found 196.1368.

IR Spectroscopic Analyses. IR spectra were recorded using an in situ IR spectrometer fitted with a 30-bounce, silicon-tipped probe.[30] The spectra were acquired in 16 scans at a gain of 1 and a resolution of 4 cm^{-1}. A representative reaction was carried out as follows: The IR probe was inserted through a nylon adapter and an O-ring seal into an oven-dried, cylindrical flask fitted with a magnetic stir bar and a T-joint. The T-joint was capped by a septum for injections and a nitrogen line. After evacuation under full vacuum, heating, and flushing with nitrogen, the flask was cooled to 0 °C and charged with LDA (108 mg, 1.01 mmol) and the quantities of THF and *i*-Pr_2NH required to achieve the final molarities. After recording a background spectrum, arene **1** was added (0.050 mmol) as a 0.50 M solution in THF, affording **3** instantaneously. The disappearance of aryllithium **3** was monitored via the absorbance at 1576 cm^{-1}.

NMR Spectroscopic Analyses. All samples were prepared using stock solutions and sealed under partial vacuum. Standard ^{6}Li, ^{13}C, ^{15}N, and ^{19}F NMR spectra were recorded on a 500 MHz spectrometer at 73.57, 125.79, 50.66, and 470.35 MHz (respectively). The ^{6}Li, ^{13}C, ^{15}N, and ^{19}F resonances are referenced to 0.30 M [^{6}Li]LiCl/MeOH at -90 °C (0.0 ppm), the CH_2O resonance of THF at -90 °C (67.57 ppm), neat Me_2NEt at -90 °C (25.7 ppm), and C_6H_5F in neat THF at -78 °C (-113.15 ppm), respectively.

APPENDIX I

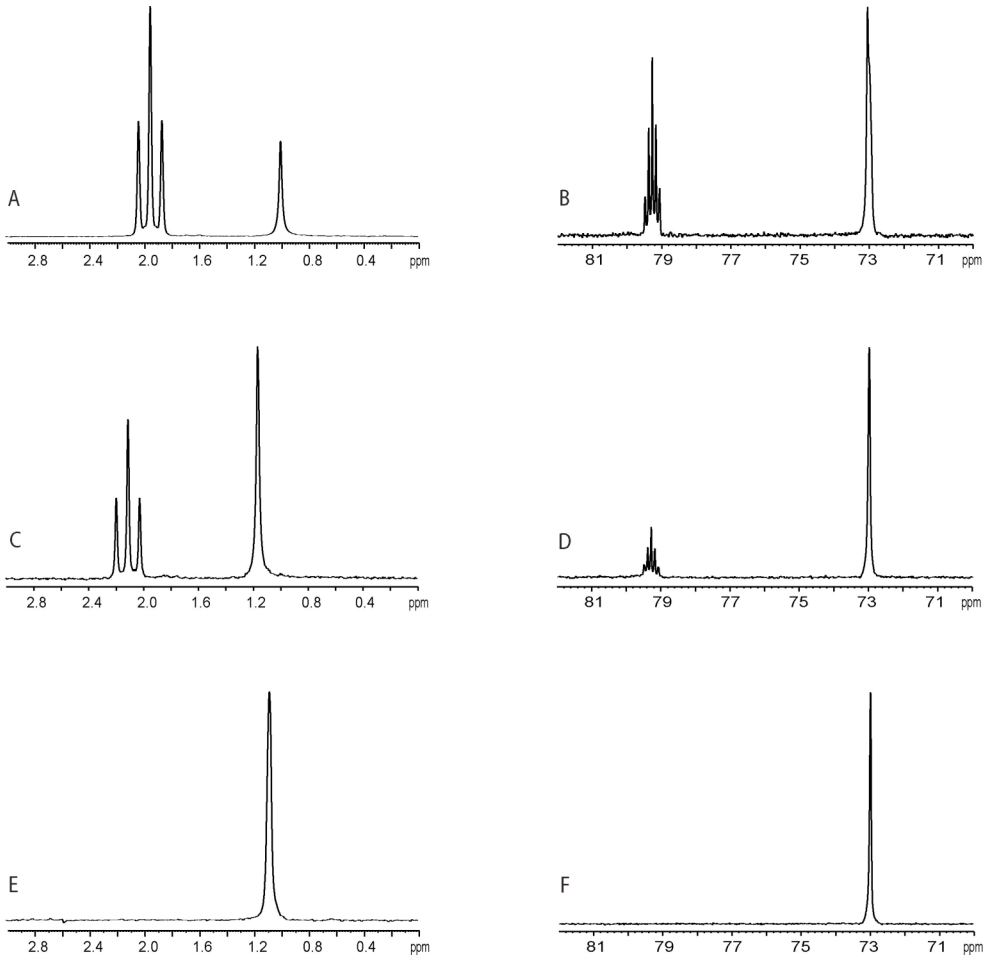

Figure AI.1. ^{6}Li and ^{15}N NMR spectra of 0.10 M [^{6}Li,^{15}N]LDA in 10.3 M THF/pentane recorded at -90 °C in the presence of: (A) 0.025 M 2,6-difluoropyridine, ^{6}Li spectrum; (B) 0.025 M 2,6-difluoropyridine, ^{15}N spectrum; (C) 0.050 M 2,6-difluoropyridine, ^{6}Li spectrum; (D) 0.050 M 2,6-difluoropyridine, ^{15}N spectrum; (E) 0.10 M 2,6-difluoropyridine, ^{6}Li spectrum; (F) 0.10 M 2,6-difluoropyridine, ^{15}N spectrum.

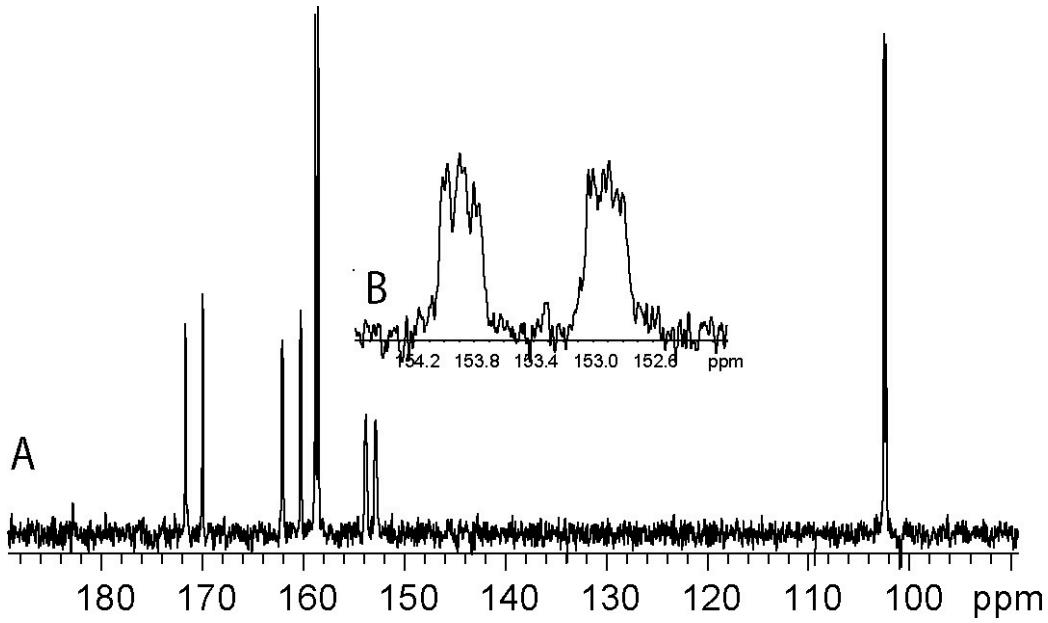

Figure AI.2. $^{13}C\{^{1}H\}$ NMR spectrum (125 MHz) of 0.050 M 2,6-difluoro-3-lithiopyridine (**3**) in 10.25 M THF/pentane at -110 ºC: (A) *d* 170.78 (dd, $^{1}J_{C\text{-}F}$ = 213.7 Hz, $^{3}J_{C\text{-}F}$ = 7.6 Hz), 161.14 (dd, $^{1}J_{C\text{-}F}$ = 228.8 Hz, $^{3}J_{C\text{-}F}$ = 15.1 Hz), 158.62 (d, $^{2}J_{C\text{-}F}$ = 37.6 Hz), 153.41 (dtd, $^{2}J_{C\text{-}F}$ = 122.5 Hz, $^{1}J_{C\text{-}Li}$ = 12.9 Hz, $^{4}J_{C\text{-}F}$ = 4.2 Hz), 102.44 (dd, $^{3}J_{C\text{-}F}$ = 26.0 Hz, $^{3}J_{C\text{-}F}$ = 4.6 Hz). (B) □□153.41 (dtd, $^{2}J_{C\text{-}F}$ = 122.5 Hz, $^{1}J_{C\text{-}Li}$ = 12.9 Hz, $^{4}J_{C\text{-}F}$ = 4.2 Hz).

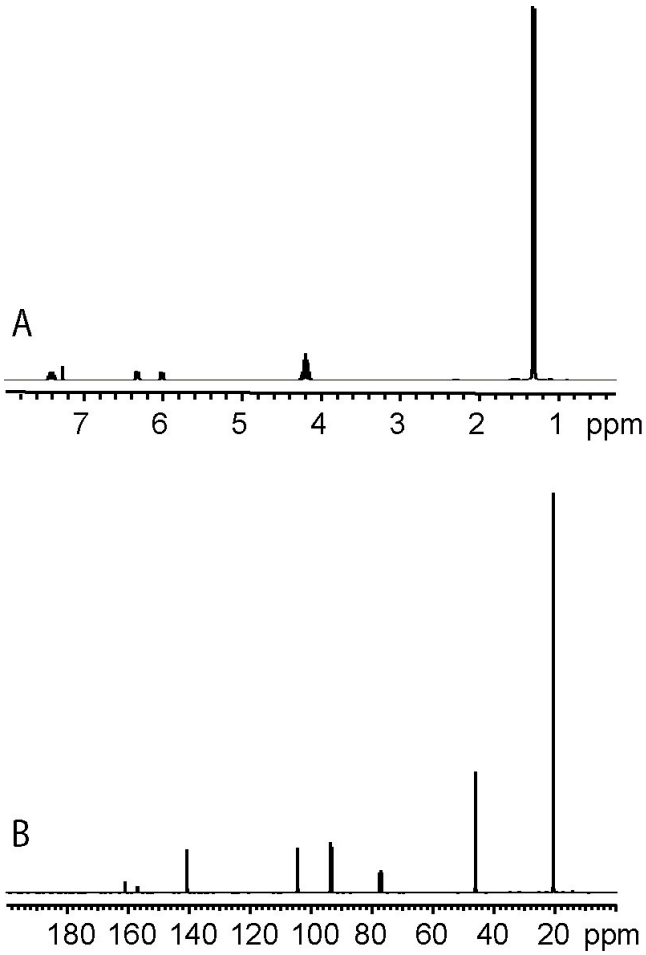

Figure AI.3. ^{1}H and ^{13}C NMR spectra of 2-fluoro-6-(diisopropylamino)-pyridine (**2**): (A) ^{1}H NMR (300 MHz, $CDCl_3$, 20 °C)□□□7.39 (q, *J* = 8.4 Hz, 1H), 6.30 (dd, *J* = 8.3 Hz, 2.9 Hz, 1H), 5.99 (dd, *J* = 7.6 Hz, 3.2 Hz, 1H), 4.17 (sept, *J* = 6.8 Hz, 2H), 1.29 (d, *J* = 6.5 Hz, 12H) (B) ^{13}C NMR (75 MHz, $CDCl_3$, 20 °C) □□162.60 (d, *J* = 232.5 Hz), 156.99 (d, *J* = 16.7 Hz), 140.77 (d, *J* = 8.5 Hz), 104.40 (d, *J* = 4.0 Hz), 93.46 (d, *J* = 38.4 Hz), 46.14 (s), 20.62 (s).

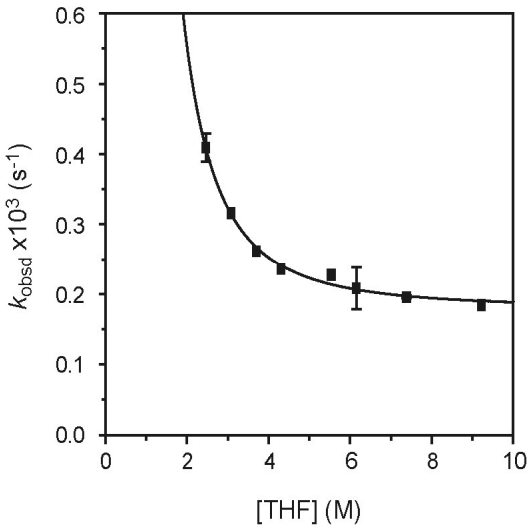

Figure AI.4. Plot of k_{obsd} vs [THF] in hexane cosolvent for the nucleophilic substitution of 2,6-difluoropyridine (0.005 M) with LDA (0.10 M) and diisopropylamine (0.10 M) at 0 °C. The curve depicts an unweighted least-squares fit to $k_{obsd} = k[\text{THF}]^n + k'$ ($k = (1.9 \pm 0.7) \times 10^{-3}$, $n = -2.4 \pm 0.4$, $k' = (1.8 \pm 0.1) \times 10^{-4}$).

[THF] (M)	$k_{obsd}1$ x 10^3 (s^{-1})	$k_{obsd}2$ x 10^3 (s^{-1})	k_{obsd}avg x 10^3 (s^{-1})
2.460	0.395	0.423	0.41 $\pm$ 2E-2
3.075	0.316	—	—
3.700	0.262	—	—
4.300	0.236	—	—
5.535	0.227	—	—
6.150	0.187	0.229	0.21 $\pm$ 3E-2
7.380	0.197	0.194	0.195 $\pm$ 2E-3
9.220	0.184	—	—

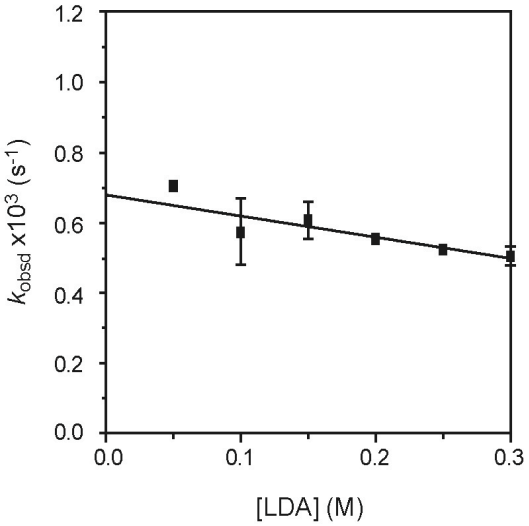

Figure AI.5. Plot of k_{obsd} vs [LDA] in 2.5 M THF/hexane and 0.10 M diisopropylamine for the nucleophilic substitution of 2,6-difluoropyridine (0.005 M) at 0 °C. The curve depicts an unweighted least-squares fit to $k_{obsd} = k[\text{LDA}] + k'$ ($k = (-6 \pm 2) \times 10^{-4}$, $k' = (6.8 \pm 0.4) \times 10^{-4}$).

[LDA] (M)	$k_{obsd}1$ x 10^3 (s^{-1})	$k_{obsd}2$ x 10^3 (s^{-1})	k_{obsd}avg x 10^3 (s^{-1})
0.05	0.706	—	—
0.10	0.642	0.507	0.57 ± 9E-2
0.15	0.571	0.646	0.61 ± 5E-2
0.20	0.556	—	—
0.25	0.525	—	—
0.30	0.487	0.526	0.51 ± 3E-2

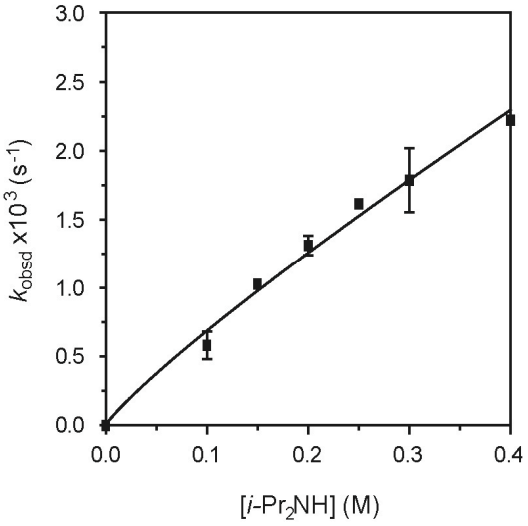

Figure AI.6. Plot of k_{obsd} vs [i-Pr$_2$NH] in 2.5 M THF/hexane for the nucleophilic substitution of 2,6-difluoropyridine (0.005 M) with LDA (0.10 M) at 0 °C. The curve depicts an unweighted least-squares fit to $k_{obsd} = k[i\text{-Pr}_2\text{NH}]^n$ ($k = (5.1 \pm 0.5) \times 10^{-3}$, $n = 0.87 \pm 0.07$).

[i-Pr$_2$NH] (M)	k_{obsd}1 x 10^3 (s^{-1})	k_{obsd}2 x 10^3 (s^{-1})	k_{obsd}avg x 10^3 (s^{-1})
0.10	0.642	0.507	0.57 $\pm$ 9E-2
0.15	1.025	—	—
0.20	1.360	1.260	1.31 $\pm$ 7E-2
0.25	1.615	—	—
0.30	1.950	1.620	1.8 $\pm$ 2E-1
0.40	2.220	—	—

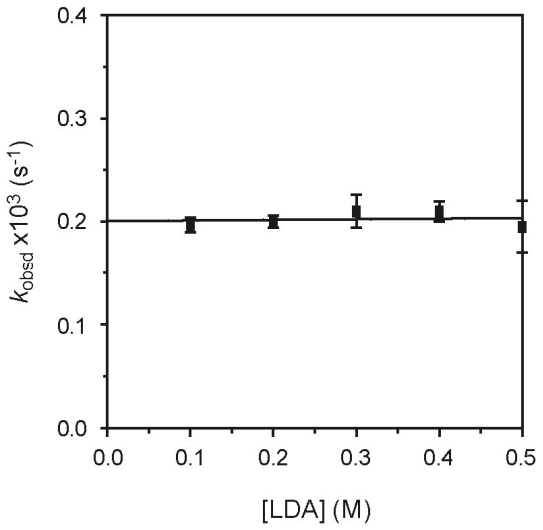

Figure AI.7. Plot of k_{obsd} vs [LDA] in 7.4 M THF/hexane and 0.10 M diisopropylamine for the nucleophilic substitution of 2,6-difluoropyridine (0.005 M) at 0 °C. The curve depicts an unweighted least-squares fit to $k_{obsd} = k[\text{LDA}] + k'$ ($k = (0.9 \pm 3.0) \times 10^{-5}$, $k' = (1.9 \pm 0.1) \times 10^{-4}$).

[LDA] (M)	$k_{obsd}1$ x 10^3 (s^{-1})	$k_{obsd}2$ x 10^3 (s^{-1})	k_{obsd}avg x 10^3 (s^{-1})
0.1	0.197	0.194	0.195 $\pm$ 6E-3
0.2	0.204	0.196	0.200 $\pm$ 6E-3
0.3	0.199	0.221	0.21 $\pm$ 2E-2
0.4	0.203	0.217	0.210 $\pm$ 9E-3
0.5	0.213	0.177	0.19 $\pm$ 2E-2

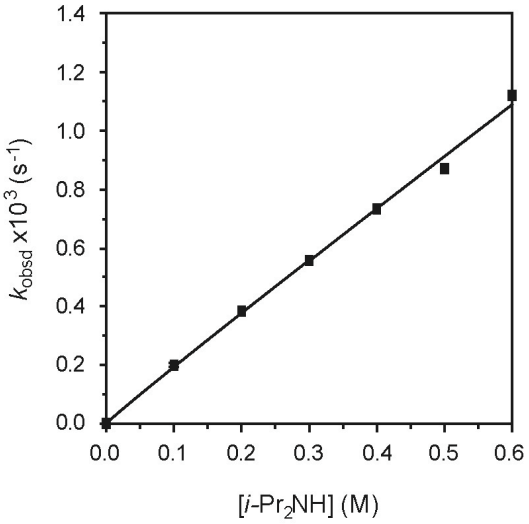

Figure AI.8. Plot of k_{obsd} vs [i-Pr$_2$NH] in 7.4 M THF/hexane for the nucleophilic substitution of 2,6-difluoropyridine (0.005 M) with LDA (0.10 M) at 0 °C. The curve depicts an unweighted least-squares fit to $k_{obsd} = k[i\text{-Pr}_2\text{NH}]^n$ ($k = (1.78 \pm 0.05) \times 10^{-3}$, $n = 0.97 \pm 0.03$).

[i-Pr$_2$NH] (M)	k_{obsd}1 x 10^3 (s^{-1})	k_{obsd}2 x 10^3 (s^{-1})	k_{obsd}avg x 10^3 (s^{-1})
0.1	0.197	0.194	0.195 $\pm$ 6E-3
0.2	0.383	—	—
0.3	0.558	—	—
0.4	0.735	—	—
0.5	0.871	—	—
0.6	1.120	—	—

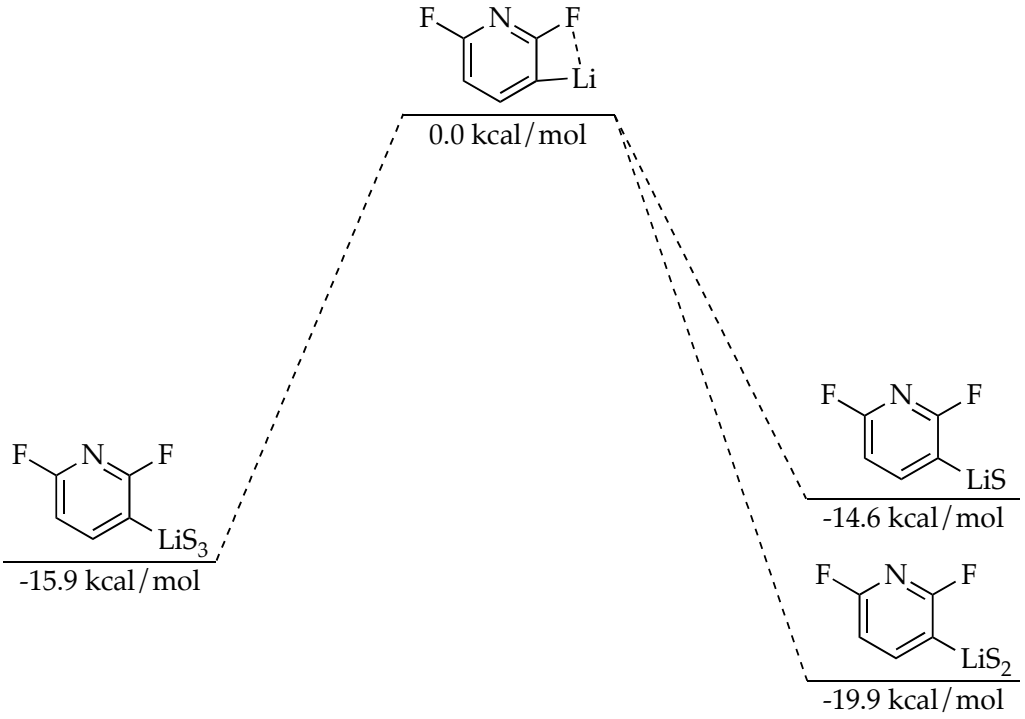

Figure AI.9. Relative free energies for the solvation (Δ*G*, kcal/mol) of 2,6-difluoro-3-lithiopyridine (**3**) at 0 °C (S = THF) calculated using B3LYP level of theory with 6-31G(d) basis set.

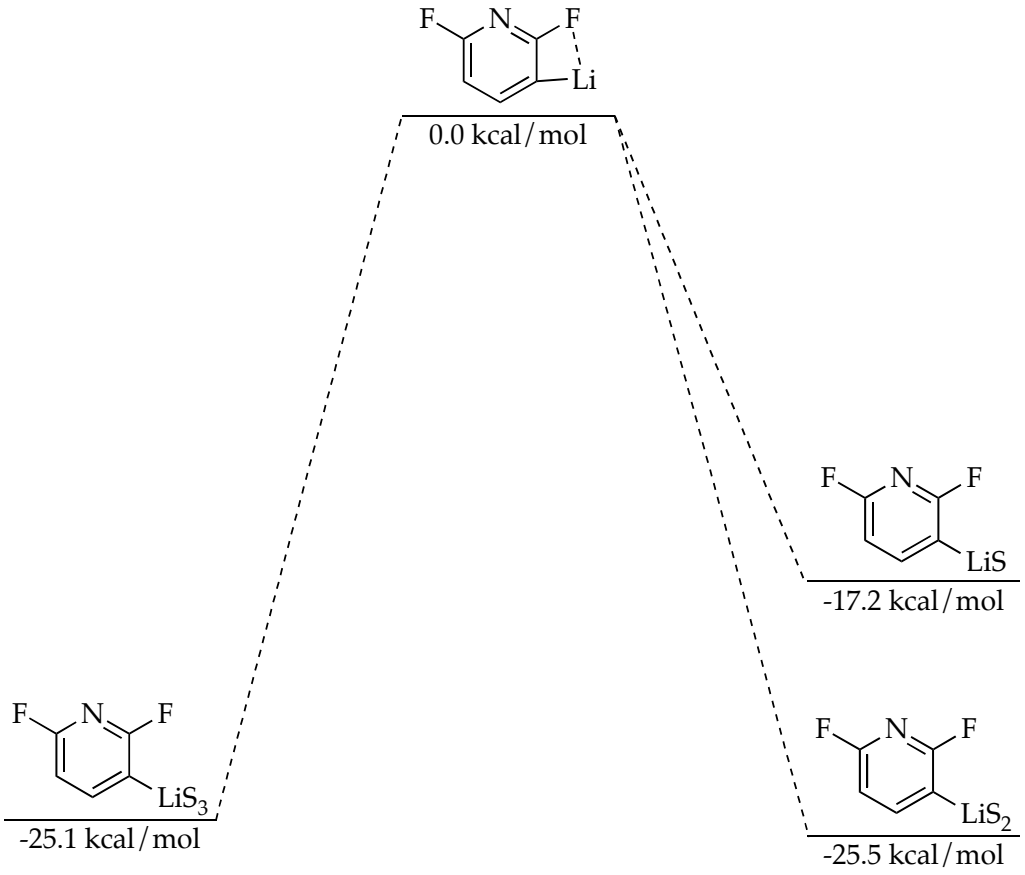

Figure AI.10. Relative free energies for the solvation (Δ*G*, kcal/mol) of 2,6-difluoro-3-lithiopyridine (**3**) at -78 °C (S = THF) calculated using B3LYP level of theory with 6-31G(d) basis set.

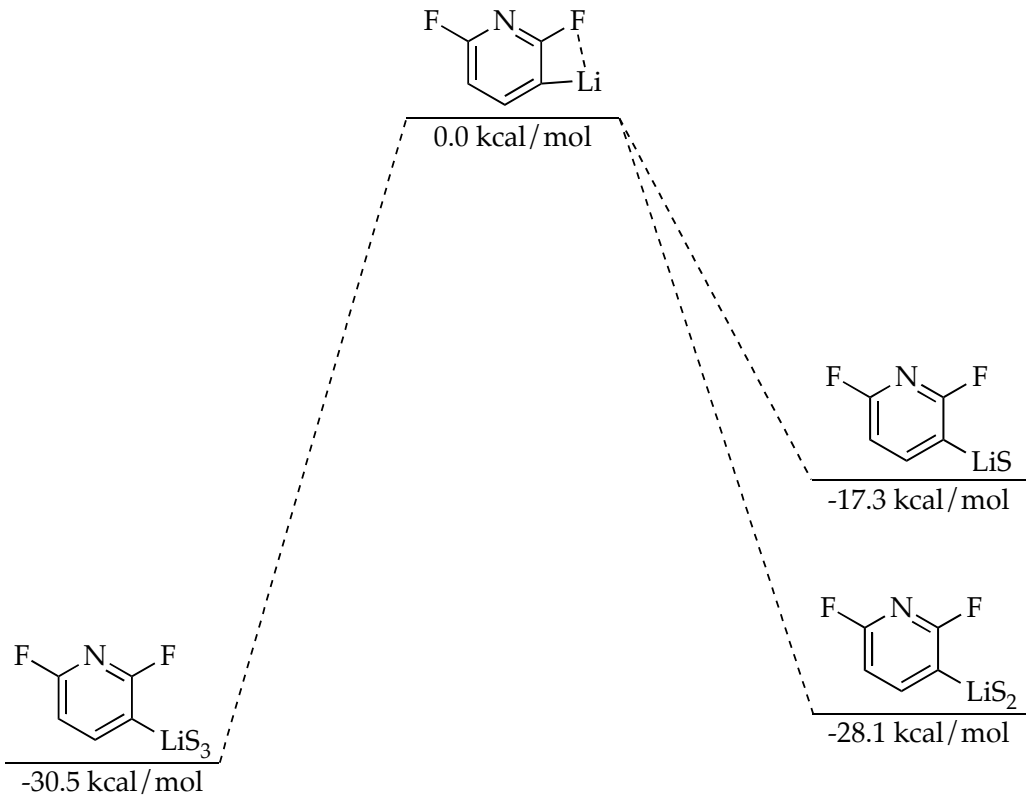

Figure AI.11. Relative free energies for the solvation (ΔG, kcal/mol) of 2,6-difluoro-3-lithiopyridine (**3**) at 0 °C (S = THF) calculated using single point MP2 corrections to B3LYP/6-31G(d) optimized structures.

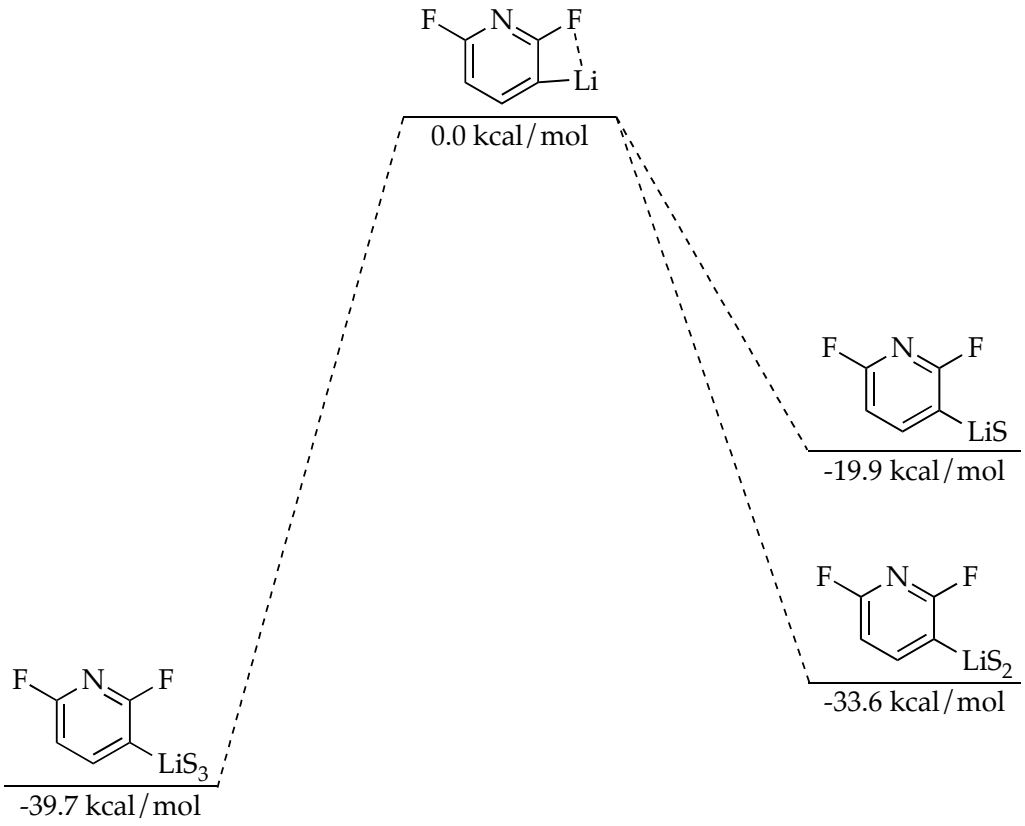

Figure AI.12. Relative free energies for the solvation (Δ*G*, kcal/mol) of 2,6-difluoro-3-lithiopyridine (**3**) at -78 °C (S = THF) calculated using calculated using single point MP2 corrections to B3LYP/6-31G(d) optimized structures.

Table AI.1. Optimized geometries at B3LYP level of theory with 6-31G(d) basis set for the serial solvation of 2,6-difluoro-3-lithiopyridine (**3**) with free energies (Hartrees) and cartesian coordinates (X, Y, Z). (Note: G_{MP2} includes single point MP2 corrections to B3LYP/6-31G(d) optimized structures)

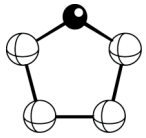

G = -232.357835 (0 °C)
G = -232.349202 (-78 °C)
G_{MP2} = -231.577985 (0 °C)
G_{MP2} = -231.569352 (-78 °C)

Atom	X	Y	Z	Atom	X	Y	Z
C	-0.77676	0.78926	-0.12614	H	1.99943	-1.03711	-0.49250
C	-1.13241	-0.69941	0.08086	H	1.31917	-0.90803	1.14900
O	-0.00028	-1.43271	-0.37154	H	1.16400	1.14893	-1.08517
C	1.13192	-0.69999	0.08156	H	1.20108	1.42138	0.65905
C	0.77743	0.78860	-0.12707	H	-1.16426	1.15158	-1.08311
H	-1.99954	-1.03544	-0.49441	H	-1.19880	1.42112	0.66158
H	-1.32099	-0.90818	1.14790				

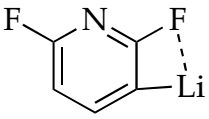

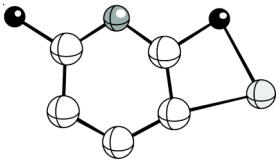

G = -453.652840 (0 °C)
G = -453.643384 (-78 °C)
G_{MP2} = -452.375354 (0 °C)
G_{MP2} = -452.365898 (-78 °C)

Atom	X	Y	Z	Atom	X	Y	Z
C	1.19546	0.56315	-0.00003	C	-1.26124	0.64286	-0.00001
C	0.93012	-0.79062	-0.00002	C	-0.01621	1.28382	0.00000
Li	3.09879	0.01350	0.00007	F	-2.43290	-1.40856	0.00003
F	2.12496	-1.60980	-0.00001	H	-2.20119	1.18413	0.00001
N	-0.17287	-1.50168	-0.00002	H	-0.00268	2.37335	0.00003
C	-1.26224	-0.75016	-0.00006				

Table AI.1 (Continued).

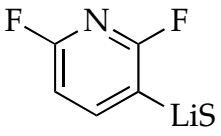

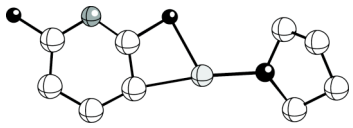

G = -686.033895 (0 °C)
G = -686.019972 (-78 °C)
G_{MP2} = -683.980860 (0 °C)
G_{MP2} = -683.966937 (-78 °C)
S = THF

Atom	X	Y	Z	Atom	X	Y	Z
C	-2.55810	1.05916	-0.12094	N	3.59752	-1.20485	-0.13846
O	-1.56124	0.07902	-0.52225	F	5.82357	-1.10665	0.25855
C	-2.07273	-1.26826	-0.32436	H	5.56391	1.48419	0.33704
C	-3.23679	-1.10522	0.64852	H	3.38499	2.66146	0.01320
C	-3.81506	0.25494	0.22589	H	-4.40660	0.73502	1.01025
Li	0.30151	0.35125	-0.61216	H	-4.45296	0.13990	-0.65761
F	1.34844	-1.32480	-0.54288	H	-3.95949	-1.92251	0.57319
C	2.49653	-0.50166	-0.29878	H	-2.86886	-1.06637	1.68014
C	2.22141	0.85245	-0.28049	H	-1.24994	-1.88275	0.04903
C	3.40837	1.57260	-0.03647	H	-2.40253	-1.66187	-1.29371
C	4.64473	0.93930	0.14954	H	-2.70154	1.76126	-0.94719
C	4.66062	-0.45057	0.08512	H	-2.16575	1.60498	0.74481

Table AI.1 (Continued).

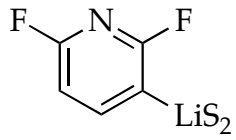

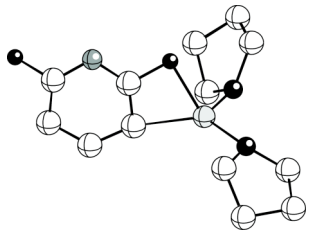

G = -918.400263 (0 °C)
G = -918.382414 (-78 °C)
G_{MP2} = -915.576090 (0 °C)
G_{MP2} = -915.558240 (-78 °C)
S = THF

Atom	X	Y	Z	Atom	X	Y	Z
C	0.39156	2.45585	1.20393	H	2.25135	-1.80815	2.44005
O	-0.41665	1.87910	0.14425	H	4.54568	-2.37239	1.63588
C	-0.33843	2.71035	-1.04651	H	-0.61203	-2.68247	-0.38146
C	0.48693	3.94063	-0.65213	H	-1.76018	-2.71761	-1.75237
C	1.35581	3.40345	0.49636	H	-2.99351	-4.05097	-0.10547
Li	-0.16844	-0.04595	-0.09555	H	-2.40014	-3.04381	1.23084
C	1.57137	-0.96097	0.55969	H	-4.59985	-2.02924	0.79634
C	2.13337	-0.76162	-0.69084	H	-4.40161	-2.23483	-0.95124
F	1.26886	-0.15318	-1.63642	H	-3.57799	0.01115	-0.82692
N	3.32570	-1.02149	-1.19408	H	-3.04139	-0.18755	0.85816
C	4.14428	-1.59330	-0.32806	H	1.73203	4.18993	1.15726
C	3.81463	-1.90128	0.98698	H	2.21115	2.84272	0.10328
C	2.51763	-1.57250	1.40829	H	1.07224	4.32843	-1.49074
F	5.37933	-1.88336	-0.78569	H	-0.16606	4.74486	-0.29327
O	-1.78513	-1.00346	-0.57018	H	0.15222	2.12469	-1.83120
C	-3.12283	-0.68530	-0.11554	H	-1.35716	2.95426	-1.36398
C	-3.86863	-2.02317	-0.01720	H	0.88018	1.62770	1.72308
C	-2.72500	-3.03079	0.18397	H	-0.27008	2.99061	1.89870
C	-1.62920	-2.44035	-0.69820				

Table AI.1 (Continued).

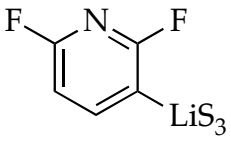

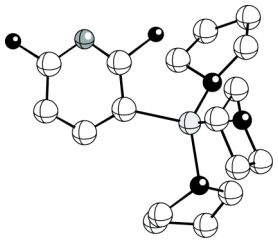

G = -1150.751744 (0 °C)
G = -1150.731071 (-78 °C)
G_{MP2} = -1147.157941 (0 °C)
G_{MP2} = -915.137268 (-78 °C)
S = THF

Atom	X	Y	Z	Atom	X	Y	Z
Li	0.00251	-0.13489	-0.07830	H	2.28500	-1.33976	2.42167
O	-0.12535	-1.17465	-1.82404	H	-3.37145	-1.36878	0.39383
C	1.04265	-1.14759	-2.66928	H	-2.85748	0.32861	0.55163
C	1.81355	-2.41948	-2.30127	H	-3.98140	0.18956	2.68463
C	0.69701	-3.41519	-1.88657	H	-3.86211	-1.57426	2.70354
C	-0.57551	-2.54115	-1.81156	H	-2.11081	-1.01540	4.29762
C	1.95005	-0.01145	0.73439	H	-1.64557	0.43085	3.38053
C	2.72903	0.89212	0.01664	H	-0.00537	-1.16617	2.53120
F	2.11403	1.54399	-1.05225	H	-1.20672	-2.49090	2.55429
N	3.99414	1.26478	0.14880	H	-1.15819	-2.67523	-0.89876
C	4.63569	0.67161	1.13732	H	-1.22546	-2.70888	-2.68251
C	4.07584	-0.27152	1.98738	H	0.92242	-3.87257	-0.91910
C	2.72948	-0.59340	1.75847	H	0.57182	-4.22397	-2.61335
F	5.92779	1.02941	1.30387	H	2.42368	-2.78664	-3.13189
O	-0.96233	1.61472	-0.49142	H	2.47193	-2.20957	-1.45457
C	-1.05864	2.04720	-1.86325	H	0.72122	-1.15506	-3.72201
C	-1.58136	3.50188	-1.81366	H	1.57686	-0.22242	-2.45457
C	-1.42379	3.90866	-0.32403	H	-0.06314	1.99861	-2.31890
C	-0.56771	2.78007	0.25937	H	-1.72148	1.34818	-2.37671
O	-1.42454	-1.05205	1.05957	H	-0.99427	4.14516	-2.47564
C	-2.81907	-0.65849	1.02017	H	-2.62557	3.56799	-2.13283
C	-3.31386	-0.65238	2.47880	H	-2.39989	3.93901	0.17107
C	-2.00795	-0.59979	3.29075	H	-0.95299	4.88797	-0.19869
C	-1.06168	-1.41011	2.40948	H	0.50324	2.95527	0.10841
H	4.66851	-0.72226	2.77680	H	-0.75278	2.56834	1.31492

Table AI.2. Optimized geometries of reactants and monomer-based transition structures at B3LYP level of theory with 6-31G(d) basis set for the nucleophilic substitution of 2,6-difluoropyridine with free energies (Hartrees), and cartesian coordinates (X,Y,Z). (Note: G_{MP2} includes single point MP2 corrections to B3LYP/6-31G(d) optimized structures)

i-Pr_2NH

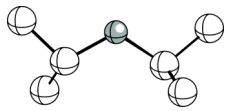

G = -292.249737
G_{MP2} = -291.164958
(0 °C)

Atom	X	Y	Z	Atom	X	Y	Z
C	1.24910	-0.14802	0.16912	H	-3.25645	0.89733	-0.39385
N	0.01667	-0.00296	-0.62039	H	-1.98369	1.51946	-1.47490
C	-1.23745	0.23551	0.11083	H	-1.05830	1.08725	0.77909
C	-1.71244	-0.95470	0.96596	H	-0.10569	-0.83728	-1.19491
C	-2.31459	0.65098	-0.89758	H	0.97067	1.68300	1.34524
C	1.71507	1.21758	0.69025	H	2.64071	1.11215	1.26819
C	2.32260	-0.77825	-0.72399	H	1.89911	1.89793	-0.14884
H	-0.95787	-1.25730	1.70017	H	2.48970	-0.15821	-1.61244
H	-2.62862	-0.70690	1.51567	H	3.27147	-0.87689	-0.18593
H	-1.93087	-1.82281	0.32926	H	2.02320	-1.77972	-1.05909
H	-2.52065	-0.16487	-1.60386	H	1.10833	-0.81327	1.04200

Table AI.2 (Continued).

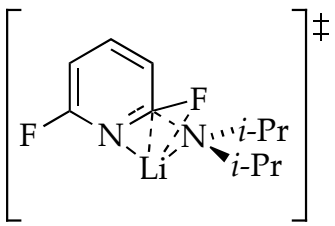

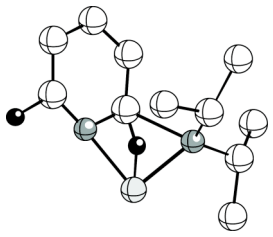

11a
G = -745.889359
G_{MP2} = -743.538202
(0 °C)

Atom	X	Y	Z	Atom	X	Y	Z
C	-2.03362	-0.42115	-0.34145	H	-1.65051	1.95737	1.10780
N	-0.63571	-0.04956	-0.65930	H	-0.49959	3.19632	0.60452
C	-0.44812	1.41222	-0.65262	H	1.07600	1.36201	-2.22665
C	-0.64302	2.11352	0.71017	H	1.73930	1.59398	-0.59614
C	0.89883	1.83757	-1.25293	H	0.91002	2.92262	-1.40916
Li	0.22036	-1.24685	-1.87935	H	-1.22231	1.83060	-1.32414
C	0.92305	-1.20159	0.25335	H	4.48103	0.16488	0.78672
F	0.08005	-2.31654	0.14127	H	2.86044	0.04707	2.73386
N	1.82870	-1.22305	-0.75899	H	0.56924	-0.88200	2.37159
C	3.02752	-0.70707	-0.53356	H	-1.95302	-0.09591	1.82822
C	3.47481	-0.21787	0.67751	H	-3.39780	-0.95618	1.27739
C	2.55558	-0.28984	1.74657	H	-1.84129	-1.79786	1.35176
C	1.28657	-0.79886	1.56504	H	-1.97639	-2.44991	-1.17031
F	3.84836	-0.69890	-1.59800	H	-3.59421	-1.75377	-1.13021
C	-2.31783	-0.84248	1.11742	H	-2.44401	-1.18473	-2.34823
C	-2.53754	-1.51547	-1.30392	H	-2.66285	0.46370	-0.53642
H	0.07798	1.74775	1.44816				

Table AI.2 (Continued).

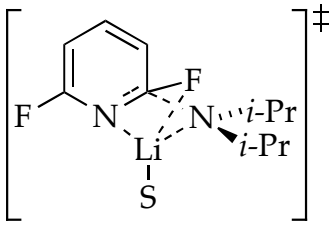

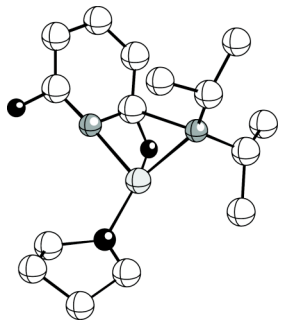

10a
G = -978.263965
G_{MP2} = -975.139814
(0 °C)
S = THF

Atom	X	Y	Z	Atom	X	Y	Z
C	1.52643	-2.08614	-0.33085	H	3.10227	-0.33951	2.96066
N	1.06513	-0.77224	0.16076	H	-0.36679	0.61180	2.00777
C	1.42771	-0.56846	1.57101	H	1.09843	1.59173	1.79160
C	2.93986	-0.47956	1.88383	H	0.86946	0.65955	3.27320
C	0.71664	0.64544	2.18732	H	1.05767	-1.44965	2.13397
Li	-0.67222	-0.15163	-0.48301	H	1.47238	4.52519	0.21448
N	0.19256	1.62030	-0.92395	H	3.61626	3.33910	-0.45320
C	1.33506	0.94528	-1.19632	H	3.49274	1.03078	-1.40387
F	1.15242	0.06821	-2.24642	H	-2.69885	1.80920	-0.82275
C	2.60638	1.56791	-1.09078	H	-3.60741	0.79675	-1.97856
C	2.65635	2.84194	-0.56542	H	-4.35084	1.42742	0.93008
C	1.47619	3.52175	-0.19073	H	-5.41947	1.47830	-0.48571
C	0.30064	2.83172	-0.40749	H	-5.37056	-0.96413	-0.70346
F	-0.87927	3.41637	-0.09461	H	-5.44256	-0.77661	1.05660
O	-2.57984	-0.22277	-0.48239	H	-3.33651	-2.13095	-0.17624
C	-3.42987	-1.13269	0.26159	H	-3.06811	-1.16561	1.29612
C	-4.84608	-0.55411	0.16721	H	3.65763	-1.59805	-0.56590
C	-4.57959	0.94726	-0.02847	H	3.17989	-3.13126	-1.30926
C	-3.34275	0.93409	-0.92228	H	2.74862	-1.59859	-2.08491
C	2.85793	-2.09864	-1.11901	H	0.19493	-2.18186	-2.06444
C	0.43170	-2.77273	-1.17109	H	0.74738	-3.76712	-1.51237
H	3.40106	0.36351	1.35894	H	-0.48585	-2.90043	-0.58081
H	3.46622	-1.39334	1.59188	H	1.68663	-2.73749	0.54729

Table AI.2 (Continued).

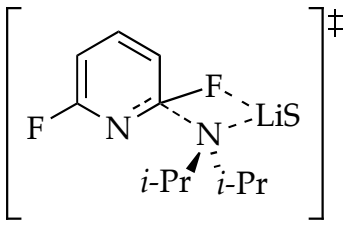

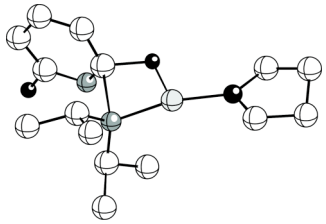

10b
G = -978.259657
G_{MP2} = -975.137701
(0 °C)
S = THF

Atom	X	Y	Z	Atom	X	Y	Z
C	3.28159	-2.04667	0.43582	H	-0.97002	-1.83964	-2.07417
O	2.72555	-0.71514	0.27837	H	0.60196	0.65774	2.48054
C	3.76853	0.22785	-0.08669	H	-0.83848	0.86587	3.47316
C	5.08231	-0.55551	-0.00490	H	-0.67201	-0.60511	2.51388
C	4.62763	-1.99791	-0.28244	H	-1.48947	3.29960	0.77576
Li	0.85908	-0.37659	0.37312	H	-1.29499	3.01693	2.50585
F	-0.17256	-1.89501	0.43575	H	0.11344	2.93050	1.42837
C	-1.49079	-1.43380	0.00713	H	-2.27729	0.99699	1.47844
C	-1.76745	-1.78372	-1.34193	H	0.72692	1.98651	-1.77012
C	-3.08876	-2.02910	-1.67005	H	-0.62268	2.63551	-2.72403
C	-4.08732	-1.99543	-0.68271	H	-0.32060	3.23723	-1.08640
C	-3.64282	-1.75904	0.61239	H	-2.89818	2.52678	-0.53425
N	-2.39614	-1.54461	0.97698	H	-3.00347	1.93878	-2.19431
F	-4.54144	-1.79198	1.61598	H	-3.36041	0.84694	-0.84978
N	-0.73114	0.61221	0.07022	H	-1.16590	0.42028	-1.92064
C	-1.19548	1.17894	1.34286	H	5.32721	-2.75031	0.09239
C	-0.48597	0.47041	2.51380	H	4.49280	-2.16018	-1.35807
C	-0.95592	2.69551	1.51239	H	5.82463	-0.19091	-0.72035
C	-1.22589	1.22115	-1.16687	H	5.51333	-0.47875	0.99973
C	-0.31044	2.34016	-1.71276	H	3.56303	0.58366	-1.10280
C	-2.70564	1.66075	-1.17568	H	3.72092	1.07724	0.60076
H	-5.13145	-2.19420	-0.88816	H	3.39947	-2.25466	1.50670
H	-3.35302	-2.27185	-2.69633	H	2.56733	-2.75741	0.01311

Table AI.2 (Continued).

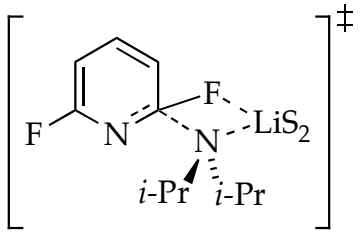

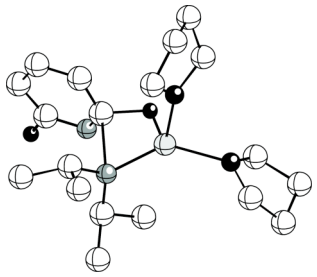

12a
G = -1210.615041
G_{MP2} = -1206.724820
(0 °C)
S = THF

Atom	X	Y	Z	Atom	X	Y	Z
Li	0.62316	-0.03746	-0.19172	H	-3.54524	0.92692	2.57567
F	-0.44404	-0.02320	-1.78568	H	-3.74041	0.01897	1.07021
C	-1.78168	0.14053	-1.28704	H	-1.63404	1.32918	1.18581
C	-2.16585	1.50060	-1.14645	H	0.42462	-2.79298	-0.04877
C	-3.50961	1.79663	-1.28883	H	-0.98146	-3.85716	-0.22715
C	-4.42862	0.78862	-1.62347	H	-0.82481	-2.44134	-1.27366
C	-3.88414	-0.47207	-1.84026	H	-1.77445	-2.20720	2.96025
N	-2.61288	-0.79610	-1.74231	H	-1.43981	-3.71412	2.10735
F	-4.70611	-1.46417	-2.23724	H	-0.12081	-2.57293	2.44547
N	-1.02509	-0.56926	0.70495	H	-2.49054	-2.09783	0.55005
C	-1.41571	-1.97992	0.78431	H	-5.48692	0.97178	-1.75965
C	-0.65345	-2.81099	-0.26197	H	-3.85466	2.81964	-1.15958
C	-1.17816	-2.64885	2.15865	H	-1.42487	2.25658	-0.91568
C	-1.65564	0.33742	1.66837	H	1.31914	1.95054	-2.17922
C	-0.85021	0.52018	2.97780	H	2.93348	2.05820	-1.42961
C	-3.14725	0.09091	1.98639	H	2.51555	4.42278	-1.83570
O	1.33405	1.85345	-0.11842	H	0.77446	4.22874	-1.56265
C	1.88668	2.37816	-1.34853	H	1.51959	5.06669	0.62688
C	1.76693	3.89820	-1.23471	H	2.99637	4.08995	0.55059
C	1.93506	4.11725	0.27683	H	1.61768	2.55684	1.80805
C	1.19820	2.90924	0.86162	H	0.13086	3.11259	1.00894
O	2.32190	-0.95443	-0.71683	H	2.55931	-0.89253	-2.77176
C	2.51624	-1.64330	-1.97738	H	1.65235	-2.29343	-2.15292
C	3.81168	-2.44137	-1.81389	H	3.82942	-3.33646	-2.44233
C	3.80896	-2.75630	-0.30948	H	4.68047	-1.82520	-2.07438
C	3.23008	-1.47053	0.28333	H	4.80129	-2.98901	0.08784
H	0.20163	0.73492	2.75331	H	3.14767	-3.60411	-0.09838
H	-1.25095	1.35811	3.56631	H	2.66475	-1.62781	1.20688
H	-0.87353	-0.37044	3.61298	H	4.01081	-0.72104	0.46871
H	-3.31152	-0.82205	2.56811				

Table AI.2 (Continued).

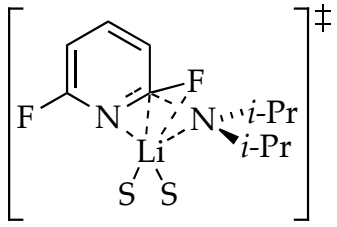

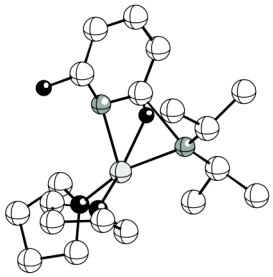

12b
G = -1210.614205
G_{MP2} = -1206.723027
(0 °C)
S = THF

Atom	X	Y	Z	Atom	X	Y	Z
Li	-0.54566	0.18282	-0.31459	H	-1.25576	4.92817	0.46980
N	0.58284	-1.39503	0.19460	H	0.38781	5.00524	1.13952
C	0.24846	-2.69567	-0.41285	H	-1.18220	2.82565	1.72729
C	-0.31398	-2.56755	-1.83989	H	0.53966	2.58437	1.29787
C	1.36066	-3.77448	-0.41990	H	-2.36698	-1.71420	1.01355
C	0.96010	-1.56029	1.60882	H	-3.26214	-2.17012	-0.45613
C	0.37717	-0.42600	2.47380	H	-5.11662	-1.65696	1.07168
C	2.47187	-1.68681	1.91857	H	-4.21815	-0.30201	1.78496
F	0.78698	0.07318	-1.85797	H	-5.56891	0.86991	0.10364
C	1.91356	-0.06880	-1.01324	H	-5.39965	-0.47002	-1.03875
N	2.07500	1.01825	-0.24945	H	-3.56131	0.77712	-1.88342
C	3.29865	1.30760	0.14408	H	-3.33278	1.66347	-0.35860
C	4.45584	0.64549	-0.22768	H	-0.71500	-0.37130	2.36780
C	4.27457	-0.42046	-1.13217	H	0.60120	-0.57604	3.53836
C	3.01239	-0.77407	-1.56563	H	0.80024	0.54037	2.18027
F	3.39020	2.39057	0.95137	H	3.00094	-0.74823	1.73116
O	-2.51664	-0.22384	-0.38945	H	2.62127	-1.94426	2.97619
C	-3.09205	-1.36787	0.27522	H	2.95174	-2.46023	1.31505
C	-4.40582	-0.85360	0.85619	H	0.49683	-2.49487	1.97910
C	-4.88374	0.09618	-0.25509	H	0.45143	-2.26369	-2.56052
C	-3.56840	0.68762	-0.79115	H	-0.70972	-3.53689	-2.16756
O	-0.83268	2.24020	-0.22134	H	-1.12794	-1.83691	-1.89092
C	-0.42176	2.97956	0.95584	H	1.67026	-4.04758	0.59301
C	-0.27990	4.42755	0.49347	H	0.99797	-4.69005	-0.90599
C	0.27084	4.23313	-0.92707	H	2.24825	-3.43287	-0.96260
C	-0.50452	3.00517	-1.41173	H	-0.57289	-3.14203	0.18961
H	0.07512	2.36665	-2.08083	H	2.84674	-1.57355	-2.27640
H	-1.44642	3.28489	-1.90212	H	5.14128	-0.95986	-1.50533
H	1.34076	4.00643	-0.88225	H	5.42755	0.96508	0.12622
H	0.12345	5.10147	-1.57640				

Table AI.2 (Continued).

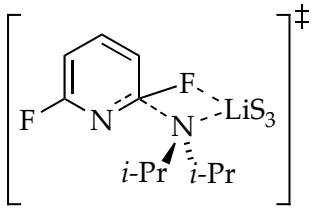

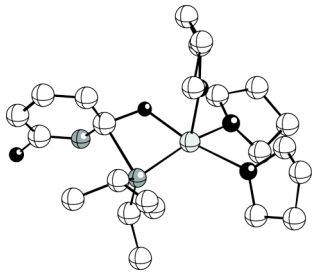

8a
G = -1442.960433
G_{MP2} = -1438.301908
(0 °C)
S = THF

Atom	X	Y	Z	Atom	X	Y	Z
Li	0.25361	0.29434	0.00257	H	5.05568	-2.00998	-0.21087
N	-1.34269	-0.52402	-0.93382	H	3.47318	-2.77878	0.02420
C	-1.75625	0.01882	-2.22791	H	3.61030	-2.89682	-2.39688
C	-1.15416	1.42090	-2.42093	H	4.51535	-1.38282	-2.48681
C	-1.36961	-0.81552	-3.47447	H	2.45154	-0.29888	-2.81460
C	-1.79820	-1.87847	-0.61952	H	1.51958	-1.71153	-2.27944
C	-0.79158	-2.99073	-1.00551	H	0.20400	-2.75372	-0.61284
C	-3.22085	-2.27178	-1.08128	H	-1.09927	-3.96144	-0.58917
F	-1.27872	1.42974	0.83273	H	-0.70299	-3.11155	-2.09045
C	-2.50359	0.77143	0.60512	H	-3.29548	-2.40531	-2.16540
C	-2.91237	-0.08697	1.65676	H	-3.51316	-3.22312	-0.61790
C	-4.26970	-0.31258	1.80166	H	-3.95636	-1.51935	-0.78425
C	-5.19015	0.33912	0.96547	H	-1.84636	-1.92220	0.48267
C	-4.64356	1.22968	0.04782	H	-0.05881	1.35653	-2.49284
N	-3.36533	1.49897	-0.10626	H	-1.52067	1.87404	-3.35062
F	-5.48421	1.93559	-0.73538	H	-1.41835	2.08468	-1.59677
O	2.16719	-0.49895	-0.75999	H	-1.81246	-1.81421	-3.47928
O	0.74612	-0.44455	1.96516	H	-1.70787	-0.30509	-4.38658
O	1.32217	2.28365	0.04511	H	-0.28026	-0.93107	-3.54102
C	2.14315	2.74203	-1.03669	H	-2.85583	0.14770	-2.26729
C	2.91188	3.94125	-0.46471	H	-0.04266	1.16639	2.98765
C	1.93220	4.51592	0.59458	H	1.70486	0.90107	3.21931
C	0.78794	3.47919	0.64079	H	0.89732	-0.14181	5.25388
C	0.72809	0.40672	3.13419	H	-0.62069	-0.63212	4.48327
C	0.45806	-0.51765	4.32499	H	0.66865	-2.71951	4.36790
C	1.07209	-1.84380	3.85084	H	2.15948	-1.83529	3.99380
C	0.72526	-1.83355	2.36119	H	1.44092	-2.37550	1.73628
C	2.39036	-1.09246	-2.05964	H	-0.27516	-2.24189	2.17386
C	3.70492	-1.89864	-1.95996	H	-6.26173	0.20637	1.04524
C	3.98959	-1.93430	-0.44672	H	-4.62750	-0.98530	2.57733
C	3.36684	-0.61848	0.01506	H	-2.17551	-0.55341	2.29850
H	3.07450	-0.58651	1.06553	H	2.76764	1.90612	-1.35201
H	4.04089	0.22885	-0.19082	H	1.50355	3.04673	-1.87838
H	3.84076	3.60772	0.00908	H	3.17488	4.66735	-1.23982
H	1.55461	5.50453	0.31680	H	-0.08188	3.81338	0.06101
H	2.42148	4.61374	1.56831	H	0.45534	3.22711	1.64815

Table AI.3. Optimized geometries of reactants and monomer-based transition structures at B3LYP level of theory with 6-31+G(d) basis set for the nucleophilic substitution of 2,6-difluoropyridine with free energies (Hartrees), and cartesian coordinates (X,Y,Z).

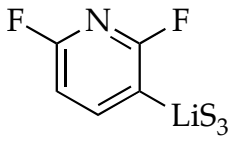

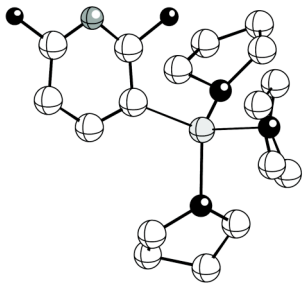

G = -1150.797843
(0 °C)
S = THF

Atom	X	Y	Z	Atom	X	Y	Z
Li	0.02911	-0.14039	-0.05877	H	2.18286	-1.17073	2.47038
O	-1.37324	-0.92242	1.18009	H	-3.16104	-1.56802	0.34096
C	-1.08929	-1.05151	2.59156	H	-2.94016	0.19625	0.44643
C	-2.26573	-0.37706	3.29362	H	-4.28145	-0.05666	2.44237
C	-3.44055	-0.75404	2.37376	H	-3.81386	-1.75374	2.62619
C	-2.79855	-0.75144	0.97608	H	-2.39745	-0.72466	4.32330
C	1.98202	0.09146	0.71235	H	-2.12177	0.70998	3.31556
C	2.68876	-0.47173	1.79989	H	-0.12024	-0.58131	2.77040
C	4.03629	-0.19205	2.08423	H	-1.02606	-2.11901	2.84884
C	4.66799	0.69170	1.22160	H	-0.92949	-2.84696	-0.62284
N	4.10064	1.26291	0.17995	H	-1.15336	-2.96866	-2.39018
C	2.82844	0.93326	-0.00485	H	1.23687	-3.87019	-0.77786
F	2.30015	1.56322	-1.13175	H	0.74333	-4.37090	-2.39908
F	5.97389	1.01381	1.43678	H	2.39147	-2.84030	-3.22941
O	-0.91366	1.59082	-0.60303	H	2.62050	-2.18045	-1.59994
C	-0.60223	2.77977	0.14966	H	0.55124	-1.33178	-3.67948
C	-1.47611	3.87022	-0.48187	H	1.47381	-0.29571	-2.54718
C	-1.58823	3.42821	-1.96701	H	0.02181	1.99991	-2.40786
C	-0.98944	2.00280	-1.98241	H	-1.60160	1.26371	-2.50424
O	-0.09341	-1.32455	-1.70609	H	-1.02695	4.09071	-2.63337
C	-0.44080	-2.71664	-1.59060	H	-2.63029	3.43057	-2.30196
C	0.87997	-3.50346	-1.74478	H	-2.46431	3.88767	-0.00939
C	1.87052	-2.46639	-2.34213	H	-1.03323	4.86469	-0.36857
C	0.98017	-1.26075	-2.66780	H	0.46777	2.99967	0.04851
H	4.57085	-0.62979	2.92155	H	-0.82598	2.56996	1.19840

Table AI.3 (Continued).

i-Pr_2NH 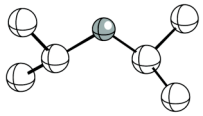 *G* = -292.261790 (0 °C)

Atom	X	Y	Z	Atom	X	Y	Z
C	1.25205	-0.10825	0.19533	H	-2.00776	1.06652	-1.82798
N	0.01598	-0.15608	-0.60098	H	-1.06959	1.26476	0.45157
C	-1.24103	0.26150	0.04114	H	-0.10634	-1.09537	-0.97955
C	-1.70735	-0.65538	1.18950	H	0.96873	1.94424	0.92274
C	-2.32344	0.37624	-1.03901	H	2.63924	1.37196	0.98027
C	1.71423	1.34213	0.39131	H	1.90110	1.81419	-0.58069
C	2.32837	-0.92485	-0.52887	H	2.50240	-0.52193	-1.53419
H	-0.94806	-0.74952	1.97402	H	3.27451	-0.89820	0.02353
H	-2.61983	-0.26482	1.65780	H	2.03132	-1.97740	-0.62896
H	-1.93021	-1.66321	0.81217	H	1.11099	-0.55702	1.19680
H	-2.51569	-0.60203	-1.50187				
H	-3.26961	0.73254	-0.61409				

 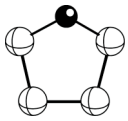 *G* = -232.367778 (0 °C)

Atom	X	Y	Z	Atom	X	Y	Z
C	-0.77749	0.78984	-0.12470	H	1.99931	-1.03598	-0.49993
C	-1.13763	-0.69731	0.08036	H	1.32321	-0.91394	1.14655
O	-0.00025	-1.43373	-0.36726	H	1.16584	1.15203	-1.08284
C	1.13720	-0.69784	0.08098	H	1.19941	1.42106	0.66359
C	0.77808	0.78927	-0.12552	H	-1.16605	1.15436	-1.08102
H	-1.99940	-1.03451	-0.50161	H	-1.19740	1.42083	0.66581
H	-1.32482	-0.91407	1.14559				

Table AI.3 (Continued).

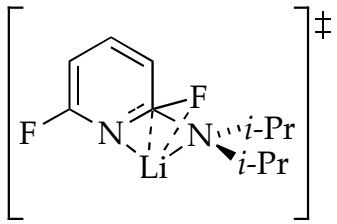

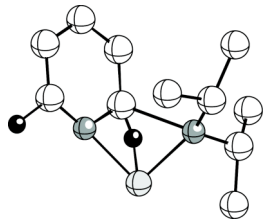

11a
G = -745.919026
(0 °C)

Atom	X	Y	Z	Atom	X	Y	Z
C	-2.03433	-0.46884	-0.35232	H	-1.72686	1.97619	1.02016
N	-0.63697	-0.08375	-0.65702	H	-0.56998	3.20636	0.50819
C	-0.47008	1.38220	-0.68582	H	1.08749	1.32035	-2.23283
C	-0.70860	2.12613	0.64803	H	1.71722	1.58041	-0.59242
C	0.88670	1.80695	-1.26795	H	0.89385	2.88932	-1.44375
Li	0.29894	-1.18252	-1.89023	H	-1.23337	1.76869	-1.38960
C	0.93722	-1.18088	0.32901	H	4.51611	0.19769	0.73450
F	0.10614	-2.30237	0.32925	H	2.91219	0.22198	2.70332
N	1.82866	-1.25674	-0.69637	H	0.60940	-0.70841	2.42311
C	3.03185	-0.73811	-0.50959	H	-1.98507	-0.05570	1.80679
C	3.50525	-0.18267	0.66106	H	-3.43766	-0.90654	1.26060
C	2.59419	-0.17526	1.74260	H	-1.90244	-1.77886	1.40611
C	1.31774	-0.68016	1.60416	H	-1.90696	-2.52846	-1.09457
F	3.83919	-0.78860	-1.59762	H	-3.54626	-1.87608	-1.09910
C	-2.35149	-0.82369	1.11963	H	-2.39916	-1.32957	-2.32971
C	-2.49366	-1.61752	-1.27241	H	-2.67245	0.39596	-0.60491
H	-0.00679	1.79250	1.41971				

Table AI.3 (Continued).

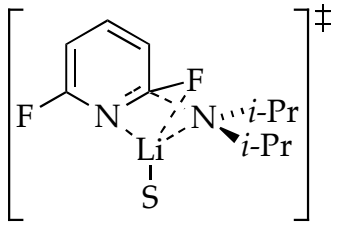

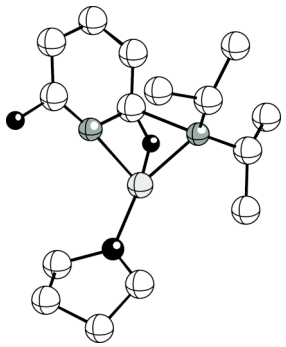

10a
G = -978.299402
(0 °C)
S = THF

Atom	X	Y	Z	Atom	X	Y	Z
C	1.36379	-2.13000	-0.36441	H	3.06652	-0.56641	2.96193
N	1.01228	-0.78889	0.14485	H	-0.28422	0.71669	2.00344
C	1.38959	-0.63426	1.55894	H	1.27345	1.54684	1.80400
C	2.90196	-0.69663	1.88348	H	0.94360	0.62402	3.27253
C	0.79675	0.63823	2.18552	H	0.93056	-1.48168	2.11042
Li	-0.66992	0.00986	-0.42002	H	1.81980	4.48582	0.25590
N	0.34861	1.68215	-0.91678	H	3.88535	3.14968	-0.38346
C	1.44627	0.93486	-1.18803	H	3.60875	0.85889	-1.35065
F	1.23033	0.09420	-2.26428	H	-2.79159	2.02056	-0.70953
C	2.75870	1.45772	-1.04691	H	-3.50434	0.95089	-1.94721
C	2.89359	2.72438	-0.51557	H	-4.60235	1.55473	0.85394
C	1.75815	3.48667	-0.15651	H	-5.50955	1.49827	-0.67019
C	0.54144	2.87924	-0.39290	H	-5.26632	-0.93776	-0.81490
F	-0.60364	3.54731	-0.08118	H	-5.53728	-0.72126	0.92371
O	-2.57702	-0.00349	-0.34907	H	-3.22329	-1.94756	-0.03104
C	-3.43243	-0.94454	0.35254	H	-3.17272	-0.90926	1.41748
C	-4.86700	-0.47360	0.09483	H	3.53175	-1.80649	-0.56733
C	-4.68790	1.04027	-0.11079	H	2.94941	-3.30907	-1.30090
C	-3.36412	1.10456	-0.86950	H	2.65398	-1.75748	-2.10409
C	2.70545	-2.25134	-1.12915	H	0.05987	-2.08525	-2.12484
C	0.22903	-2.70506	-1.23556	H	0.46623	-3.71934	-1.58375
H	3.45111	0.09293	1.35869	H	-0.70788	-2.76234	-0.66455
H	3.33684	-1.66137	1.60381	H	1.44840	-2.80565	0.50710

Table AI.3 (Continued).

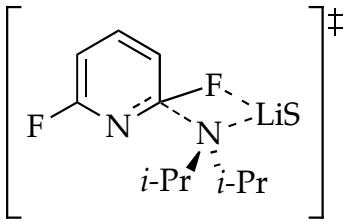

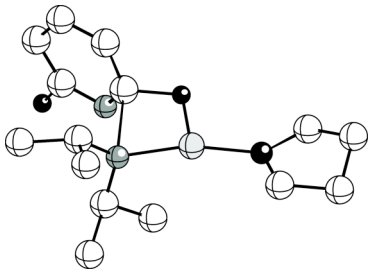

10b
G = -978.296603
(0 °C)
S = THF

Atom	X	Y	Z	Atom	X	Y	Z
C	-1.05833	1.02392	1.38255	H	-1.30664	-1.63332	-2.33582
N	-0.72859	0.57733	0.02178	H	3.52868	1.05857	0.43294
C	-1.30377	1.32751	-1.09865	H	3.76755	0.53343	-1.25456
C	-2.76111	1.81147	-0.93419	H	5.93500	-0.08535	-0.34576
C	-0.39447	2.47001	-1.60939	H	5.24396	-0.44142	1.24828
Li	0.84723	-0.46368	0.05909	H	5.40454	-2.69127	0.27498
F	-0.23540	-1.97284	0.04975	H	4.90630	-2.09409	-1.31935
C	-1.57645	-1.43559	-0.17683	H	2.74026	-2.80932	-0.49153
C	-2.01512	-1.62651	-1.51514	H	3.16910	-2.39751	1.18940
C	-3.37423	-1.80049	-1.71418	H	0.62156	2.09553	-1.78993
C	-4.25766	-1.84501	-0.62041	H	-0.77911	2.87069	-2.55830
C	-3.65839	-1.76387	0.62997	H	-0.32194	3.30187	-0.90166
N	-2.37446	-1.62564	0.87318	H	-2.86496	2.61915	-0.20195
F	-4.44604	-1.87993	1.73132	H	-3.13388	2.19329	-1.89349
O	2.71845	-0.78721	-0.04450	H	-3.41852	0.99167	-0.62792
C	3.76798	0.20528	-0.20788	H	-1.33949	0.60852	-1.93228
C	5.06692	-0.50909	0.16831	H	0.81233	0.35553	2.30554
C	4.77089	-1.96227	-0.23917	H	-0.53937	0.48029	3.43083
C	3.29702	-2.11079	0.13857	H	-0.48488	-0.88414	2.31675
C	-0.74745	2.50927	1.68190	H	-1.32695	3.20412	1.07055
C	-0.27325	0.18305	2.40949	H	-0.97859	2.72871	2.73296
H	-5.32578	-1.98959	-0.72569	H	0.31775	2.72257	1.51874
H	-3.75965	-1.92387	-2.72353	H	-2.13105	0.86104	1.59525

Table AI.3 (Continued).

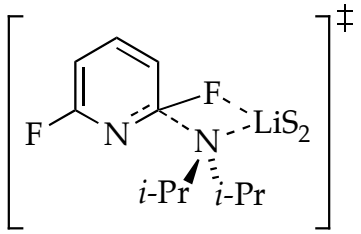

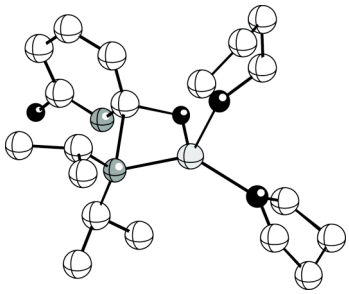

12a
G = -1210.657993
(0 °C)
S = THF

Atom	X	Y	Z	Atom	X	Y	Z
Li	0.58190	-0.09018	-0.18342	H	-3.39201	-0.52268	2.60350
F	-0.50087	-0.09001	-1.79335	H	-3.53273	1.23383	2.49902
C	-1.83432	0.13674	-1.30898	H	-3.77902	0.24277	1.05486
C	-2.18335	1.51222	-1.24011	H	-1.59642	1.45182	1.10675
C	-3.51897	1.83692	-1.40533	H	0.26265	-2.84578	0.13939
C	-4.46651	0.83639	-1.68766	H	-1.20257	-3.83122	-0.02480
C	-3.95048	-0.44563	-1.83408	H	-0.93326	-2.48641	-1.13709
N	-2.69189	-0.80079	-1.71511	H	-1.93858	-1.98443	3.06627
F	-4.80404	-1.44543	-2.18096	H	-1.63468	-3.54164	2.29651
N	-1.09346	-0.49813	0.72305	H	-0.28739	-2.42038	2.59323
C	-1.54522	-1.88421	0.88276	H	-2.62344	-1.96842	0.64695
C	-0.80928	-2.80960	-0.10233	H	-5.51977	1.04078	-1.83562
C	-1.34355	-2.48229	2.29721	H	-3.83615	2.87473	-1.33311
C	-1.67591	0.48860	1.63810	H	-1.42338	2.26277	-1.05602
C	-0.86762	0.69435	2.94499	H	1.37146	1.85916	-2.24283
C	-3.17984	0.34156	1.96481	H	2.99644	1.79324	-1.50926
O	1.40016	1.76119	-0.18044	H	2.82860	4.19023	-1.91728
C	1.99055	2.22504	-1.41918	H	1.07998	4.18529	-1.61942
C	2.03575	3.74908	-1.30491	H	1.93732	4.93640	0.55934
C	2.25035	3.94955	0.20432	H	3.30874	3.81756	0.46067
C	1.40619	2.82230	0.80669	H	1.81345	2.42007	1.73895
O	2.21869	-1.11900	-0.69234	H	0.36945	3.13275	0.98445
C	2.37457	-1.88439	-1.91453	H	2.27054	-1.19425	-2.75651
C	3.75288	-2.53847	-1.80952	H	1.56979	-2.62677	-1.96554
C	3.88451	-2.76892	-0.29450	H	3.81900	-3.46215	-2.39281
C	3.20811	-1.52258	0.28449	H	4.53390	-1.85446	-2.16410
H	0.20178	0.79676	2.72423	H	4.92172	-2.87160	0.03982
H	-1.19845	1.60814	3.46090	H	3.33997	-3.67280	0.00273
H	-0.97974	-0.13891	3.64594	H	2.69707	-1.70427	1.23544
H	3.91736	-0.69445	0.41578				

Table AI.3 (Continued).

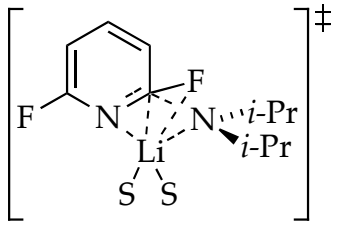

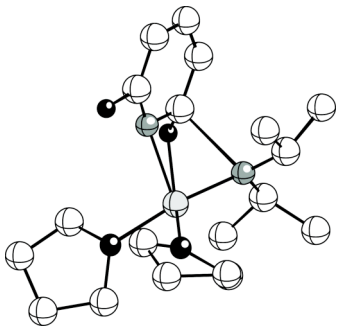

12b
G = -1210.655548
(0 °C)
S = THF

Atom	X	Y	Z	Atom	X	Y	Z
C	1.56317	-0.38561	2.28872	H	2.68721	2.62667	-1.01032
N	1.45858	0.03059	0.87228	H	2.51241	0.98590	-1.63369
C	2.34820	1.15950	0.55365	H	2.07481	2.00876	1.20771
C	3.86350	0.91988	0.78193	H	2.51192	-0.89100	-4.31773
C	2.14193	1.68284	-0.87748	H	4.38521	-1.67226	-2.78347
Li	-0.33984	-0.22385	-0.02844	H	3.85892	-2.19694	-0.39292
N	0.76446	-1.32206	-1.45781	H	-2.93749	-1.43709	2.02651
C	1.76985	-1.66231	-0.61472	H	-3.35186	-0.11180	0.90777
F	1.38625	-2.55730	0.36018	H	-4.83501	-2.55946	1.18110
C	3.10251	-1.83266	-1.07813	H	-4.94364	-1.51309	-0.23561
C	3.37442	-1.55006	-2.40186	H	-3.64751	-2.96622	-1.53272
C	2.34863	-1.12095	-3.27236	H	-3.74541	-4.15914	-0.23092
C	1.09150	-1.03698	-2.70265	H	-1.66305	-3.41514	0.74923
F	0.04712	-0.63200	-3.48168	H	-1.29410	-2.99744	-0.94473
O	-1.96946	-1.43724	0.19263	H	-1.43463	1.45339	-2.50397
C	-1.99732	-2.83993	-0.12707	H	-2.93096	0.85301	-1.75460
C	-3.46682	-3.12661	-0.46486	H	-2.74865	3.48850	-2.64805
C	-4.24908	-2.08711	0.38593	H	-3.67209	3.08339	-1.19007
C	-3.14395	-1.18206	0.97674	H	-2.03444	4.67121	-0.28658
O	-1.44188	1.41815	-0.43055	H	-0.74822	4.01290	-1.31757
C	-1.33452	2.67181	0.28409	H	-0.32891	2.72821	0.70770
C	-1.64870	3.75596	-0.74701	H	-2.06629	2.67193	1.10456
C	-2.67572	3.04927	-1.64812	H	0.85961	1.47618	3.21219
C	-2.14549	1.61195	-1.68515	H	1.67394	0.36592	4.32913
C	1.69923	0.77360	3.31039	H	2.62799	1.34233	3.21156
C	0.32608	-1.19244	2.72863	H	0.11943	-2.03372	2.06722
H	4.27444	0.23594	0.03371	H	0.47157	-1.58981	3.74207
H	4.41372	1.86823	0.70598	H	-0.56126	-0.54302	2.75465
H	4.07207	0.49589	1.76970	H	2.44491	-1.04030	2.43874
H	1.08267	1.87374	-1.08393				

Table AI.3 (Continued).

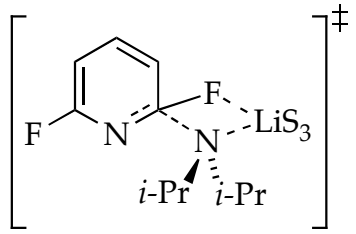

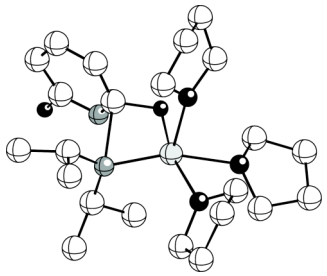

8a
G = -1443.002678
(0 °C)
S = THF

Atom	X	Y	Z	Atom	X	Y	Z
Li	0.25361	0.29434	0.00257	H	4.51535	-1.38282	-2.48681
N	-1.34269	-0.52402	-0.93382	H	2.45154	-0.29888	-2.81460
C	-1.75625	0.01882	-2.22791	H	1.51958	-1.71153	-2.27944
C	-1.15416	1.42090	-2.42093	H	0.20400	-2.75372	-0.61284
C	-1.36961	-0.81552	-3.47447	H	-1.09927	-3.96144	-0.58917
C	-1.79820	-1.87847	-0.61952	H	-0.70299	-3.11155	-2.09045
C	-0.79158	-2.99073	-1.00551	H	-3.29548	-2.40531	-2.16540
C	-3.22085	-2.27178	-1.08128	H	-3.51316	-3.22312	-0.61790
F	-1.27872	1.42974	0.83273	H	-3.95636	-1.51935	-0.78425
C	-2.50359	0.77143	0.60512	H	-1.84636	-1.92220	0.48267
C	-2.91237	-0.08697	1.65676	H	-0.05881	1.35653	-2.49284
C	-4.26970	-0.31258	1.80166	H	-1.52067	1.87404	-3.35062
C	-5.19015	0.33912	0.96547	H	-1.41835	2.08468	-1.59677
C	-4.64356	1.22968	0.04782	H	-1.81246	-1.81421	-3.47928
N	-3.36533	1.49897	-0.10626	H	-1.70787	-0.30509	-4.38658
F	-5.48421	1.93559	-0.73538	H	-0.28026	-0.93107	-3.54102
O	2.16719	-0.49895	-0.75999	H	-2.85583	0.14770	-2.26729
O	0.74612	-0.44455	1.96516	H	-0.04266	1.16639	2.98765
O	1.32217	2.28365	0.04511	H	1.70486	0.90107	3.21931
C	2.14315	2.74203	-1.03669	H	0.89732	-0.14181	5.25388
C	2.91188	3.94125	-0.46471	H	-0.62069	-0.63212	4.48327
C	1.93220	4.51592	0.59458	H	0.66865	-2.71952	4.36790
C	0.78794	3.47919	0.64079	H	2.15948	-1.83529	3.99380
C	0.72809	0.40672	3.13419	H	1.44092	-2.37550	1.73628
C	0.45806	-0.51766	4.32499	H	-0.27516	-2.24189	2.17386
C	1.07209	-1.84381	3.85084	H	-6.26173	0.20637	1.04524
C	0.72526	-1.83355	2.36119	H	-4.62750	-0.98530	2.57733
C	2.39036	-1.09246	-2.05964	H	-2.17551	-0.55341	2.29850
C	3.70492	-1.89864	-1.95996	H	2.76764	1.90612	-1.35201
C	3.98959	-1.93430	-0.44672	H	1.50355	3.04673	-1.87838
C	3.36684	-0.61848	0.01506	H	3.84076	3.60772	0.00908
H	3.07450	-0.58651	1.06553	H	3.17488	4.66735	-1.23982
H	4.04089	0.22885	-0.19082	H	1.55461	5.50453	0.31680
H	5.05568	-2.00998	-0.21087	H	2.42148	4.61374	1.56831
H	3.47318	-2.77878	0.02420	H	-0.08188	3.81338	0.06101
H	3.61030	-2.89682	-2.39688	H	0.45534	3.22711	1.64815

Table AI.4. Optimized geometries at B3LYP level of theory with 6-31G(d) basis set for the solvation of LDA monomer with free energies (Hartrees), and cartesian coordinates (X,Y,Z). (Note: G_{MP2} includes single point MP2 corrections to B3LYP/6-31G(d) optimized structures)

i-$Pr_2NLi \bullet S_2$

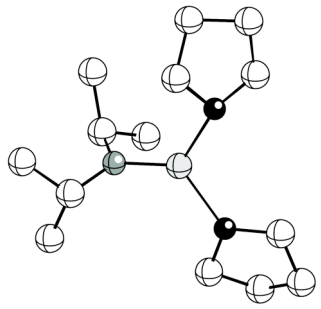

G = -763.921827
G_{MP2} = -761.242814
(0 °C)
S = THF

Atom	X	Y	Z	Atom	X	Y	Z
C	0.53584	-2.31846	-1.11557	H	-2.34804	-1.31446	0.22222
N	0.54228	-1.32502	-0.04871	H	-3.40247	-1.03144	-1.19260
C	1.23590	-1.71823	1.16664	H	-0.18239	3.68916	0.46720
C	2.65946	-1.11706	1.29862	H	0.75791	2.52348	1.43574
C	0.41645	-1.31502	2.40970	H	1.82060	4.64663	-0.49727
Li	-0.28135	0.31461	-0.36284	H	2.45225	4.22679	1.10609
O	-2.20978	0.56437	-0.57645	H	3.31466	2.07890	0.28078
C	-3.01619	-0.59767	-0.25994	H	3.67824	3.14913	-1.08653
C	-4.14305	-0.05168	0.61037	H	2.06743	0.89858	-1.39927
C	-4.41849	1.30833	-0.05429	H	1.71145	2.40651	-2.30325
C	-3.01785	1.76028	-0.50223	H	2.59834	-0.01980	1.34288
O	0.58515	2.08541	-0.58902	H	3.17692	-1.46017	2.20752
C	1.84656	1.96591	-1.30764	H	3.27774	-1.37958	0.43458
C	2.87076	2.73693	-0.47431	H	-0.55856	-1.81522	2.40479
C	2.00615	3.81693	0.19501	H	0.92795	-1.55505	3.35263
C	0.70989	3.05516	0.47581	H	0.23397	-0.22827	2.40357
C	1.92773	-2.71287	-1.67360	H	1.36333	-2.81540	1.22780
C	-0.25703	-3.61264	-0.79002	H	-1.28169	-3.36672	-0.48788
H	-3.01951	2.25151	-1.48109	H	-0.30743	-4.28879	-1.65526
H	-2.55232	2.43651	0.22440	H	0.20519	-4.17195	0.03271
H	-4.89142	2.03155	0.61671	H	2.52640	-3.23743	-0.91803
H	-5.07438	1.17812	-0.92251	H	1.84331	-3.37850	-2.54454
H	-5.01925	-0.70655	0.62649	H	2.48421	-1.81790	-1.97729
H	-3.79498	0.08189	1.64150	H	0.00011	-1.85081	-1.96365

Table AI.4 (Continued).

i-$Pr_2NLi \cdot S_3$

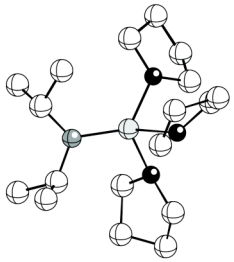

G = -996.270707
G_{MP2} = -992.824425
(0 °C)
S = THF

Atom	X	Y	Z	Atom	X	Y	Z
Li	0.19850	0.00829	-0.10075	H	-0.28373	-3.24415	2.81719
N	-1.35509	-0.69168	0.79093	H	-0.53892	-3.30828	1.05717
C	-2.66311	-0.29169	0.28843	H	-1.95141	0.03676	3.42365
C	-3.52636	-1.45068	-0.28560	H	-1.26053	-1.40749	4.19145
C	-3.55264	0.53438	1.25753	H	-0.21480	-0.26283	3.32163
C	-1.39567	-1.52589	1.98122	H	-2.36776	-2.04681	2.08229
C	-0.33161	-2.63946	1.90048	H	-1.22387	1.08943	-2.63241
C	-1.19919	-0.74928	3.31083	H	0.33930	1.81160	-3.08011
O	-0.09301	1.83406	-1.05923	H	-0.50845	4.06479	-2.77778
C	-0.73055	2.86302	-0.26371	H	-1.99215	3.27950	-3.34924
C	-1.82521	3.45978	-1.15078	H	-2.75184	2.88566	-1.04501
C	-1.23608	3.27393	-2.55827	H	-2.03934	4.50423	-0.90461
C	-0.53529	1.91926	-2.43190	H	0.02651	3.61459	0.00098
O	0.89142	-1.08095	-1.74852	H	-1.10640	2.39148	0.64756
C	0.01344	-2.19728	-2.04284	H	2.29032	2.07277	-0.60030
C	0.90948	-3.43222	-1.99998	H	3.68297	0.95952	-0.54752
C	2.23425	-2.88226	-2.55212	H	4.51968	2.73575	0.89431
C	2.26555	-1.46149	-1.97278	H	2.90228	3.04721	1.55631
O	2.08314	0.49953	0.70192	H	3.85735	1.56613	3.27624
C	2.47985	0.34053	2.08602	H	4.64485	0.56870	2.04168
C	3.75563	1.17172	2.26090	H	2.62215	-0.72532	2.28773
C	3.57903	2.26393	1.19451	H	1.66435	0.70531	2.71896
C	2.92585	1.47827	0.05854	H	2.72795	-0.73446	-2.65067
H	-2.99748	1.38957	1.66150	H	2.78922	-1.42250	-1.01080
H	-4.45465	0.91410	0.75511	H	2.20554	-2.85085	-3.64786
H	-3.88833	-0.07204	2.10816	H	3.10841	-3.47046	-2.25560
H	-3.77502	-2.18785	0.48794	H	1.03286	-3.77096	-0.96478
H	-4.47612	-1.08559	-0.70283	H	0.50915	-4.26376	-2.58806
H	-2.98767	-1.97653	-1.08213	H	-0.77103	-2.17368	-1.28142
H	-2.46686	0.37551	-0.57075	H	-0.42257	-2.05276	-3.04213
H	0.66375	-2.20011	1.73936				

Table AI.5. Optimized geometries at B3LYP level of theory with 6-31G(d) basis set from the IRC calculations on monosolvated (**10a**) and trisolvated (**8**) monomeric transition structures with free energies (Hartrees), and cartesian coordinates (X,Y,Z).

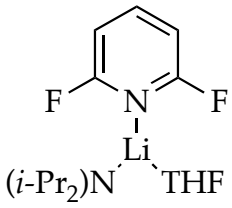

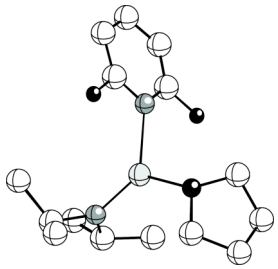

13
G = -978.284647
(0 °C)
S = THF

Atom	X	Y	Z	Atom	X	Y	Z
C	0.46810	2.65236	-0.65972	H	0.12577	2.71721	3.40233
N	0.50805	1.46642	0.18083	H	1.98400	-0.11029	1.79790
C	0.85628	1.74230	1.55917	H	0.28299	-0.22472	2.31387
C	-0.20750	2.52448	2.37165	H	1.46259	0.60425	3.33854
C	1.16824	0.42939	2.29603	H	1.78245	2.35995	1.61554
Li	0.01022	-0.24489	-0.35959	H	-4.24142	-2.24612	1.87631
O	1.14670	-1.71325	-0.98863	H	-5.80638	-1.36277	0.09788
C	2.52199	-1.32654	-1.27226	H	-4.81273	-0.27914	-1.95871
C	3.41720	-2.41814	-0.65169	H	0.24864	-3.13951	0.18013
C	2.45941	-3.18842	0.27621	H	1.04730	-3.77378	-1.28529
C	1.12939	-3.05116	-0.46006	H	2.39306	-2.70075	1.25482
N	-1.97522	-1.04553	-0.31005	H	2.75473	-4.23104	0.42853
C	-2.81414	-0.59985	-1.23435	H	3.81060	-3.08243	-1.42915
F	-2.23298	-0.03636	-2.29815	H	4.27008	-1.99221	-0.11570
C	-4.19780	-0.67534	-1.16023	H	2.64547	-1.25069	-2.35794
C	-4.73066	-1.27645	-0.01822	H	2.65743	-0.33694	-0.82766
C	-3.87984	-1.76951	0.97361	H	-1.53709	3.32194	-0.07182
C	-2.51867	-1.61813	0.75320	H	-0.96579	4.06678	-1.58212
F	-1.64277	-2.07090	1.66198	H	-1.49822	2.37260	-1.56472
C	-0.96561	3.14063	-0.98765	H	0.78308	1.55663	-2.52056
C	1.22318	2.41034	-1.98335	H	1.18262	3.27878	-2.65607
H	-1.14756	1.95646	2.41098	H	2.27523	2.17423	-1.78650
H	-0.42302	3.49352	1.90910	H	0.98263	3.49657	-0.15839

Table AI.5 (Continued).

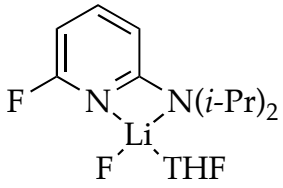

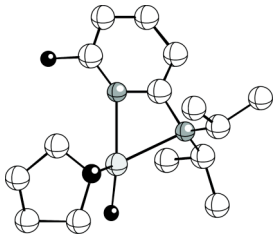

14
G = -978.347810
(0 °C)
S = THF

Atom	X	Y	Z	Atom	X	Y	Z
C	2.05838	-1.42304	-0.97928	H	2.88826	-1.42516	3.01965
N	1.34502	-0.55233	0.01931	H	-0.52710	-0.25149	2.00402
C	1.51205	0.85160	-0.17817	H	0.79129	0.85859	2.43656
C	2.74014	1.52080	-0.22599	H	0.54307	-0.62107	3.36891
C	2.74933	2.90176	-0.43259	H	1.10420	-2.02073	1.44983
C	1.54784	3.58964	-0.58363	H	1.49474	4.65957	-0.74583
C	0.38995	2.82127	-0.52858	H	3.69115	3.44160	-0.47365
N	0.35003	1.51869	-0.34286	H	3.66566	0.96804	-0.11767
Li	-0.87265	-0.26451	-0.63487	H	-3.16487	1.27493	1.86596
O	-2.53464	-0.13639	0.47321	H	-2.68617	1.90952	0.27641
C	-3.21864	1.09945	0.78468	H	-5.33262	0.68043	1.11823
C	-4.66723	0.93733	0.28578	H	-5.04883	1.85373	-0.17469
C	-4.56654	-0.24025	-0.70010	H	-4.23194	0.10211	-1.68595
C	-3.47965	-1.10051	-0.06565	H	-5.51313	-0.77544	-0.82435
F	-1.15600	-1.35321	-1.86031	H	-2.90948	-1.70350	-0.77659
F	-0.79914	3.42764	-0.68059	H	-3.87454	-1.71247	0.75841
C	1.45688	-0.98675	1.45069	H	2.22700	0.12324	-2.54918
C	2.88721	-0.97584	2.01999	H	2.40294	-1.54178	-3.10170
C	0.50626	-0.19695	2.35917	H	0.78397	-0.94433	-2.64771
C	1.85295	-0.89602	-2.40805	H	0.43078	-2.80954	-1.16025
C	1.50039	-2.85258	-0.92524	H	2.00443	-3.45595	-1.68873
H	3.27511	0.04463	2.11909	H	1.66253	-3.35319	0.03469
H	3.58315	-1.55114	1.40076	H	3.13844	-1.44039	-0.75312

Table AI.5 (Continued).

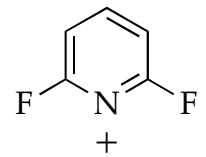

i-$Pr_2NLi(THF)_3$

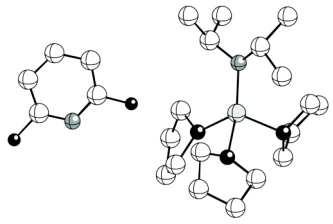

G = -1442.979555
(0 °C)
S = THF

Atom	X	Y	Z	Atom	X	Y	Z
Li	0.98827	-0.15210	0.28350	H	5.56399	-0.78653	-1.58133
N	0.86880	1.75616	0.14832	H	4.62032	0.12802	0.36129
C	-0.04269	2.23205	-0.88527	H	3.32162	0.94952	-0.55272
C	0.62320	2.68457	-2.21731	H	1.33536	1.92080	-2.55338
C	-1.06699	3.30911	-0.44901	H	-0.12229	2.83368	-3.01483
C	1.38608	2.75770	1.06057	H	1.17915	3.62256	-2.10810
C	2.02201	2.06652	2.27943	H	-0.59614	4.27851	-0.24507
C	2.42220	3.75980	0.47776	H	-1.81624	3.47520	-1.23640
O	-0.05536	-1.43804	-1.06549	H	-1.58415	2.99493	0.46703
C	-0.44498	-1.12038	-2.40989	H	-0.66159	1.36260	-1.17015
C	-0.53962	-2.47829	-3.12844	H	2.85175	1.41534	1.97217
C	-0.83121	-3.48190	-1.97765	H	2.41801	2.79426	2.99996
C	-0.82300	-2.60065	-0.71253	H	1.28046	1.44492	2.79429
F	-2.88646	-0.08080	-0.15633	H	1.98886	4.36260	-0.32636
C	-4.20168	0.20950	-0.17070	H	2.78832	4.45573	1.24778
N	-5.01056	-0.83202	-0.15339	H	3.28708	3.22580	0.06178
C	-6.30324	-0.56136	-0.16663	H	0.57782	3.39628	1.47860
C	-6.85791	0.71475	-0.19637	H	-1.84002	-2.29096	-0.44151
C	-5.96274	1.78477	-0.21393	H	-0.34458	-3.05301	0.15696
C	-4.58837	1.54463	-0.20118	H	-0.05501	-4.25191	-1.92730
F	-7.12139	-1.62116	-0.14938	H	-1.79182	-3.99115	-2.09928
O	2.89641	-0.97459	-0.03480	H	-1.32188	-2.47443	-3.89331
C	3.87809	0.01603	-0.43887	H	0.40522	-2.72160	-3.62444
C	4.51843	-0.50428	-1.74649	H	0.30207	-0.43814	-2.81922
C	3.67440	-1.74453	-2.10304	H	-1.41724	-0.61007	-2.39278
C	3.17039	-2.19306	-0.73227	H	-7.93296	0.84776	-0.20516
O	0.42363	-1.25241	1.95134	H	-6.33469	2.80463	-0.23751
C	-0.78178	-0.84715	2.62443	H	-3.84692	2.33419	-0.21436
C	-0.97523	-1.87181	3.76074	H	2.11543	-2.26148	2.51163
C	0.44300	-2.47492	3.96688	H	1.76769	-0.80070	3.46833
C	1.32164	-1.68094	2.98499	H	0.44917	-3.54014	3.71537
H	2.24294	-2.76799	-0.76386	H	0.79897	-2.37628	4.99677
H	3.93862	-2.77295	-0.19563	H	-1.35938	-1.39117	4.66545
H	4.24561	-2.51915	-2.62466	H	-1.68976	-2.64868	3.47281
H	2.82159	-1.46351	-2.73069	H	-0.64939	0.17033	3.01501
H	4.50141	0.25041	-2.53816	H	-1.58074	-0.83334	1.88200

Table AI.5 (Continued).

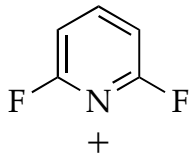

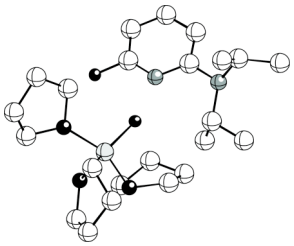

G = -1443.053274
(0 °C)
S = THF

Atom	X	Y	Z	Atom	X	Y	Z
Li	-2.35889	-0.06713	-0.12736	H	-2.69127	-3.33174	-3.58417
F	-0.80181	0.29945	-0.66020	H	-1.79969	-3.28989	-1.37860
C	1.21955	2.35597	0.27413	H	-1.10445	-1.64522	-1.59204
F	0.30994	2.56378	1.25428	H	5.73511	-0.89053	-2.00082
N	2.01103	1.32484	0.44851	H	7.11769	-0.19555	-1.12920
C	2.92906	1.06499	-0.49953	H	6.30158	-1.62205	-0.49016
C	3.06486	1.89821	-1.62830	H	5.68382	-0.32478	1.81751
C	2.23810	3.00865	-1.74730	H	6.68533	0.98219	1.17692
C	1.27277	3.26596	-0.77281	H	5.01013	1.30571	1.66501
N	3.75426	-0.06944	-0.34863	H	5.27401	1.23496	-0.78025
C	3.15420	-1.16263	0.46665	H	2.08120	-2.04323	-1.19943
C	1.85249	-1.63785	-0.20523	H	1.41668	-2.44830	0.39362
C	4.06987	-2.38259	0.63387	H	1.09393	-0.85712	-0.31188
C	5.20060	0.28155	-0.25005	H	4.99444	-2.17285	1.17607
C	5.66859	0.57091	1.18942	H	3.52395	-3.13884	1.20878
C	6.13810	-0.67376	-1.00614	H	4.32630	-2.82550	-0.33464
O	-2.49058	-0.43364	1.84740	H	2.90952	-0.77948	1.46781
C	-1.17413	-0.27508	2.44296	H	-4.94329	1.09538	1.04958
C	-0.82253	-1.66243	2.97063	H	-5.41528	2.45301	-0.01182
C	-2.18936	-2.17903	3.45017	H	-4.41433	3.67635	1.86443
C	-3.15639	-1.58405	2.41377	H	-3.20296	2.39993	2.10043
O	-3.63036	1.48780	-0.47175	H	-1.82327	3.73841	0.73136
C	-2.81292	2.61853	-0.87380	H	-3.19616	4.59002	0.00496
C	-2.82513	3.60802	0.31719	H	-3.25269	3.06435	-1.77612
C	-3.77527	2.95223	1.34906	H	-1.82852	2.20013	-1.09415
C	-4.57096	1.96253	0.49818	H	0.58789	4.10363	-0.82619
O	-3.10058	-1.67878	-1.12962	H	2.32443	3.66062	-2.61257
C	-1.95889	-2.29307	-1.80541	H	3.78058	1.64867	-2.40389
C	-2.31570	-2.34114	-3.30089	H	-4.10643	-1.26217	2.85694
C	-3.43420	-1.29284	-3.42565	H	-3.37158	-2.28165	1.59646
C	-4.14999	-1.44314	-2.08562	H	-2.41120	-1.78933	4.45065
H	-4.68792	-0.54706	-1.76746	H	-2.25117	-3.27078	3.49479
H	-4.84202	-2.29906	-2.09397	H	-0.43583	-2.28560	2.15622
H	-4.09410	-1.46355	-4.28225	H	-0.07086	-1.63284	3.76540
H	-3.00901	-0.28631	-3.50646	H	-0.51944	0.10005	1.65539
H	-1.45115	-2.11629	-3.93222	H	-1.23965	0.45948	3.25802

REFERENCES I

1. Review of nucleophilic aromatic substitution of arylfluorides: Amii, H.; Uneyama, K. *Chem. Rev.* **2009**, *109*, 2119.

2. Pasumansky, L.; Hernandez, A. R.; Gamsey, S.; Goralski, C. T.; Singaram, B. *Tetrahedron Lett.* **2004**, *45*, 6417. For related examples of amination of 2-fluoropyridine, see: Thomas, S.; Roberts, S.; Pasumansky, L.; Gamsey, S.; Singaram, B. *Org. Lett.* **2003**, *5*, 3867. Penney, J. M. *Tetrahedron Lett.* **2004**, *45*, 2667.

3. "Pharmaceuticals & Intermediates 1986-1997 Update". Becker, A., Ed.; Becker Associates, 1997.

4. Fort, Y. *2-Fluoropyridine* In *e-EROS Encyclopedia of Reagents for Organic Synthesis*; John Wiley & Sons, NewYork; 2001. Bhardwaj, P.; Forgione, P. *2,6-Difluoropyridine.* In *e-EROS Encyclopedia of Reagents for Organic Synthesis*; John Wiley & Sons, NewYork; 2001.

5. (a) Schlosser, M. *Angew. Chem., Int. Ed.* **2005**, *44*, 376. (b) Schlosser, M.; Rausis, T. *Eur. J. Org. Chem.* **2004**, 1018. (c) Kuethe, J. T.; Zhong, Y.-L.; Alam, M.; Alorati, A. D.; Beutner, G. L.; Cai, D.; Fleitz, F. J.; Gibb, A. D.; Kassim, A.; Linn, K.; Man- cheno, D.; Marcune, B.; Pye, P. J.; Scott, J. P.; Tellers, D. M.; Xiang, B.; Yasuda, N.; Yin, J.; Davies, I. W. Tetrahedron **2009**, *65*, 5013. (d) Güngör, T.; Marsais, F.; Queguiner, G. *J. Organomet. Chem.* **1981**, *215*, 139.

6. (a) Cottet, F.; Schlosser, M. *Eur. J. Org. Chem.* **2004**, 3793. (b) Trecourt, F.; Mallet, M.; Marsais, F.; Quéguiner, G. *J. Org. Chem* **1988**, *53*, 1367. (c) Comins, D. L.; LaMunyon, D. H. *Tetrahedron Lett.* **1988**, *29*, 773. (d) Eaton, P. E.; Cunkle, G. T.; Marchioro, G.; Martin, R. M. *J. Am. Chem. Soc.* **1987**, *109*, 948. (e) Bridges. A. J.; Patt, W. C.; Stickney, T. M. *J. Org. Chem.* **1990**, *55*, 773. (f) Trécourt, F.; Marsais, F.; Güngör, T.; Quéguiner, G. *J. Chem. Soc., Perkin Trans. 1* **1990**, 2409. (g) Gros, P. C.; Fort, Y. *Eur. J. Org. Chem.* **2009**, 4199. (h) Cottet, F.; Marull, M.; Lefebvre, O.; Schlosser, M. *Eur. J. Org. Chem.* **2003**, 1559.

7. Collum, D. B.; McNeil, A. J.; Ramirez, A. *Angew. Chem., Int. Ed.* **2007**, *46*, 3002.

8. (a) Gribble, G. W.; Saulnier, M. G. *Heterocycles* **1993**, *35*, 151. (b) Mariet, N.; Ibrahim-Ouali, M.; Parrain, J.-L.; Santelli, M. *Theochem.* **2004**, *679*, 53. (c)

Cramer, C. J.; Debbert, S. *Chem. Phys. Lett.* **1998**, *287*, 320. (d) Walters, M. A.; Shay, J. J. *Synth. Commun.* **1997**, *27*, 3573. (e) Iwayama, T.; Sato, Y. *J. Chem. Soc., Chem. Commun.* **2009**, 5245.

9. (a) Di Nunno, L.; Vitale, P.; Scilimati, A. *Tetrahedron* **2008**, *64*, 11198. (b) Kivala, M.; Mitzel, F.; Boudon, C.; Gisselbrecht, J.-P.; Seiler, P.; Gross, M.; Diederich, F. *Chem.—Asian J.* **2006**, *1*, 479. (c) Hickey, M. R.; Allwein, S. P.; Nelson, T. D.; Kress, M. H.; Sudah, O. S.; Moment, A. J.; Rodgers, S. D.; Kaba, M.; Fernandez, P. *Org. Process Res. Dev.* **2005**, *9*, 764. (d) Dabrowski, M.; Kubicka, J.; Lulinski, S.; Serwatowski, J. *Tetrahedron Lett.* **2005**, *46*, 4175.

10. (a) Ramirez, A.; Candler, J.; Bashore, C. G.; Wirtz, M. C.; Coe, J. W.; Collum, D. B. *J. Am. Chem. Soc.* **2004**, *126*, 14700. (b) Riggs, J. C.; Ramirez, A.; Cremeens, M. E.; Bashore, C. G.; Candler, J.; Wirtz, M. C.; Coe, J. W.; Collum, D. B. *J. Am. Chem. Soc.* **2008**, *130*, 3406.

11. Examples of electrophilicity of organolithiums within mixed aggregates that are *superficially* related to the hypothesis in eq 2 are reviewed by Boche: Boche, G.; Lohrenz, J. C. W. *Chem. Rev.* **2001**, *101*, 697.

12. (a) Kim, Y.-J.; Bernstein, M. P.; Galiano-Roth, A. S.; Romesberg, F. E.; Fuller, D. J.; Harrison, A. T.; Collum, D. B.; Williard, P. G. *J. Org. Chem.* **1991**, *56*, 4435. (b) Collum, D. B. *Acc. Chem. Res.* **1993**, *26*, 227.

13. Review of ^{6}Li NMR spectroscopy: Günther, H. *J. Brazil. Chem.* **1999**, *10*, 241.

14. Review of ^{19}F NMR spectroscopy in organometallic chemistry: Espinet, P.; Albeniz, A. C.; Casares, J. A.; Martinez-Ilarduya, J. M. *Coor. Chem. Rev.* **2008**, *252*, 2180.

15. Similar $^{2}J_{C\text{-}F}$ values have been observed for related 2-fluorophenyllithiums: (a) Singh, K. J.; Collum, D. B. *J. Am. Chem. Soc.* **2006**, *128*, 13753. (b) Menzel, K.; Fisher, E. L.; DiMichele, L.; Frantz, D. E.; Nelson, T. D.; Kress, M. H. *J. Org. Chem.* **2006**, *71*, 2188.

16. $^{2}J_{C\text{-}F}$ values have been correlated with π-bond orders and total electronic charge at the ^{13}C atom: (a) Doddrell, D.; Jordan, D.; Riggs, N. V. *J. Chem. Soc., Chem. Commun.* **1972**, 1158. (b) Doddrell, D.; Barfield, M.; Adcock, W.; Aurangzeb, M.; Jordan, D. *J. Chem. Soc., Perkin Trans. 2* **1976**, 402.

17. Gaussian 03, Revision B.04, Frisch, M. J.; Trucks, G. W.; Schlegel, H. B.;

Scuseria, G. E.; Robb, M. A.; Cheeseman, J. R.; Montgomery, Jr., J. A.; Vreven, T.; Kudin, K. N.; Burant, J. C.; Millam, J. M.; Iyengar, S. S.; Tomasi, J.; Barone, V.; Mennucci, B.; Cossi, M.; Scalmani, G.; Rega, N.; Petersson, G. A.; Nakatsuji, H.; Hada, M.; Ehara, M.; Toyota, K.; Fukuda, R.; Hasegawa, J.; Ishida, M.; Nakajima, T.; Honda, Y.; Kitao, O.; Nakai, H.; Klene, M.; Li, X.; Knox, J. E.; Hratchian, H. P.; Cross, J. B.; Bakken, V.; Adamo, C.; Jaramillo, J.; Gomperts, R.; Stratmann, R. E.; Yazyev, O.; Austin, A. J.; Cammi, R.; Pomelli, C.; Ochterski, J. W.; Ayala, P. Y.; Morokuma, K.; Voth, G. A.; Salvador, P.; Dannenberg, J. J.; Zakrzewski, V. G.; Dapprich, S.; Daniels, A. D.; Strain, M. C.; Farkas, O.; Malick, D. K.; Rabuck, A. D.; Raghavachari, K.; Foresman, J. B.; Ortiz, J. V.; Cui, Q.; Baboul, A. G.; Clifford, S.; Cioslowski, J.; Stefanov, B. B.; Liu, G.; Liashenko, A.; Piskorz, P.; Komaromi, I.; Martin, R. L.; Fox, D. J.; Keith, T.; Al-Laham, M. A.; Peng, C. Y.; Nanayakkara, A.; Challacombe, M.; Gill, P. M. W.; Johnson, B.; Chen, W.; Wong, M. W.; Gonzalez, C.; and Pople, J. A.; Gaussian, Inc., Wallingford CT, 2004.

18. (a) Kottke, T.; Sung, K.; Lagow, R. J. *Angew. Chem., Int. Ed. Engl.* **1995**, *34*, 1517. (b) Reich, H. J.; Green, D. P.; Medina, M. A.; Goldenberg, W. S.; Gudmundsson, B. Ö.; Dykstra, R. R.; Phillips, N. H. *J. Am. Chem. Soc.* **1998**, *120*, 7201. (c) Bonasia, P. J.; Arnold, J. *J. Organometal. Chem.* **1993**, *449*, 147.

19. The concentration of LDA, although expressed in units of molarity, refers to the concentration of the monomer unit (normality). The concentration of THF is expressed as total concentration of free (uncoordinated) ligand.

20. The most stable form of LDA monomer is calculated to be a trisolvate.

21. (a) A solution of diisopropylamine (50 mL, 0.35 mol) in 100 mL of methylene chloride was washed with deuterium oxide (10 x 10 mL) containing NaCl. The organic layer was dried over Na_2SO_4 and distilled to give *N*-deuterated diisopropylamine (30 mL, 0.21 mol). The absence of N-H resonance in ^{1}H NMR spectrum confirmed the quantitative deuteration of the sample. (b) Newcomb, M.; Reeder, R. A. *J. Org. Chem.* **1980**, *45*, 1489.

22. Edwards, J. O.; Greene, E. F.; Ross, J. *J. Chem. Educ.* **1968**, *45*, 381.

23. (a) Streitwieser, A.; Abu-Hasanyan, F.; Neuhaus, A.; Brown, F. *J. Org. Chem.* **1996**, *61*, 3151. (b) Pratt, L. M.; Ramachandran, B.; Xidos, J. D.; Cramer, C. J.; Truhlar, D. G. *J. Org. Chem.* **2002**, *67*, 7607. (c) Singh, K. J.; Hoepker, A. C.; Collum, D. B. *J. Am. Chem. Soc.* **2008**, *130*, 18008. (d) Chadwick, S. T.; Rennels, R. A.; Rutherford, J. L.; Collum, D. B. *J. Am. Chem. Soc.* **2000**, *122*, 8640.
24. Selected examples of fully-characterized through-space Li-F interactions: (a) Armstrong, D. R.; Khandelwal, A. H.; Kerr, L. C.; Peasey, S.; Raithby, P. R.;

Shields, G. P.; Snaith, R.; Wright, D. S. *Chem. Commun.* **1998**, 1011. (b) Plenio, H.; Diodone, R. *J. Am. Chem. Soc.* **1996**, *118*, 356. (c) Henderson, K. W.; Dorigo, A. E.; Liu, Q.-Y.; Williard, P. G. *J. Am. Chem. Soc.* **1997**, *119*, 11855. (d) Kessar, S. V.; Singh, P.; Singh. K. N.; Bharatam, P. V.; Sharma, A. K.; Lata, S.; Kaur, A. *Angew. Chem., Int. Ed.* **2008**, *47*, 4703. (e) Lee, W.-Y.; Liang, L.-C. *Inorg. Chem.* **2008**, *47*, 3298. (f) Sini, G.; Tessier, A.; Pytkowicz, J.; Brigaud, T. *Chem. Eur. J.* **2008**, *14*, 3363 and references cited therein.

25. Foresman, J. B.; Frisch, A. E. *Exploring Chemistry with Electronic Structure Methods,* 2nd ed.; Gaussian, Inc.: Pittsburgh, 1993; p 99.

26. Lin, Z. *Coord. Chem. Rev.* **2007**, *251*, 2280.

27. Seebach, D.; Laube, T.; Dunitz, J. D. H*elv. Chim. Acta* **1985**, *68*, 1373.

28. Rennels, R. A.; Maliakal, A. J.; Collum, D. B. *J. Am. Chem. Soc.* **1998**, *120*, 421.

29. Kofron, W. G.; Baclawski, L. M. *J. Org. Chem.* **1976**, *41*, 1879.

30. Rein, A. J.; Donahue, S. M.; Pavlosky, M. A. *Curr. Opin. Drug Discovery Dev.* **2000**, *3*, 734.

CHAPTER II

Lithium Diisopropylamide-Mediated Ortholithiations: Lithium Chloride Catalysis*

*Reprinted with permission from Gupta, L.; Hoepker. A. C; Singh, K. J.; Collum, D. B. *J. Org. Chem*. **2009**, *74*, 2231. Copyright 2010 American Chemical Society.

Lithium Diisopropylamide-Mediated Ortholithiations: Lithium Chloride Catalysis

Abstract

Ortholithiations of a range of arenes mediated by lithium diisopropylamide (LDA) in THF at -78 °C reveal substantial accelerations by as little as 0.5 mol % LiCl (relative to LDA). Substrate dependencies suggest a specific range of reactivity within which the LiCl catalysis is optimal. Standard protocols using unpurified commercial samples of *n*-butyllithium to prepare LDA or commercially available LDA show marked batch-dependent rates--up to 100-fold--that could prove significant to the unwary practitioner. Other lithium salts elicit more modest accelerations. The mechanism is not discussed.

Introduction

We report herein lithium diisopropylamide (LDA)-mediated ortholithiations[1] that are markedly accelerated by LiCl (eq 1). Beneficial effects of LiCl on the chemistry of LDA and other organolithium reactions have been documented.[2-4] Nevertheless, the magnitudes of these accelerations of ortholithiation are striking and the implications in synthesis are potentially significant.

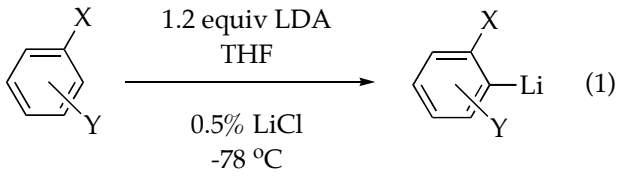

(1)

Results

We preface the results with several comments about protocol. Most investigators either purchase LDA as a THF solvate or prepare it in situ from commercially available *n*-BuLi.[5] The implications of these procedures are discussed below. The LDA used in this study was prepared from recrystallized *n*-BuLi,[6] further recrystallized from hexane,[7] and shown to contain <0.02% LiCl by potentiometry[8] and ion chromatography.[9] The added LiCl was generated in situ from recrystallized $Et_3N{\cdot}HCl$.[10] The Et_3N by-product is a poor ligand[11] that has no effect on the ortholithiations.

Ortholithiations were monitored using in situ IR spectroscopy[12] following both the disappearance of the arene and the formation of the resulting aryllithium.[13] ^{19}F NMR spectroscopic analysis provided comparable results in a number of instances. Trapping experiments were consistent with lithiation but are unreliable measures of the rates because they generate catalytically active lithium salts. Trimethylchlorosilane, for example, generates LiCl,[3c] making LiCl-sensitive arene lithiations nearly instantaneous.

Although some metalations display normal (exponential) decays, autocatalysis[14] arising from the aryllithiums was evident in the form of linear and sigmoidal decays for many substrates (supporting information). Consequently, the rates of uncatalyzed ortholithiation are simply reported as half-lives ($t_{1/2}$), and the LiCl-mediated accelerations as the ratios of $1/t_{1/2}$'s with and without added 0.5% LiCl (k_{LiCl}).[15] The approximation is crude but adequate for our needs.

The results from LiCl-free and LiCl-catalyzed LDA-mediated metalations are illustrated in Table II.1. The accelerations reflected by k_{LiCl} values derive from adding only 0.5 mol % LiCl. Higher concentrations of LiCl

produce greater accelerations (resulting in immeasurably high rates in many instances.) The substrates in Table II.1 are ordered from the most reactive (small $t_{1/2}$) to the least reactive (large $t_{1/2}$), revealing an interesting pattern: Substrates of intermediate reactivity are most prone to catalysis. Both the fastest metalations ($t_{1/2} < 200$ s) and the slowest ($t_{1/2} > 10^5$ s) metalations are relatively insensitive to external LiCl.

Table II.1. Rates of lithium diisopropylamide-mediated ortholithiation (eq 1) listed in order of decreasing reactivity.

Entry	Substrate	$t_{1/2}$ (in s) (-78 °C)	$k_{\mathrm{LiCl}}{}^{a}$
1	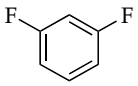	80	2
2	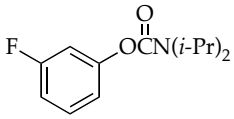	170	2
3	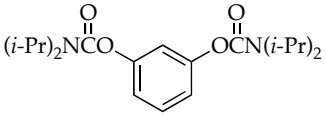	190	2
4	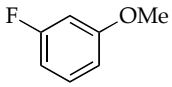	240	5
5	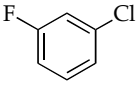	450	9
6	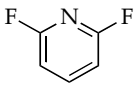	1950	11
7	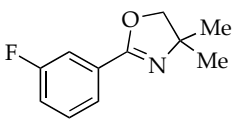	2800	10

Table II.1 (Continued).

Entry	Substrate	$t_{1/2}$ (in s) (-78 °C)	k_{LiCl} [a]
8	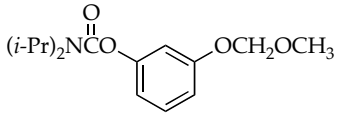	2900	2
9	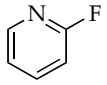	3600	45
10	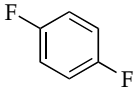	4300	60
11	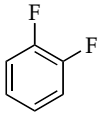	5600	55
12	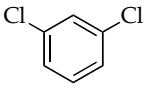	7900	55
13	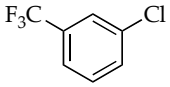	10^4	10
14	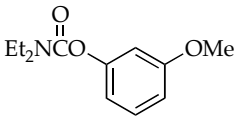	$>10^5$	1 (-65 °C)
15	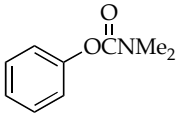	$>10^5$	1 (-30 °C)
16	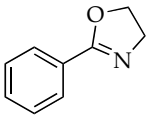	$>10^5$	1 (0 °C)
17	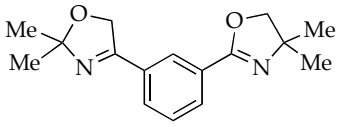	$>10^5$	1 (20 °C)

[a]Measured at -78 °C unless otherwise noted.

We draw the readers attention to entry 8, which does not follow the pattern. Notably, increasing the LiCl concentration to 10 mol % has no effect. In short, a k_{LiCl} of 2 appears to be within the experimental error of unity. But why is entry 8 aberrant? Curiously, the LiCl-sensitive ortholithiations involve substrates containing halogen-based directing groups (F, Cl, or CF_3). Similarly, the ortholithiation in entry 3 shows only a marginal increase in k_{LiCl} with larger aliquots of LiCl. This result may foreshadow conclusions from ongoing mechanistic studies.

It would be especially provocative if the accelerations elicited significant changes in regioselectivity. Schlosser, for example, noted advantageous regiochemical effects of a brew containing both *i*-$Pr_2NCOOLi$ and catalytic LiBr.[4] Metalations of **1** and **2**, however, reveal strong LiCl catalysis, but the regioselectivities (indicated by the arrows) remains unchanged, as expected for reversible metalations.[4,16,17]

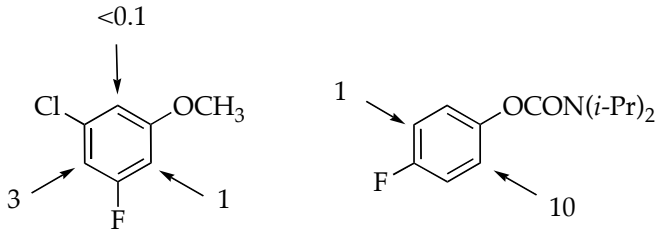

1 $k_{cat} = 7$ **2** $k_{cat} = 12$

Using standard protocols in which the LDA is unpurified, we observed >10^2-fold swings in the reaction rate depending on the commercial source of the *n*-BuLi or LDA. These variations were not supplier dependent per se, but rather batch dependent. A statistically marginal sampling suggests that

commercially available LDA may have a lower LiCl titer and be less prone to inadvertent accelerations compared to LDA generated from commercial *n*-BuLi. Lloyd-Jones noted batch dependencies of aryl triflate metalations that appeared to stem from lithium halides.[3d] Nonetheless, the variations were enormous, inspiring us to repeat a timeless maxim: buyer beware.

Cursory investigation of the influence of other lithium salts (10 mol %) revealed the accelerations illustrated in eq 2. Clearly, LiCl is the most efficient catalyst.

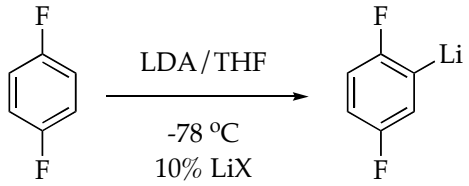

(2)

LiX	$k_{cat\,(10\%)}$
LiCl	>300
LiBr	90
PhCCLi	90
PhCOOLi	30
PhOLi	2

We have explicitly deferred mechanistic speculation. The dramatic LiCl-mediated accelerations do, however, appear to correlate with arene metalations that are also prone to autocatalysis.[14]

Conclusions

LDA/THF/-78 °C-mediated ortholithiations are anomalous in many respects,[14] including a marked penchant for LiCl catalysis. The catalysis is observed in a narrow but potentially consequential window. Unsuspecting academic chemists may have detected irregularities--batch dependencies--that

proved a source of annoyance. The results suggest opportunities to optimize protocols. We believe, however, that industrial chemists should be especially wary of these results. Rate variations that go undetected on small scales could give way to unexpected and potentially costly variations on process and plant scales. Our advice to both communities is the same: try adding a few mol % $Et_3N{\cdot}HCl$ to LDA at the outset.

Experimental Section

Reagents and Solvents. THF and hexane were distilled from blue or purple solutions containing sodium benzophenone ketyl. The hexane contained 1% tetraglyme to dissolve the ketyl. Both *n*-BuLi and LDA were recrystallized.[6,7] Solutions of *n*-BuLi and LDA were titrated using a literature method.[18] Arenes were either commercially available or prepared via literature protocols.[19] $Et_3N{\cdot}HCl$ was recrystallized from THF/2-propanol.

IR Spectroscopic Analyses. Spectra were recorded using an in situ IR spectrometer fitted with a 30-bounce, silicon-tipped probe. The spectra were acquired in 16 scans at a gain of 1 and a resolution of 4 cm^{-1}. A representative reaction was carried out as follows: The IR probe was inserted through a nylon adapter and O-ring seal into an oven-dried, cylindrical flask fitted with a magnetic stir bar and a T-joint. The T-joint was capped by a septum for injections and a nitrogen line. After evacuation under full vacuum, heating, and flushing with nitrogen, the flask was charged with LDA (129 mg, 1.20 mmol) in THF and cooled in a dry ice-acetone bath prepared from fresh acetone. LiCl (0.5 mol% relative to LDA) was added as a stock solution (0.50 mL) containing $Et_3N{\cdot}HCl$ (8.3 mg, 0.06 mmol) and LDA (13.5 mg, 0.12 mmol) in 5 mL THF. After recording a background spectrum, we added an arene (1.0

mmol) with stirring. IR spectra were recorded over the course of the reaction. Absorbances corresponding to the arene moieties (1350-1650 cm^{-1}) were monitored in most cases. Spectra were recorded every 3 s.

Measurement of chloride concentration:

Potentiometry. The chloride concentration was determined potentiometrically by measuring the potential against a saturated potassium chloride solution. After calibrating with known concentrations of chloride, the concentration was calculated with the Nernst equation ($E=E°-(RT/zF)log_{10}Q$, where $Q=[Cl^-]$; RT/zF is determined via calibration and is ideally 59.1 mV). The potential was measured with a potentiostat of low impedence. Both reference and indicating electrodes are made of silver plated with silver chloride (Ag/AgCl). Samples were prepared by quenching 25 mg of LDA or 100 μl of 1.6 M *n*-BuLi with high-purity water (from Abruña group), evacuating to dryness and redissolving in water. Because the electrodes require a near neutral pH, the quenched base solutions needed to be neutralized with HNO_3. The LiCl standards were accordingly enriched with $NaNO_3$ to ensure comparable activity. Both HNO_3 and $NaNO_3$ contained <0.5 ppm and <0.0003% Cl^-, respectively. The lower detection limit for Cl^- is approximately 0.5 ppm.

Ion Chromatography. Ion chromatography was performed on a Dionex ICS-2000 system (Sunnyvale, CA) with a Dionex Ionpac AG18 guard column and a Dionex Ionpac AS18 separation column. Samples and standards were run in the isocratic mode (1.0 ml/min) using 38 mM KOH as eluent. Elution time of chloride varied from 3.94 to 4.23 min. The suppression was achieved by a Dionex ASRS ULTRA II 4 mm self-regenerating suppressor. The column temperature was 30 °C and the working electric current was 100 mA.

The eluent flow rate is 1.0 ml/min. The injection volume is 25 μl. Samples were prepared by quenching 25 mg of LDA or 100 μl of 1.6 M *n*-BuLi with high-purity water (from Abruña group), evacuating to dryness and redissolving in water. Aqueous samples of pH 12-13 were injected in duplicate into the chromatograph. The lower detection limit is approximately 10 ppb.

APPENDIX II

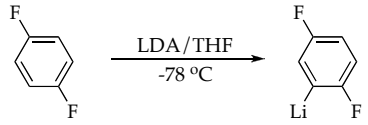

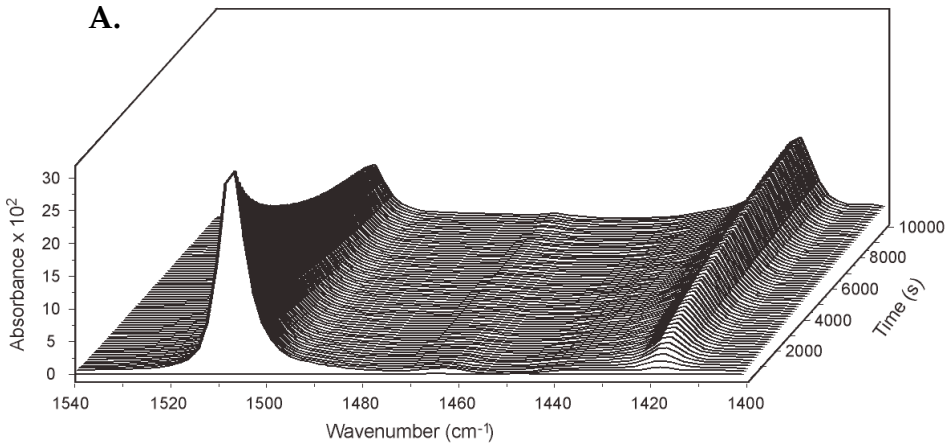

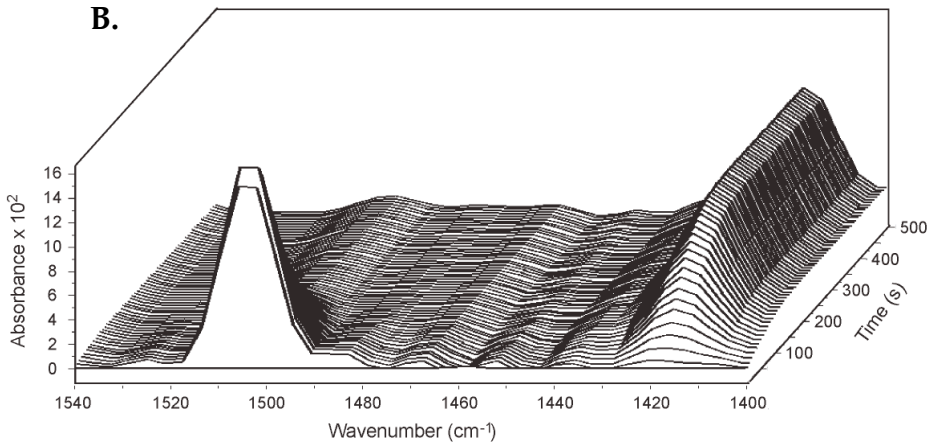

Figure AII.1. Representative in situ IR spectroscopic analysis of the ortholithiation of 1,4-difluorobenzene (0.1 M) with LDA (0.12 M) in neat THF at -78 °C: (A) no added LiCl; (B) 0.5 mol % LiCl. The IR absorbance at 1507 cm^{-1} corresponds to 1,4-difluorobenzene, whereas the absorbance at 1418 cm^{-1} corresponds to its lithiated form.

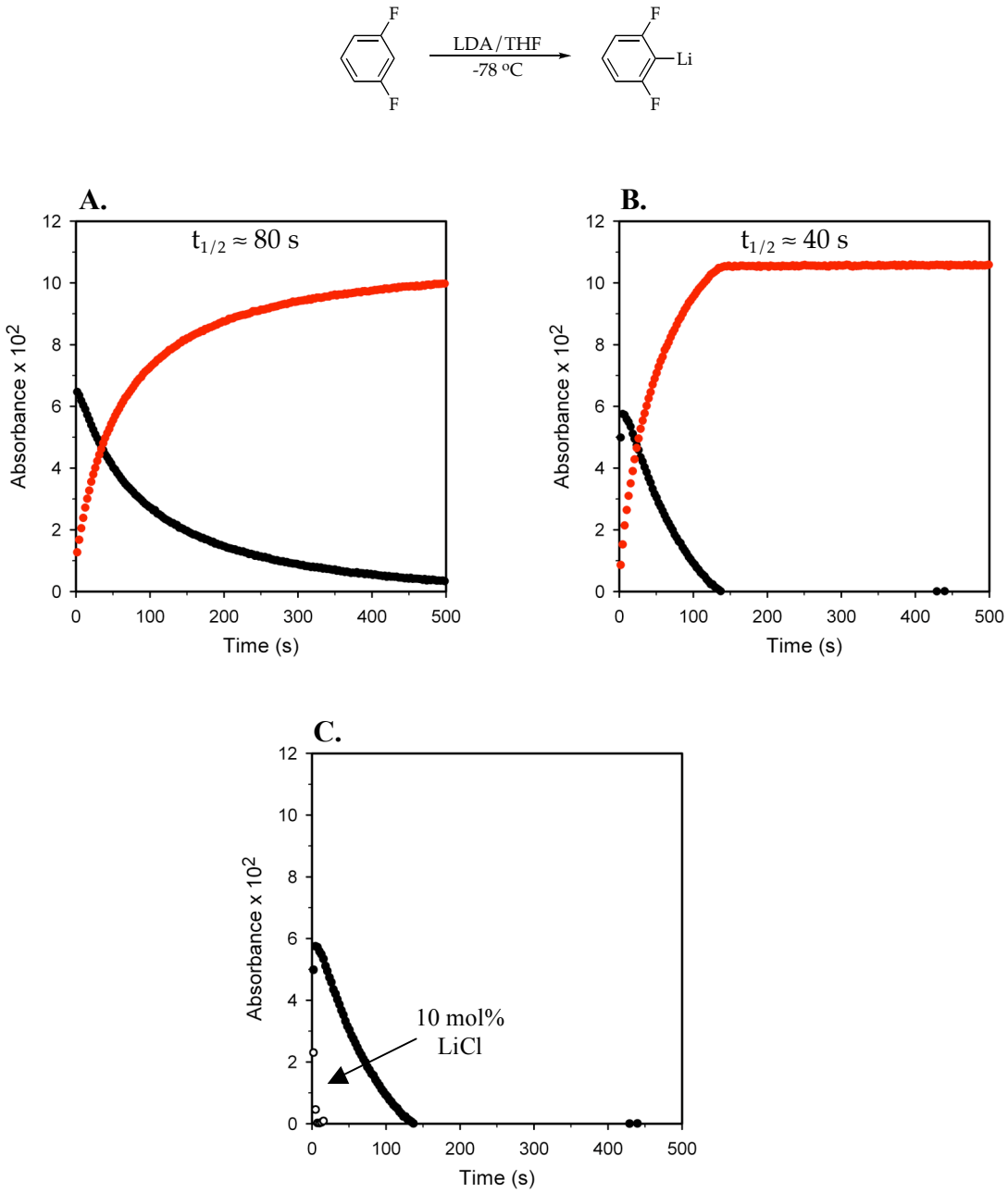

Figure AII.2. Plot of IR absorbances (black – 1606 cm^{-1}, red – 1406 cm^{-1}) versus time for the ortholithiation of 1,3-difluorobenzene (0.10 M) with LDA (0.12 M) in neat THF at -78 °C: (A) no added LiCl; (B) 0.5 mol% LiCl; (C) 0.5 and 10 mol% LiCl.

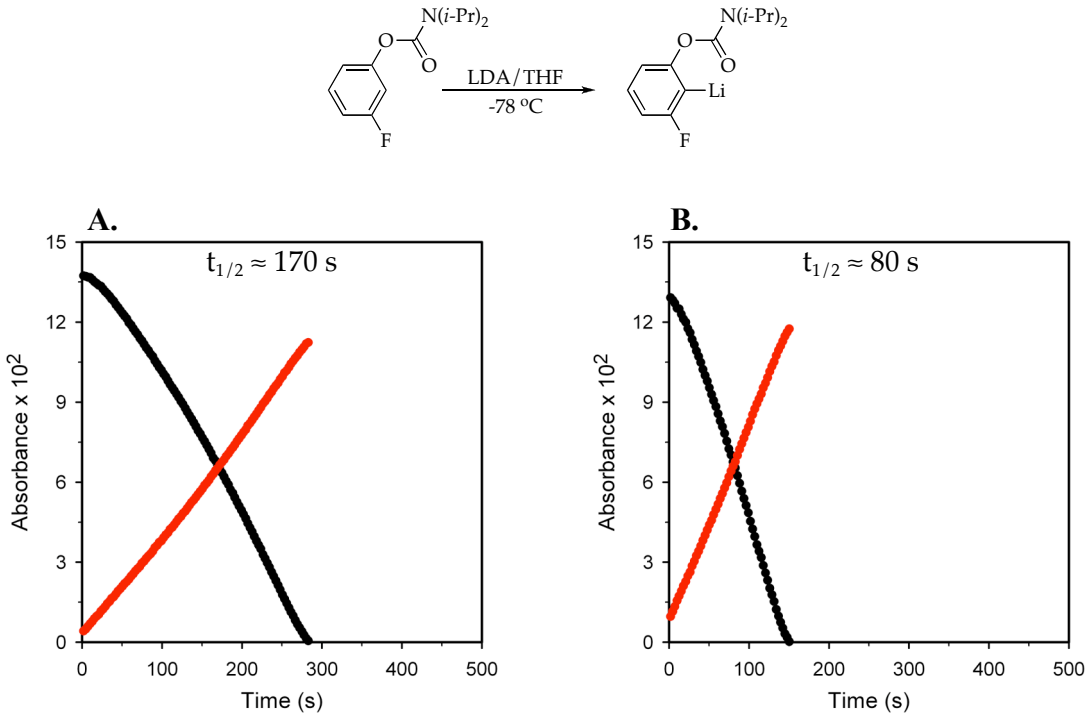

Figure AII.3. Plot of IR absorbances (black – 1715 cm^{-1}, red – 1657 cm^{-1}) versus time for the ortholithiation of 3-fluorophenyl-*N*,*N*-diisopropylcarbamate (0.10 M) with LDA (0.12 M) in neat THF at -78 °C: (A) no added LiCl; (B) 0.5 mol% LiCl.

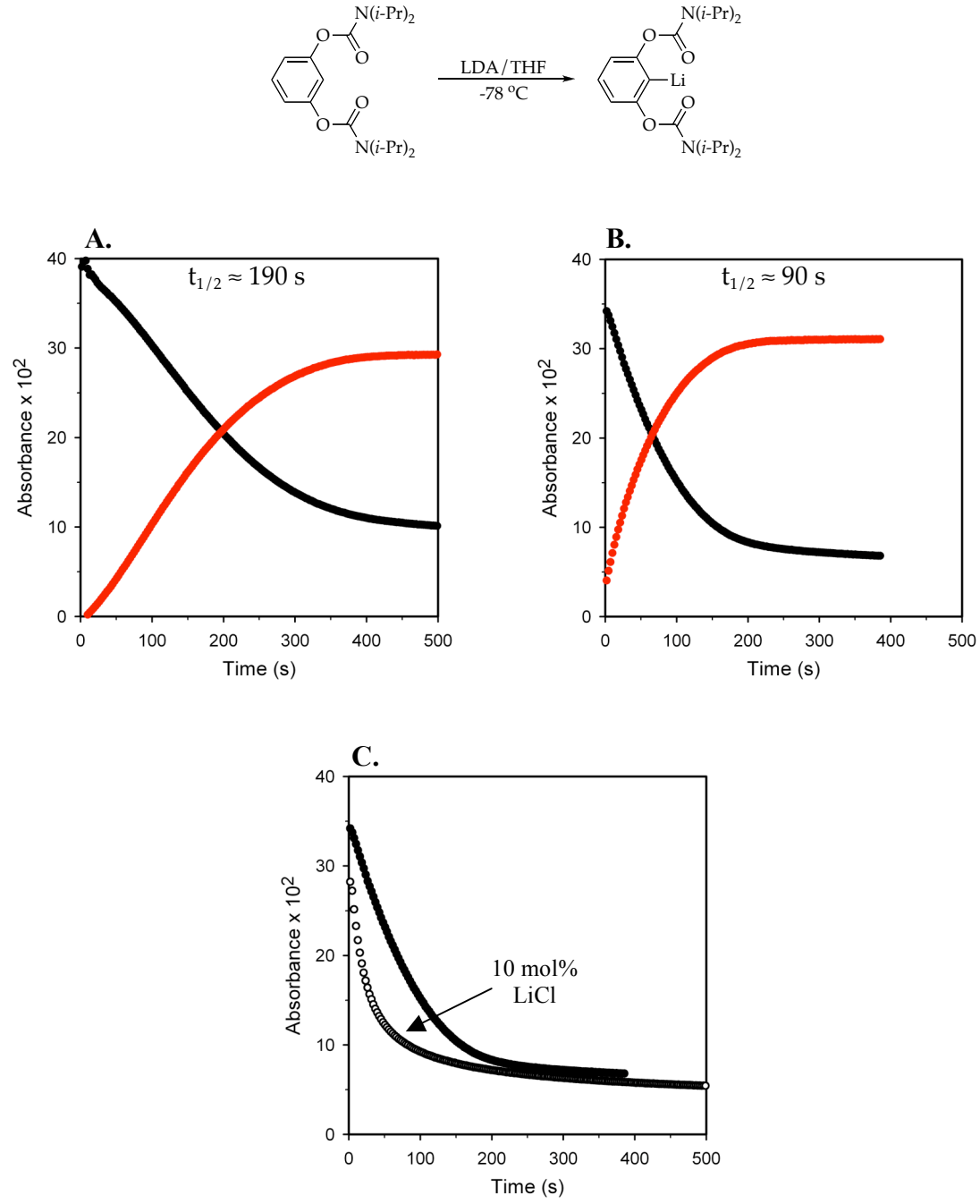

Figure AII.4. Plot of IR absorbances (black – 1721 cm^{-1}, red – 1661 cm^{-1}) versus time for the ortholithiation of 1,3-bis(*N*,*N*-diisopropylcarbamoyl)benzene (0.10 M) with LDA (0.12 M) in neat THF at -78 °C: (A) no added LiCl; (B) 0.5 mol% LiCl; (C) 0.5 and 10 mol% LiCl.

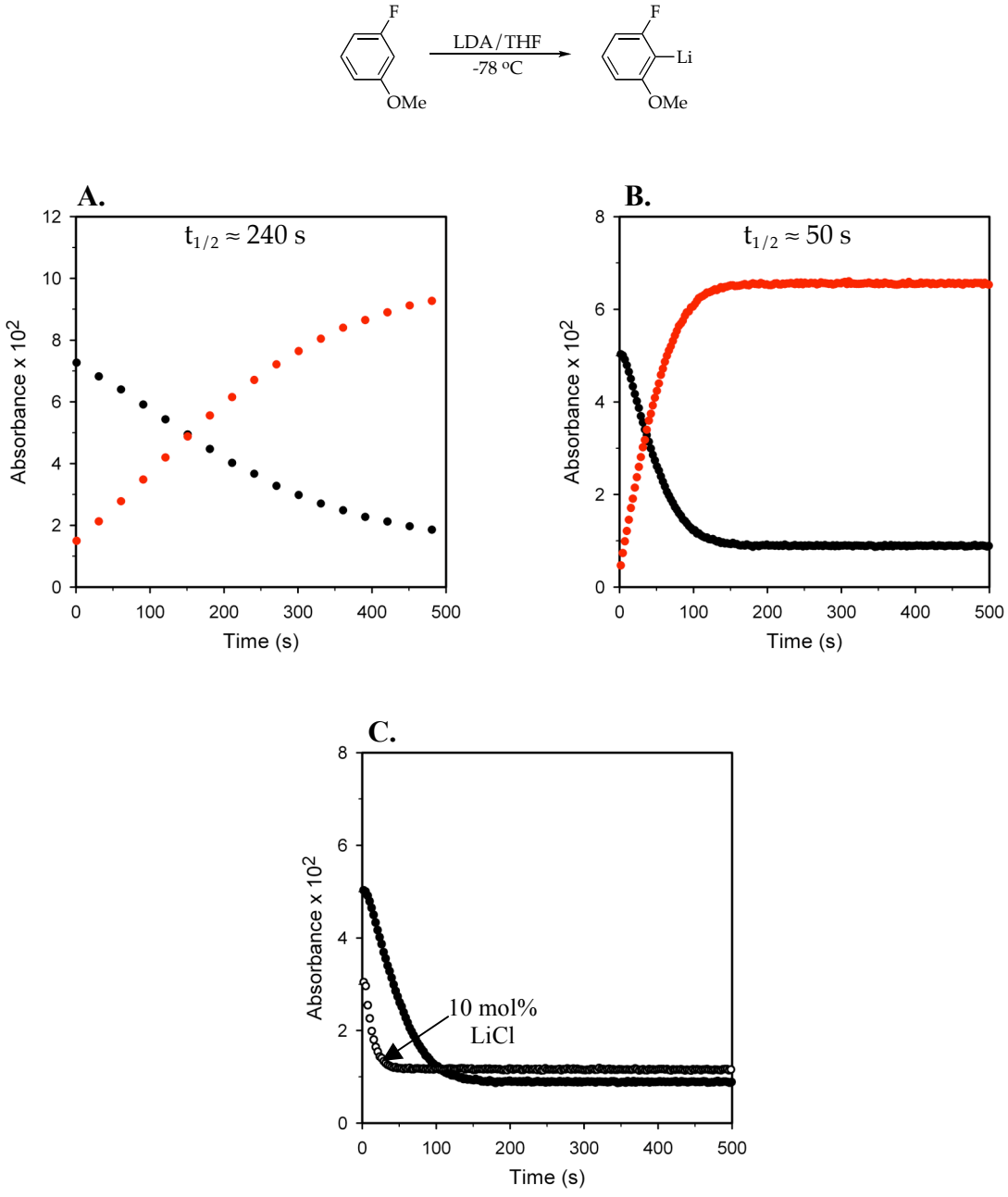

Figure AII.5. Plot of IR absorbances (black – 1617 cm^{-1}, red – 1412 cm^{-1}) versus time for the ortholithiation of 3-fluoroanisole (0.10 M) with LDA (0.12 M) in neat THF at -78 °C: (A) no added LiCl; (B) 0.5 mol% LiCl (C) 0.5 and 10 mol% LiCl.

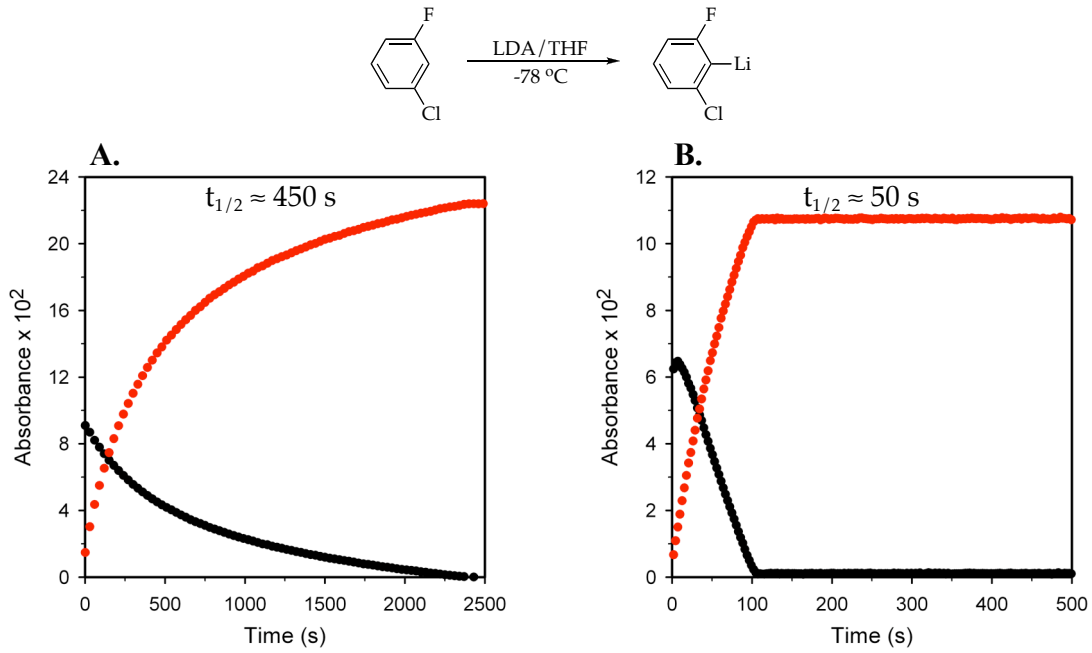

Figure AII.6. Plot of IR absorbances (black – 1595 cm^{-1}, red – 1397 cm^{-1}) versus time for the ortholithiation of 1-chloro-3-fluorobenzene (0.10 M) with LDA (0.12 M) in neat THF at -78 °C: (A) no added LiCl; (B) 0.5 mol% LiCl.

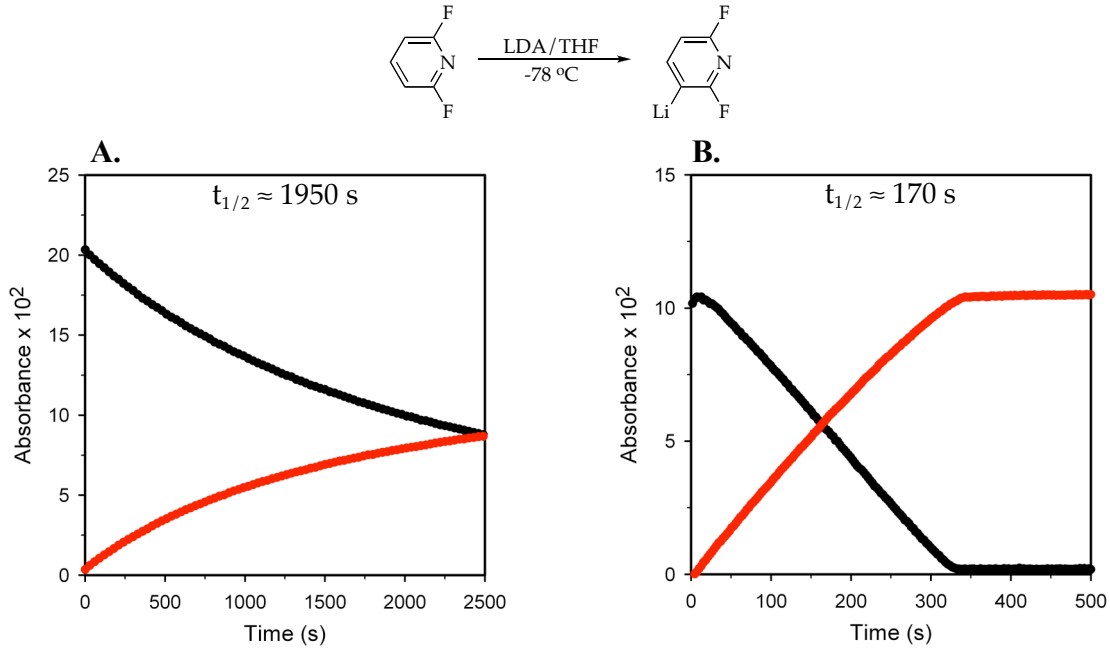

Figure AII.7. Plot of IR absorbances (black – 1610 cm^{-1}, red – 1514 cm^{-1}) versus time for the ortholithiation of 2,6-difluoropyridine (0.10 M) with LDA (0.12 M) in neat THF at -78 °C: (A) no added LiCl; (B) 0.5 mol% LiCl.

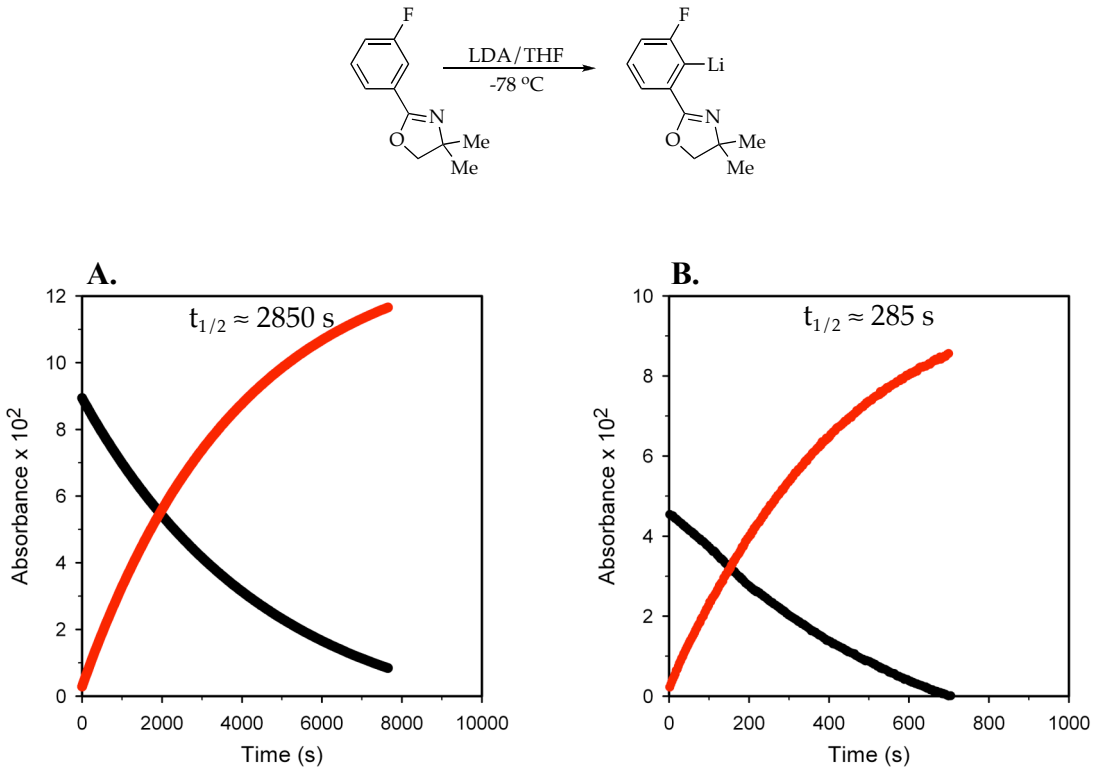

Figure AII.8. Plot of IR absorbances (black – 1653 cm^{-1}, red – 1622 cm^{-1}) versus time for the ortholithiation of 2-(3-fluorophenyl)-4,4-dimethyl-4,5-dihydro-1,3-oxazole (0.10 M) with LDA (0.12 M) in neat THF at -78 °C: (A) no added LiCl; (B) 0.5 mol% LiCl.

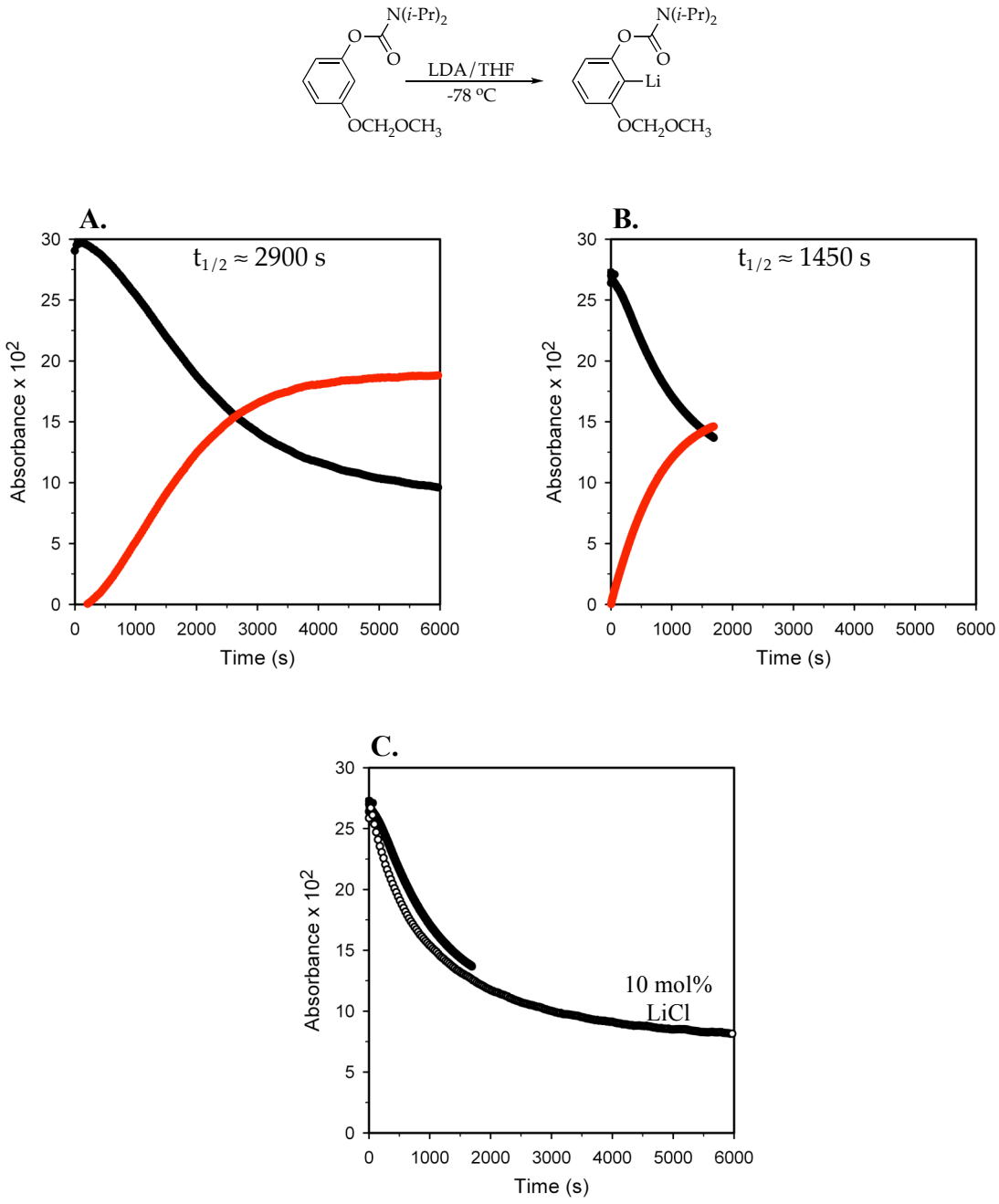

Figure AII.9. Plot of IR absorbances (black – 1719 cm^{-1}, red – 1659 cm^{-1}) versus time for the ortholithiation of 3-methoxymethoxyphenyl-*N*,*N*-diisopropylcarbamate (0.10 M) with LDA (0.12 M) in neat THF at -78 °C: (A) no added LiCl; (B) 0.5 mol% LiCl; (C) 0.5 and 10 mol% LiCl.

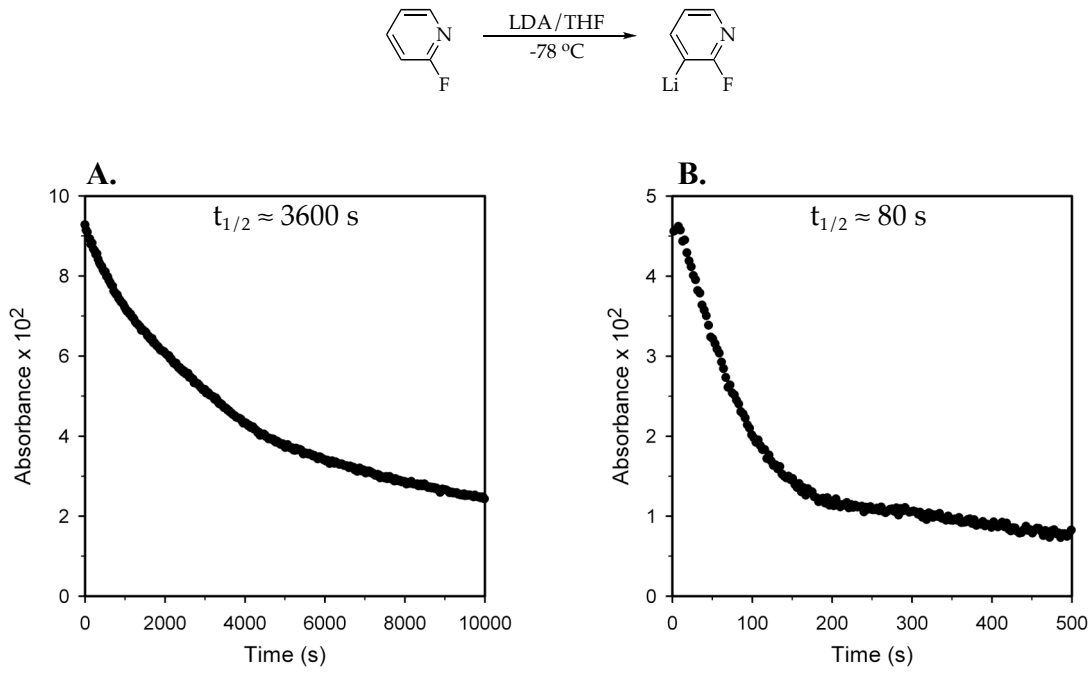

Figure AII.10. Plot of IR absorbances (black – 1597 cm^{-1}) versus time for the ortholithiation of 2-fluoropyridine (0.10 M) with LDA (0.12 M) in neat THF at -78 °C: (A) no added LiCl; (B) 0.5 mol% LiCl.

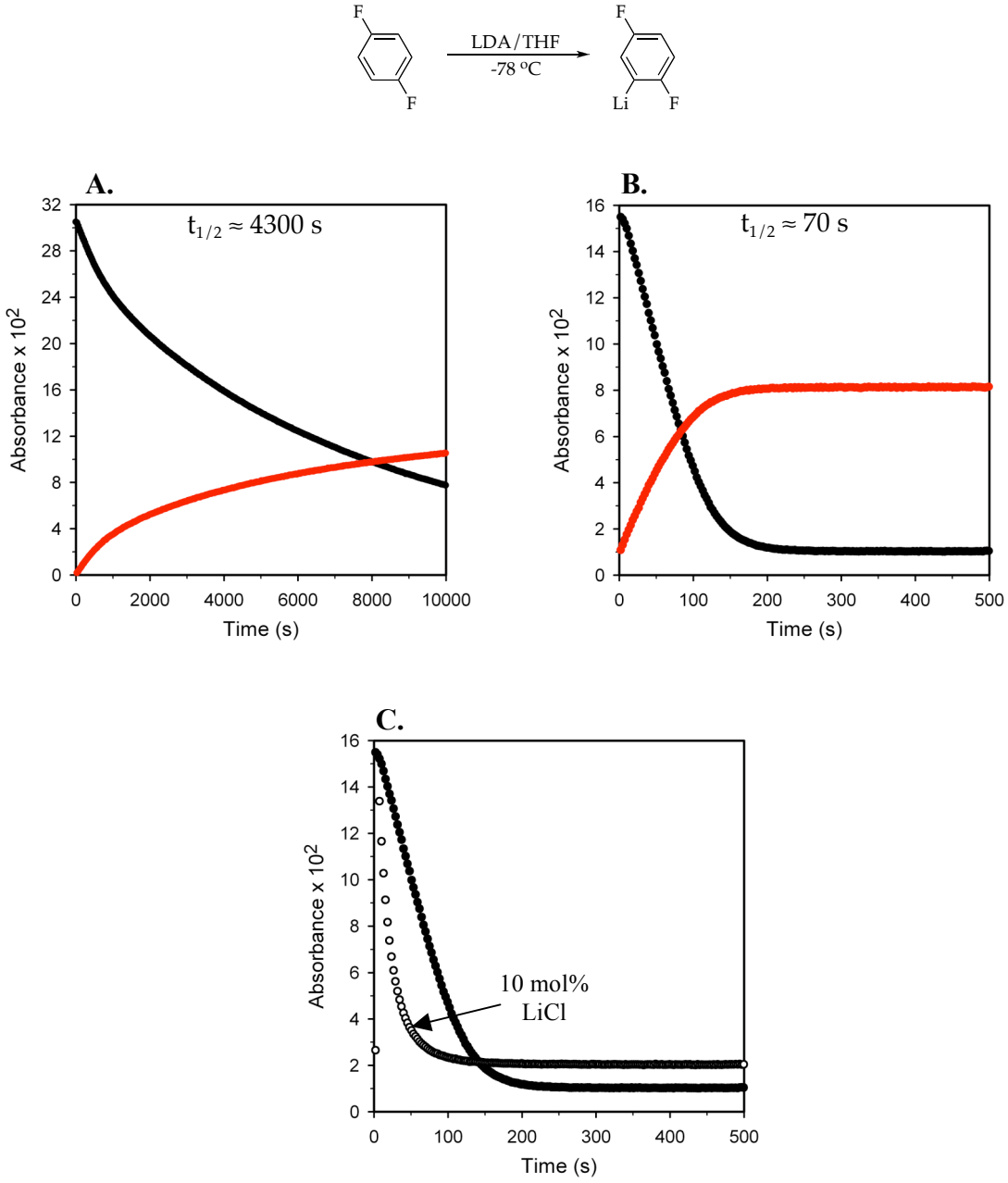

Figure AII.11. Plot of IR absorbances (black – 1507 cm^{-1}, red – 1418 cm^{-1}) versus time for the ortholithiation of 1,4-difluorobenzene (0.10 M) with LDA (0.12 M) in neat THF at -78 °C: (A) no added LiCl; (B) 0.5 mol% LiCl; (C) 0.5 and 10 mol% LiCl.

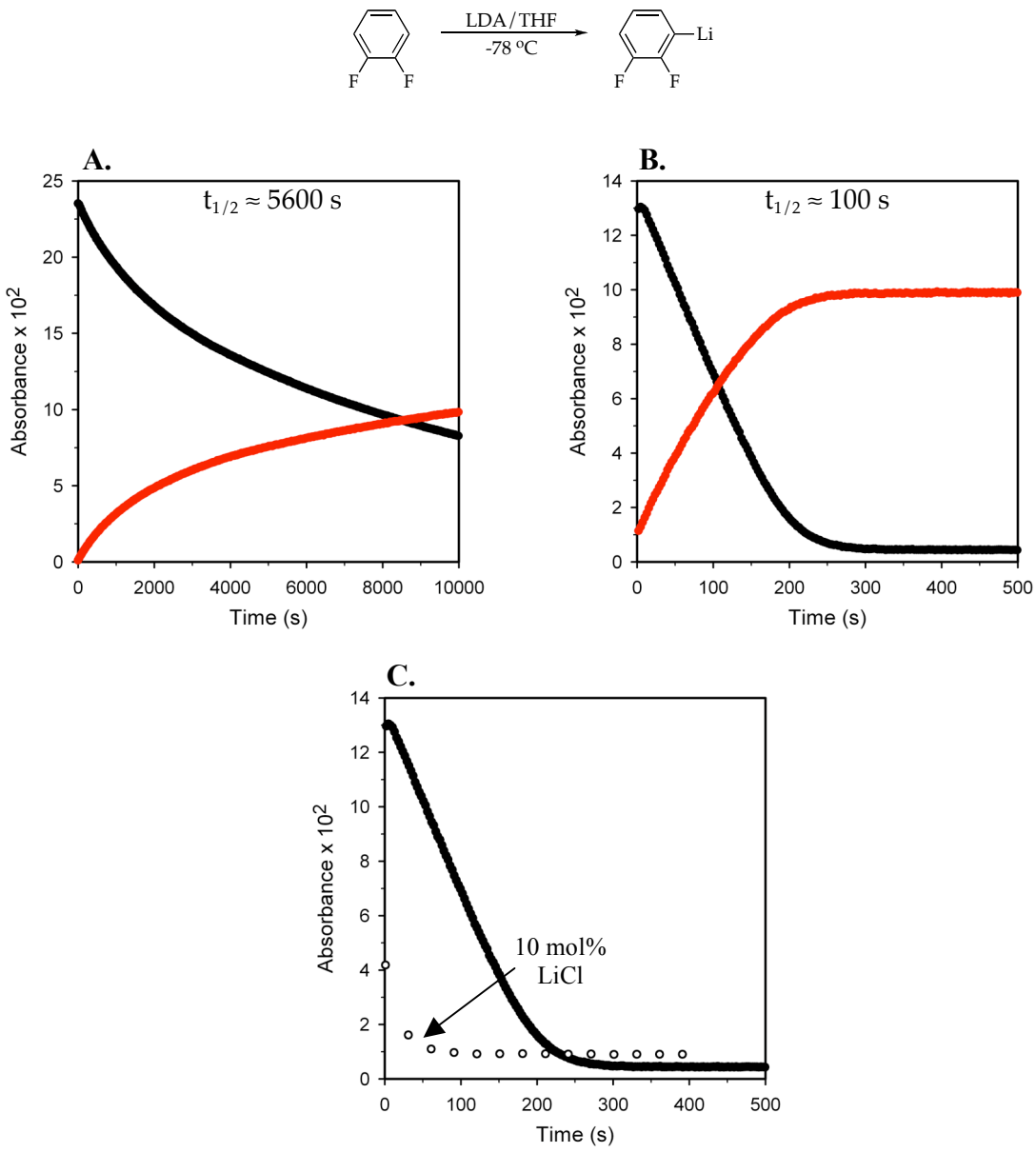

Figure AII.12. Plot of IR absorbances (black – 1509 cm^{-1}, red – 1391 cm^{-1}) versus time for the ortholithiation of 1,2-difluorobenzene (0.10 M) with LDA (0.12 M) in neat THF at -78 °C: (A) no added LiCl; (B) 0.5 mol% LiCl; (C) 0.5 and 10 mol% LiCl.

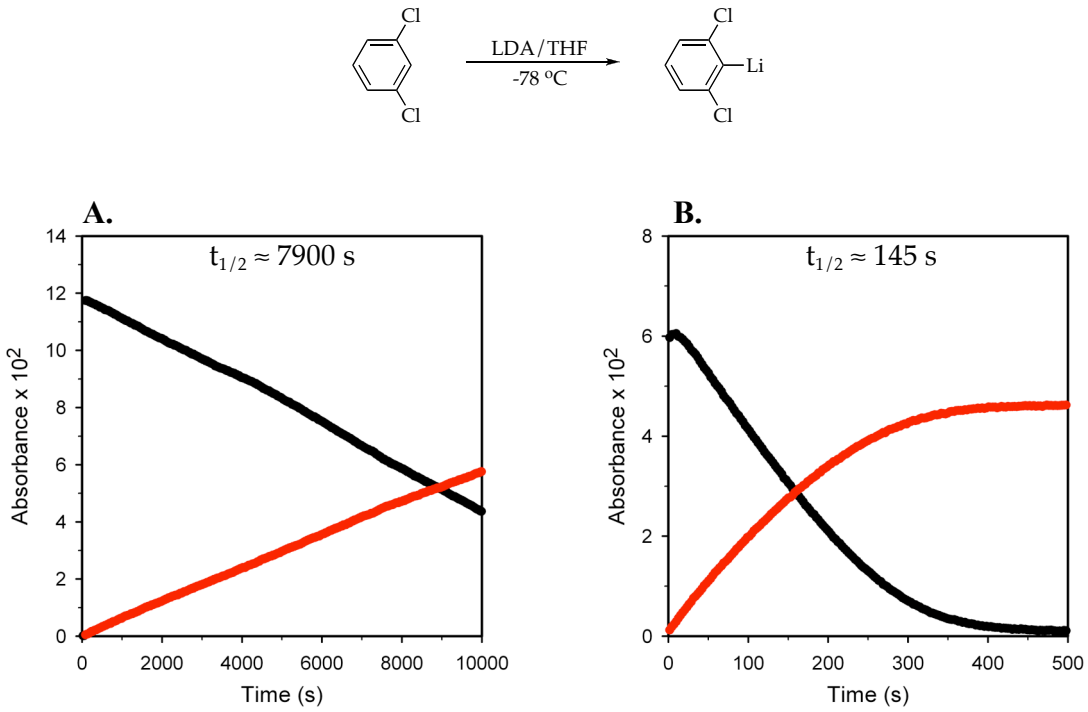

Figure AII.13. Plot of IR absorbances (black – 1576 cm^{-1}, red – 1534 cm^{-1}) versus time for the ortholithiation of 1,3-dichlorobenzene (0.10 M) with LDA (0.12 M) in neat THF at -78 °C: (A) no added LiCl; (B) 0.5 mol% LiCl.

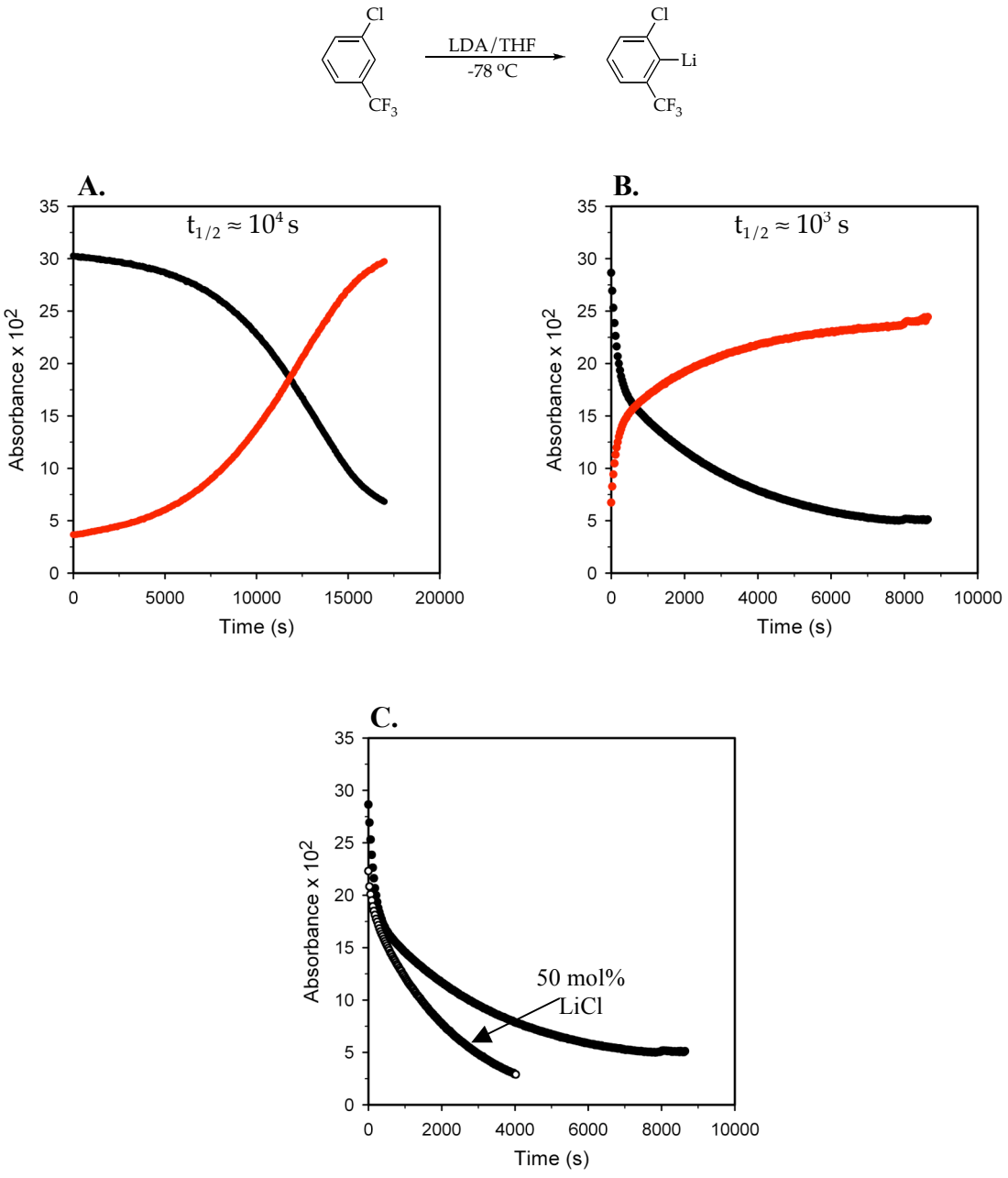

Figure AII.14. Plot of IR absorbances (black – 1326 cm^{-1}, red – 1306 cm^{-1}) versus time for the ortholithiation of 3-chlorobenzotrifluoride (0.10 M) with LDA (0.12 M) in neat THF at -78 °C: (A) no added LiCl; (B) 0.5 mol% LiCl; (C) 0.5 and 50 mol% LiCl.

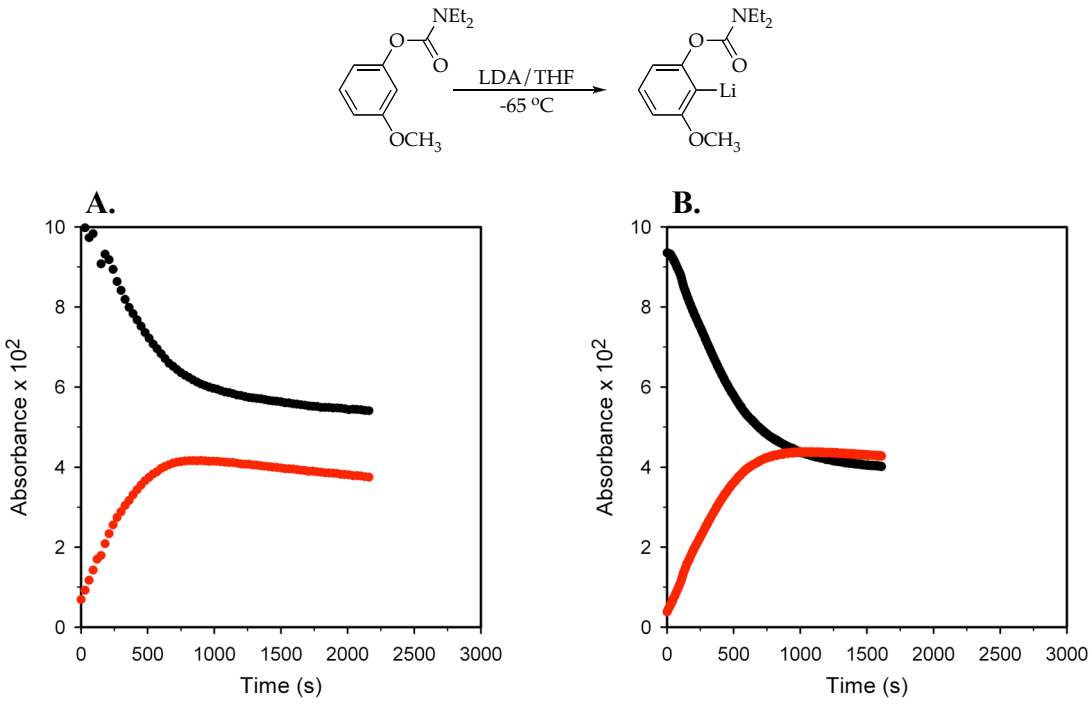

Figure AII.15. Plot of IR absorbances (black – 1725 cm^{-1}, red – 1675 cm^{-1}) versus time for the ortholithiation of 3-methoxyphenyl-*N*,*N*-diethylcarbamate (0.10 M) with LDA (0.12 M) in neat THF at -65 °C: (A) no added LiCl; (B) 0.5 mol% LiCl.

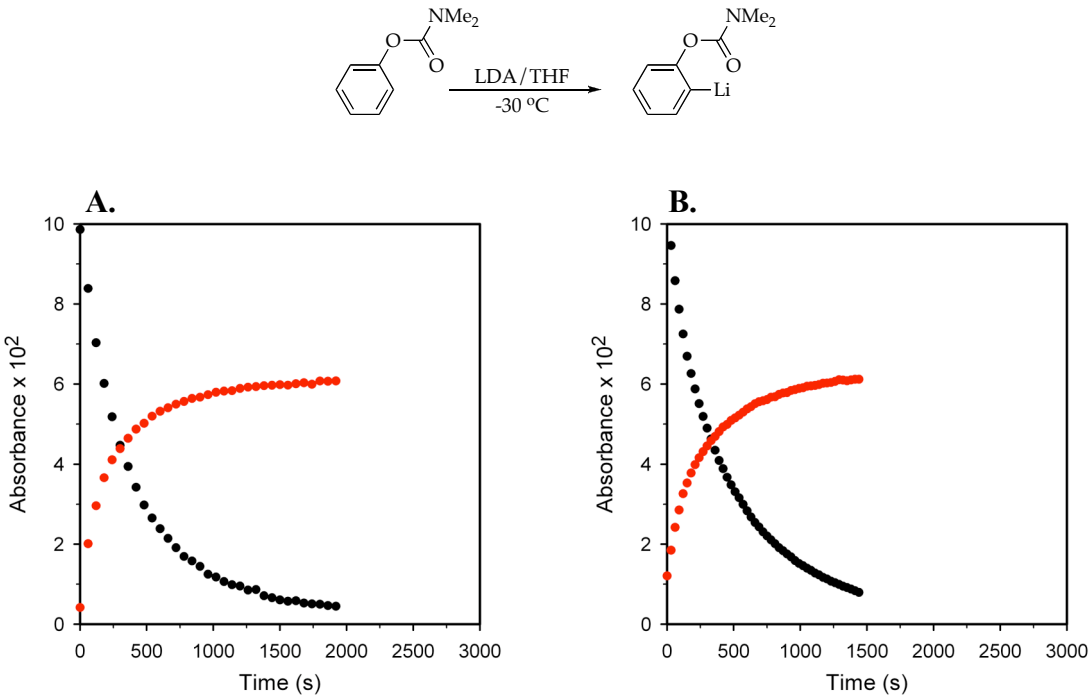

Figure AII.16. Plot of IR absorbances (black – 1725 cm^{-1}, red – 1675 cm^{-1}) versus time for the ortholithiation of phenyl-*N*,*N*-dimethylcarbamate (0.10 M) with LDA (0.12 M) in neat THF at -30 °C: (A) no added LiCl; (B) 0.5 mol% LiCl.

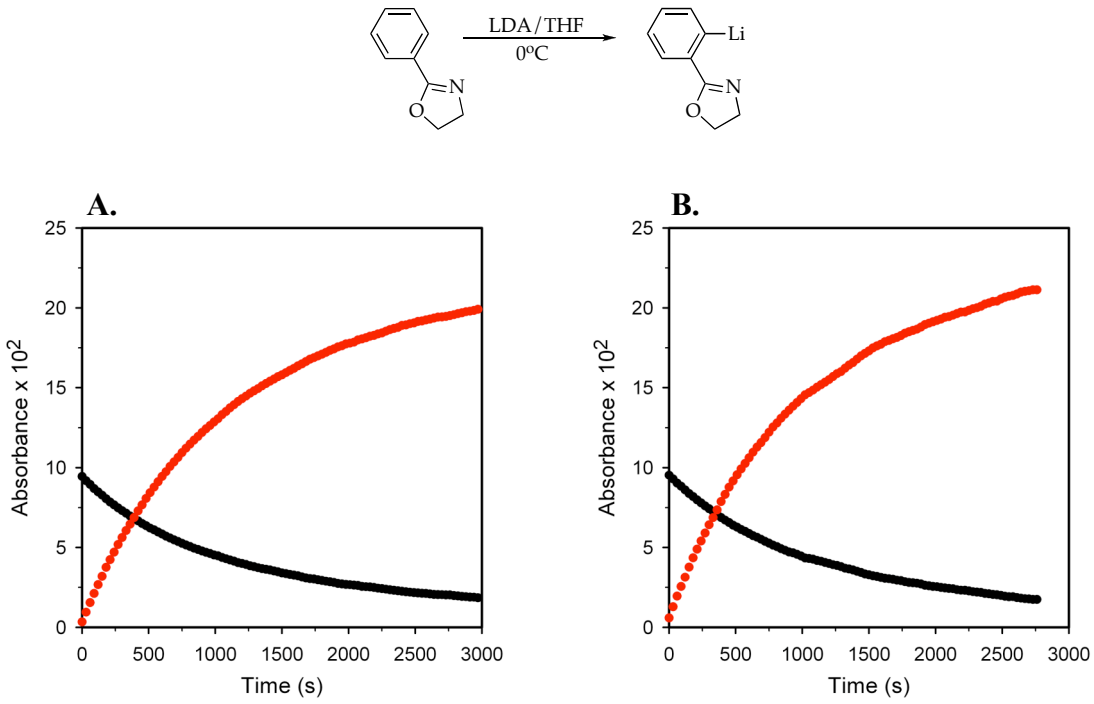

Figure AII.17. Plot of IR absorbances (black – 1652 cm^{-1}, red – 1526 cm^{-1}) versus time for the ortholithiation of 2-phenyl-2-oxazoline (0.10 M) with LDA (0.12 M) in neat THF at 0 °C: (A) no added LiCl; (B) 0.5 mol% LiCl.

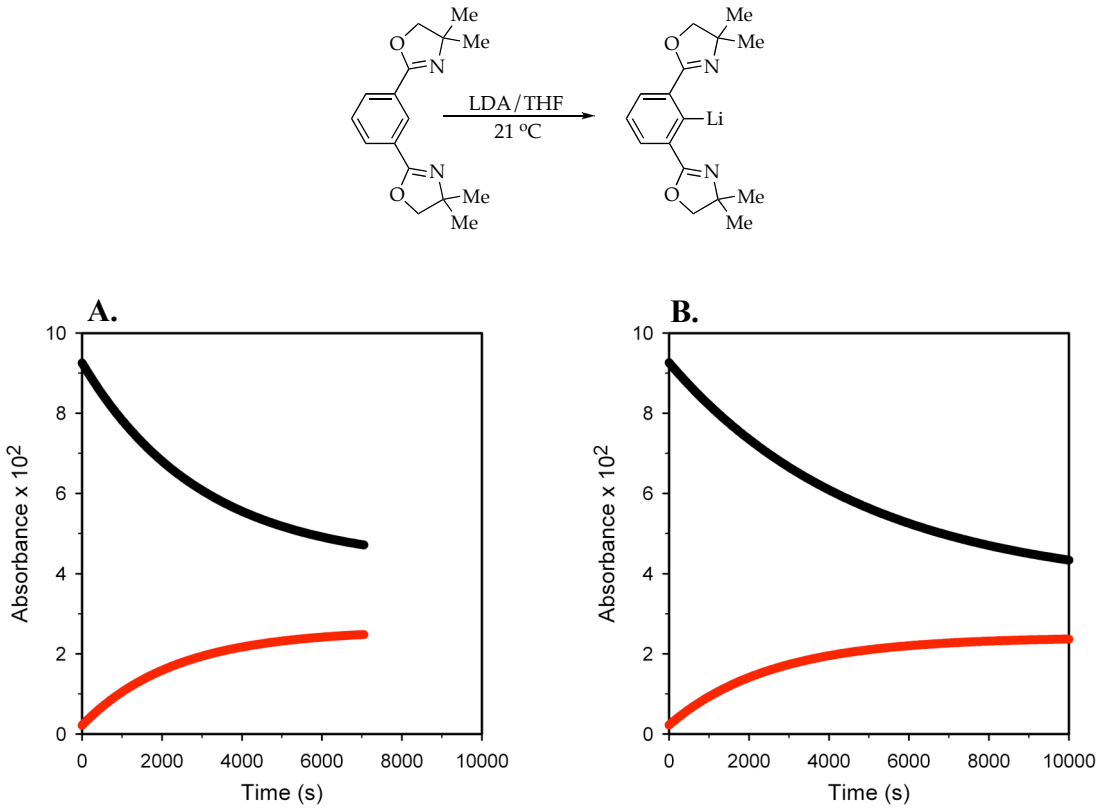

Figure AII.18. Plot of IR absorbances (black – 1654 cm^{-1}, red – 1520 cm^{-1}) versus time for the ortholithiation of 1,3-bis(4′,4′-dimethyl-2′-oxazolinyl)benzene (0.10 M) with LDA (0.12 M) in neat THF at 21 °C: (A) no added LiCl; (B) 0.5 mol% LiCl.

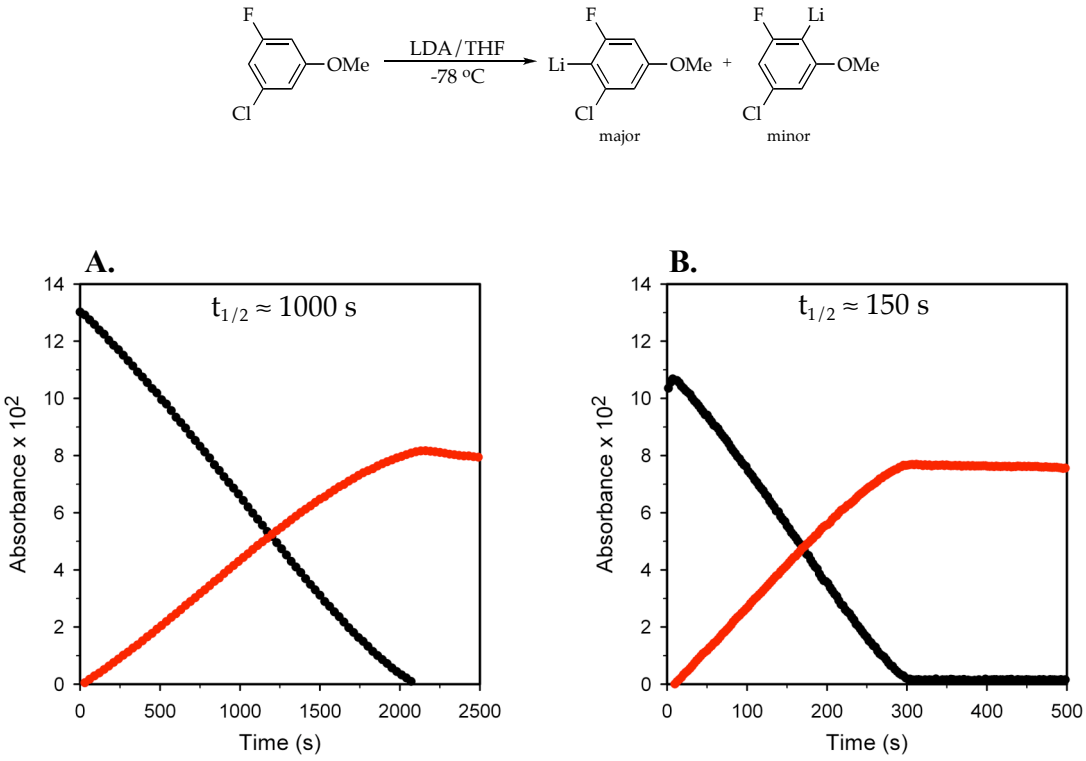

Figure AII.19. Plot of IR absorbances (black – 1611 cm^{-1}, red – 1553 cm^{-1}) versus time for the ortholithiation of 3-chloro-5-fluoroanisole (0.10 M) with LDA (0.12 M) in neat THF at -78 °C: (A) no added LiCl; (B) 0.5 mol% LiCl.

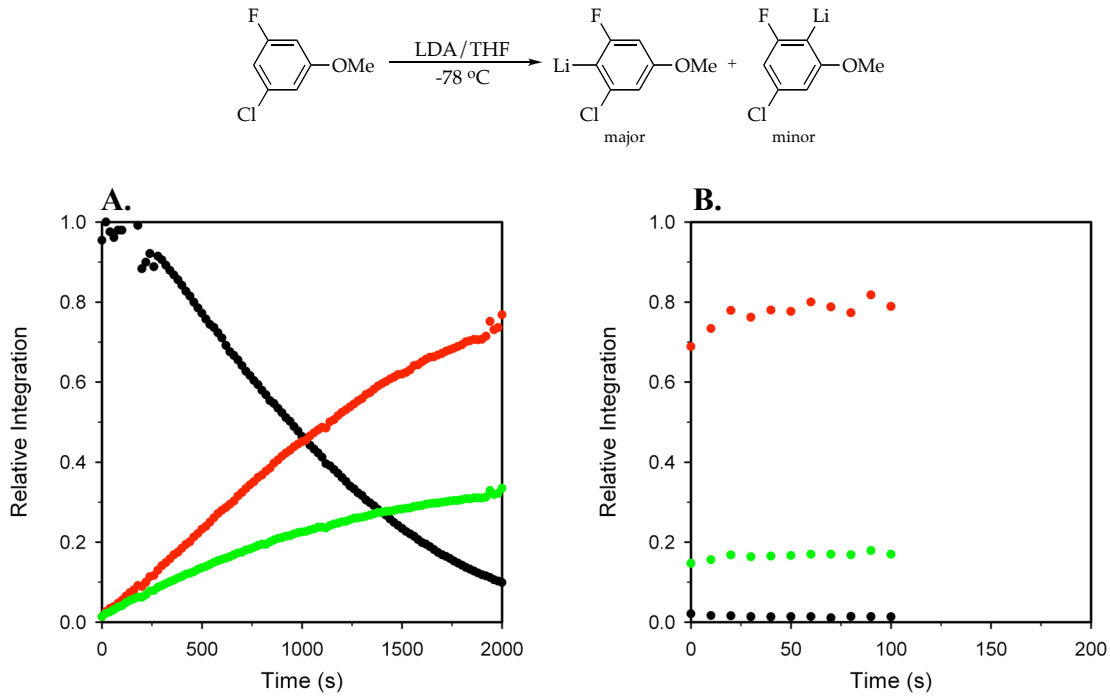

Figure AII.20. Plot of ^{19}F NMR peak integrations (black: δ -110.1, red: δ -77.8, green: δ -76.6) versus time for the ortholithiation of 3-chloro-5-fluoroanisole (0.05 M) with LDA (0.20 M) in neat THF at -78 °C: (A) no added LiCl; (B) 10 mol% LiCl.

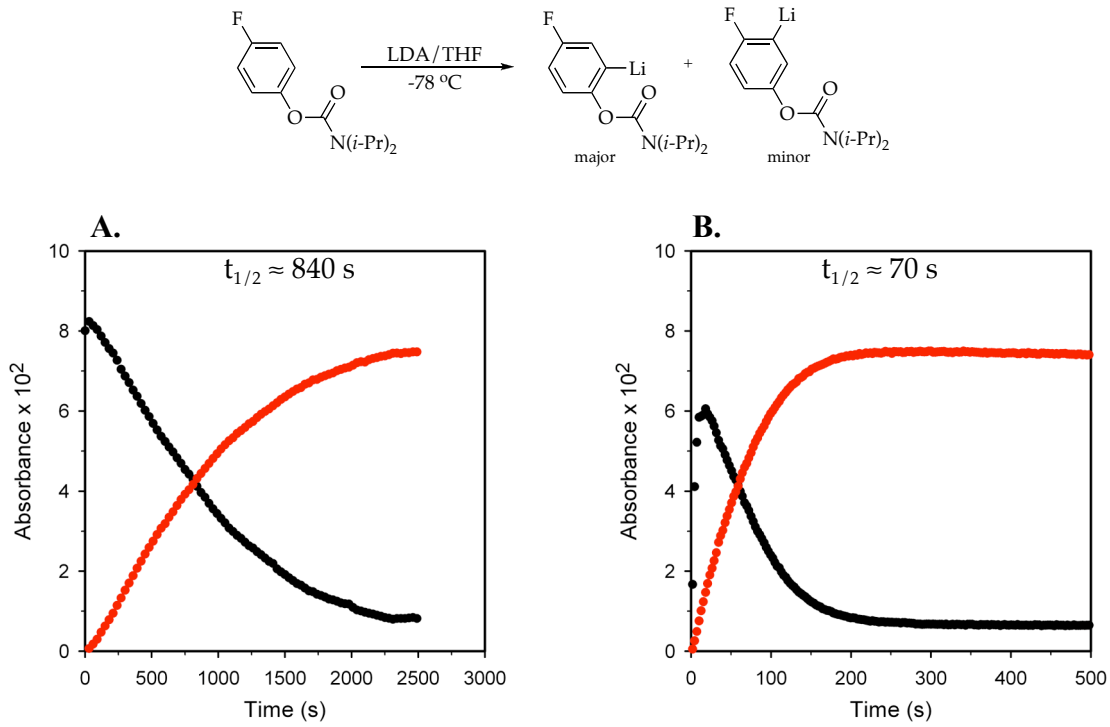

Figure AII.21. Plot of IR absorbances (black – 1717 cm^{-1}, red – 1657 cm^{-1}) versus time for the ortholithiation of 4-fluorophenyl-*N*,*N*-diisopropylcarbamate (0.025 M) with LDA (0.12 M) in neat THF at -78 °C: (A) no added LiCl; (B) 0.5 mol% LiCl.

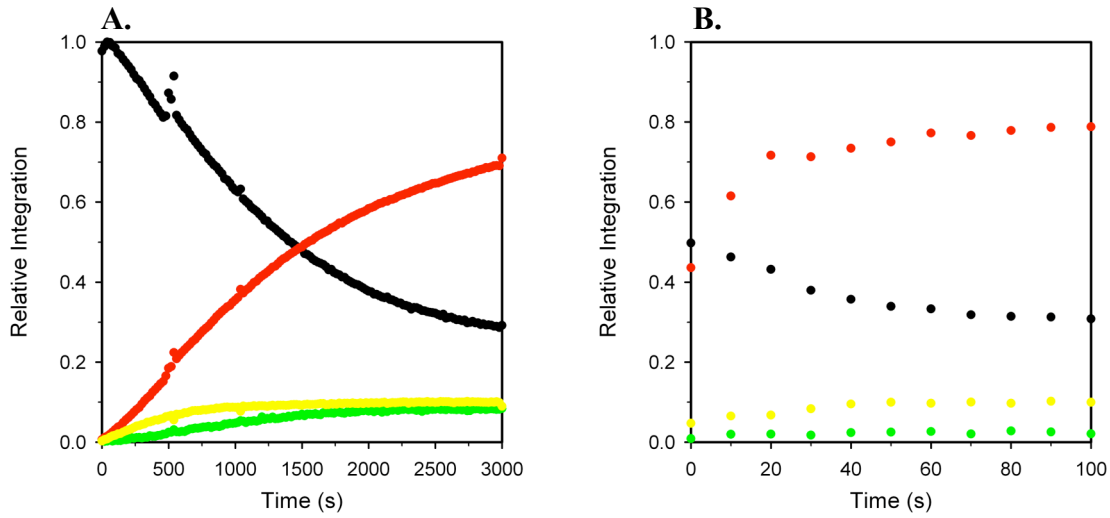

Figure AII.22. Plot of ^{19}F NMR peak integrations (black: δ -118.8, red: δ -123.7, green: δ 85.5, yellow: δ -124.1) versus time for the ortholithiation of 4-fluorophenyl-*N*,*N*-diisopropylcarbamate (0.05 M) with LDA (0.20 M) in neat THF at -78 °C: (A) no added LiCl; (B) 10 mol% LiCl.

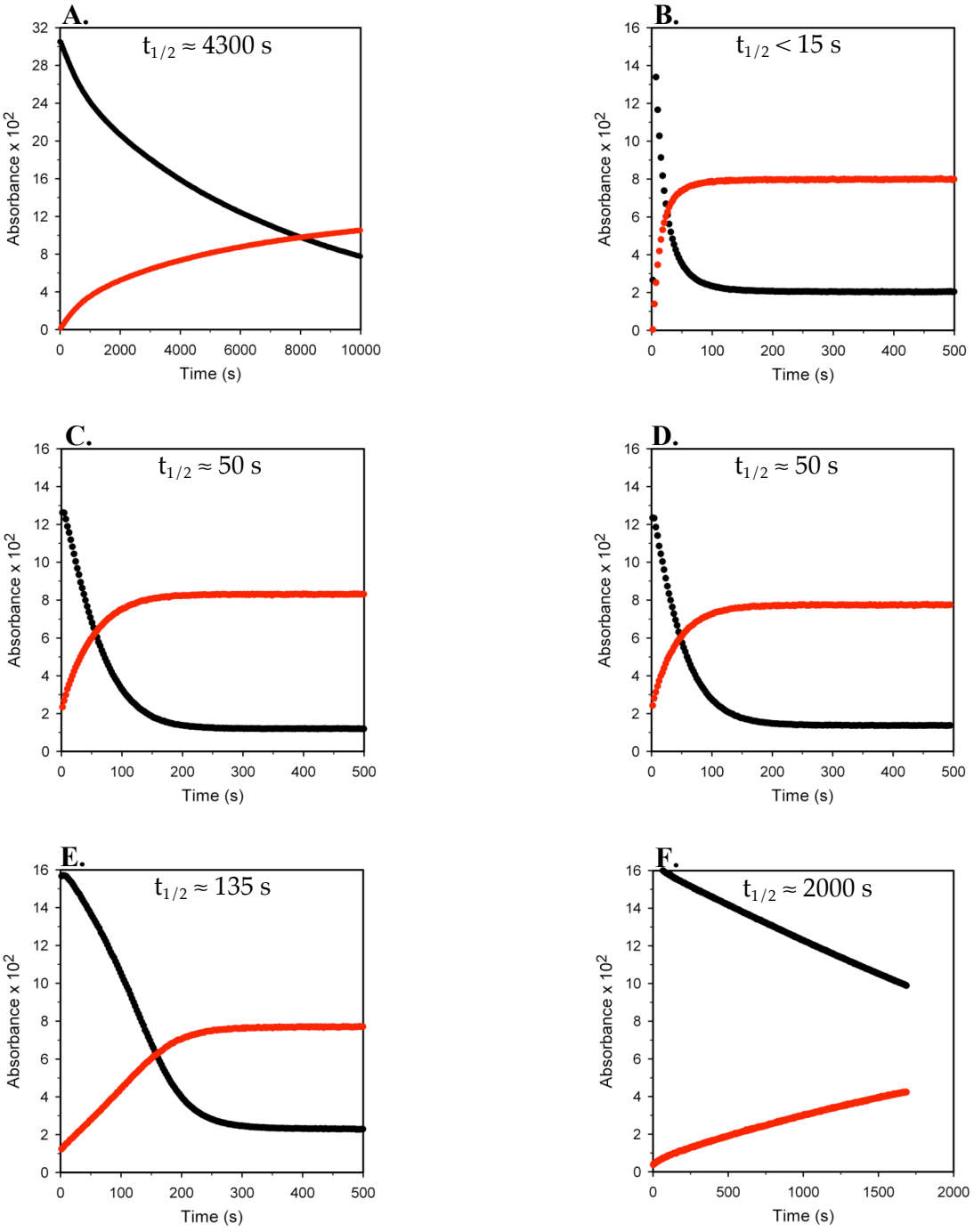

Figure AII.23. Plot of IR absorbances (black – 1507 cm^{-1}, red – 1418 cm^{-1}) versus time for the ortholithiation of 1,4-difluorobenzene (0.10 M) with LDA (0.12 M) in neat THF at -78 °C: (A) no additive; (B) 10 mol% LiCl; (C) 10 mol% LiBr; (D) 10 mol% PhCCLi; (E) 10 mol% PhCOOLi; (F) 10 mol% PhOLi.

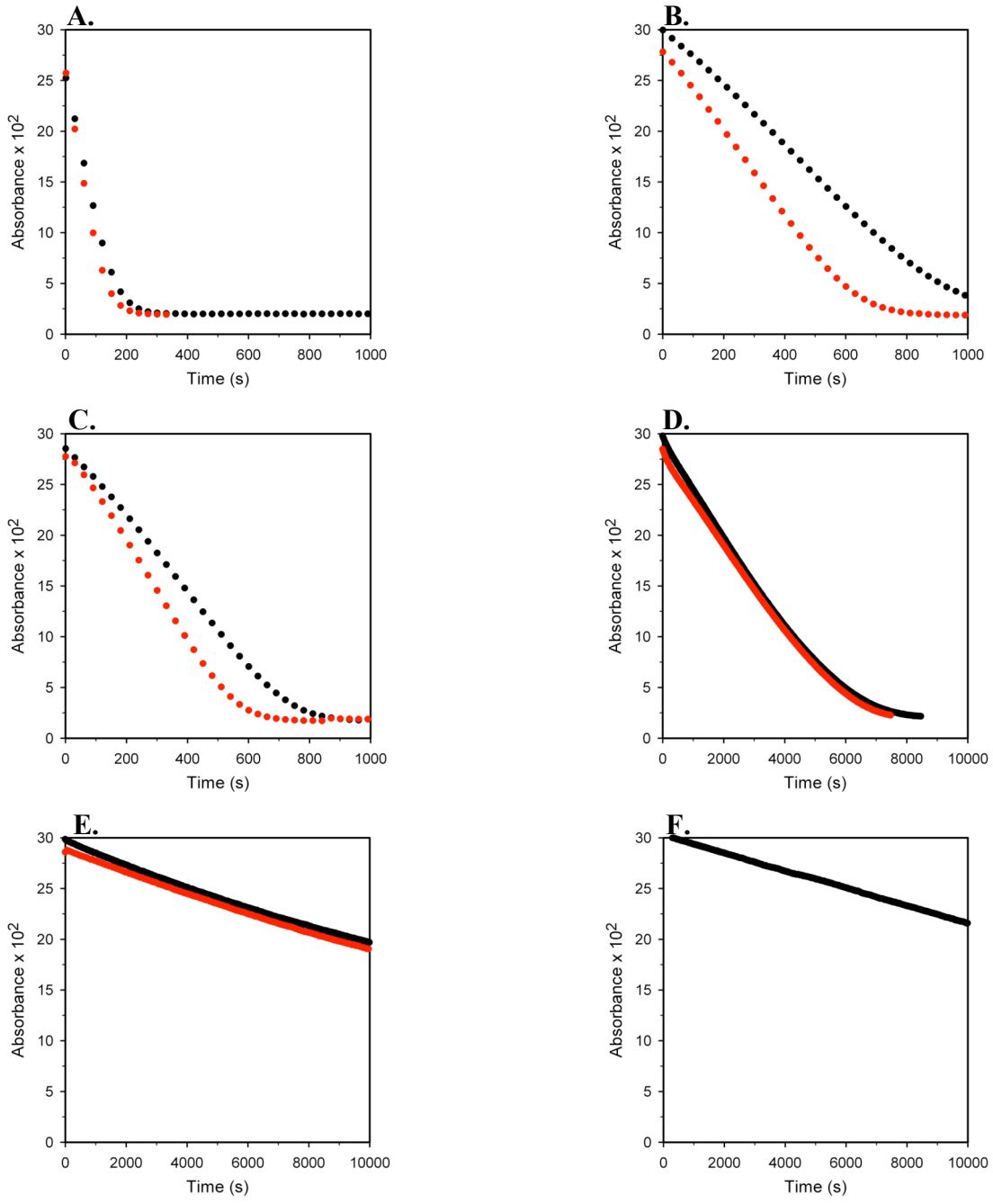

Figure AII.24. Plot of IR absorbances (black/red – duplicated rates) versus time for the ortholithiation of 1,4-difluorobenzene (0.10 M) with LDA (0.12 M) in 10.0 M THF/hexane at -78 °C using: (A) Acros *n*-BuLi – batch1; (B) Acros *n*-BuLi – batch2; (C) Aldrich *n*-BuLi – batch1; (D) Aldrich *n*-BuLi – batch2; (E) Acros LDA; (F) Aldrich LDA

REFERENCES II

1. (a) Hartung, C. G.; Snieckus, V. In *Modern Arene Chemistry*, Astruc, D. (Ed.), Wiley-VCH: Weinheim, 2002; Chapter 10. (b) Snieckus, V. *Chem. Rev.* **1990**, *90*, 879. (c) Schlosser, M.; Mongin, F. *Chem. Soc. Rev.* **2007**, *36*, 1161. (d) Mongin, F.; Quéguiner, G. *Tetrahedron* **2001**, *57*, 4059.

2. (a) Seebach, D. *Angew. Chem., Int. Ed. Engl.* **1988**, *27*, 1624. (b) Seebach, D. In *Proceedings of the Robert A. Welch Foundation Conferences on Chemistry and Biochemistry*; Wiley: New York, 1984. (c) Tchoubar, B.; Loupy, A. *Salt Effects in Organic and Organometallic Chemistry*; VCH Publishers: New York, 1992; Chapters 4, 5, and 7. (d) Caubère, P. *Chem. Rev.* **1993**, *93*, 2317. (e) Juaristi, E.; Beck, A. K.; Hansen, J.; Matt, T.; Mukhopadhyay, T.; Simson, M.; Seebach D. *Synthesis* **1993**, 1271.

3. (a) Kummer, D. A.; Chain, W. J.; Morales, M. R.; Quiroga, O.; Myers, A. G. *J. Am. Chem. Soc.* **2008**, *130*, 13231. (b) Galiano-Roth, A. S.; Kim, Y.-J.; Gilchrist, J. H.; Harrison, A. T.; Fuller, D. J.; Collum, D. B. *J. Am. Chem. Soc.* **1991**, *113*, 5053. (c) Lipshutz, B. H.; Wood, M. R.; Lindsley, C. W. *Tetrahedron Lett.* **1995**, *36*, 4385.
(d) Dyke, A. M.; Gill, D. M.; Harvey, J. N.; Hester. A. J.; Lloyd-Jones, G. C.; Munoz, M. P.; Shepperson, I. R. *Angew. Chem., Int. Ed.* **2008**, *47*, 5067.

4. For beneficial effects of other lithium salts on ortholithiation, see: Cottet, F.; Schlosser, M. *Eur. J. Org. Chem.* **2004**, 3793.

5. (a) Bakker, W. I. I.; Wong, P. L.; Snieckus, V. Lithium Diisopropylamide. In *e-EROS*; Paquette, L. A., Ed.; John Wiley & Sons: New York, 2001. (b) Clayden, J. *Organolithiums: Selectivity for Synthesis*; Baldwin, J. E., Williams, R. M., Eds.; Pergamon: New York, 2002.

6. Rennels, R. A.; Maliakal, A. J.; Collum, D. B. *J. Am. Chem. Soc.* **1998**, *120*, 421.

7. Kim, Y.-J.; Bernstein, M. P.; Galiano-Roth, A. S.; Romesberg, F. E.; Fuller, D. J.; Harrison, A. T.; Collum, D. B.; Williard, P. G. *J. Org. Chem.* **1991**, *56*, 4435.

8. Evans, A. *Potentiometry and Ion-Selective Electrodes*. New York: Wiley, 1987.

9. Dasgupta, D. K. *Anal. Chem.* **1992**, *64*, 775A.

10. (a) Snaith and coworkers clearly articulated the merits of NH_4X salts as precursors to anhydrous LiX salts: Barr, D.; Snaith, R.; Wright, D. S.; Mulvey, R. E.; Wade, K. *J. Am. Chem. Soc.* **1987**, *109*, 7891. (b) Also, see: Hall, P. L.; Gilchrist, J. H.; Collum, D. B. *J. Am. Chem. Soc.* **1991**, *113*, 9571.

11. Zhao, P.; Collum, D. B. *J. Am. Chem. Soc.* **2003**, *125*, 14411.

12. Rein, A. J.; Donahue, S. M.; Pavlosky, M. A. *Curr. Opin. Drug Discovery Dev.* **2000**, *3*, 734.

13. Weymeels, E.; Awad, H.; Bischoff, L.; Mongin, F.; Trécourt, F.; Quéguiner, G.; Marsais, F. *Tetrahedron* **2005**, *61*, 3245.

14. Singh, K. J.; Hoepker, A. C.; Collum, D. B. *J. Am. Chem. Soc.* **2008**, *130*, 18008.

15. We define $k_{\mathrm{LiCl}} = t_{1/2}(\text{no LiCl})/t_{1/2}(0.5\%\ \text{LiCl})$

16. The regioselectivity for **2** is assigned based on a marked upfield shift of the ^{19}F resonance in one isomer but not the other. The regioselectivity in **1** is based on a literature report: Dabrowski, M.; Kubicka, J.; Lulinski, S.; Serwatowski *Tetrahedron Lett.* **2005**, *46*, 4175.

17. Trecourt, F.; Mallet, M.; Marsais, F.; Queguiner, G. *J. Org. Chem* **1988**, *53*, 1367.

18. Kofron, W. G.; Baclawski, L. M. *J. Org. Chem.* **1976**, *41*, 1879.

19. Arene preparations: (a) Table 1, entries 2, 3, 14, 15, and compound **2**: Lustig, E.; Benson, W. R.; Duy, N. *J. Org. Chem.* **1967**, *32*, 851. Yamagami, C.; Takao, N.; Nishioka, T.; Fujita, T.; Takeuchi, Y. *Org. Magn. Reson.* **1984**, *22*, 439. (b) Table 1, entry 7: Newman, M. S.; Kannan, R. *J. Org. Chem.* **1979**, *44*, 3388. (c) Table 1, entry 8: Tsukazaki, M.; Snieckus, V. *Can. J. Chem.* **1992**, *70*, 1486. (d) Table 1, entry 17: Harris, T. D.; Neuschwander, B.; Boekelheide, V. *J. Org. Chem.* **1978**, *43*, 727.

CHAPTER III

Lithium Diisopropylamide-Mediated Ortholithiation of 2-Fluoropyridines: Rates, Mechanisms, and the Role of Autocatalysis

Lithium Diisopropylamide-Mediated Ortholithiation of 2-Fluoropyridines: Rates, Mechanisms, and the Role of Autocatalysis

Abstract

Lithium diisopropylamide (LDA)-mediated ortholithiations of 2-fluoropyridine and 2,6-difluoropyridine in tetrahydrofuran at -78 °C were studied using a combination of IR and NMR spectroscopies and computational methods. The dominant reaction pathway at the outset of the reaction involves substrate-assisted, rate-limiting deaggregation of LDA dimer. Standard and competitive isotope effects confirm post-rate-limiting proton transfer. Rate studies show a direct deaggregation of LDA dimer occurs parallel with an unprecedented tetramer-based pathway. Autocatalysis that emerges as the reaction proceeds originates from ArLi-catalyzed deaggregation of LDA that, paradoxically, proceeds through 2:2 LDA-ArLi mixed tetramers. A hypersensitivity of the ortholithiation rates to traces of LiCl derives from lithium chloride-catalyzed dimer-monomer exchange and a subsequent monomer-based ortholithiation. Once again, 2:2 LDA-LiCl mixed tetramers are suggested to be key intermediates. The mechanisms of the uncatalyzed and catalyzed deaggregations are discussed. A general mechanistic paradigm is delineated to explain a number of seemingly disparate LDA-mediated reactions, all of which occur in tetrahydrofuran at -78 °C.

Introduction

We describe herein mechanistic studies of the lithium diisopropylamide (LDA)-mediated ortholithiation of 2-fluoropyridines (eq

1).[1,2,3] The ortholithiations of **1** and **2** join the ranks of a growing number of LDA-mediated reactions carried out in THF at –78 °C—conditions used routinely by synthetic chemists[4]—in which especially high substrate reactivities cause aggregation events to become partially or totally rate limiting.[5,6] Reactions in this emerging class often display virulent autocatalysis, a penchant toward catalysis by added lithium salts (LiCl in particular), and hypersensitivity to impurities. The mechanistic complexity—a spike in the number of variables that influence the time course of the lithiations—is unlike anything we've detected during studies of organolithium reaction mechanisms that span 25 years.[7] The particular case of fluoropyridine metalation brings two baffling contributions to the developing picture: (1) a substrate-catalyzed deaggregation of LDA dimer **5** that is difficult to explain using conventional models of ligand-based catalysis, and (2) reaction orders in LDA and catalytically active lithium salts (aryllithium **3** and LiCl) that attest to *associative* aggregation events. Both of these new mechanistic wrinkles are, to date, affiliated only with 2-fluoropyridine metalations.

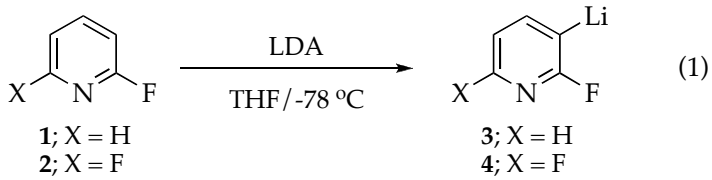

1; X = H
2; X = F

3; X = H
4; X = F

(1)

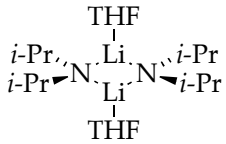

5

While browsing through the paper, those who use LDA routinely should note that commercial samples of LDA behave quite similarly to the

analytically pure LDA used in the rate studies below. By contrast, LDA generated in situ from *n*-BuLi and diisopropylamine is equivalent to LDA/LiCl mixtures by manifesting substantially greater reactivity than LiCl-free LDA. As a final reference point, the results section details the protocols and data for specialists. The discussion assumes a more tutorial format, offering a mechanistic paradigm that covers a number of LDA-mediated reactions, summarizes what we have learned, and discusses issues that linger. We begin, however, with background material that will aid in understanding the results.

Background

During studies of LDA/THF-mediated imine metalations we noticed that one particularly reactive imine—the only imine for which a reaction temperature of –78 °C is required for monitoring the metalation rate (eq 2)—failed to follow the standard exponential decay, instead showing an oddly linear decay throughout the first two half lives. We spent little time pondering the underlying cause of this aberration.[8]

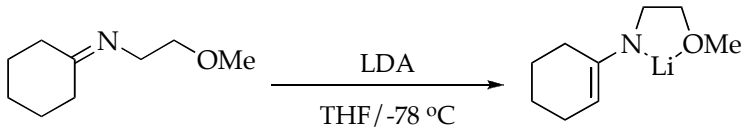

(2)

During studies of LDA/THF-mediated ortholithiations of carbamates, the most reactive 3-fluorocarbamate (eq 3) displayed a decidedly linear decay to full conversion (more than five half-lives) that was impossible to ignore.[5a] We suspected that the linear losses of arene **6**—an apparent zeroth-order

dependence[9]—derived from a rate-limiting deaggregation of LDA dimer followed by post-rate-limiting proton transfer. Relatively minor changes in conditions, however, afforded sigmoidal decays characteristic of autocatalysis.[10] Rate studies showed a first-order rather than a zeroth-order dependence on **6** that did *not* derive from a simple (uncatalyzed) deaggregation of LDA dimer **5**. The linear and sigmoidal decays were traced to an autocatalytic condensation of aryllithium **7** with LDA dimer **5**. Isomeric LDA-ArLi mixed dimers **8** and **9** were shown to react rapidly on the time scales of aggregate exchanges. Whether **8** and **9** reacted directly or by facile dissociation remained open to speculation. The metalation was also markedly catalyzed by low concentrations of LiCl (<0.5 mol %).

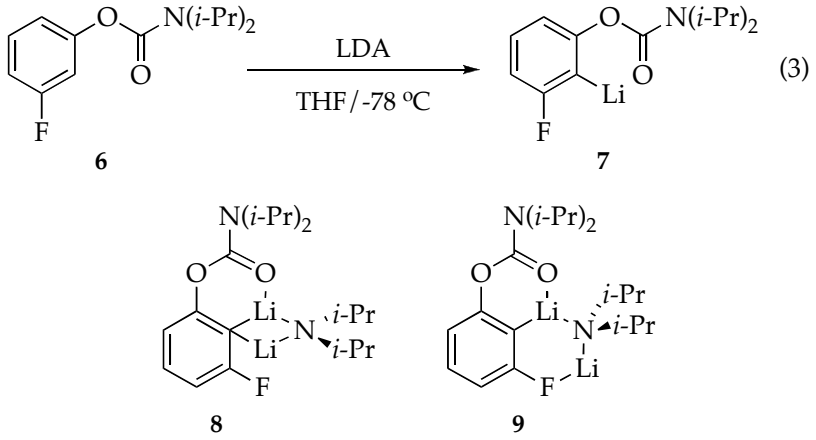

(3)

Subsequent studies showed that a number of LDA/THF-mediated lithiations of fluorinated arenes at –78 °C display strange time-dependent decays and are susceptible to autocatalysis and LiCl catalysis.[11] For example, LDA/THF-mediated ortholithiation of arene **10** at –78 °C follows a linear disappearance of **10** and the kinetically-controlled formation of regioisomeric aryllithiums **11** and **12** followed by a slower equilibration (eq 4).[5c] Rate studies

reveal a true zeroth-order dependence on **10** with an overlay of autocatalysis. The uncatalyzed deaggregation proceeds via a disolvated dimer; transition structure **13** is supported by density functional theory (DFT) computations. Marked acceleration with LiCl was traced to the catalysis of LDA dimer-monomer exchange with an accompanying shift in the rate-limiting step from deaggregation to proton transfer. Catalysis allowed us to peer beyond the deaggregation and discover that the critical proton transfer proceeds through a monomer-based transition structure (**14**).

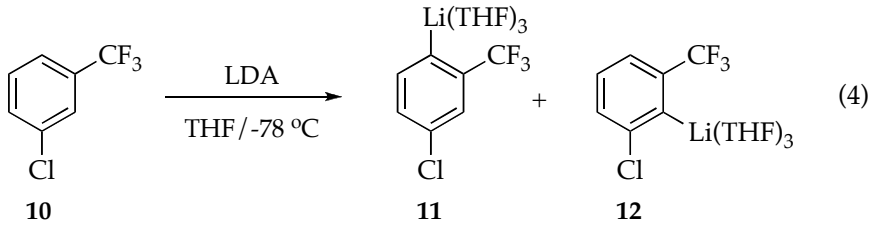

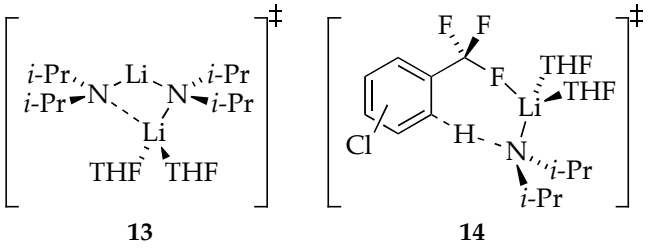

Studies of LDA/THF-mediated 1,4-addition to unsaturated ester **15** at –78 °C (eq 5) revealed a linear loss of substrate, confirming that the strange kinetics are restricted to neither ortholithiations nor fluorinated substrates.[5b] In analogy to the ortholithiation in eq 4, the linear decay results from a zeroth-order dependence in substrate—a rate-limiting deaggregation. Notably, the critical deaggregation occurs via a *trisolvated*-dimer-based transition structure suggested by DFT computations to be trisolvate **17** rather than disolvate **13**.

The existence of distinctly different rate-limiting deaggregations is emerging as a central issue. Autocatalysis, although muted because of the low catalytic efficacy of enolates,[5b] elicits counterintuitive rate changes. Once again, LiCl markedly accelerates the reaction by catalyzing dimer-monomer exchange. By shifting the rate-limiting step, LiCl catalysis allowed us to show that the 1,4-addition proceeds via a monosolvated-monomer-based transition structure; computations supported **18**.

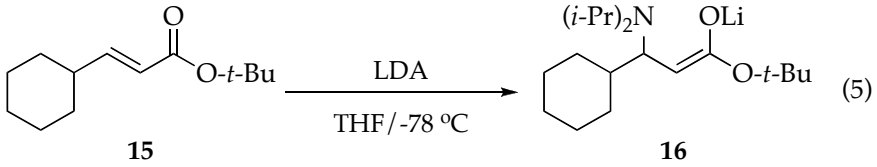

15 **16** (5)

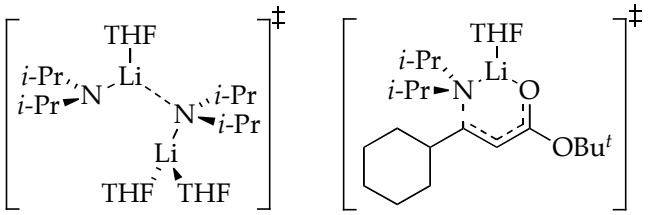

17 **18**

Recognizing the importance of LDA aggregation events for reactions in THF at –78 °C, we carried out detailed NMR spectroscopic and DFT computational studies of the dynamic behavior of LDA.[12] NMR spectroscopic studies showed that subunit exchanges (at least nuclear exchanges) occur on approximately the same time scales as the reactions described above (half-life > 1 h at 0.10 M LDA in THF at –78 °C). The dominant mechanism of exchange, however, involved an associative pathway via a *tetrasolvated tetramer*. Computational studies probed the role of ladders (Scheme III.1).[13] We could not ascertain, however, whether nuclear exchange involves symmetrized

cyclic tetramer (**20**) or monomer (**22**). The notion that tetramers are possible sources of monomers, however, has a mechanistic appeal that is discussed below.

Scheme III.1

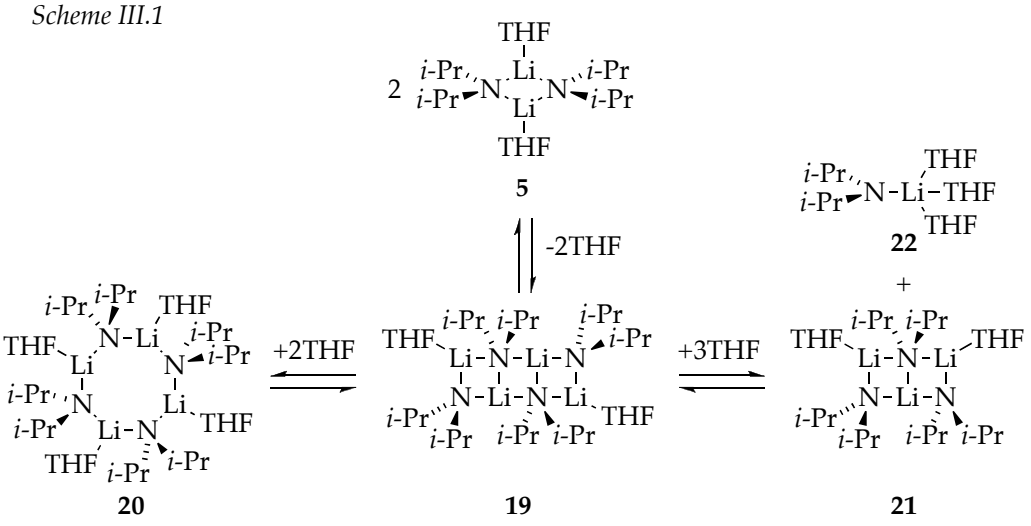

Computational studies of the apparently slower direct (dissociative) conversion of dimer **5** to monomer **22** revealed a complex series of transformations; the most notable intermediates are shown in Scheme III.2.[12] The computed activation barriers for the exchanges in Scheme III.2 rise monotonically on progression from dimer **5** to monomer **22**. Thus, an uncatalyzed, dissociative conversion of dimer **5** to monomer **22** is predicted to involve reversible formation of **23**-**25** and rate-limiting cleavage of **25** via transition structure **17**. Intermediates **23**-**25**, however, are potentially important determinants of LDA reactivity (vide infra).

Scheme III.2

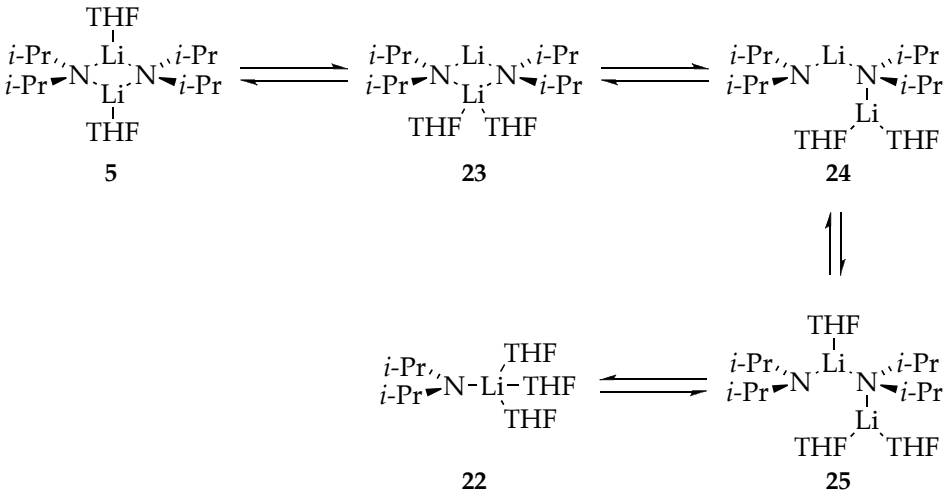

Results

Solution Structures.[14] Structural assignments of LDA and aryllithiums are required to interpret the rate data. Previous studies of [^{6}Li,^{15}N]LDA using ^{6}Li and ^{15}N NMR spectroscopies reveal exclusively disolvated dimer **5**.[15,16] The ^{13}C NMR spectrum of ArLi **3** shows the lithiated carbon as two 1:1:1 triplets (doublet of triplets) arising from the superposition of ^{6}Li-^{13}C coupling ($^{1}J_{\text{Li-C}}$ = 11.7 Hz) that is split further by especially large ^{13}C-^{19}F coupling ($^{2}J_{\text{F-C}}$ = 124.3 Hz) emblematic of 2-fluoroaryllithiums.[17,18,19] The ^{19}F{^{1}H}NMR spectrum displays a singlet.[20] Aryllithium **3** in the presence of [^{6}Li,^{15}N]LDA shows no ^{6}Li-^{15}N splitting in **3**, confirming the absence of mixed aggregation.[15] Aryllithium **4** displays spectroscopic properties similar to those of **3** with additional splitting arising from the fluoro moiety at the 6 position. DFT computations of **3** and **4** at the B3LYP/6-31G(d) level[21] with single point calculations at the MP2 level of theory implicate trisolvated monomers (**3a** and **4a**) in accord with other monomeric aryllithiums.[22,23] Numbers **3** and **4** are

often used interchangeably with **3a** and **4a** throughout the text, depending on the specific context.

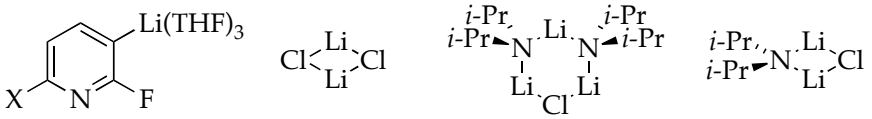

3a; X = H
4a; X = F

26

27

28

Catalysis by LiCl is discussed in light of the structures of LiCl homoaggregate and LDA-LiCl mixed aggregates. Previous studies showed LiCl to be dimeric (**26**) in THF solution.[7,24] Mixtures of LDA with very low LiCl concentrations (≤2 mol % LiCl) used in the rate studies described below afford a [LiCl]-independent 8:1 mixture of **27** and **28** to the exclusion of free LiCl.[5b,24] Solutions containing [^{6}Li]LiCl and **3a** or **4a** show no evidence of LiCl-ArLi mixed aggregates.

Rate Studies: General Protocols. We have historically used recrystallized *n*-BuLi[25] to prepare LDA and then recrystallized the resulting LDA.[18] Although potentiometry[26] and ion chromatography[27] have shown that LDA prepared in this manner contains <0.02 mol % LiCl,[5a] the purity proved inadequate for the studies described below because of detectable accelerations elicited by as little as 0.001 mol % LiCl. Accordingly, we prepared LiCl-free LDA from lithium metal and diisopropylamine using a modified[5b] literature protocol[28] and recrystallized the resulting LDA from hexane, rendering the residual variability tolerable.[29] Explicitly added anhydrous LiCl was generated in THF solution by lithiation of $Et_3N{\cdot}HCl$ with LDA.[30] Et_3N is a poor ligand[31] that has no effect on solution structures or reaction rates. Similarly, added diisopropylamine does not influence the ortholithiation.[17]

Reactions were monitored using in situ IR[34] or ^{19}F NMR spectroscopy,[20] the former offering convenience and the latter affording resolution of all ArH and ArLi-related species. The choice of method depended on specific needs. In a broader sense, we tactically attempted to study the mechanisms in isolation (under limiting conditions) to the maximum extent possible. Autocatalysis placed an importance on the method of initial rates,[33a] obtained by fitting the raw data measured at early conversion and extracting the first derivative from a polynomial fit.[34] Rate laws were routinely assessed using their integral forms. Numeric integrations of the corresponding differential forms allowed us to include provisions for autocatalysis and other nonlimiting behaviors.

Substrate Dependence. Lithiation using LDA at 0.10 M[35] and **1** at 0.002 M concentrations affords a linear decay (Figure III.1, curve A). Increasing the substrate concentration to 0.004 M causes detectable downward curvature, which becomes prominent at elevated substrate concentrations (Figure III.1, curve B). Downward curvatures are characteristic of autocatalysis.[10] Plotting initial rates—the rates displayed before the onset of autocatalysis—versus substrate concentration (Figure III.2) reveals a first-order dependence on substrate along with a nonzero y-intercept that is either small or simply experimental error. Thus, the linear decay at the lowest substrate concentration could arise from (1) the reduction (but not complete elimination) of autocatalysis by the low concentrations of ArLi,[36] or (2) a zeroth-order substrate dependence accompanying the small nonzero intercept. Throughout the remainder of the text, allusions to low and high substrate concentrations (0.002 and 0.10 M, respectively) represent probes of a minor (or nonexistent) substrate-independent pathway and the dominant substrate-dependent pathway, respectively.

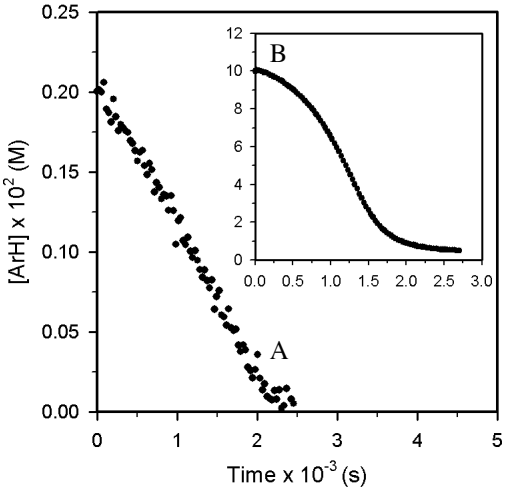

Figure III.1. Plot of [**1**] vs time for the ortholithiation of **1** with LDA (0.10 M) in THF (12.20 M) at -78 °C: (A) [**1**] = 0.002 M; (B) [**1**] = 0.10 M.

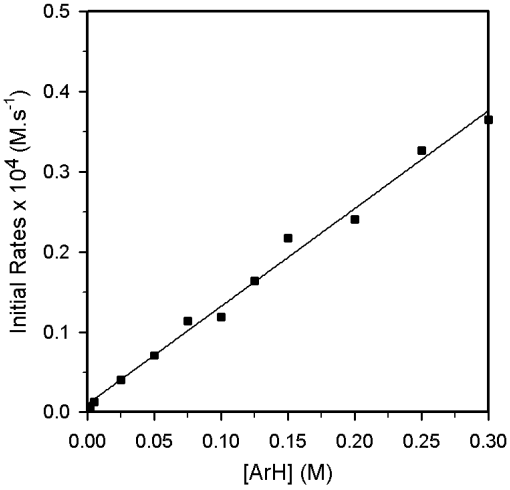

Figure III.2. Plot of initial rates vs [**1**] for the ortholithiation of **1** with LDA (0.10 M) in THF (12.20 M) at -78 °C. The curve depicts an unweighted least-squares fit to $-d[\mathbf{1}]/dt = k[\mathrm{ArH}] + k'$ ($k = (1.22 \pm 0.04) \times 10^{-4}$, $k' = (1.0 \pm 0.6) \times 10^{-6}$).

THF Dependence. A plot of initial rates versus THF concentration[35] at low substrate concentration (Figure III.3, curve A) shows an inverse dependence that is oddly linear. (Normal inverse dependencies are hyperbolic.)[7,33a] The inhibition by THF was shown to derive from secondary-shell solvation (medium effects) using a well-tested protocol[37] in which 2,5-dimethyltetrahydrofuran is used as a polar but noncoordinating cosolvent[38] to maintain a constant polarity of the medium (curve B).

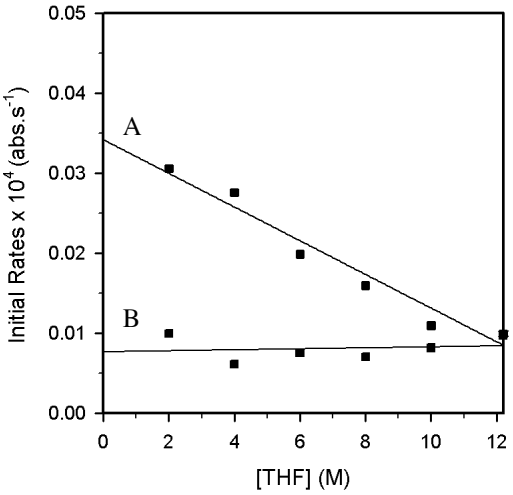

Figure III.3. Plot of initial rates vs [THF] for the ortholithiation of **1** (0.002 M) with LDA (0.10 M) at -78 °C in: (A) hexane cosolvent. The curve depicts an unweighted least-squares fit to $-d[\mathbf{1}]/dt = -k[\mathrm{THF}] + k'$ ($k = (2.1 \pm 0.2) \times 10^{-7}$, $k' = (3.4 \pm 0.2) \times 10^{-6}$); (B) 2,5-dimethyltetrahydrofuran cosolvent. The curve depicts an unweighted least-squares fit to $-d[\mathbf{1}]/dt = -k[\mathrm{THF}] + k'$ ($k = (6 \pm 19) \times 10^{-9}$, $k' = (8 \pm 1) \times 10^{-7}$).

LDA Dependence. Plots of initial rates versus LDA concentration reveal perplexing orders of 1.7 ± 0.3 and 1.5 ± 0.3 at low and high substrate concentrations, respectively (Figure III.4). These orders are significantly higher than *any* LDA orders measured to date.[7] We cannot exclude the intervention of an uncontrolled variable; the kinetics are extraordinarily sensitive, as reflected

by the large error. Nonetheless, any temptation to dismiss the unusual orders summarily is tempered by the analogously high LDA orders observed for metalations of difluoropyridine **2** (vide infra) as well as by a value of 1.2 for 3-deutero-2-fluoropyridine, **1-d_1**.

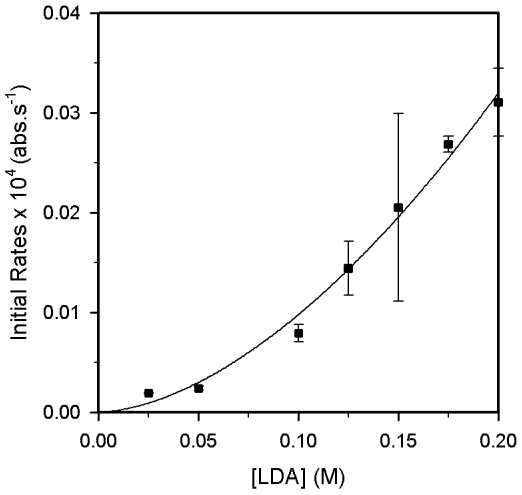

Figure III.4. Plot of initial rates vs [LDA] in THF (11.50 M) using hexane as the cosolvent for the ortholithiation of **1** (0.002 M) at -78 °C. The curve depicts an unweighted least-squares fit to $-d[\mathbf{1}]/dt = k[\mathrm{LDA}]^n$ ($k = (5 \pm 2) \times 10^{-5}$, $n = 1.7 \pm 0.3$).

Partial Mechanisms. It is instructive to amalgamate the data described to this point into partial rate laws and mechanisms. Zeroth-order THF dependencies and first-order pyridine dependencies are observed under all conditions. The high, noninteger LDA orders, however, present special challenges that force us to consider several mechanisms and their combinations. We introduce the following shorthand: A = an LDA subunit; S = THF (e.g., A_2S_2 = **5**); ArH = fluoropyridine **1**; and ArLi = aryllithium **3**.

Dimer Mechanism. The most obvious mechanism is the dimer-based pathway described by eqs 6 and 7. Such dimer-based reactions of LDA have

been observed on many occasions[7,39] but cannot account for the high LDA orders.

$$-d[\mathrm{ArH}]/d\mathrm{t} = k'[\mathrm{ArH}][\mathrm{A_2S_2}][\mathrm{S}]^0 \quad (6)$$

$$\mathrm{A_2S_2} + \mathrm{ArH} \longrightarrow [\mathrm{A_2S_2(ArH)}]^{\ddagger} \quad (7)$$

Trimer Mechanism. A 1.5 LDA order could arise from a dimer-trimer preequilibrium (eqs 8-10). The substrate must participate in the rate-limiting transition structure, although the specific timing of this involvement is unknowable. A dimer-trimer preequilibrium, however, seems to demand the intermediacy of monomers en route to trimers, which is nonsensical given evidence that the lithiation proceeds via LDA monomers (vide infra).

$$-d[\mathrm{ArH}]/d\mathrm{t} = k''[\mathrm{ArH}][\mathrm{A_2S_2}]^{1.5}[\mathrm{S}]^0 \quad (8)$$

$$3\mathrm{A_2S_2} \rightleftharpoons 2\mathrm{A_3S_3} \quad (9)$$

$$\mathrm{A_3S_3} + \mathrm{ArH} \longrightarrow [\mathrm{A_3S_3(ArH)}]^{\ddagger} \quad (10)$$

Tetramer Mechanism. A tetramer-based reaction (eqs 11 and 12) is without precedent in lithium amides[40,41] but receives support from the dynamic NMR and computational studies showing tetramer-based (associative) LDA exchange (Scheme III.1).[12] A tetramer-based mechanism cannot, in isolation, account for the high and fractional LDA orders.

$$-d[\mathrm{ArH}]/d\mathrm{t} = k'''[\mathrm{ArH}][\mathrm{A_2S_2}]^2[\mathrm{S}]^0 \quad (11)$$

$$2\mathrm{A_2S_2} + \mathrm{ArH} \longrightarrow [\mathrm{A_4S_4(ArH)}]^{\ddagger} \quad (12)$$

Dimer/Tetramer Composite Mechanism. Combinations of the dimer- and tetramer-based mechanisms in parallel are described by eq 13. The composite mechanism includes provisions for any LDA order in the range of 1.0-2.0.

$$-d[\mathrm{ArH}]/d\mathrm{t} = k'[\mathrm{ArH}][\mathrm{A_2S_2}][\mathrm{S}]^0 + k'''[\mathrm{ArH}][\mathrm{A_2S_2}]^2[\mathrm{S}]^0 \qquad (13)$$

Isotope Effects. The first-order substrate dependence appears to implicate mechanism(s) that, although disquieting in detail, involves rate-limiting proton transfer(s). Isotopic labeling studies, however, show that *the critical proton transfer step is post rate limiting.*

The loss of 0.002 M **1-*d*$_1$** versus time displays a substantial upward curvature that contrasts with the linear decay of **1** (Figure III.5). Comparing initial rates for **1** and **1-*d*$_1$** measured independently (rather than in direct competition) reveals a small isotope effect ($k_H/k_D = 1.82 \pm 0.08$; Scheme III.3).[42]

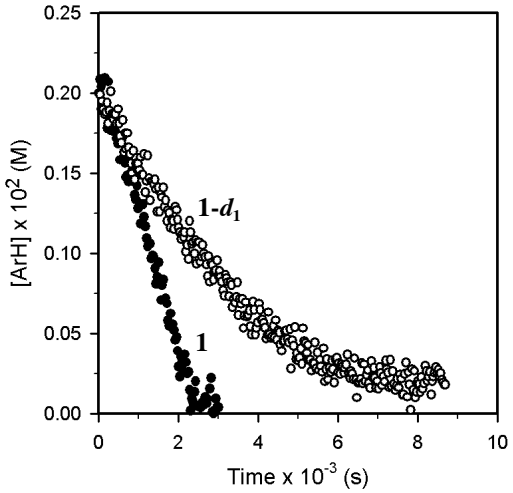

Figure III.5. Plot of [ArH] vs time for the ortholithiation of 0.002 M **1** and **1-*d*$_1$** with LDA (0.10 M) in THF (12.20 M) at -78 °C.

An even smaller value is obtained at high substrate concentrations (k_H/k_D = 1.1 ± 0.3). Metalations of **1** and **1-*d*$_1$** *in competition* can be monitored using ^{19}F NMR spectroscopy by exploiting isotopically sensitive ^{19}F chemical shifts.[43] The resulting isotope effect—loosely referred to as a competitive isotope effect and discussed extensively below[44]—is large (k_H/k_D = 35 ± 1; Scheme III.3) but within the normal range for such lithiations.[45]

The combination of small standard and large competitive isotope effects offers compelling evidence of a post-rate-limiting proton transfer. This conclusion is supported by following the competition of **1** and **1-*d*$_1$** to full conversion (Figure III.6). Arene **1-*d*$_1$** reacts in earnest only after **1** is fully consumed. Such biphasic behavior is observed over a large (0.002-0.10 M) range of substrate concentrations. The curves in Figure III.6 correspond to a best-fit numerical integration to the simplified model in Scheme III.3. (A model in which the key intermediate is an activated dimer, A_2*, rather than two monomers fits equally well.)

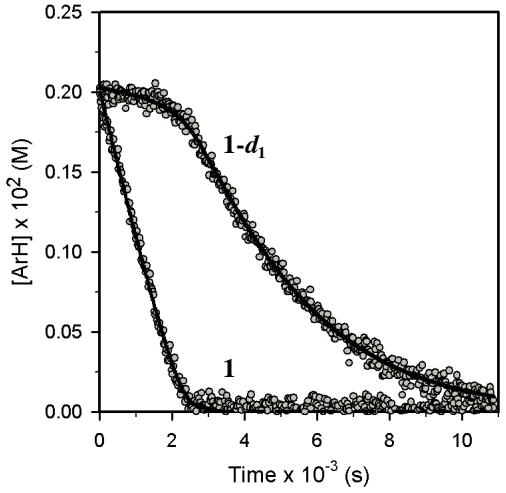

Figure III.6. Plot of [ArH] vs time for the ortholithiation of a mixture of fluoropyridines **1** and **1-*d*$_1$** (0.002 M each) with LDA (0.10 M) in THF (12.20 M) at -78 °C, monitored by ^{19}F NMR spectroscopy. The functions result from best-fit numerical integration to the model in Scheme III.3.

Scheme III.3

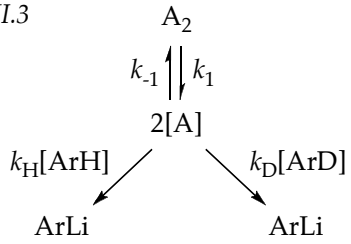

Two additional observations are subtle but important. First, the large competitive isotope effect following the rate-limiting deaggregation *requires* that facile ArH/ArD ligand exchange occurs on the fleeting deaggregated form of LDA (monomer A in Scheme III.3, for example) *before* the proton transfer. Second, the small but measurable standard isotope effect and upward curvature arising from **1-*d*$_1$** (Figure III.5, curve B) indicate that deuterium transfer is *partially* rate limiting, which is supported by the fit showing a 20:1 ratio of the forward to back reaction rates (k_D[ArD][A]/k_{-1}[A]^2 = 20).

Ligand Catalysis. We attempted to mimic substrate-catalyzed deaggregation with a variety of added ligands, including pyridine (**29**), fluorobenzene (**30**), and silylated fluoropyridine **31**; none detectably catalyzed the metalation of **1**. Curiously, 6-silyl pyridine **32** metalates nearly as efficiently as **1** despite the hindrance about the nitrogen, and it appears to be susceptible to the same substrate-catalyzed deaggregation. Catalysis of deaggregation is a recurring theme in subsequent sections.

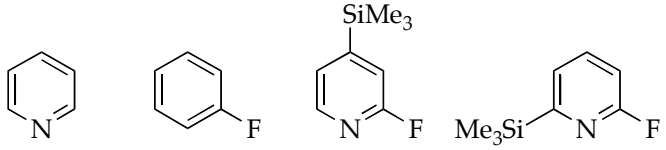

29 **30** **31** **32**

LiCl Catalysis. The curvature arising from autocatalysis[5a,9] as well as previous studies of ortholithiation[11] foreshadow catalysis by LiCl. Indeed, traces of LiCl elicit marked rate accelerations accompanied by distinct upward curvatures (Figure III.7). First-order decays are observed at >0.3 mol % LiCl. A plot of the initial rates versus LiCl concentration shows saturation kinetics (Figure III.8). Sigmoidal curvature evident at the low LiCl concentrations signifies a high (possibly second) order in LiCl.

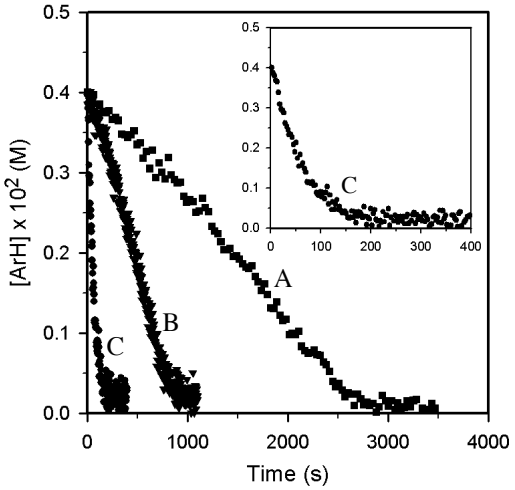

Figure III.7. Plot of [**1**] vs time for the ortholithiation of **1** (0.004 M) with LDA (0.10 M) in 12.20 M THF at -78 °C in the presence of varying mol percentages of LiCl: (A) no LiCl; (B) 0.05 mol% LiCl; (C) 0.6 mol% LiCl.

The saturation behavior in Figure III.8 is *not* Michaelis-Menten kinetics, which would require stoichiometric LiCl to attain saturation. Seemingly analogous LiCl saturation behavior (absent the sigmoid) observed for 1,4-additions of LDA to unsaturated esters was traced to LiCl-catalyzed deaggregation of LDA accompanied by a shift in the rate-limiting step.[5b] Indeed, monitoring the ortholithiation of **1** at full saturation (2 mol % LiCl)

reveals large standard and competitive isotope effects (k_H/k_D = 33 and 23, respectively).

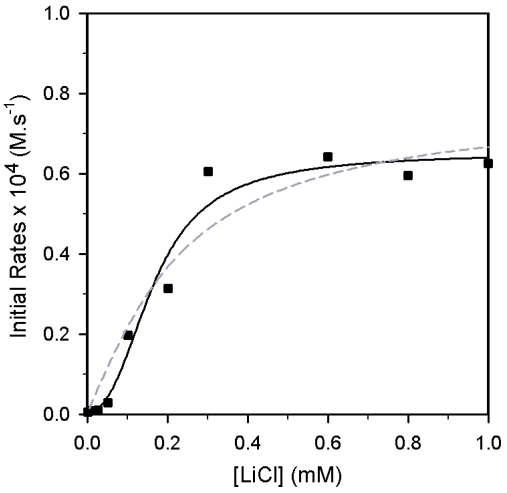

Figure III.8. Plot of initial rates vs [LiCl] for the ortholithiation of **1** (0.004 M) with LDA (0.10 M) in THF (12.20 M) at -78 °C. The curve depicts an unweighted least-squares fit to eq 16. See supporting information for derivation. [ArH] = 0.004 M, $[A_2S_2]_0$ = 0.05 M, c = (5 $\pm$ 1) x 10^{-7}, n = 2 and k_1 = (1.6 $\pm$ 0.1) x 10^{-2}, k_{-1} = (1.03 $\pm$ 0.03) x 10^4, k_2 = (5.901 $\pm$ 0.002) x 10^1. The dashed curve represents a fit to the data where n = 1 in the given equation.

LiCl catalysis causes proton transfer to become rate limiting. In doing so, it offers a view beyond what had been a rate-limiting deaggregation. Plotting k_{obsd} versus LDA concentration (Figure III.9) affords a generic half-order dependence implicating a dimer-monomer preequilibrium. A plot of k_{obsd} versus THF concentration (Figure III.10) shows an ambiguous dependence that could be interpreted as either (1) a first-order dependence with a single renegade point at the highest THF concentration (solid line), or (2) a second-order dependence with a nonzero intercept (dashed line). Although the former seems most palatable by inspection, the latter is supported by the analogous plot using **1-*d*$_1$**, which shows a more distinct

upward curvature (Figure III.10, inset). Thus, we remain agnostic on the solvation number at the rate-limiting transition structure and present the mechanism according to eqs 14-17. The rate law in eq 14 includes provisions for second-order saturation by LiCl (Figure III.8). The odd mathematical form of eq 16 stems from the quadratic equation required by the deaggregation.[22] In the limit of full saturation (>0.3 mol % LiCl), eq 16 reduces to eq 17.

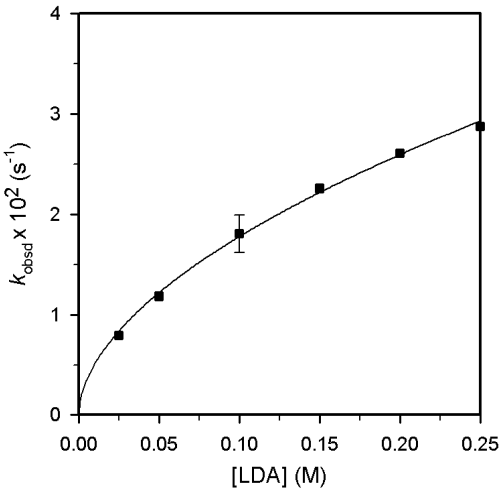

Figure III.9. Plot of k_{obsd} vs [LDA] for the ortholithiation of **1** (0.004 M) in 12.20 M THF in the presence of 2 mol% LiCl at -78 °C. The curve depicts an unweighted least-squares fit to $k_{obsd} = k[\mathrm{LDA}]^n$ ($k = (6.2 \pm 0.4) \times 10^{-2}$, $n = (0.54 \pm 0.03)$).

$$A_2S_2 + 2m\mathrm{THF} \underset{k_{-1}[\mathrm{LiCl_{total}}]^n}{\overset{k_1[\mathrm{LiCl_{total}}]^n}{\rightleftharpoons}} 2AS_{m+1} \qquad (14)$$

$$AS_{m+1} + \mathrm{ArH} \xrightarrow{k_2} [AS_{m+1}(\mathrm{ArH})]^{\ddagger} \qquad (15)$$

$$-\frac{d[\mathrm{ArH}]}{dt} = \frac{k_2[\mathrm{ArH}]}{4k_{-1}[\mathrm{LiCl}]^n}\left(\sqrt{k_2^2[\mathrm{ArH}]^2 + 16k_1k_{-1}[A_2S_2]_0[\mathrm{LiCl}]^{2n}[\mathrm{THF}]^{2m}} - k_2[\mathrm{ArH}]\right) + c$$

$$(-d[\mathrm{ArH}]/d\mathrm{t} = -\Delta[\mathrm{ArH}]/\Delta\mathrm{t}_{(\mathrm{t}=0)}) \qquad (16)$$

$$-d[\mathrm{ArH}]/dt = (k_1/k_{-1})^{1/2}k_2[\mathrm{ArH}][\mathrm{THF}]^{2m}[\mathrm{LDA}]^{0.5} \quad (17)$$

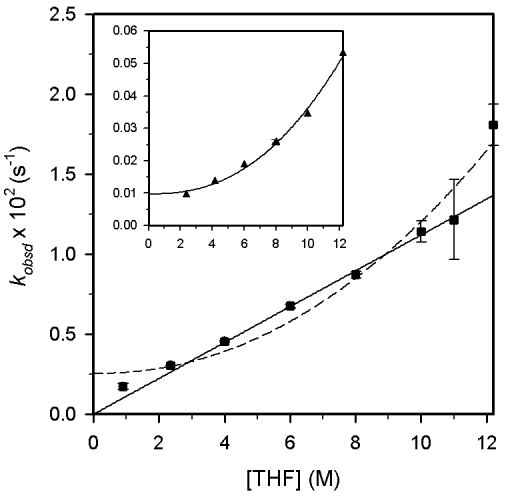

Figure III.10. Plot of k_{obsd} vs [THF] in hexane cosolvent for the ortholithiation of **1** (0.004 M) with LDA (0.10 M) in the presence of 2 mol% LiCl at -78 °C. The solid line depicts an unweighted least-squares fit to $k_{obsd} = k[\mathrm{THF}]$, with the point at 12.2 M THF excluded. ($k = (1.12 \pm 0.03) \times 10^{-3}$) .The dashed line depicts an unweighted least-squares fit to $k_{obsd} = k[\mathrm{THF}]^n + k'$ ($k = (8 \pm 7) \times 10^{-5}$, $n = (2.0 \pm 0.4)$, $k' = (2.5 \pm 0.7) \times 10^{-3}$). Inset shows the corresponding plot for the ortholithiation of **1-*d*$_1$** (0.004 M). The curve depicts an unweighted least-squares fit to $k_{obsd} = k[\mathrm{THF}]^n + k'$ ($k = (1.1 \pm 0.6) \times 10^{-6}$, $n = (2.4 \pm 0.2)$, $k' = (10 \pm 1) \times 10^{-5}$).

A highly attenuated saturation behavior is observed for LiCl-catalyzed lithiations of **1-*d*$_1$** (supporting information). The barely discernible catalysis supports the previous assertion that deuteration renders the proton transfer partially rate limiting.

Partial Mechanisms Revisited. With the LiCl catalysis implicating monomer-based metalation of somewhat ambiguous solvation number, we turned to DFT computations to fill in some details. Mono-, di-, and trisolvated-monomer-based transition structures **33**-**35** are all viable; the

disolvate is suggested to be the preferred form. As noted previously, Li-F interactions are important determinants of organolithium reaction mechanisms.[5a,46,47] Intrinisic reaction coordinate (IRC) calculations show that the minima preceding and succeeding **34** correspond to **36** and **37**, respectively (eq 18).

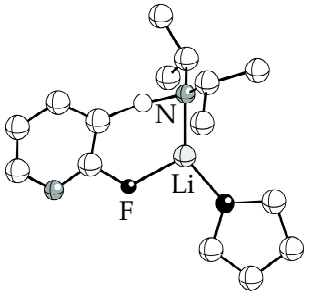

33

$\Delta G^{\ddagger}$ = 16.9 kcal/mol

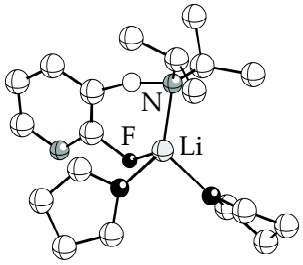

34

$\Delta G^{\ddagger}$ = 7.5 kcal/mol

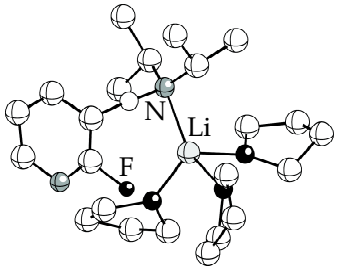

35

$\Delta G^{\ddagger}$ = 11.5 kcal/mol

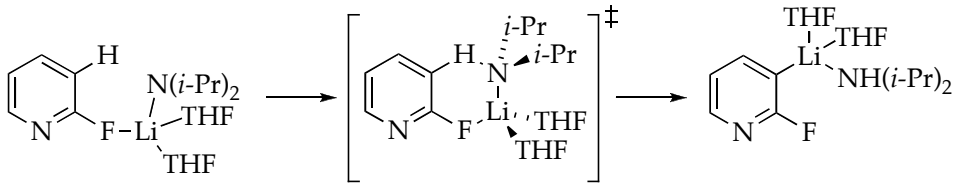

36 **34** **37** (18)

Autocatalysis. Eqs 6-13 describe various rate-limiting deaggregations that would be prevalent at early conversion. By contrast, eqs 14, 15, and 17 describe lithiation under conditions of a fully established dimer-monomer equilibrium (LiCl catalyzed). We can now consider the autocatalysis illustrated in Figure III.1 (curve B). Recall that no *observable* mixed aggregates are formed from LDA and aryllithium **3**.

A standard control experiment that we have historically used to show the *absence* of autocatalysis under pseudo-first-order conditions is carried out

by zeroing the IR baseline at the end of a kinetic run and measuring a rate constant from a second aliquot. The second rate constant should be indistinguishable from the first except for a very small reduction in rate resulting from loss of LDA titer. We noted a rate *increase* from a second aliquot of **1**, suggesting that aryllithium **3** accelerates the reaction. The impact of autocatalysis is readily discerned by incrementally additing arene **1** to a solution of LDA and monitoring the initial rates. Overall, a molar equivalent of substrate is added in small aliquots, which minimizes the influence of substrate-catalyzed deaggregation. The first notable observation is that the presence of ArLi elicits upward curvatures in the decay of ArH, suggesting that ArLi-derived catalysis at least partially shifts the rate-limiting step from LDA deaggregation to a reaction in which substrate **1** participates. A plot of the initial rates versus the mole fraction of aryllithium (X_{ArLi}) is illustrated in Figure III.11. The positive deviation from the dashed line represents the contribution of autocatalysis. This variant of a Job plot[48,49,50] is meritorious in that it detects even low levels of autocatalysis that could be concealed as slight distortions in decays that are already distorted by rate-limiting deaggregation. The maximum in the curve corresponding to 1:1 ArLi and LDA titer (normality *not* molarity) shows the optimum stoichiometry to be equal proportions of ArLi and LDA subunits, $[(i\text{-Pr})_2\text{NLi}]_m(\text{ArLi})_n$ ($m = n$). The fit to $m = n = 1$ (dashed curve in Figure III.11), however, is obviously inadequate. A nonlinear least squares fit to eq 19[22] to ascertain the order (solid line in Figure III.11) is excellent and implicates a mixed tetramer, $[(i\text{-Pr})_2\text{NLi}]_m(\text{ArLi})_n$ ($m = 1.9 \pm 0.1$; $n = 1.9 \pm 0.1$).

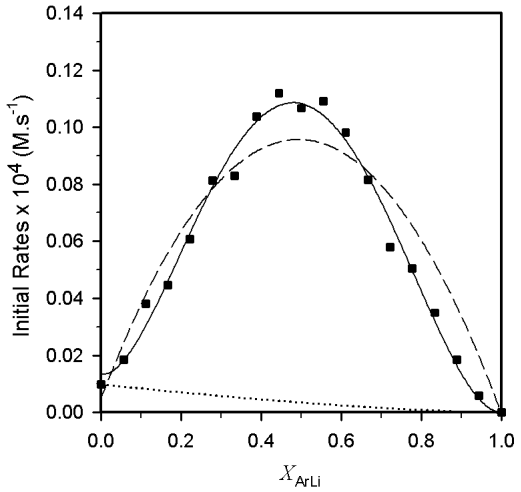

Figure III.11. Plot of initial rates versus mole fraction of 3-lithio-2-fluoropyridine (X_{ArLi}) for the serial injections of 0.0055 M aliquots of **1** to 0.10 M LDA in 12.20 M THF at -78 °C. The dotted line depicts the theoretical initial rates in the absence of autocatalysis, assuming an LDA order of 1.5. The solid line depicts an unweighted least-squares fit to eq 19. See supporting information for derivation. ($m = 1.9 \pm 0.1$, $n = 1.9 \pm 0.1$, $k = (1.5 \pm 0.3) \times 10^{-4}$, $k' = (1.3 \pm 0.4) \times 10^{-6}$). The dashed curve represents a fit to the data where $m = 1$ and $n = 1$ in the given equation.

$$-d[\mathrm{ArH}]/dt = k(X_{\mathrm{ArLi}})^n(1-X_{\mathrm{ArLi}})^m + k'(1-X_{\mathrm{ArLi}})^{1.5} \qquad (19)$$

We carried out a more traditional experiment by monitoring initial rates versus ArLi concentration at constant LDA concentration (Figure III.12), revealing saturation behavior akin to that observed for LiCl (Figure III.8). A nonlinear least squares fit with the ArLi order as an adjustable parameter reveals a best-fit order of 1.7 ± 0.4, supporting the putative high-order dependence on ArLi. Rate studies at full saturation ($\geq$0.03 M ArLi) reveal a half-order dependence on LDA and second-order dependence on THF, confirming the dominance of the same monomer-based metalation as that observed under LiCl catalysis.

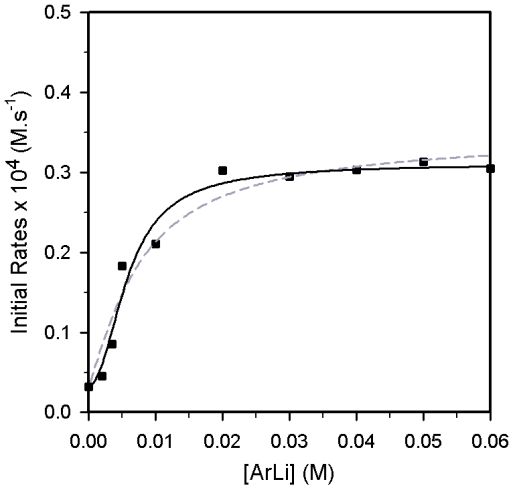

Figure III.12. Plot of initial rates vs [ArLi] for the ortholithiation of **1** (0.005 M) with LDA (0.10 M) in THF (12.20 M) at -78 °C. The curve depicts an unweighted least-squares fit to eq 16. See supporting information for derivation. [ArH] = 0.005 M, $[A_2S_2]_0$ = 0.05 M, c = (3.2 $\pm$ 0.5) x 10^{-6} and n = 1.7 $\pm$ 0.4, k_1 = 1.2 $\pm$ 2.6, k_{-1} = (1.6 $\pm$ 0.2) x 10^3, k_2 = (9.2 $\pm$ 11.5) x 10^{-1}. The dashed curve represents a fit to the data where n = 1 in the given equation.

We are poised to assess the relative contribution of autocatalysis to the decays shown in Figure III.1. (THF was shown to promote autocatalysis, but we did not examine the role of THF in detail nor is it needed in the model.) The mathematical model for autocatalysis (eq 20) is constructed by assuming that (1) the mixed-tetramer-based transition structure for autocatalysis, $[A_2(ArLi)_2]^‡$, affords an $A_2(ArLi)_2$ mixed tetramer as a transient intermediate, and (2) $A_2(ArLi)_2$ reacts with ArH—be it directly or by facile dissociation to monomer or reactive mixed dimers—in post-rate-limiting steps (eq 21). (Given the absence of observable LDA-ArLi mixed aggregates, dissociation of demonstrably unstable mixed aggregates would certainly be facile.) Combining the contribution of autocatalysis in eq 20 with the uncatalyzed metalations in eq 13, best-fit numerical integration affords the curves shown in

Figure III.1. We view the quality of these fits as constituting consistency with, rather than confirmation of, the model.

$$-d[\mathrm{ArH}]/d\mathrm{t} = k_{\mathrm{cat}}[\mathrm{ArLi}]^2[\mathrm{LDA}] \qquad (20)$$

$$\mathrm{A_2} + 2\mathrm{ArLi} \xrightarrow{k_{\mathrm{cat}}} [\mathrm{A_2(ArLi)_2}] \xrightarrow[\textit{fast}]{2\mathrm{ArH}} 4\mathrm{ArLi} \qquad (21)$$

The data for the uncatalyzed and autocatalyzed pathways allow us to ascertain the percent contribution from the two pathways. The calculated contributions based on equimolar LDA and pyridine **1** versus percent conversion are illustrated in Figure III.13. Although the catalytic efficiency of ArLi pales compared to that of LiCl, autocatalyzed deaggregation becomes the dominant mechanism at 6% conversion.

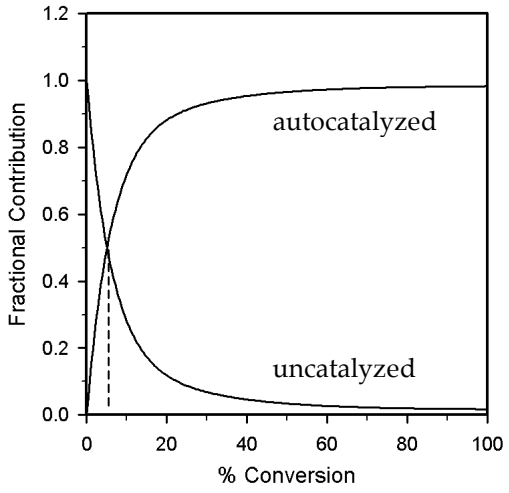

Figure III.13. Plot of fractional contribution of the autocatalyzed and uncatalyzed pathway to the total reaction rates versus percent conversion derived from the data in Figure III.11. Equal contribution from the two pathways (dashed line) occurs at 6% conversion.

2,6-Difluoropyridine (2). Extensive data was amassed on the ortholithiation of difluoropyridine **2**. Because of significant parallels with **1**, the data have been relegated largely to supporting information. Several differences are notable:

(i) The metalation of **2** is decidedly less susceptible to autocatalysis, which could stem from either a muted susceptibility of the metalation to catalysis or a muted activity of ArLi **4** as a catalyst. Control experiments involving added mono- and difluoroaryllithiums **3** or **4** to metalations of arenes **1** or **2** show that the lower autocatalysis results from a low catalytic activity of aryllithium **4**.

(ii) Plots of initial rate versus concentration of **2** show a first-order dependence analogous to that in Figure III.2 but with a 7-fold greater slope. Although it is tempting to attribute the higher metalation rates to an enhanced acidity of **2** (see part iii below) the proton transfer is post rate limiting. Consequently, the greater metalation rates of **2** relative to **1** stem from a more efficient substrate-mediated deaggregation. Competition of **1** and **2** shows biphasic kinetics consistent with a post-rate-limiting proton transfer (Figure III.14). The 7-fold greater rate of the metalation of **2** when measured separately and the 30-fold greater rate when measured in competition suggest that substrate properties that influence the deaggregation differ from those that influence the proton transfer.

(iii) Small standard isotope effects in conjunction with large competitive isotope effects and biphasic kinetics (analogous to those illustrated in Figure III.6) confirm a post-rate-limiting proton transfer at low substrate concentration. At high substrate concentration, however, an intermediate

standard isotope effect ($k_H/k_D = 14$) suggests that deuterium transfer is largely rate limiting.

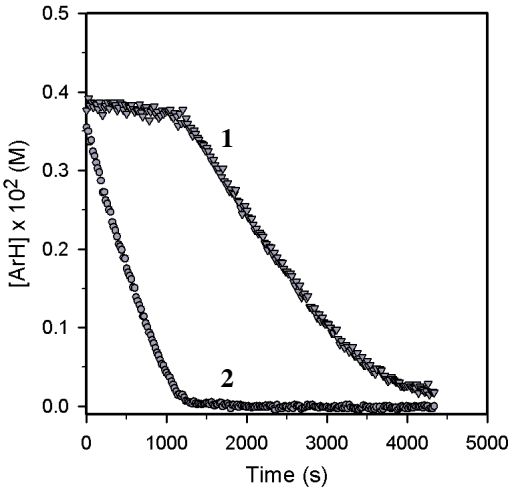

Figure III.14. Plot of [ArH] vs time for the ortholithiation of a mixture of fluoropyridines **1** and **2** (0.004 M each) with LDA (0.10 M) in THF (12.20 M) at -78 °C, monitored by ^{19}F NMR spectroscopy.

(iv) The measured LDA orders remain large at both low and high substrate concentrations (1.48 $\pm$ 0.09 at 0.005 M **2** and 1.25 $\pm$ 0.09 at 0.10 M **2**, respectively.)

(v) Pronounced LiCl catalysis makes the rates to become unmeasurably fast at concentrations that might have afforded saturation behavior. In contrast to the greater catalytic efficiency of **2** compared to **1** (described in part ii above), the higher reactivity of **2** versus **1** under LiCl catalysis is due to the 30-fold greater kinetic acidity of **2** (see part ii). A second-order dependence on LiCl (Figure III.8) seems uncontestable for pyridine **2** (Figure III.15), providing support to the second-order saturation behavior of pyridine **1**.

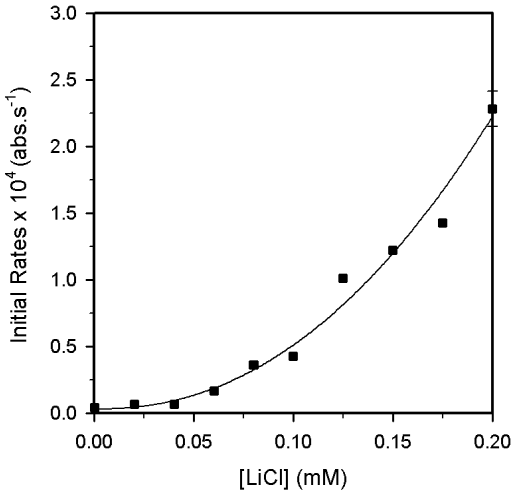

Figure III.15. Plot of initial rates vs [LiCl] for the ortholithiation of **2** (0.004 M) with LDA (0.10 M) in THF (12.20 M) at -78 °C. The curve depicts an unweighted least-squares fit to $-d[\mathbf{2}]/dt = k[\mathrm{LiCl}]^n + k'$ ($k = (7 \pm 3) \times 10^{-3}$, $n = 2.2 \pm 0.3$, $k' = (3 \pm 7) \times 10^{-6}$).

Discussion

Mechanistic studies of the LDA-mediated ortholithiation of 2-fluoropyridine (**1**) afforded results that are surprising, in some cases unprecedented, and at times seemingly paradoxical. The complexity stems from three primary factors: (1) a rate-limiting deaggregation mediated by pyridine **1**, (2) autocatalysis by aryllithium **3**, and (3) highly efficient catalysis by LiCl. There is a natural tension between our need as authors to compartmentalize the variables for presentation and the inherent correlations of these variables. Additional pedagogic challenges arise from comparisons of fluoropyridine metalations with the LDA/THF-mediated reactions summarized in the background section that, although mechanistically related, can display strikingly different behaviors.

Summary. The sum of our efforts are described by Scheme III.4. We had taken the liberty in the results to introduce a shorthand as follows: A = an

LDA subunit; S = THF, pyr = fluoropyridine **1**, and ArLi = aryllithium **3**. The importance of the three notations in Scheme III.4—deaggregation, complexation, and proton transfer—will become apparent below.

Scheme III.4

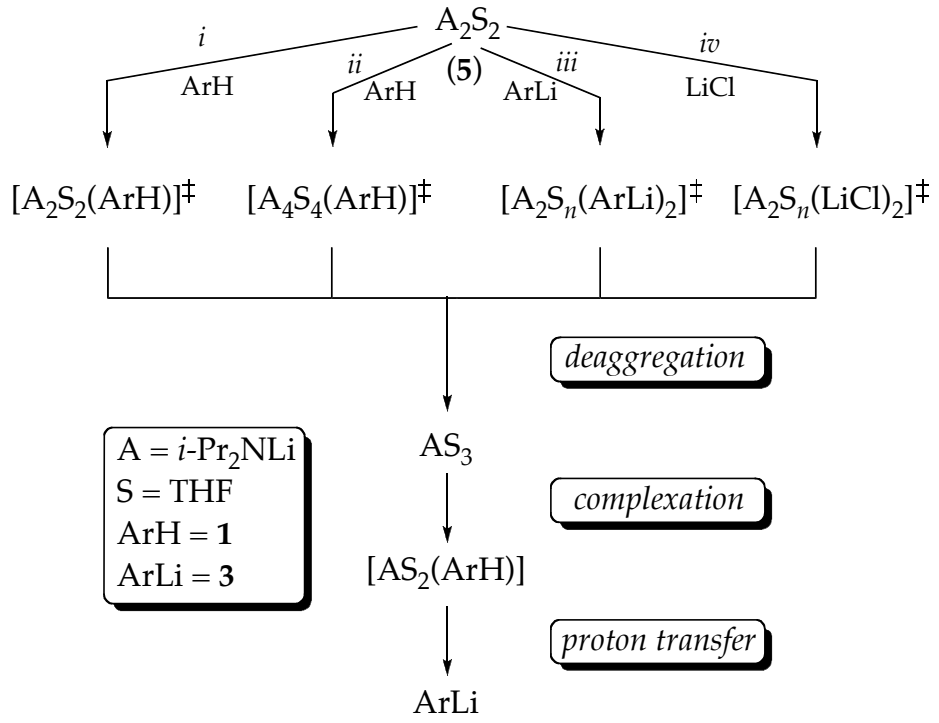

Monitoring the lithiation of pyridine **1** at early conversion—before the onset of autocatalysis—reveals evidence of parallel pathways involving disolvated dimers and tetrasolvated tetramers (Scheme III.4, pathways *i* and *ii*.) Although both display seemingly generic first-order substrate dependencies, isotopic labeling studies show that the proton transfers occur *subsequent* to rate-limiting aggregation events.

As the metalation proceeds to full conversion, reaction of aryllithium **3** with LDA dimer **5** elicits autocatalysis (Scheme III.4, pathway *iii*). A 2:2 stoichiometry in the transition structure, $[A_2(ArLi)_2]^‡$, is gleaned using the

method of continuous variations[48,49,50] (the Job Plot in Figure III.11); the role of tetramers is discussed in detail below. More conventional methods revealed saturation behavior (Figure III.12) that does *not* derive from Michaelis-Menten kinetics but rather from a shift in the rate-limiting step from LDA deaggregation to proton transfer. In conjunction with studies of LiCl catalysis (below), the autocatalysis is shown to derive from ArLi-catalyzed deaggregation of LDA dimer **5** to monomer (Scheme III.5; LiX = aryllithium **3**). Although some parallels are observed for autocatalytic metalations of 2-fluoropyridine (eq 1) and fluorocarbamates (eq 3), the reactions differ in two respects: (1) autocatalysis of the carbamate metalations appears to occur via a mixed-trimer-based transition structure, $[A_2(ArLi)]^{‡}$, rather than via mixed tetramers, and (2) LDA-ArLi mixed dimers are observable for carbamate-derived aryllithiums whereas no mixed aggregates of any kind are observed for pyridyllithium **3**.

Autocatalysis foreshadowed accelerations by LiCl (Scheme III.4, pathway *iv*). Catalysis by as little as 0.001 mol % LiCl wreaked havoc on the rate studies until rigorously LiCl-free LDA was prepared. Rate studies also show a second-order saturation behavior in LiCl (Figure III.8), implicating a heterotetramer-based pathway (Scheme III.4, pathway *iv*). The resting state of LiCl as mixed aggregates **27** and **28**, however, renders this conclusion a guarded one (vide infra). Saturation of the rates above 0.3 mol % LiCl and subsequent rate studies at full saturation are consistent with the mechanism in Scheme III.5 (LiX = LiCl). Thus, LiCl catalysis allowed us to investigate the mechanism of proton transfer occurring beyond the formerly rate-limiting deaggregation. Rate studies under conditions of full LiCl catalysis reveal the intermediacy of a di- or trisolvated LDA monomer at the proton transfer step.

Computational studies support disolvated transition structure **34** as the most favorable.

Scheme III.5

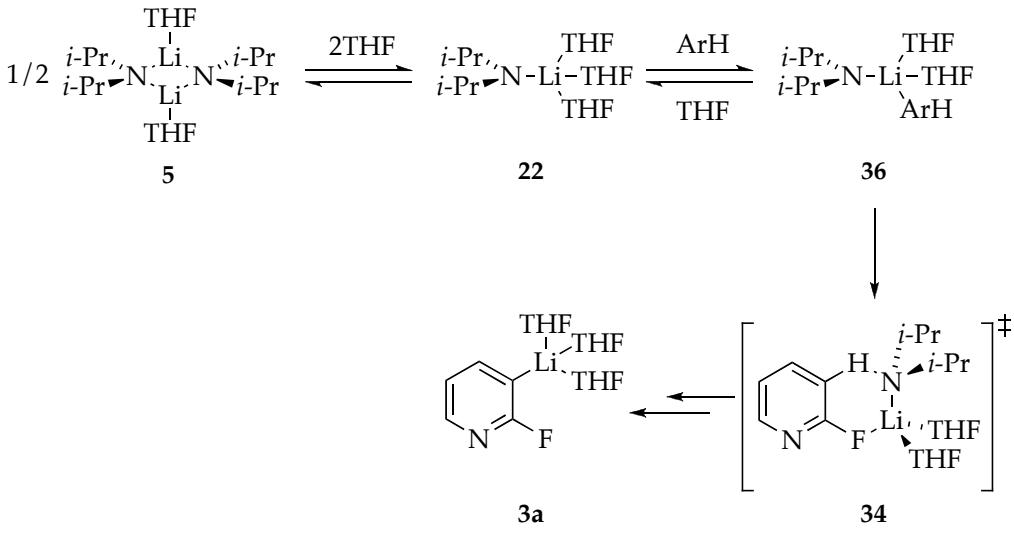

Aside from the obvious omission of a few niggling details, this summary paints a seemingly coherent picture of LDA-mediated lithiation of fluoropyridine **1**. These details, however, are quite perplexing as discussed below.

Role of the Rate-Limiting Steps: A Mechanistic Paradigm. In this section we develop a mechanistic paradigm that includes provisions for a seemingly disparate collection of observations all revolving around rate-limiting aggregation or substrate complexation. The approach may seem overly methodical, but it is imperative that the reader understand the determinants of rate limitation. With the nonspecialist in mind, we begin from first principles using the simplest possible model (eq 22).

$$\text{SM} \underset{k_{-1}}{\overset{k_1}{\rightleftharpoons}} [\text{I}] \xrightarrow{k_2} \text{P} \qquad (22)$$

Assume that intermediate, I, is relatively unstable ($k_{-1} >> k_1$). The rate-limiting step of the overall conversion of starting material (SM) to product (P) is determined by the fate of I. If $k_2 << k_{-1}$, then I will return to SM with high fidelity, only occasionally giving P; conversion of I to P is rate limiting. By contrast, if $k_2 >> k_{-1}$, then I always affords P; conversion of SM to I is rate limiting. Thus, it is the k_2/k_{-1} ratio—the penchant of I to give product or return to starting material—that dictates rate limitation. This is an important concept that we will rely on heavily in the forthcoming discussion.

To understand the role of catalysis and autocatalysis, let us assume again that $k_2/k_{-1} >> 1$ (formation of I is rate limiting) and introduce a catalyst to facilitate the conversion of SM to I. Using a minor short cut, catalysis can be thought of as simply increasing k_1,[51] which will afford higher reaction rates. Less obvious, perhaps, is that the reverse reaction of I to SM is necessarily accelerated proportionately as mandated by the principle of microscopic reversibility.[52] At some elevated level of catalysis, the catalyzed back reaction becomes so efficient that I returns to SM faster than it reacts to give P ($k_2/k_{-1} << 1$); conversion of I to P becomes rate limiting. Thus, catalysis of the conversion of SM to I (the forward reaction) causes the acceleration, whereas catalysis of I to SM (the back reaction) causes the shift in the rate-limiting step.

Now we can bring elements of organolithium chemistry to the model. Scheme III.6 depicts the simplest representation of a monomer-based metalation that is not oversimplified. (We recycle rate constants such as k_1 and k_2 to keep the model and discussion simple; they are, of course, not the same as k_1 and k_2 in eq 22.) Monomer **38** is arbitrarily drawn with only two

solvents, although the resting state is more likely trisolvate **22**—that is unimportant. What *is* important is that by considering three limiting behaviors of this simple mechanism we can begin to understand the consequences and nuances of rate-limiting aggregation or substrate complexation.

Scheme III.6

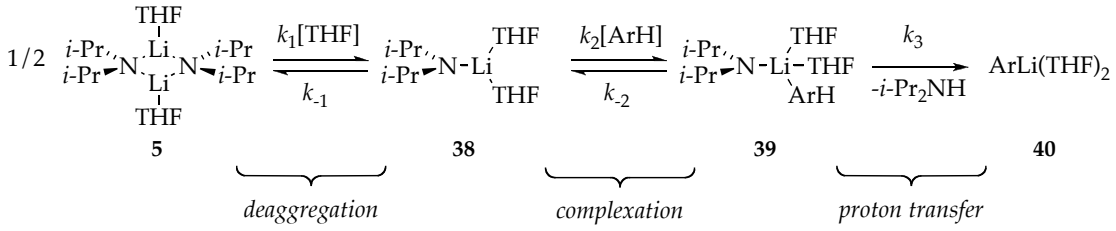

Case 1: Rate-limiting proton transfer. Under most circumstances—circumstances that have dominated our rate studies of LDA-mediated metalations for 25 years—the proton transfer described by k_3 would be rate limiting. Fleeting intermediates **38** and **39** are formed reversibly. Complex **39** has a much greater probability of returning to dimer **5** than forming aryllithium **40**. In short, k_3[**39**] << k_{-2}[**39**] and k_{-1}[**38**]^2. The equilibrium approximation[33] affords a rate law showing first-order dependencies on both substrate and THF concentrations (eq 23). The half-order dependence on LDA concentration is emblematic of the reversible dimer-monomer preequilibrium.[7] Comparing ArH and ArD would reveal a large standard isotope effect (typically $k_H/k_D > 7$, but it can be quite large).[53] Competition of ArH and ArD in the same vessel would afford what we loosely refer to as a competitive isotope effect[44] that would be of comparable magnitude to the standard isotope effect, confirming that the isotopically sensitive proton transfer is also rate limiting.

$$d[\mathrm{ArLi}]/d\mathrm{t} = k'[\mathrm{ArH}][\mathrm{LDA}]^{1/2}[\mathrm{THF}] \qquad (23)$$

Before proceeding to additional limiting cases, it is instructive to consider how we discovered post-rate-limiting proton transfers. Imagine the metalation of increasingly more reactive substrates. The elevated kinetic acidities—increasing values of k_3—demand lower reaction temperatures to maintain rates that can be conveniently monitored (half-life = 100-1000 s). At some critical point, the proton transfer becomes so efficient that one of the preceding steps (deaggregation or complexation) becomes rate limiting. By coincidence, this critical point appears for LDA/THF-mediated reactions within a few degrees of –78 °C. Under these synthetically prominent conditions, aggregation events occur on minute rather than microsecond time scales.[12]

Case 2: Rate-limiting complexation. In case 2, we assume the proton transfer is fast, **5** deaggregates to give **38** reversibly, and complexation to form **39** is rate limiting (k_2[ArH][**38**] << k_{-1}[**38**]^2 and k_3[**39**]). There are two possible outcomes, depending on whether a post-rate-limiting exchange of ArH and ArD occurs before proton transfer (Scheme III.7). In the first scenario, **39** metalates to give **40** as quickly as it is formed—ArH does not dissociate from **39** nor do **39** and **39-*d*$_1$** exchange by any mechanism. The rate law is still described by eq 23, and the metalation rates would depend on both the structure and concentration of ArH. The standard and competitive isotope effects, however, would both be unity ($k_\mathrm{H}/k_\mathrm{D}$ = 1).

In the second scenario, formation of **39** is rate limiting but exchange of **39** and **39-*d*$_1$** with free arene occurs before proton transfer. Whereas the standard isotope effect would be unity because the proton transfer is post rate

limiting, the facile ArH-ArD exchange gives the LDA monomer a choice of which substrate to metalate: the preference for ArH over ArD would be pronounced, making the competitive isotope effect large. If the reaction is followed to full conversion, one would observe biphasic kinetics akin to that shown in Figure III.6. The rapid ArH-ArD exchange (or lackthereof) is critical to interpreting competitive isotope effects. This particular scenario has the added constraint that rapid ArH-ArD exchange would have to be an associative substitution of the arenes rather than a dissociation to uncomplexed monomer **38**. To assume that **38** and **39** are at equilibrium is tantamount to assuming proton transfer (k_3) is rate limiting, which conflicts with the central tenet of case 2—that complexation is rate limiting.

Scheme III.7

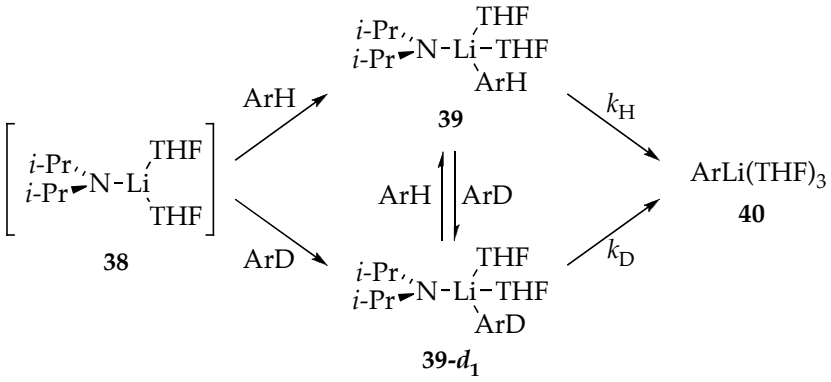

Case 3: Rate-limiting deaggregation. Assuming that deaggregation of dimer **5** to form monomer **38** is rate limiting, the reassociation of two monomers would be slow compared to complexation and all subsequent steps (k_{-1}[**38**]^2 << k_2[ArH][**38**] and k_3[**39**]). The rate law would show a first-order dependence on LDA concentration, an order in THF reflecting the number of additional ligands required to deaggregate dimer **5**, and an independence of

the rate from the concentration of ArH (zeroth order). Whereas the standard isotope effect would be unity, the competitive isotope effect would be large *provided that ArH-ArD exchange on monomer **39** is efficient before proton transfer.* Unlike the more restrictive case 2, a facile **38**-**39** equilibrium would suffice. Case 3 corresponds to an uncatalyzed/unmediated rate-limiting LDA deaggregation, a deaggregation that should occur in LDA/THF solution in the absence of any other species.

Case 4: Partial rate-limiting proton transfer. This simple example offers an excellent opportunity to illustrate the concept of partial rate limitation. Allusions are made throughout the text to the appearance of upward curvature arising from either catalysis or deuteration (see Figures III.5 and III.6 for examples). Curvature will appear if a rate-limiting deaggregation (zeroth-order decays; case 3) shifts to a rate-limiting proton transfer (first-order decays; case 1). This shift can occur either by facilitating the reaggregation (k_{-1}[**38**]^2) or by suppressing the proton transfer (k_3[**39**]). Acceleration of the reaggregation was discussed generically in the context of catalysis and eq 22 and becomes germane to the mixed aggregation effects discussed below. Suppression of proton transfer is achieved through deuteration and the affiliated >20-fold kinetic isotope effect.

We have described very complex behavior—changes in curvatures, reaction orders, and isotope effects—that could stem from a relatively simple mechanism by assuming that deaggregation, complexation, or proton transfer could be rate limiting. Reality may be even more complex. We draw the reader's attention to the computational studies of LDA deaggregation described in the background section. For the time being, readers should ignore the possible intermediacy of the tetramers illustrated in Scheme III.1—we will

return to these shortly—and focus on the cascade leading from LDA dimer **5** to monomer **22** (Scheme III.2). Recall that the activation barriers rise monotonically across the sequence.[12] One would predict, therefore, that dimers **23**-**25** form reversibly and that cleavage of **25** would be the rate-limiting step en route to monomer **22**.

What would happen if one of the dimeric intermediates in Scheme III.2 could react with ArH? Take, for example, a reaction involving open dimer **24** (Scheme III.8). If **24** and corresponding complex **41** are both formed reversibly, proton transfer will be rate limiting. Such open-dimer-based reactions are well-precedented.[39] Using an analogy to the monomer-based metalation in Scheme III.5, however, we posit that the rate limiting step could be proton transfer, complexation, or deaggregation. On repeating the very same analysis, we find that reaction orders and kinetic isotope effects (standard and competitive) would again change markedly depending on the assumptions. We need not repeat this analysis here.

Now imagine that *any* of the intermediates in Scheme III.2 could be intercepted, depending on the choice of substrate. Because of the monotonic rise in the barriers along the cascade, intercepting an early intermediate would, all other parameters being equal, afford observed reaction rates that are higher than if an intermediate later in the cascade is intercepted. Moreover, the observed rates, reaction orders, and kinetic isotope effects would depend on which intermediate is intercepted by substrate and which step—deaggregation, complexation, or proton transfer—is rate limiting.

Scheme III.8

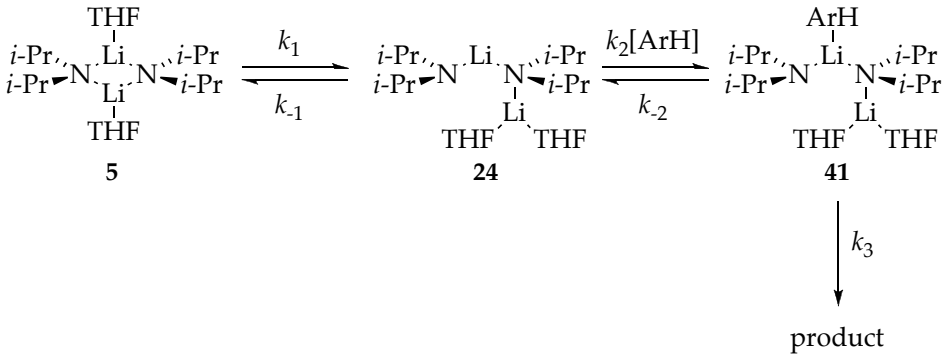

The evidence collected to date seems to fit this general paradigm. Metalation of carbamate **6** shows a distinct ArH concentration dependence via a rate limiting $[A_2S_2(ArH)]^{‡}$, which could correspond to rate-limiting complexation (**42**) or ArH-dependent deaggregation (**43**). Prompted by the studies described in this manuscript, follow-up studies showed that the proton transfer is post rate limiting and the analogous deuterium transfer is partially rate limiting.[54] Metalation of arene **10** (eq 4) displays a zeroth-order dependence on substrate traced to a rate-limiting deaggregation via a disolvated-dimer-based transition structure (**13**); complexation and metalation of substrate occur post rate limiting. The large competitive isotope effect shows that the post-rate-limiting proton transfer is necessarily preceded by a facile ArH-ArD exchange. With the aid of the efficient LiCl-catalyzed dimer-monomer exchange that causes a shift in the rate-limiting step, we showed that the critical deprotonation involves monomer-based transition structure **14**.

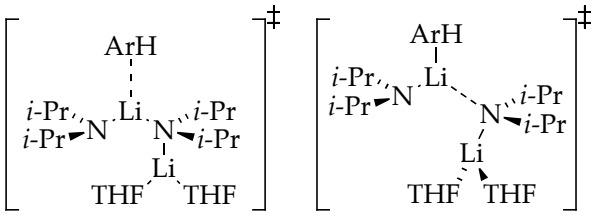

42 **43**

The notion of two different rate-limiting deaggregations emerges from comparing studies of the metalation of **10** (eq 4) with studies of 1,4-additions of LDA (eq 5). Whereas metalation of arene **10** proceeds via rate-limiting transition structure **13**, 1,4-additions occur via transition structure **17**. The different solvation numbers of **13** and **17** distinguish them as distinctly different rate-limiting deaggregation events. Aided by LiCl-catalyzed dimer-monomer exchange, we showed that the actual 1,4-addition involves monomer-based transition structure **18**. We find the evidence convincing that transition structure **18** implicated under LiCl catalysis is the same as the post-rate-limiting transition structure without catalysis. By contrast, although the metalation of **10** also occurs via monomer-based pathways under LiCl catalysis, the evidence that monomers are the key post-rate-limiting intermediates without catalysis is more circumstantial.

We can now place the metalation of pyridine **1** in context as well. Standard isotope effects approaching unity for metalations of **1** and **1-*d*$_1$** in conjunction with large competitive isotope effects and biphasic kinetics (Figure III.6) offer compelling evidence of a post-rate-limiting proton transfer. The first-order substrate dependence corresponds to either rate-limiting complexation (**42**) or deaggregation (**43**). A large competitive isotope effect and biphasic kinetics (Figure III.6) show that facile ArH-ArD exchange (akin to that illustrated in Scheme III.7) must occur after the rate-limiting step but

before the proton transfer. The requisite ArH-ArD exchange does not necessarily exclude substrate complexation (**42**) as rate limiting, but it does require that such an exchange be associative. We strongly favor rate-limiting deaggregation (**43**) and suspect that rate-limiting complexations are rare or nonexistent.

On the Role of Tetramers. The analysis described above explicitly defers discussions of LDA orders in the unprecedented range of 1.2-1.7. What makes these orders so odd is that other reactions involving rate-limiting deaggregations (eqs 3-5) seem to proceed only via dimer-based pathways. We must confess that we still worry that unseen variables in the metalations of **1** are causing mischief, but no amount of experimental tinkering caused the high orders to reduce to unity. We also admit that the evidence supporting a central importance of tetrameric intermediates is considerable.

A trimer-based mechanism to explain the high, fractional orders (eqs 8-10) was dismissed for the simple reason that trimer formation seems to require LDA monomer as an intermediate, and monomers were shown to be efficacious intermediates in their own right. Consequently, we turned to a composite mechanism invoking parallel pathways via LDA dimers (eqs 6 and 7) and tetramers (eqs 11 and 12).[41] Spectroscopic and computational studies of tetramer-based aggregate exchanges summarized in Scheme III.1 are telling. (Despite the chronology of publication, the metalations of pyridine **1** prompted the dynamic studies in Scheme III.1.) Moreover, rate studies of LiCl- and ArLi-catalyzed deaggregations implicate mixed tetrameric intermediates (below) as do analogous studies of LDA-lithium enolate condensations.[5b]

We have two fundamental questions for which we can only offer some rather speculative answers:

(1) Could tetramers serve as intermediates en route to monomers? The high energetic cost of deaggregating LDA dimer **5** via transition structure **17** stems, at least in part, from the concurrent formation of *two* high energy species. To use an analogy, this might be akin to a solvolysis that forms a carbocation and an alkoxide. Circumventing the dilemma in solvolyses requires stabilizing one of the two fragments, making it a good leaving group. We can push the analogy into the realm of the deaggregation in Scheme III.1. For the dissociation of tetramers to trimers and monomers, trimeric ladder **21** assumes the role as leaving group, demanding liberation of only *one* highly destabilized monomer. Further deaggregation of **21** reaps the benefits of a dimer-based leaving group. If tetramers are indeed the intermediates en route to monomers (eq 24), however, the principle of microscopic reversibility demands that tetramers are also the preferred intermediates by which monomers form dimers.[52] That is an odd concept.

$$2A_2 \rightleftharpoons A_4 \rightleftharpoons A_3 + A \rightleftharpoons A_2 + 2A \qquad (24)$$

(2) Why would LDA tetramers appear uniquely (to date at least) for the metalation of 2-fluoropyridines? The short answer is that we don't know. A slightly more constructive answer is that the first-order substrate dependence presents the possibility of substrate specificity. The properties that allow fluoropyridines to intercept a particular dimeric intermediate in Scheme III.2 might correlate with the properties allowing them to intercept ladders (see **44** or **45**). Further speculation should probably await additional examples.[41b-e,13,55]

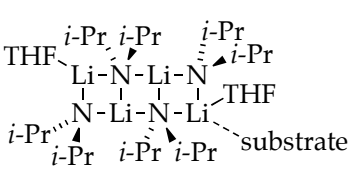

44

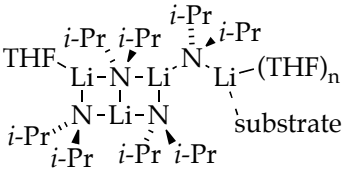

45

LiCl-Catalyzed Deaggregation. LiCl catalysis has many interesting facets. Recall from the tutorial on rate limitation that catalysis of the deaggregation causes acceleration whereas catalysis of the *reaggregation* elicits a shift in the rate-limiting step. Rate studies show that catalyzing the dimer-monomer preequilibrium shifts the rate-limiting step from dimer deaggregation to proton transfer (eqs 14-17). In light of the discussion of tetramer-based intermediates, the high order in LiCl seems more than coincidental, suggesting the intermediacy of LDA-LiCl mixed tetramers. We hasten to add that the resting state of LiCl is a mixture of mixed trimer **27** and dimer **28**; we have minimal insights into the fate of the mixed aggregates during the metalation. That said, however, we are willing to offer a few speculations to provoke thought.

In light of the discussions of tetrameric ladders in Scheme III.1, one could imagine transiently forming mixed tetrameric ladder **46** from a dimer-dimer condensation (Scheme III.9).[13,61] Alternatively, serial condensation of LDA dimer **5** with two LiCl monomers would afford isomeric ladder **48** that could split into mixed dimers and eventually yield monomeric LDA.

Scheme III.9

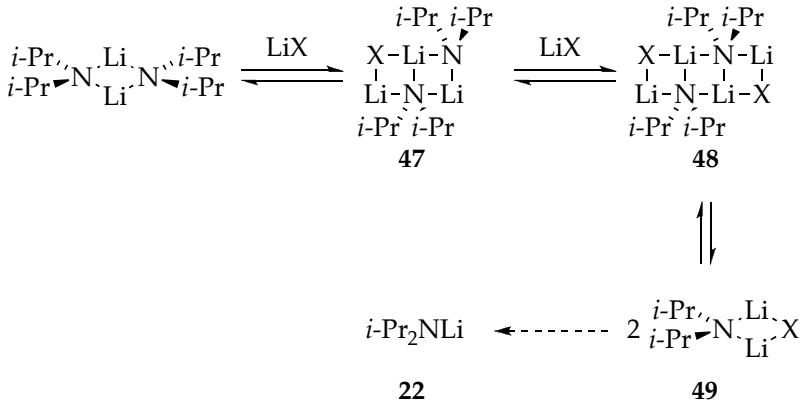

As one last suggestion, we submit that chloride ion should be a particularly good ligand—a strongly binding THF equivalent to facilitate deaggregation. The intermediacy of complex ions **50** or **51** is consistent with both the high LiCl order and positive order in THF. The cationic triple ion fragment (Li–Cl–Li)[57] as well as the chloride adduct of a lithium amide open dimer[58] have computational and experimental support.[59]

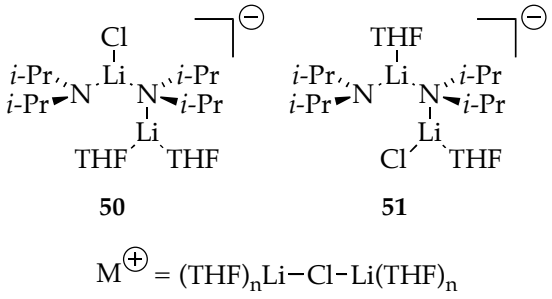

Autocatalysis. The Job plot in Figure III.11 also points to a mixed-tetramer-based mechanism for autocatalysis. The maximum at equal parts LDA and ArLi shows a 1:1 stoichiometry. The quality of the fit excludes a 1:1 mixed dimer, strongly supporting a 2:2 stoichiometry instead. The emergence

of yet another putative mixed-tetramer-based pathway cannot be mere coincidence. Is it possible that ArLi also operates through the mechanism in Scheme III.9 (X = Ar) previously invoked for LiCl? Rate studies implicated a mixed-tetramer-based ArLi-catalysis, and eventual formation of LDA monomer seems plausible. We cannot rigorously exclude that low ArLi concentrations (below the levels required to attain saturation kinetics) allow for direct reaction of fleeting mixed tetramers by substrate. This idea of substrate intercepting a mixed tetramer would account for the unique penchant of fluoropyridines to react via mixed-tetramer-based autocatalysis.

Lingering Issues. We sought evidence that the miniscule nonzero intercept in Figure III.2 corresponds to a rate-limiting deaggregation in which substrate plays no role whatsoever. In principle, all LDA-mediated reactions that share a common rate-limiting deaggregation would necessarily share common transition structures and reaction rates. Similar rates observed at ultralow concentrations of **1**, **1-d_1**, **3, and 3-d_2** support this notion.[60] Similar rates are also observed for several arene ortholithiations[5] as well as for several LDA-mediated 1,4-additions.[5b] The intervention of a putative tetramer-based pathway, however, even at ultralow substrate concentration, precludes a simple analysis.

The implication of tetramers—homotetrameric LDA as well as LDA-LiCl and LDA-ArLi mixed tetramers—suggest an inescapable theme in fluoropyridine metalations. The fact that tetramer-based chemistry is uniquely attributable to fluoropyridine may simply reflect substrate specificity for trapping fleeting intermediates. Failed attempts to mimic the catalysis by adding **29**-**32**, however, underscore an inability to identify what makes fluoropyridines special. Limited evidence that difluoropyridine **2** is more

efficient than **1** at mediating the rate-limiting deaggregation simply adds to the mystery of how substrates assist deaggregations.

Despite emerging evidence that different substrates intercept different intermediates along the dimer-monomer and dimer-tetramer cascades, we suspect that the chemistry may funnel through LDA monomers in most if not all instances; possibly only the rate limiting steps vary. The evidence that LiCl and ArLi accelerate the reaction by catalyzing the LDA dimer-monomer equilibration is compelling. That is not to say, however, that the uncatalyzed reactions of LDA necessarily share a common monomer-based reactive form. Whereas the case for monomer-based 1,4-additions (eq 5) is compelling, the evidence of monomer-based intermediates in the metalation of **1** is strong but still circumstantial.

It is clear that different lithium salts display markedly varying capacities to elicit accelerations of LDA-mediated reactions by catalyzing the deaggregation. We have made progress toward understanding the dynamics of LDA aggregate exchanges in THF. The mechanisms of deaggregation and aggregate-aggregate exchange for LDA dimer **5** and LDA-LiX mixed aggregates remain poorly defined and likely to be revealed only reluctantly.

Conclusions

For years we studied LDA-mediated reactions between –55 °C and 0 °C. At these temperatures, all aggregation and solvation events are rapid relative to easily monitored reactions. It is now clear that LDA dimer **5** deaggregates and exchanges with LiX aggregates with half-lives of many minutes in THF at –78 °C. Consequently, any reaction of LDA that proceeds at measurable rates in THF at –78 °C is likely to be influenced by the rates at which aggregates

exchange. Such rate-limiting aggregation events prove highly susceptible to autocatalysis as well as to catalysis by added lithium salts. Evidence is also mounting that different transiently stable aggregates of LDA can be intercepted depending on the precise structure of the substrate.

Lithiations of 2-fluoropyridine described herein are probably the most vexing reported to date, but a coherent mechanistic paradigm is emerging. Progress is incremental largely because of our profoundly limited understanding of how organolithium aggregates exchange. The notion that two substrates can react via rate-limiting deaggregations in which the critical deaggregation steps are *different* is odd. Moreover, we argue that the most efficient pathway from LDA dimers to LDA monomers is via homo- and mixed-aggregated *tetramers*, which is a conclusion that we drew with some trepidation. As we have stated previously, some of the conclusions are vulnerable to revision. We will be watching for additional support as these studies continue.

In closing, we ask a simple question: Are the efforts to untangle this mess justifiable? We believe the answer is yes. Of immediate practical importance, commercial LDA is free of LiCl, whereas LDA generated in situ from *n*-BuLi contains sufficient LiCl to efficiently catalyze deaggregation. The relative reactivities of the two forms of LDA can vary by as much as 10^3. At a more academic level, the rate-limiting aggregation events observed for LDA/THF are offering what may be an unparalleled window into the details of aggregate exchanges. LDA is one of the most commonly used reagents—suggested by one extensive survey to be *the* most commonly used reagent[61]—in organic synthesis. It seems self-evident that understanding its chemistry is worthy of considerable effort.

Experimental Section

Reagents and Solvents. THF and hexanes were distilled from blue or purple solutions containing sodium benzophenone ketyl. The hexane contained 1% tetraglyme to dissolve the ketyl. LiCl-free LDA was prepared and multiply recrystallized as described previously.[5b] Solutions of LDA were titrated using a literature method.[62] Arenes **1** and **2** are commercially available. Deuterated analogues were prepared as described below. $Et_3N{\cdot}HCl$ was recrystallized from THF/2-propanol.

Synthesis of deuterated pyridine derivatives:

3-deutero-2-fluoropyridine: A 1.6 M solution of *n*-butyllithium (22.2 mL, 35.6 mmol) in hexanes was added via syringe to a solution of dry diisopropylamine (5.0 mL, 3.61 g, 35.6 mmol) in dry THF at –78 °C under argon. After the solution was stirred for 20 minutes, 1.0 equiv of 2-fluoropyridine (3.0 mL) was added to the LDA solution. Th solution was stirred at –78 °C for 1.0 h, after which 1.0 equiv of *n*-butyllithium was added to the solution via syringe and the reaction was quenched with a THF/D_2O (10:1, 10 mL) after 15-20 minutes of stirring. The organic layer was washed with aqueous NaCl (3 x 10 mL), dried over Na_2SO_4 and filtered. Distillation and flash chromatography (pentane/ether) afforded 3-deutero-2-fluoropyridine (2.4 g, 27.6 mmol) as a colorless liquid in 80% yield and 98% deuteration as shown by ^1H NMR spectroscopy.

3,5-dideutero-2,6-difluoropyridine: The dideuterated compound was synthesized using the above procedure with 2 equiv of LDA. Quantitative deuteration was obtained after recycling the partially deuterated compound successively through five such lithiation cycles.

Synthesis of silylated pyridine derivatives:

Typical Procedure[63,64]: A 1.3 M solution of *i*-PrMgCl·LiCl (31.5 mL, 40.9 mmol) in THF was added via syringe to a solution of commercially available 4-bromo-2-fluoropyridine (6.0 g, 34.1 mmol) in dry THF (25 mL) at 0 °C under Ar. After the completion of Br/Mg exchange (checked by GC analysis of quenched reaction aliquots), the supernatant obtained from centrifuging ~3 equiv of 3:1 Me_3SiCl/Et_3N was added to the reaction and the solution was stirred at rt for ~15 h. The reaction was quenched with water and the organic layer was washed with aqueous NaCl (3 x 10 mL), dried over Na_2SO_4, filtered and evaporated to dryness under reduced pressure. Distillation under reduced pressure followed by flash chromatography (pentane/ether) afforded 2-fluoro-4-(trimethylsilyl)-pyridine (5.2 g, 30.7 mmol) as a colorless liquid in 90% yield.

2-fluoro-3-(trimethylsilyl)pyridine and 2,6-difluoro-3,5-bis(trimethylsilyl)-pyridine[1b]: A 1.6 M solution of *n*-butyllithium (22.2 mL, 35.6 mmol) in hexaness was added via syringe to a solution of dry diisopropylamine (5.0 mL, 3.61 g, 35.6 mmol) in dry THF at -78 °C under Ar. After the solution was stirred for 20 minutes, the supernatant obtained from centrifuging ~3 equiv of 3:1 Me_3SiCl/Et_3N was added to the LDA solution. 1.0 equiv of 2-fluoropyridine (0.5 equiv of 2,6-difluoropyridine) was added to the solution via syringe and the solution was stirred at -78 °C for 1 h. The reaction was quenched with wet THF, and the organic layer was washed with aqueous NaCl (3 x 10 mL), dried over Na_2SO_4, filtered and evaporated to dryness under reduced pressure. Distillation under reduced pressure followed by flash chromatography (pentane/ether) afforded silylated fluoropyridine as a colorless liquid in 90% yield.

IR Spectroscopic Analyses. IR spectra were recorded using an in situ IR spectrometer fitted with a 30-bounce, silicon-tipped probe. The spectra were acquired in 16 scans at a gain of 1 and a resolution of 4 cm^{-1}. A representative reaction was carried out as follows: The IR probe was inserted through a nylon adapter and an O-ring seal into an oven-dried, cylindrical flask fitted with a magnetic stir bar and a T-joint. The T-joint was capped with a septum for injections and a nitrogen line. After evacuation under full vacuum, heating, and flushing with nitrogen, the flask was charged with LDA (107 mg, 1.00 mmol) in THF (9.9 mL) and cooled in a dry ice-acetone bath prepared from fresh acetone. After recording a background spectrum, arene **1** (100 μL) was added with stirring. IR spectra were recorded at 30-second intervals over the course of the reaction. Absorbances corresponding to the arene moieties (Table 1) were monitored.

NMR Spectroscopic Analyses. All NMR tubes were prepared using stock solutions and sealed under partial vacuum. Standard ^{6}Li, ^{13}C, and ^{19}F NMR spectra were recorded on a 500 MHz spectrometer at 73.57, 125.79, 50.66 and 470.35 MHz (respectively). The ^{6}Li, ^{13}C, ^{15}N, and ^{19}F resonances are referenced to 0.30 M [^{6}Li]LiCl/MeOH at –90 °C (0.0 ppm), the CH_2O resonance of THF at –90 °C (67.57 ppm), neat Me_2NEt at –90 °C (25.76 ppm), and C_6H_5F in neat THF at -78 °C (-113.15 ppm), respectively.

Computations. DFT computations were optimized at using B3LYP/6-31G(d) level[21] with single point calculations at the MP2 level of theory. Saddle points were verified by a single negative frequency.

APPENDIX III

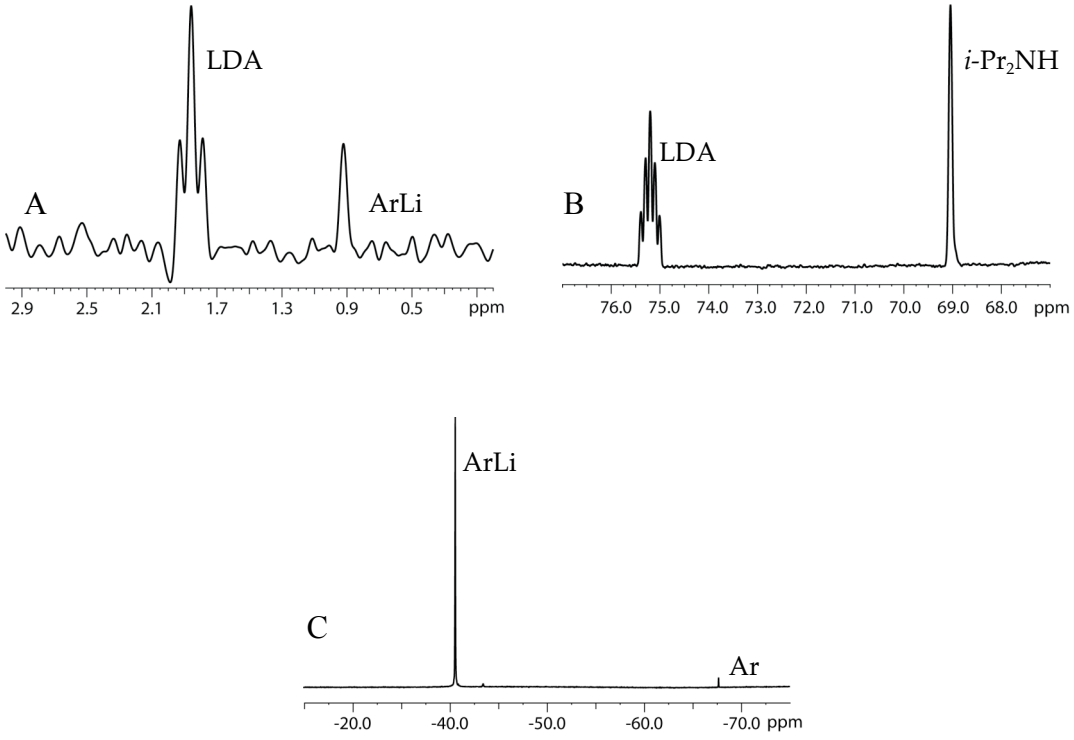

Figure AIII.1. ^{6}Li, ^{15}N and ^{19}F NMR spectra of 0.10 M [^{6}Li,^{15}N]LDA in neat THF recorded at -90 °C in the presence of 0.025 M 2-fluoropyridine (**1**): (A) ^{6}Li spectrum; (B) ^{15}N spectrum; (C) ^{19}F spectrum.

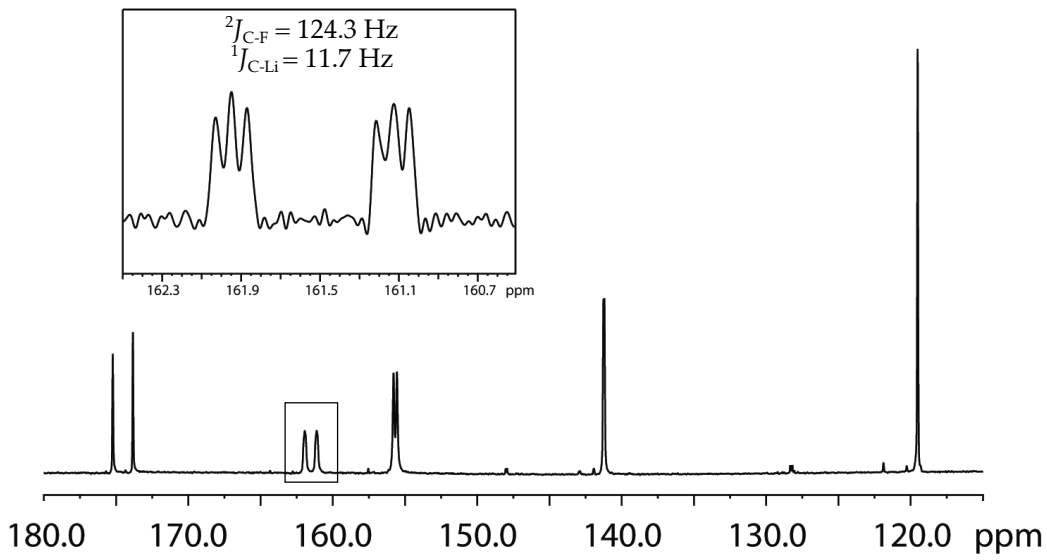

Figure AIII.2. $^{13}C\{^1H\}$ NMR spectrum (150 MHz) of 0.050 M 2-fluoro-3-lithiopyridine (**3**) in neat THF at -100 °C: δ 175.54 (d, $^1J_{C\text{-}F}$ = 210.6 Hz), 161.54 (dt, $^2J_{C\text{-}F}$ = 124.3 Hz, $^1J_{C\text{-}Li}$ = 11.7 Hz), 155.68 (d, $^3J_{C\text{-}F}$ = 35.9 Hz), 141.24 (d, $^3J_{C\text{-}F}$ = 11.8 Hz), 119.52 (s). Inset shows the multiplet at δ 161.54 and includes lorentzian to gaussian transformation to enhance resolution.

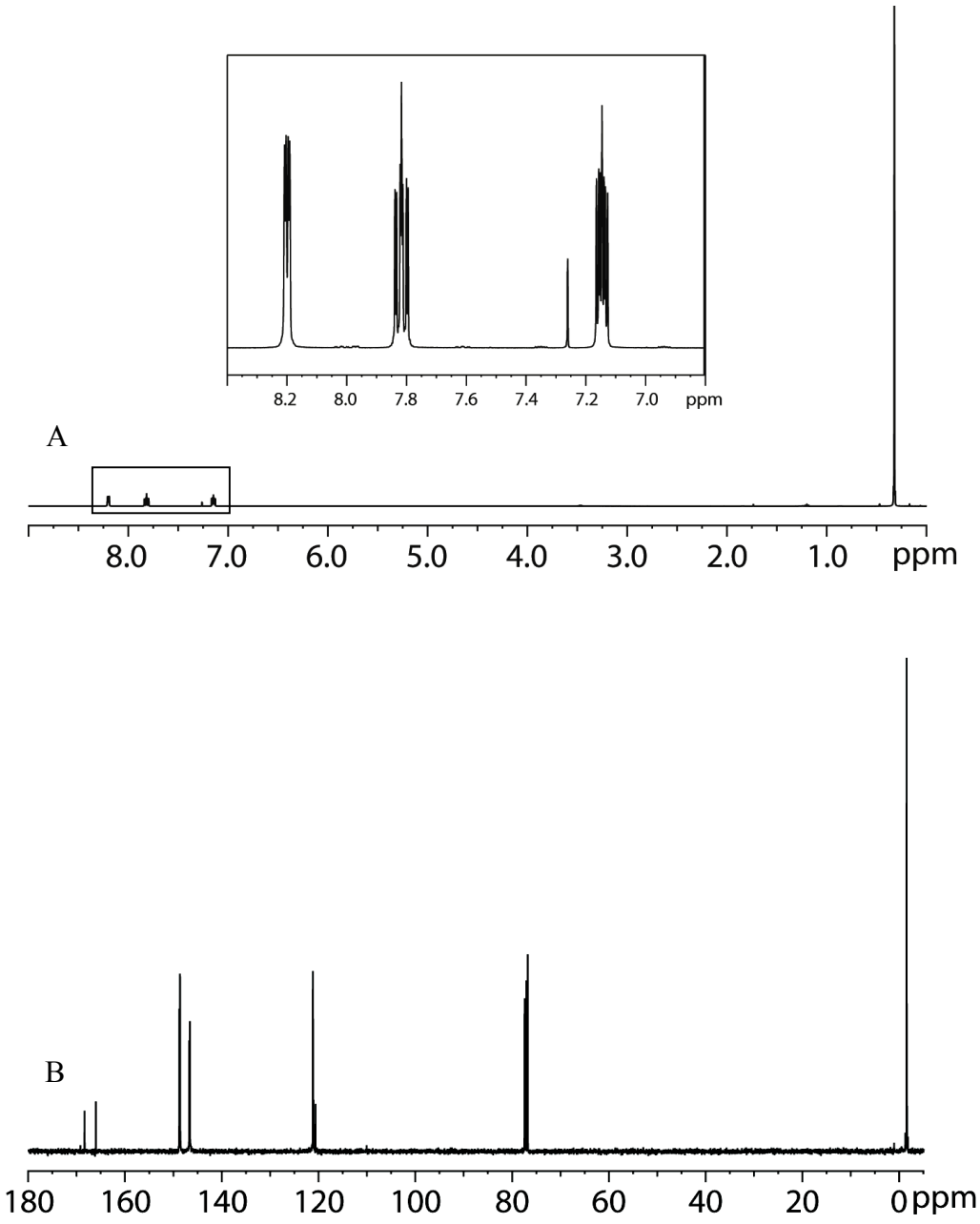

Figure AIII.3. ^{1}H and ^{13}C NMR spectra of 2-fluoro-3-(trimethylsilyl)pyridine in $CDCl_3$: (A) ^{1}H NMR, 400 MHz: δ 8.20 (dd, J = 4.9, 2.1 Hz, 1H), 7.82 (m, 1H), 7.15 (m, 1H), 0.32 (s, 9H). Inset shows the peaks in the aromatic region; (B) ^{13}C NMR, 100 MHz: δ 167.3 (d, J = 235.4 Hz), 148.8 (d, J = 14.8 Hz), 146.8 (d, J = 10.2 Hz), 121.2 (d, J = 4.0 Hz), 120.9 (d, J = 45.2 Hz), -1.4 (d, J = 1.5 Hz). HRMS [$C_8H_{12}NFSi$] requires m/z 169.0723, found 169.0726.

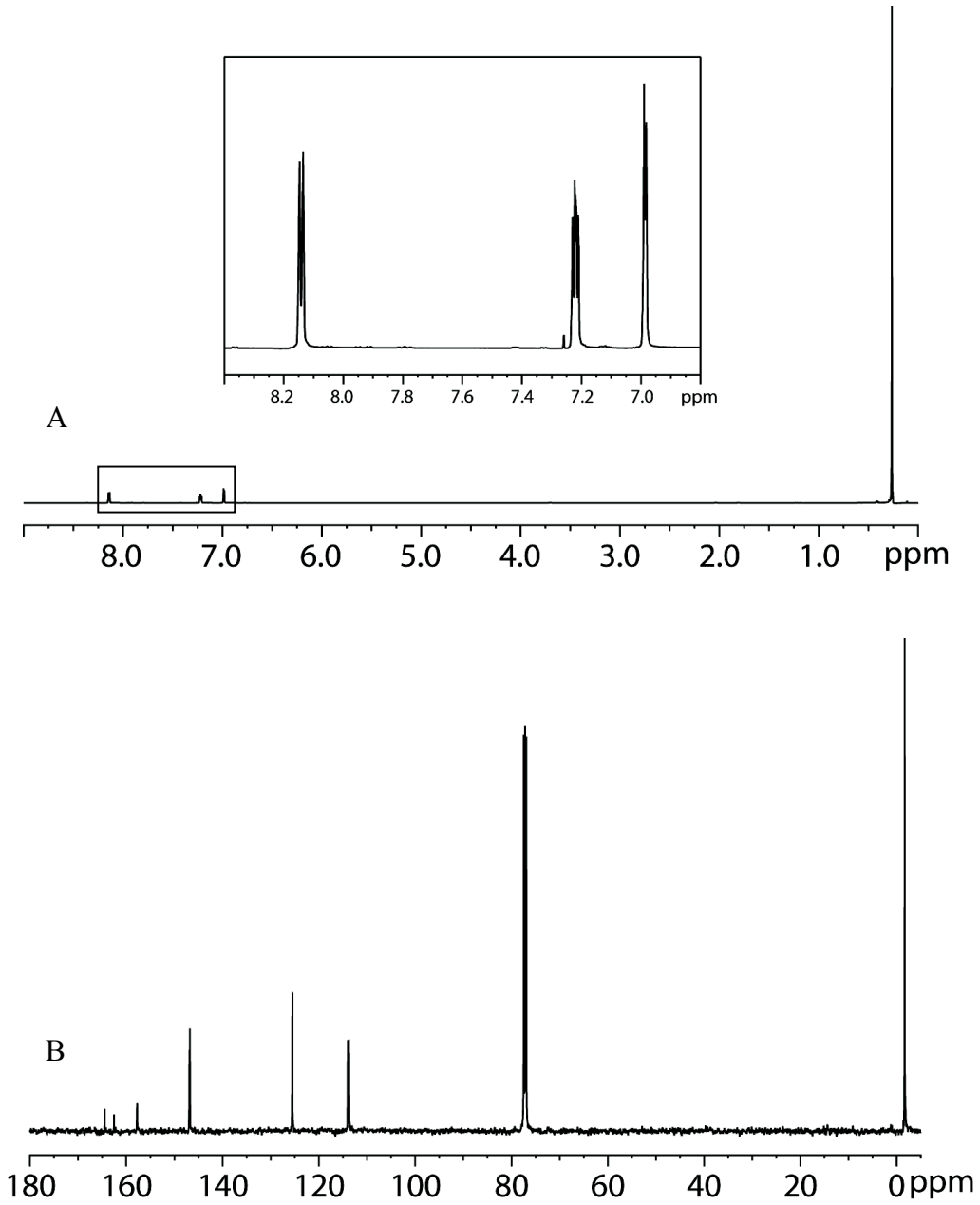

Figure AIII.4. ^{1}H and ^{13}C NMR spectra of 2-fluoro-4-(trimethylsilyl)pyridine in $CDCl_3$: (A) ^{1}H NMR, 400 MHz: δ 8.14 (dt, J = 4.8, 0.9 Hz, 1H), 7.22 (m, 1H), 6.99 (m, 1H), 0.27 (s, 9H). Inset shows the peaks in the aromatic region; (B) ^{13}C NMR, 125 MHz: δ 163.5 (d, J = 242.3 Hz), 157.7 (d, J = 4.9 Hz), 146.8 (d, J = 12.9 Hz), 125.5 (d, J = 4.0 Hz), 113.9 (d, J = 33.6 Hz), -1.6 (s). HRMS [$C_8H_{12}NFSi$] requires m/z 169.0723, found 169.0727.

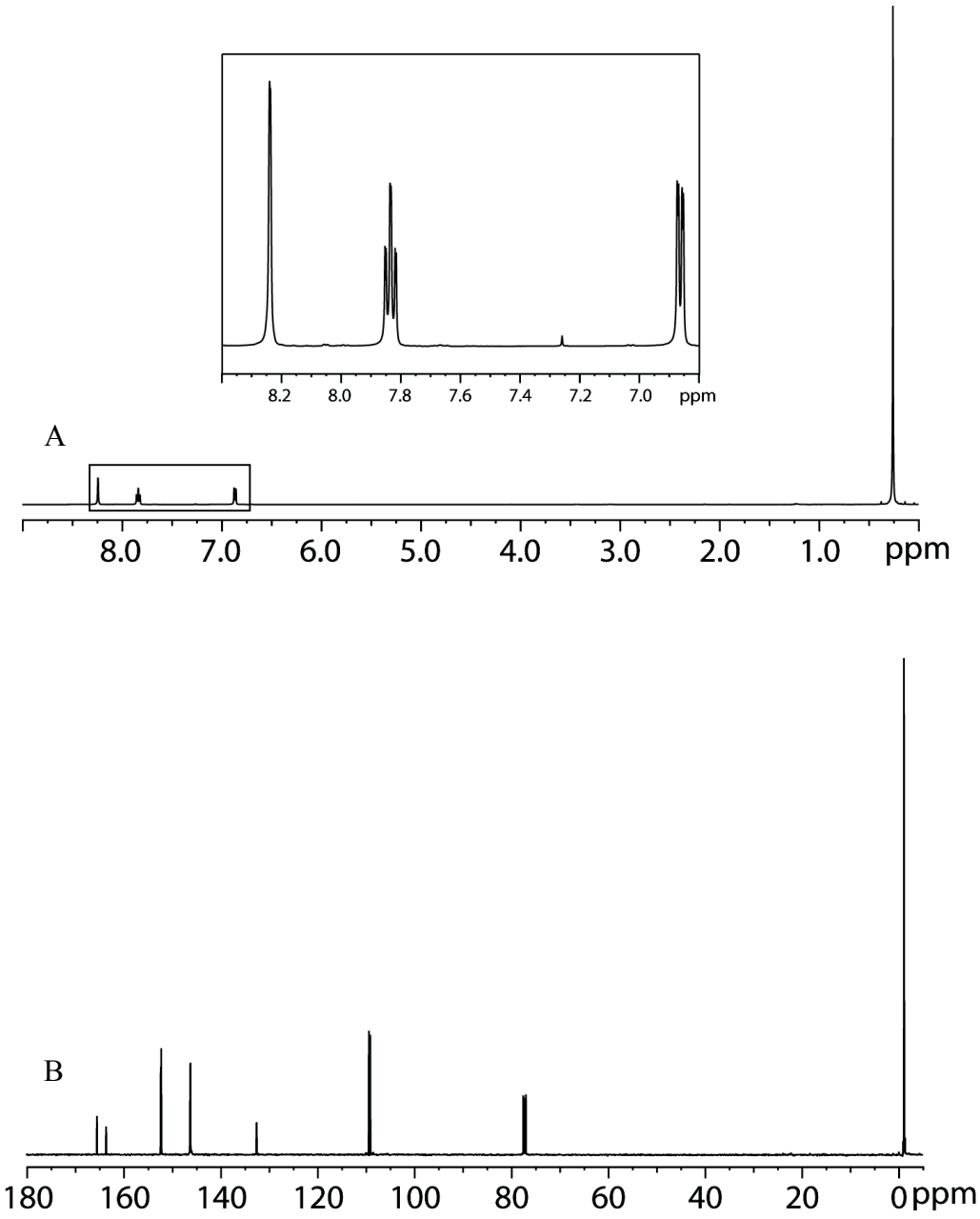

Figure AIII.5. ^{1}H and ^{13}C NMR spectra of 2-fluoro-5-(trimethylsilyl)pyridine in $CDCl_3$: (A) ^{1}H NMR, 500 MHz: δ 8.24 (s, 1H), 7.84 (td, J = 8.5, 2.0 Hz, 1H), 6.86 (dd, J = 8.1, 2.0 Hz, 1H), 0.26 (s, 9H). Inset shows the peaks in the aromatic region; (B) ^{13}C NMR, 125 MHz: δ 164.5 (d, J = 239.8 Hz), 152.2 (d, J = 13.2 Hz), 146.2 (d, J = 7.0 Hz), 132.5 (d, J = 4.4 Hz), 109.2 (d, J = 35.0 Hz), -1.2 (s). HRMS [$C_8H_{12}NFSi$] requires m/z 169.0723, found 169.0728.

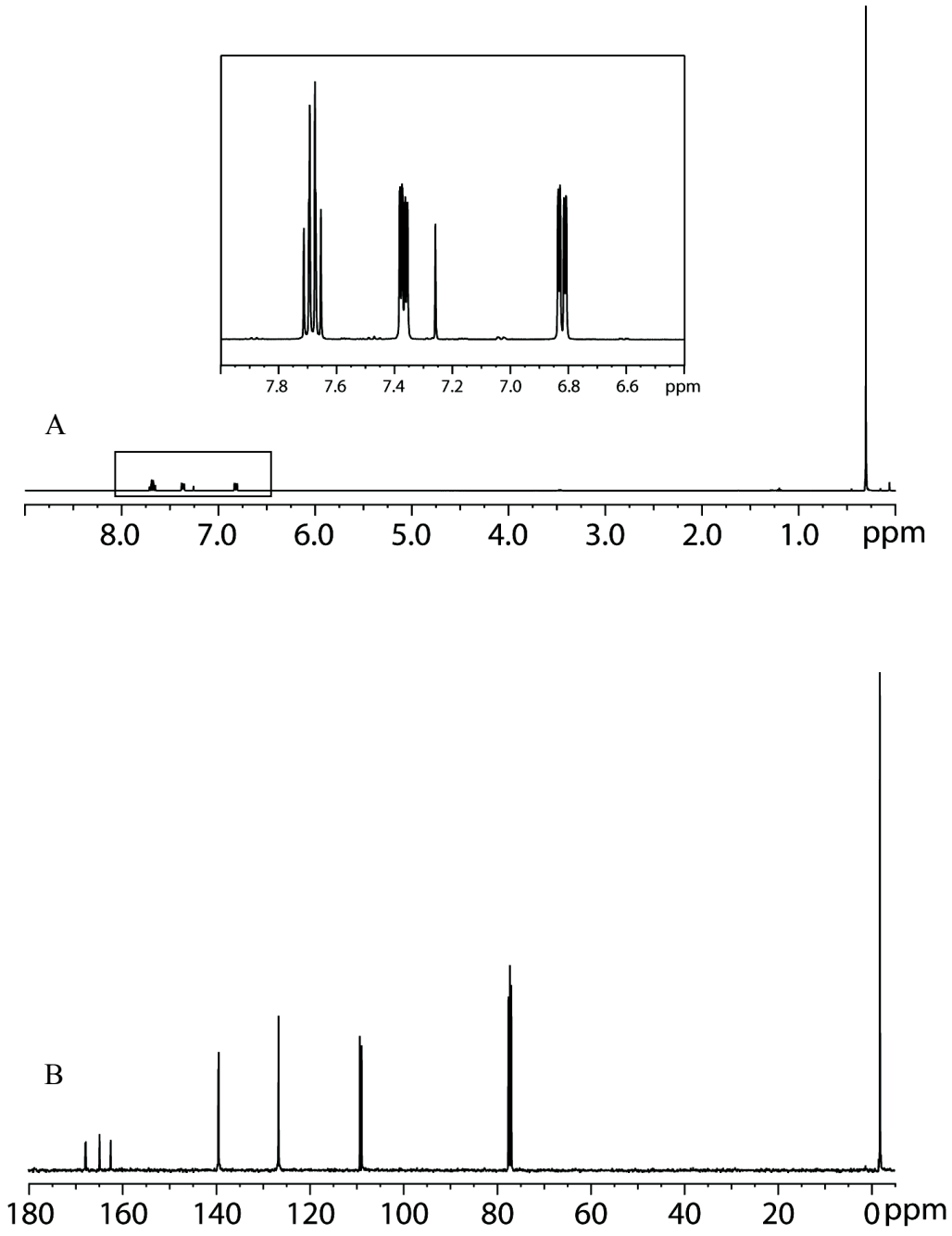

Figure AIII.6. ^{1}H and ^{13}C NMR spectra of 2-fluoro-6-(trimethylsilyl)pyridine in $CDCl_3$: (A) ^{1}H NMR, 400 MHz: δ 7.68 (m, 1H), 7.36 (m, 1H), 6.82 (m, 1H), 0.31 (s, 9H). Inset shows the peaks in the aromatic region. (B) ^{13}C NMR, 100 MHz: δ 167.8 (d, J = 11.5 Hz), 163.6 (d, J = 238.6 Hz), 139.4 (d, J = 7.5 Hz), 126.5 (d, J = 3.6 Hz), 109.0 (d, J = 38.3 Hz), -1.9 (s). HRMS [$C_8H_{12}NFSi$] requires m/z 169.0723, found 169.0730.

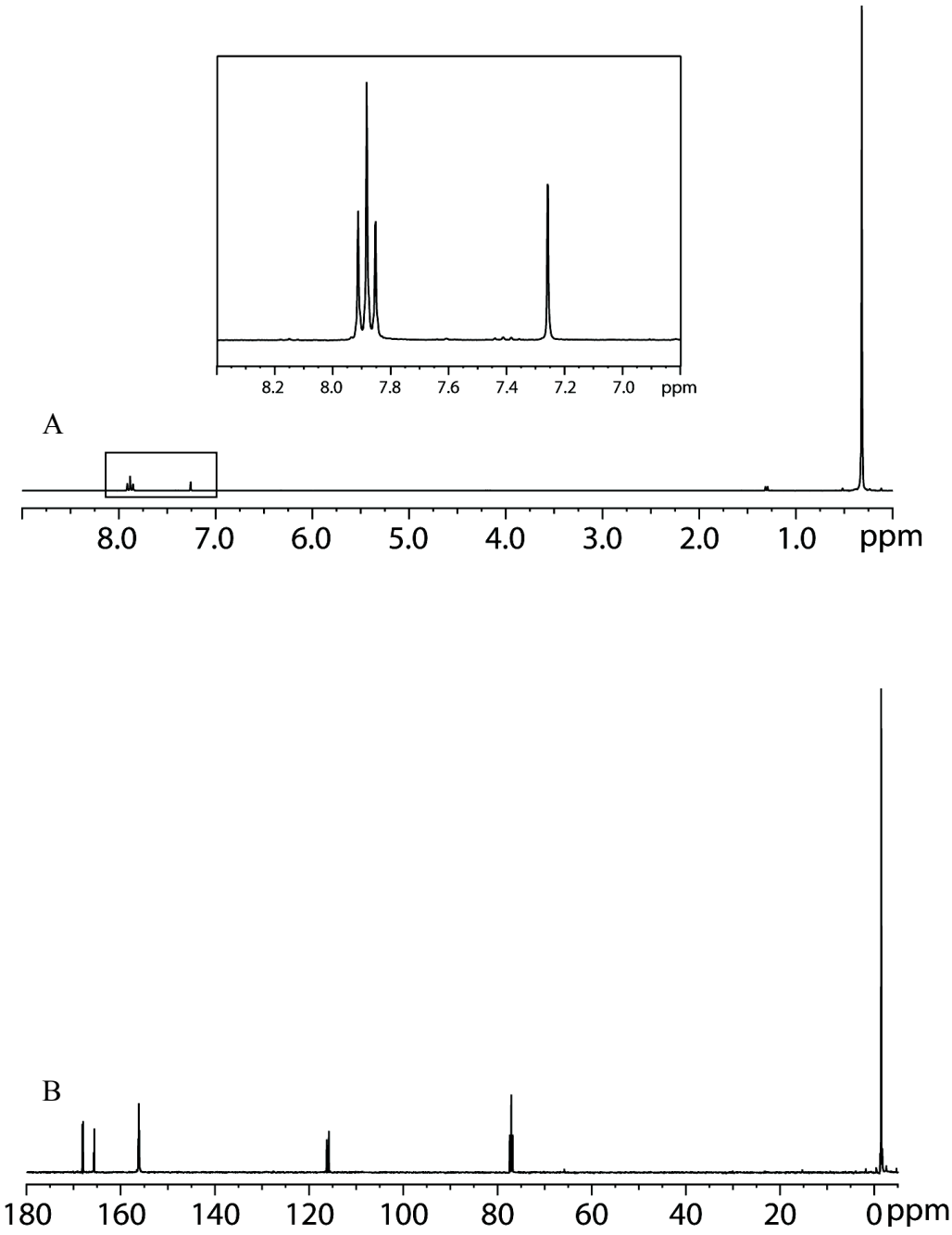

Figure AIII.7. ^{1}H and ^{13}C NMR spectra of 2,6-difluoro-3,5-bis(trimethylsilyl)pyridine in $CDCl_3$: (A) ^{1}H NMR, 300 MHz: δ 7.88 (t, J = 8.9 Hz, 1H), 0.32 (s, 18H). Inset shows the peaks in the aromatic region. (B) ^{13}C NMR, 100 MHz: δ 166.9 (dd, J = 243.4, 14.5 Hz), 156.2 (td, J = 9.7, 1.6 Hz), 116.1 (m), -1.4 (s). HRMS [$C_8H_{12}NFSi$] requires m/z 259.1024, found 259.1030.

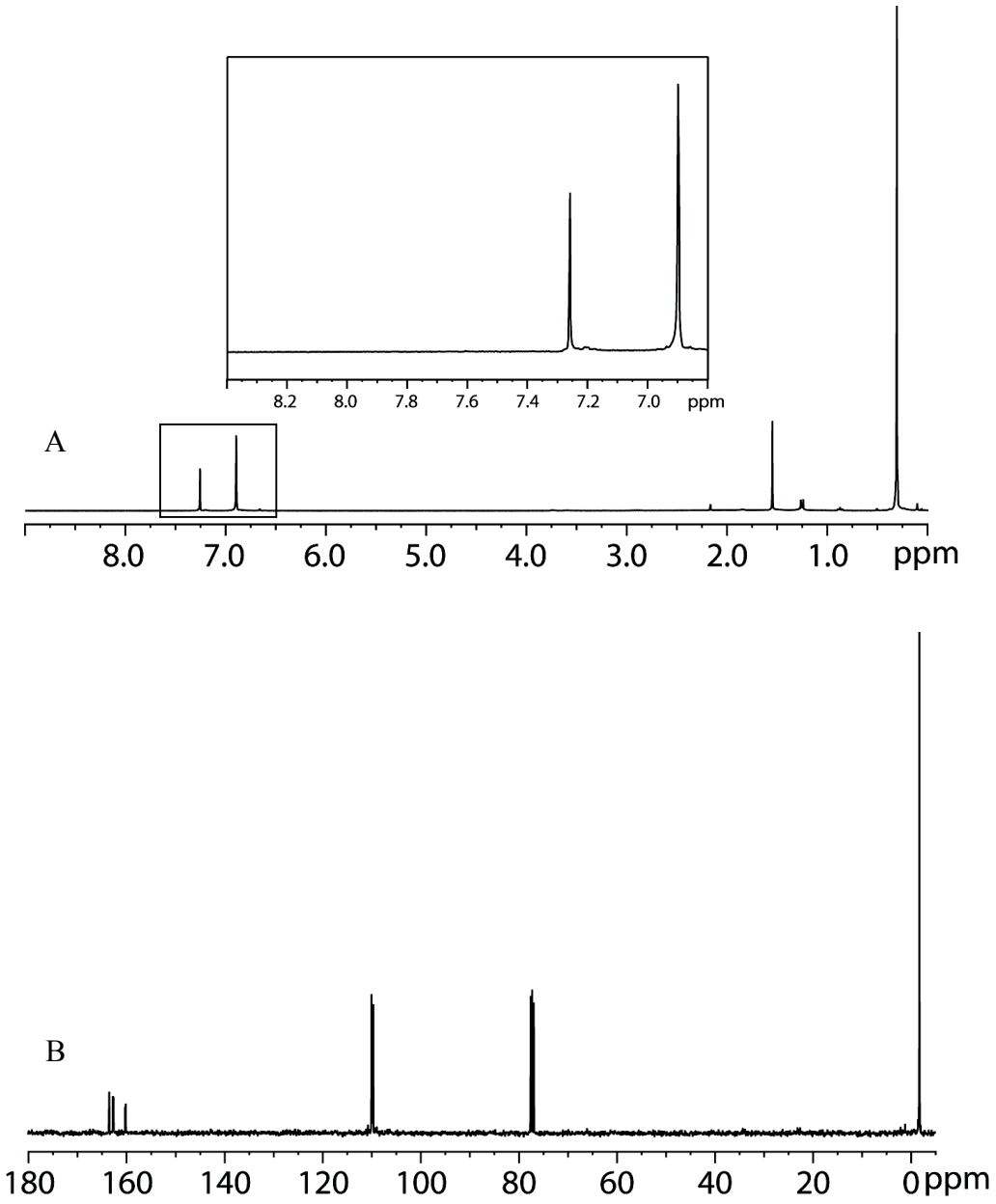

Figure AIII.8. ^{1}H and ^{13}C NMR spectra of 2,6-difluoro-4-(trimethylsilyl)pyridine in $CDCl_3$: (A) ^{1}H NMR, 500 MHz: δ 6.90 (d, J = 0.7 Hz, 2H), 0.31 (s, 9H). Inset shows the peaks in the aromatic region. (B) ^{13}C NMR, 100 MHz: δ 163.5 (t, J = 4.1 Hz), 161.4 (dd, J = 250.9, 13.0 Hz), 109.8 (m), -1.8 (s). HRMS [$C_8H_{12}NFSi$] requires m/z 187.0629, found 187.0630.

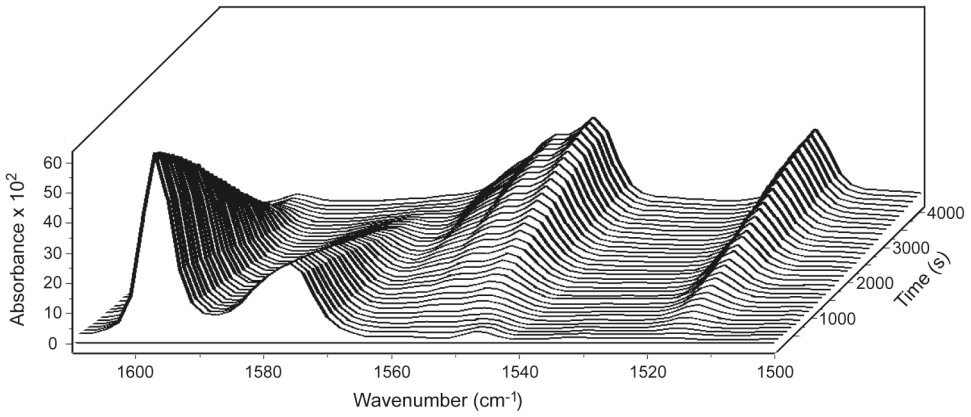

Figure AIII.9. Representative in situ IR spectroscopic analysis of the ortholithiation of **1** (0.05 M) with LDA (0.10 M) in THF at -78 °C. The IR absorbances at 1598 cm^{-1} and 1576 cm^{-1} correspond to **1**, whereas the absorbances at 1551 cm^{-1} and 1517 cm^{-1} correspond to its lithiated form **3**.

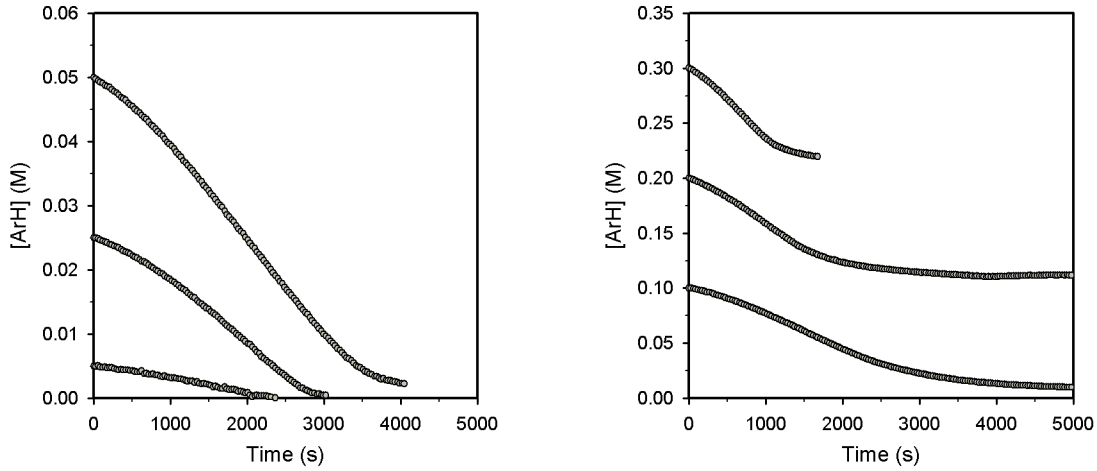

Figure AIII.10. Representative plots showing [ArH] vs time for the ortholithiation of **1** with LDA (0.10 M) in THF (12.20 M) at -78 °C.

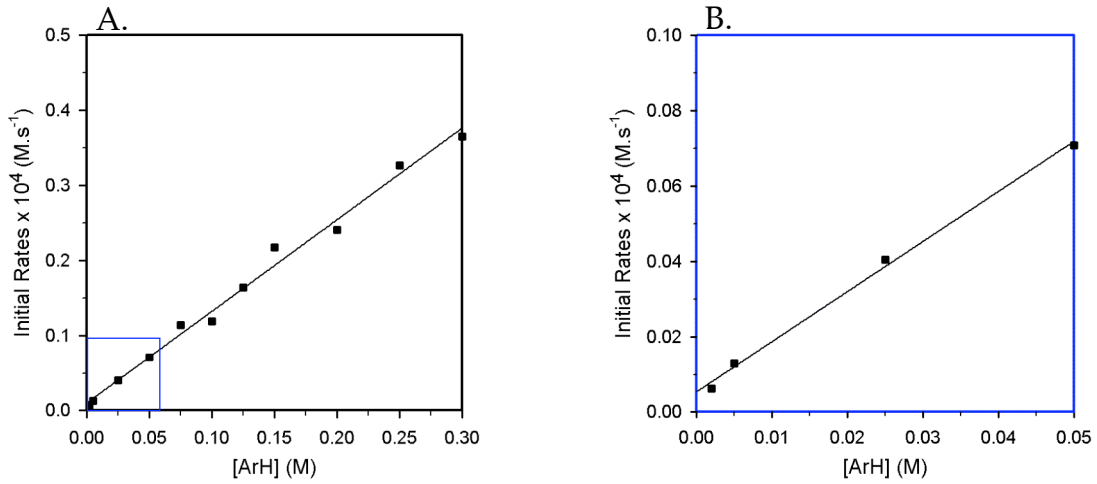

Figure AIII.11. Plot of initial rates vs [ArH] for the ortholithiation of **1** with LDA (0.10 M) in THF (12.20 M) at -78 °C. The curve depicts an unweighted least-squares fit to $y = k[ArH] + k'$ ($k = (1.22 \pm 0.04) \times 10^{-4}$, $k' = (1.0 \pm 0.6) \times 10^{-6}$); (B) Magnified plot of the regime marked in blue square in (A). The curve depicts an unweighted least-squares fit to $y = k[ArH] + k'$ ($k = (1.32 \pm 0.05) \times 10^{-4}$, $k' = (5 \pm 1) \times 10^{-7}$)

[ArH] (M)	$y_1 \times 10^4$ (M.s^{-1})
0.002	0.006 ± 2E-3
0.005	0.013 ± 2E-3
0.025	0.0405 ± 9E-4
0.050	0.0709 ± 7E-4
0.075	0.114 ± 2E-3
0.100	0.119 ± 2E-3
0.125	0.164 ± 2E-3
0.150	0.217 ± 6E-3
0.200	0.240 ± 5E-3
0.250	0.33 ± 2E-2
0.300	0.365 ± 8E-3

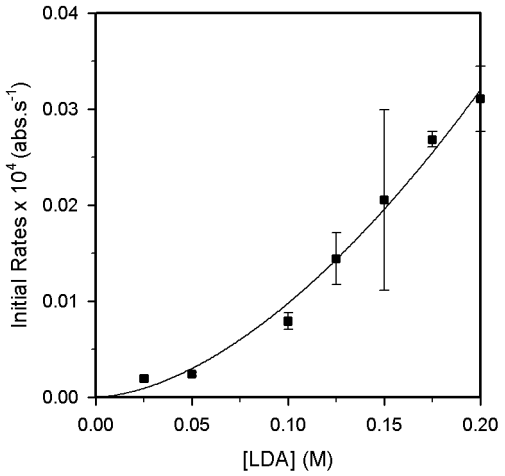

Figure AIII.12. Plot of initial rates vs [LDA] in THF (11.5 M) using hexaness as the cosolvent for the ortholithiation of **1** (0.002 M) at -78 °C. The curve depicts an unweighted least-squares fit to $y = k[\text{LDA}]^n$ ($k = (5 \pm 2) \times 10^{-5}$, $n = 1.7 \pm 0.3$).

[LDA] (M)	$y_1 \times 10^4$ (abs.s^{-1})	$y_2 \times 10^4$ (abs.s^{-1})	$y_3 \times 10^4$ (abs.s^{-1})
0.025	0.0018 ± 2E-4	0.0019 ± 2E-4	—
0.05	0.0022 ± 4E-4	0.0025 ± 4E-4	—
0.10	0.008 ± 1E-3	0.007 ± 2E-3	—
0.125	0.016 ± 4E-3	0.012 ± 3E-3	—
0.15	0.022 ± 4E-3	0.011 ± 4E-3	0.029 ± 6E-3
0.175	0.027 ± 7E-3	0.026 ± 4E-3	—
0.20	0.027 ± 3E-3	0.032 ± 1E-2	0.034 ± 9E-3

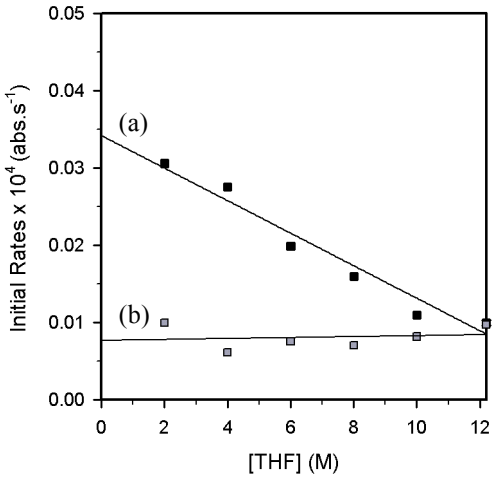

Figure AIII.13. Plot of initial rates vs [THF] for the ortholithiation of **1** (0.002 M) with LDA (0.10 M) at -78 °C in: (a) hexanes cosolvent. The curve depicts an unweighted least-squares fit to $y = -k[THF] + k'$ ($k = (2.1 \pm 0.2) \times 10^{-7}$, $k' = (3.4 \pm 0.2) \times 10^{-6}$); (b) 2,5-dimethyltetrahydrofuran cosolvent. The curve depicts an unweighted least-squares fit to $y = -k[THF] + k'$ ($k = (6 \pm 19) \times 10^{-9}$, $k' = (8 \pm 1) \times 10^{-7}$).

	(a)	(b)
[THF] (M)	$y_1 \times 10^4$ (abs.s^{-1})	$y_2 \times 10^4$ (abs.s^{-1})
2.0	0.030 ± 1E-3	0.010 ± 1E-3
4.0	0.027 ± 1E-3	0.006 ± 1E-3
6.0	0.0199 ± 8E-4	0.0075 ± 6E-4
8.0	0.0160 ± 3E-4	0.007 ± 3E-3
10.0	0.0109 ± 8E-4	0.008 ± 2E-3
12.0	0.009 ± 1E-3	0.009 ± 1E-3

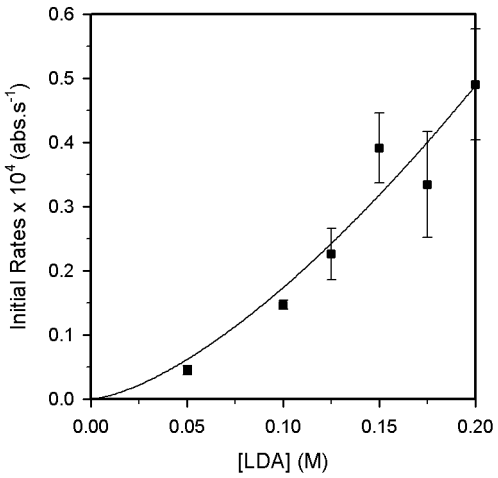

Figure AIII.14. Plot of initial rates vs [LDA] in THF (11.5 M) using hexanes as the cosolvent for the ortholithiation of **1** (0.20 M) at -78 °C. The curve depicts an unweighted least-squares fit to $y = k[\text{LDA}]^n$ ($k = (5 \pm 3) \times 10^{-4}$, $n = 1.5 \pm 0.3$).

[LDA] (M)	$y_1 \times 10^4$ (abs.s^{-1})	$y_2 \times 10^4$ (abs.s^{-1})	$y_3 \times 10^4$ (abs.s^{-1})
0.050	0.050 ± 4E-3	0.040 ± 6E-3	—
0.100	0.15 ± 1E-2	0.142 ± 7E-3	—
0.125	0.25 ± 3E-2	0.19 ± 1E-2	—
0.150	0.42 ± 3E-2	0.33 ± 1E-2	0.43 ± 2E-2
0.175	0.39 ± 3E-2	0.27 ± 1E-2	—
0.200	0.40 ± 1E-2	0.49 ± 2E-2	0.58 ± 3E-2

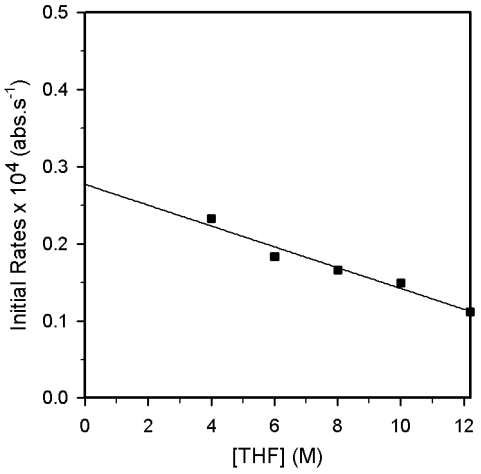

Figure AIII.15. Plot of initial rates vs [THF] in hexanes cosolvent for the ortholithiation of **1** (0.20 M) with LDA (0.10 M) at -78 °C. The curve depicts an unweighted least-squares fit to $y = -k[THF] + k'$ ($k = (1.3 \pm 0.2) \times 10^{-6}$, $k' = (2.8 \pm 0.1) \times 10^{-5}$).

[THF] (M)	$y_1 \times 10^4$ (abs.s^{-1})
4.0	0.23 ± 3E-2
6.0	0.18 ± 4E-2
8.0	0.2 ± 3E-1
10.0	0.15 ± 1E-2
12.20	0.11 ± 3E-2

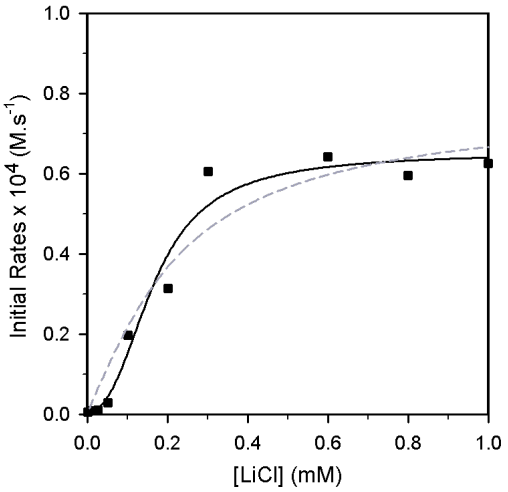

Figure AIII.16. Plot of initial rates vs [LiCl] for the ortholithiation of **1** (0.004 M) with LDA (0.10 M) in THF (12.20 M) at -78 °C. The curve depicts an unweighted least-squares fit to $-d[\mathrm{ArH}]/dt = \{k_2[\mathrm{ArH}]/4k_{-1}[\mathrm{LiCl}]^n\}\ \{(k_2^2[\mathrm{ArH}]^2 + 16k_1k_{-1}[\mathrm{A_2S_2}]_0\ [\mathrm{LiCl}]^{2n})^{0.5} - k_2[\mathrm{ArH}]\} + c$ (see page 31 for derivation). [ArH] = 0.004 M, $[\mathrm{A_2S_2}]_0$ = 0.05 M, c = $(5 \pm 1) \times 10^{-7}$, $n = 2$ and $k_1 = (1.6 \pm 0.1) \times 10^{-2}$, $k_{-1} = (1.03 \pm 0.03) \times 10^4$, $k_2 = (5.901 \pm 0.002) \times 10^1$. The dashed curve represents a fit to the data where $n = 1$ in the given equation.

[LiCl] (mM)	$y_1 \times 10^4$ ($M.s^{-1}$)
0.0	0.005 ± 1E-3
0.01	0.0084 ± 9E-4
0.025	0.010 ± 2E-3
0.05	0.028 ± 4E-3
0.10	0.20 ± 3E-2
0.20	0.31 ± 7E-2
0.30	0.61 ± 8E-2
0.60	0.64 ± 8E-2
0.80	0.6 ± 1E-1
1.0	0.6 ± 1E-1

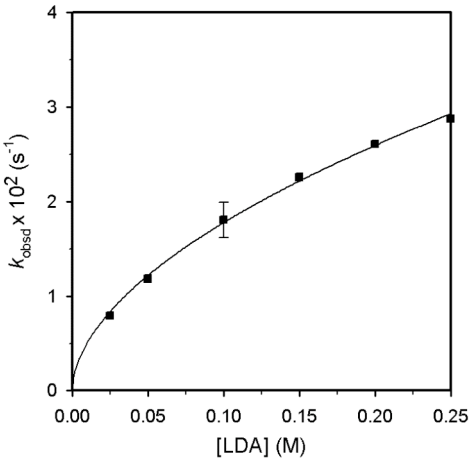

Figure AIII.17. Plot of k_{obsd} vs [LDA] in THF (12.20 M) using hexanes as the cosolvent for the ortholithiation of **1** (0.004 M) in the presence of 2 mol% LiCl at -78 °C. The curve depicts an unweighted least-squares fit to $k_{obsd} = k[\text{LDA}]^n$ ($k = (6.2 \pm 0.4) \times 10^{-2}$, $n = 0.54 \pm 0.03$).

[LDA] (M)	k_{obsd1} x 10^2 (s^{-1})	k_{obsd2} x 10^2 (s^{-1})	k_{obsd3} x 10^2 (s^{-1})
0.025	0.79 ± 1E-2	—	
0.05	1.18 ± 2E-2	—	
0.10	1.94 ± 5E-2	1.67 ± 5E-2	1.80 ± 5E-2
0.15	2.26 ± 7E-2	—	
0.20	2.6 ± 1E-1	—	
0.25	2.9 ± 1E-1	—	

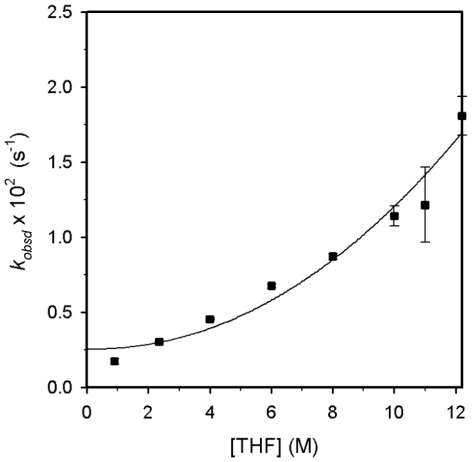

Figure AIII.18. Plot of k_{obsd} vs [THF] in hexanes cosolvent for the ortholithiation of **1** (0.004 M) with LDA (0.10 M) in the presence of 2 mol% LiCl at -78 °C. The curve depicts an unweighted least-squares fit to $k_{obsd} = k[THF]^n + k'$ ($k = (8 \pm 7) \times 10^{-5}$, $n = (2.0 \pm 0.4)$, $k' = (2.5 \pm 0.7) \times 10^{-3}$).

[THF] (M)	k_{obsd1} x 10^2 (s^{-1})	k_{obsd2} x 10^2 (s^{-1})	k_{obsd3} x 10^2 (s^{-1})
0.89	0.185 ± 4E-3	0.160 ± 5E-3	—
2.35	0.304 ± 5E-3	0.304 ± 4E-3	—
4.0	0.449 ± 8E-3	0.458 ± 9E-3	—
6.0	0.68 ± 1E-2	0.67 ± 1E-2	—
8.0	0.86 ± 2E-2	0.89 ± 2E-2	—
10.0	1.19 ± 5E-2	1.09 ± 3E-2	—
11.0	1.39 ± 6E-2	1.04 ± 4E-2	—
12.20	1.94 ± 5E-2	1.67 ± 5E-2	1.80 ± 5E-2

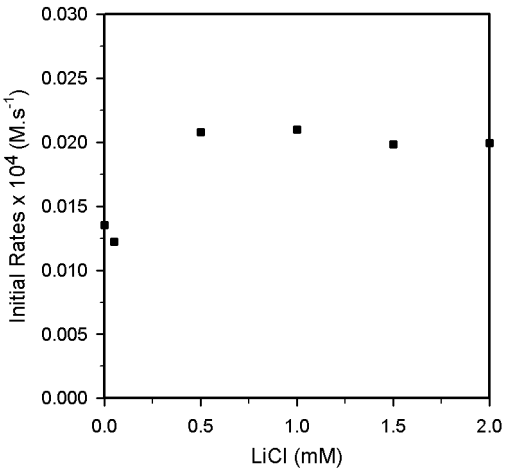

Figure AIII.19. Plot of initial rates vs [LiCl] for the ortholithiation of **1-*d*$_1$** (0.004 M) with LDA (0.10 M) in THF (12.20 M) at -78 °C.

[LiCl] (mM)	y_1 x 10^4 ($M.s^{-1}$)
0.0	0.0135 $\pm$ 2E-4
0.05	0.0122 $\pm$ 3E-4
0.5	0.0208 $\pm$ 3E-4
1.0	0.0209 $\pm$ 5E-4
1.5	0.0198 $\pm$ 5E-4
2.0	0.0199 $\pm$ 3E-4

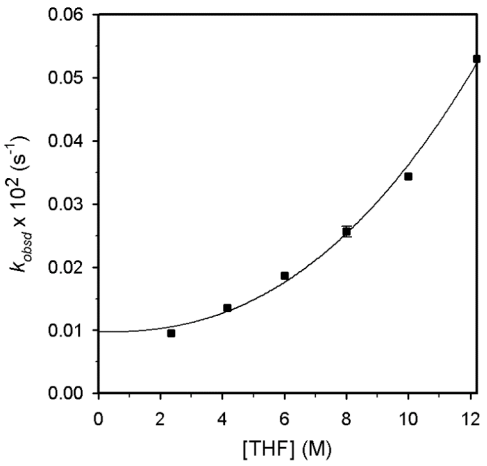

Figure AIII.20. Plot of k_{obsd} vs [THF] in hexanes cosolvent for the ortholithiation of **1-*d*$_1$** (0.004 M) with LDA (0.10 M) in the presence of 2 mol% LiCl at -78 °C. The curve depicts an unweighted least-squares fit to $k_{obsd} = k[THF]^n + k'$ ($k = (1.1 \pm 0.6) \times 10^{-6}$, $n = (2.4 \pm 0.2)$, $k' = (10 \pm 1) \times 10^{-5}$).

[THF] (M)	k_{obsd1} x 10^2 (s^{-1})	k_{obsd2} x 10^2 (s^{-1})
2.35	0.00956 ± 8E-5	—
4.15	0.01355 ± 7E-5	—
6.0	0.0186 ± 3E-4	—
8.0	0.0262 ± 3E-4	0.0251 ± 5E-4
10.0	0.0344 ± 6E-4	—
12.20	0.0530 ± 7E-4	—

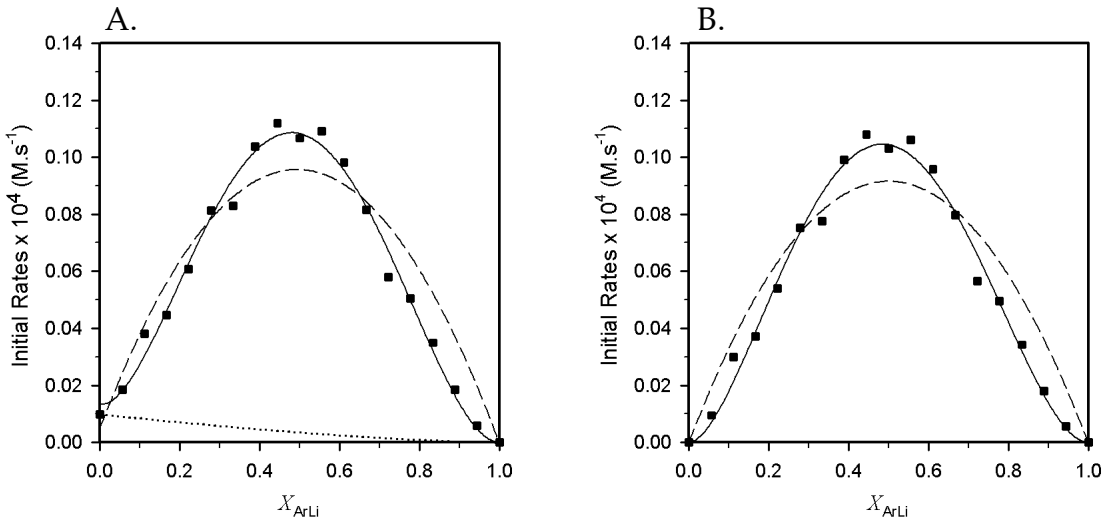

Figure AIII.21. Plot of initial rates versus mole fraction of 2-fluoro-3-lithio pyridine (X_{ArLi}) for the serial injection of 0.0055 M aliquots of pyridine **1** to 0.10 M LDA in 12.20 M THF at -78 °C. The dotted line in figure A depicts the theoretical initial rates in the absence of autocatalysis, assuming an LDA order of 1.5. The solid line depicts an unweighted least-squares fit to $-d[\mathbf{1}]/dt = k(1-X_{ArLi})^m(X_{ArLi})^n + k'(1-X_{ArLi})^{1.5}$ (see page 32 for derivation), $m = 1.9 \pm 0.1$, $n = 1.8 \pm 0.1$, $k = (1.5 \pm 0.3) \times 10^{-4}$, $k' = (1.3 \pm 0.4) \times 10^{-6}$. The dashed curve represents a fit to the data where $n = 1$ and $m = 1$ in the given equation. In figure B, the contribution of the uncatalyzed pathway (dotted line in figure A) is subtracted.

X_{ArLi}	y x 10^4 (M.s^{-1})	X_{ArLi}	y x 10^4 (M.s^{-1})
0.0000	0.0098 ± 6E-4	0.5556	0.109 ± 7E-3
0.0556	0.018 ± 1E-3	0.6111	0.098 ± 8E-3
0.1111	0.038 ± 2E-3	0.6667	0.082 ± 5E-3
0.1667	0.045 ± 4E-3	0.7222	0.058 ± 3E-3
0.2222	0.061 ± 4E-3	0.7778	0.050 ± 3E-3
0.2778	0.081 ± 6E-3	0.8333	0.035 ± 2E-3
0.3333	0.083 ± 7E-3	0.8889	0.0184 ± 6E-4
0.3889	0.10 ± 1E-2	0.9444	0.0059 ± 5E-4
0.4444	0.112 ± 9E-3	1.0000	0.0
0.5000	0.107 ± 7E-3		

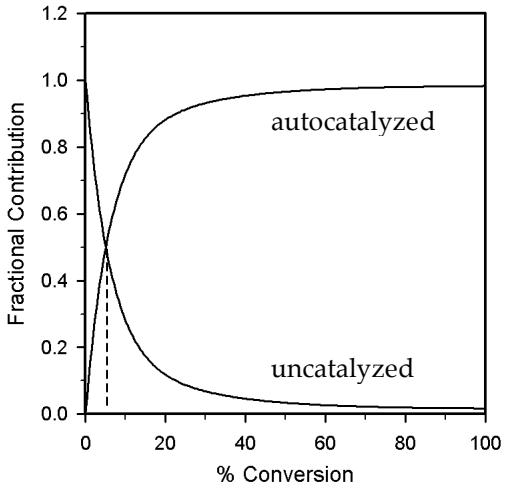

Figure AIII.22. Plot of fractional contribution of the autocatalyzed and uncatalyzed pathway to the total reaction rate versus percent conversion derived from the data in Figure AIII.21. Equal contribution from the two pathways (dashed line) occurs at 6% conversion.

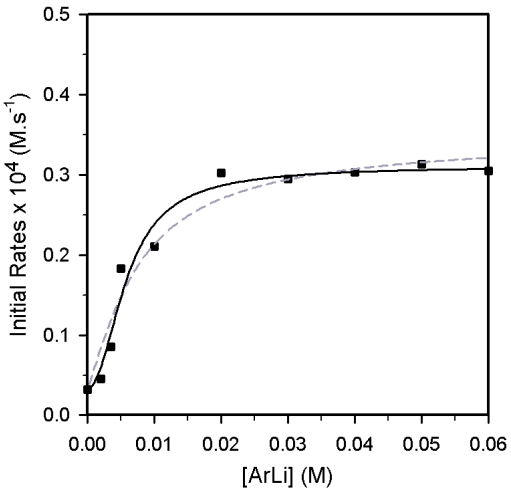

Figure AIII.23. Plot of initial rates vs [ArLi] for the ortholithiation of **1** (0.005 M) with LDA (0.10 M) in THF (12.20 M) at -78 °C. The curve depicts an unweighted least-squares fit to $-d[\mathrm{ArH}]/dt = \{k_2[\mathrm{ArH}]/4k_{-1}[\mathrm{ArLi}]^n\}\{(k_2^2[\mathrm{ArH}]^2 + 16k_1k_{-1}[\mathrm{A_2S_2}]_0\ [\mathrm{ArLi}]^{2n})^{0.5} - k_2[\mathrm{ArH}]\} + c$ (see page 31 for derivation). [ArH] = 0.005 M, $[\mathrm{A_2S_2}]_0 = 0.05$ M, c = (3.2 ± 0.5) x 10^{-6} and $n = 1.7 \pm 0.4$, $k_1 = 1.2 \pm 2.6$, k_{-1} = (1.6 ± 0.2) x 10^3, k_2 = (9.2 ± 11.5) x 10^{-1}. The dashed curve represents a fit to the data where $n = 1$ in the given equation.

[ArLi] (M)	y_1 x 10^4 ($M.s^{-1}$)
0.0	0.032 ± 5E-3
0.002	0.045 ± 5E-3
0.0035	0.085 ± 9E-3
0.005	0.18 ± 1E-2
0.01	0.21 ± 1E-2
0.02	0.30 ± 5E-2
0.03	0.29 ± 3E-2
0.04	0.30 ± 4E-2
0.05	0.31 ± 5E-2
0.06	0.30 ± 6E-2

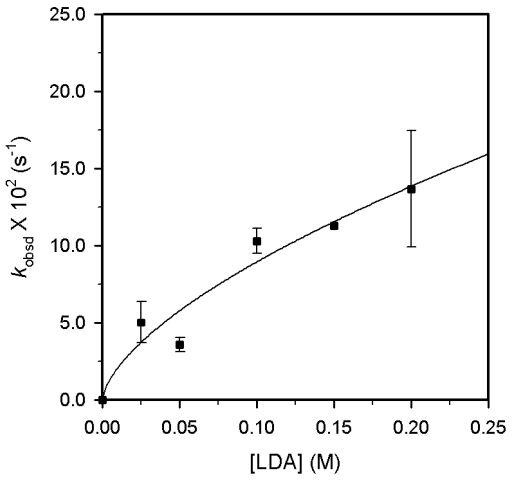

Figure AIII.24. Plot of k_{obsd} vs [LDA] in THF (12.20 M) using hexanes as the cosolvent for the ortholithiation of **1** (0.005 M) in the presence of 0.04 M ArLi at -78 °C. The curve depicts an unweighted least-squares fit to $k_{obsd} = k[\text{LDA}]^n$ ($k = (4 \pm 1) \times 10^{-2}$, $n = 0.6 \pm 0.1$).

[LDA] (M)	$k_{obsd1} \times 10^2$ (s^{-1})	$k_{obsd2} \times 10^2$ (s^{-1})
0.025	0.59 ± 1E-2	0.407 ± 6E-3
0.05	0.39 ± 1E-2	0.325 ± 7E-3
0.10	1.09 ± 2E-2	0.97 ± 2E-2
0.15	1.22 ± 3E-2	—
0.20	1.63 ± 4E-2	1.10 ± 2E-2

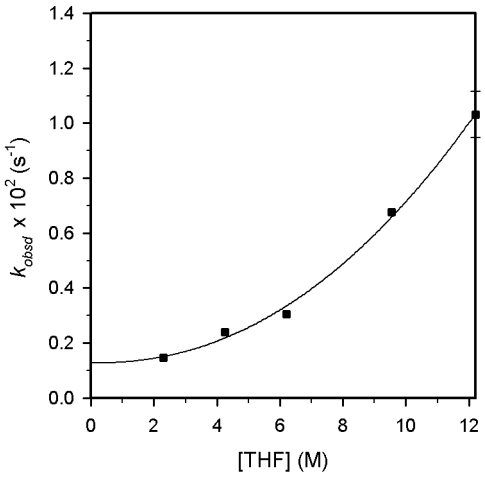

Figure AIII.25. Plot of k_{obsd} vs [THF] in hexanes cosolvent for the ortholithiation of **1** (0.005 M) with LDA (0.10 M) in the presence of 0.03 M ArLi at -78 °C. The curve depicts an unweighted least-squares fit to $k_{obsd} = k[THF]^n + k'$ ($k = (4 \pm 5) \times 10^{-5}$, $n = (2.1 \pm 0.5)$, $k' = (1.2 \pm 0.6) \times 10^{-3}$).

[THF] (M)	k_{obsd1} x 10^2 (s^{-1})	k_{obsd2} x 10^2 (s^{-1})
2.29	0.15 ± 1E-2	—
4.25	0.241 ± 3E-3	—
6.21	0.304 ± 6E-3	—
9.54	0.67 ± 1E-2	—
12.20	1.09 ± 2E-2	1.09 ± 2E-2

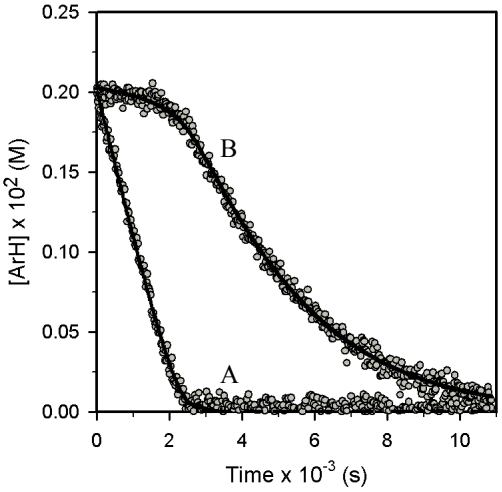

Figure AIII.26. Parametric fit to the plot of [ArH] vs time for the ortholithiation of a mixture of fluoropyridines **1** and **1-*d*$_1$** (0.002 M each) with LDA (0.10 M) in THF (12.20 M) at -78 °C, monitored by ^{19}F NMR spectroscopy: (A) **1**; (B) **1-*d*$_1$**. The functions result from best-fit numerical integration to the following model:

Model:

$$A_2 \underset{k_1}{\overset{k_{-1}}{\rightleftharpoons}} 2A$$

$$A + ArH \xrightarrow{k_H} ArLi$$

$$A + ArD \xrightarrow{k_D} ArLi$$

The model is described by the following differential equations:

$$d[A_2]/dt = -k_1[A_2] + k_{-1}[A]^2$$

$$d[A]/dt = 2k_1[A_2] - 2k_{-1}[A]^2 - k_H[ArH][A] - k_D[ArH][A]$$

$$d[ArH]/dt = -k_H[ArH][A]$$

$$d[ArD]/dt = -k_D[ArD][A]$$

where, ArH = **1**, ArD = **1-*d*$_1$**, A_2 = **5**

k_1 = (9.87 $\pm$ 0.04) x 10^{-6}
k_{-1} = 2.31 $\pm$ 0.09
k_2 = 21.7 $\pm$ 0.8
k_3 = 0.89 $\pm$ 0.02

A. Derivation of expression for fitting LiCl saturation curve (eq 16 and eq 17 in manuscript):

$$A_2S_2 + 2m\text{THF} \underset{k_{-1}[\text{LiCl}]^n}{\overset{k_1[\text{LiCl}]^n}{\rightleftharpoons}} 2AS_{m+1}$$

$$AS_{m+1} + \text{ArH} \xrightarrow{k_2} \text{product}$$

The rate of consumption of arene and its initial rate ($\text{rate}_{\text{init}}$) are defined as:

$$-\frac{d[\text{ArH}]}{dt} = k_2[AS_{m+1}][\text{ArH}] \quad (1)$$

Applying the steady-state approximation to monomer AS_{m+1},

$$\frac{d[AS_{m+1}]}{dt} = 2k_1[A_2S_2][\text{LiCl}]^n[\text{THF}]^{2m} - 2k_{-1}[AS_{m+1}]^2[\text{LiCl}]^n - k_2[AS_{m+1}][\text{ArH}] = 0 \quad (2)$$

solving for $[AS_{m+1}]$ using the quadratic equation,

$$[AS_{m+1}] = \frac{1}{4k_{-1}[\text{LiCl}]^n}\left(\sqrt{k_2^2[\text{ArH}]^2 + 16k_1k_{-1}[A_2S_2][\text{LiCl}]^{2n}[\text{THF}]^{2m}} - k_2[\text{ArH}]\right) \quad (3)$$

substituting eq 3 into eq 1 gives:

$$-\frac{d[\text{ArH}]}{dt} = \frac{k_2[\text{ArH}]}{4k_{-1}[\text{LiCl}]^n}\left(\sqrt{k_2^2[\text{ArH}]^2 + 16k_1k_{-1}[A_2S_2][\text{LiCl}]^{2n}[\text{THF}]^{2m}} - k_2[\text{ArH}]\right) \quad (4)$$

where [ArH] and $[A_2S_2]$ are evaluated at t=0. To account for the LiCl-free pathway as outlined below:

$$A_2S_2 + 2m\text{THF} \underset{k_{-1}}{\overset{k_1}{\rightleftharpoons}} 2AS_{m+1}$$

$$AS_{m+1} + \text{ArH} \xrightarrow{k_2} \text{product}$$

we add a constant c to eq 4 that reflects the initial rate without LiCl. The constant is determined experimentally rather than as an adjustable parameter.

$$-\frac{d[\text{ArH}]}{dt} = \frac{k_2[\text{ArH}]}{4k_{-1}[\text{LiCl}]^n}\left(\sqrt{k_2^2[\text{ArH}]^2 + 16k_1k_{-1}[A_2S_2]_0[\text{LiCl}]^{2n}[\text{THF}]^{2m}} - k_2[\text{ArH}]\right) + c \quad (5)$$

In the limit of full saturation ($k_2 << k_{-1}$), eq 5 reduces to eq 6

$$-\frac{d[\mathrm{ArH}]}{dt} = \frac{(k_1)^{1/2}k_2}{(k_{-1})^{1/2}}[\mathrm{ArH}][\mathrm{THF}]^{2m}[\mathrm{LDA}]^{0.5} \quad (6)$$

B. Derivation of expression for fitting incremental addition curve (eq 19 in manuscript):

In a serial injection experiment, the amount of [ArH] injected remains constant, but the concentration of LDA and ArLi varies with each successive injection.

Hence, the rate of consumption of arene and its initial rate ($\mathrm{rate_{init}}$) are defined as:

$$-d[\mathrm{ArH}]/d\mathrm{t} = k[\mathrm{ArLi}]^n[\mathrm{LDA}]^m \quad (1)$$

Writing the concentrations in terms of mole fractions:

$$-d[\mathrm{ArH}]/d\mathrm{t} = k[X_{\mathrm{ArLi}}]^n[X_{\mathrm{LDA}}]^m \quad (2)$$

where $X_{\mathrm{ArLi}} = \mathrm{N}_{\mathrm{ArLi}}/(\mathrm{N}_{\mathrm{ArLi}} + \mathrm{N}_{\mathrm{LDA}})$ (N stands for normality)

Also, $X_{\mathrm{LDA}} = 1 - X_{\mathrm{ArLi}}$ (3)

Substituting eq 3 into eq 2 gives:

$$-d[\mathrm{ArH}]/d\mathrm{t} = k[X_{\mathrm{ArLi}}]^n[1 - X_{\mathrm{ArLi}}]^m \quad (4)$$

The initial rate in the absence of autocatalysis, assuming an LDA order of 1.5 is given by:

$$-d[\mathrm{ArH}]/d\mathrm{t} = k'[X_{\mathrm{LDA}}]^{1.5} \quad (5)$$

or,

$$-d[\mathrm{ArH}]/d\mathrm{t} = k'[1 - X_{\mathrm{ArLi}}]^{1.5} \quad (6)$$

To account for the rate in the absence of autocatalysis, we add eq 6 to eq 4. Hence, eq 4 becomes:

$$-d[\mathrm{ArH}]/d\mathrm{t} = k[X_{\mathrm{ArLi}}]^n[1 - X_{\mathrm{ArLi}}]^m + k'[1 - X_{\mathrm{ArLi}}]^{1.5} \quad (7)$$

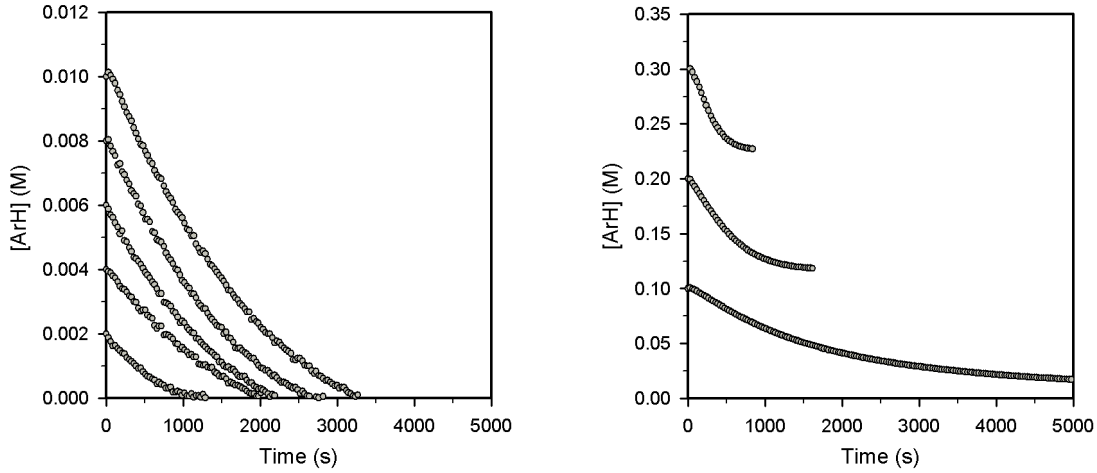

Figure AIII.27. Representative plots showing [ArH] vs time for the ortholithiation of 2,6-difluoropyridine (**2**) with LDA (0.1 M) in THF (12.20 M) at -78 °C.

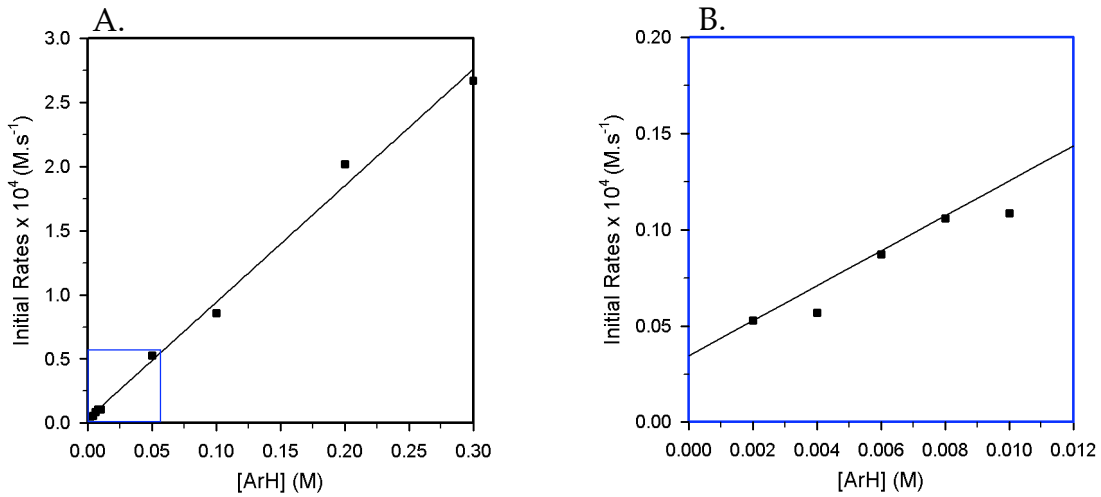

Figure AIII.28. Plot of initial rates vs [ArH] in THF (12.20 M) for the ortholithiation of **2** with LDA (0.10 M) at -78 °C. The curve depicts an unweighted least-squares fit to $y = k[ArH] + k'$ ($k = (9.1 \pm 0.3) \times 10^{-4}$, $k' = (3 \pm 3) \times 10^{-6}$); (B) Magnified plot of the pseudo-first-order regime marked in blue square in (A). The curve depicts an unweighted least-squares fit to $y = k[ArH] + k'$ ($k = (8 \pm 1) \times 10^{-4}$, $k' = (3.4 \pm 0.9) \times 10^{-6}$).

[ArH] (M)	$y_1 \times 10^4$ (abs.s^{-1})
0.002	0.053 ± 1E-3
0.004	0.0569 ± 8E-4
0.006	0.087 ± 1E-3
0.008	0.106 ± 1E-3
0.010	0.109 ± 1E-3
0.050	0.528 ± 3E-3
0.100	0.858 ± 5E-3
0.200	2.02 ± 1E-2
0.300	2.67 ± 4E-2

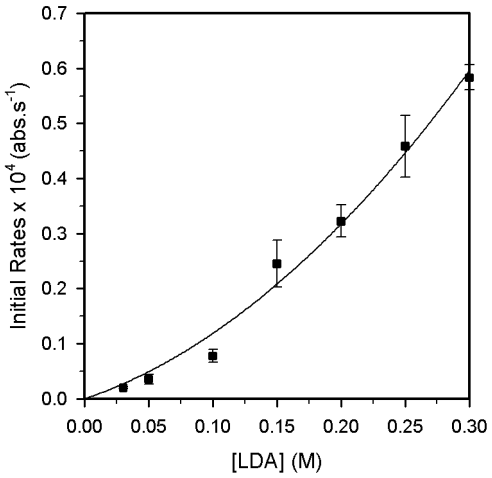

Figure AIII.29. Plot of initial rates vs [LDA] in THF (12.20 M) for the ortholithiation of **2** (0.005 M) at -78 °C. The curve depicts an unweighted least-squares fit to $y = k[\text{LDA}]^n$ ($k = (3.5 \pm 0.4) \times 10^{-5}$, $n = 1.48 \pm 0.09$).

[LDA] (M)	$y_1 \times 10^4$ (abs.s^{-1})	$y_2 \times 10^4$ (abs.s^{-1})	$y_3 \times 10^4$ (abs.s^{-1})
0.03	0.0211 ± 3E-4	0.019 ± 1E-3	0.020 ± 1E-3
0.05	0.046 ± 1E-3	0.0283 ± 4E-4	0.0336 ± 4E-4
0.10	0.074 ± 2E-3	0.069 ± 2E-3	0.091 ± 2E-3
0.15	0.29 ± 1E-2	0.234 ± 8E-3	0.209 ± 7E-3
0.20	0.356 ± 7E-3	0.301 ± 8E-3	0.31 ± 1E-2
0.25	0.42 ± 1E-2	0.49 ± 2E-2	—
0.35	0.56 ± 2E-2	0.61 ± 3E-2	0.58 ± 1E-2

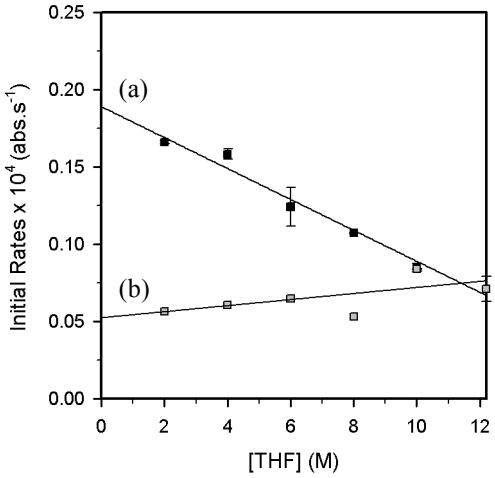

Figure AIII.30. Plot of initial rates vs [THF] for the ortholithiation of **2** (0.005 M) with LDA (0.10 M) at -78 °C in: (a) hexanes cosolvent. The curve depicts an unweighted least-squares fit to $y = -k[THF] + k'$ ($k = (1.00 \pm 0.06) \times 10^{-6}$, $k' = (1.89 \pm 0.05) \times 10^{-5}$); (b) 2,5-dimethyltetrahydrofuran cosolvent. The curve depicts an unweighted least-squares fit to $y = -k[THF] + k'$ ($k = (2 \pm 1) \times 10^{-7}$, $k' = (5.2 \pm 0.9) \times 10^{-6}$).

[THF] (M)	$y_1 \times 10^4$ (abs.s^{-1})	$y_2 \times 10^4$ (abs.s^{-1})
2.0	0.167 ± 4E-3	0.165 ± 4E-3
4.0	0.160 ± 3E-3	0.156 ± 4E-3
6.0	0.115 ± 2E-3	0.133 ± 2E-3
8.0	0.107 ± 1E-3	0.107 ± 1E-3
10.0	0.083 ± 1E-3	0.0867 ± 8E-4
12.20	0.0652 ± 8E-4	0.0767 ± 8E-4

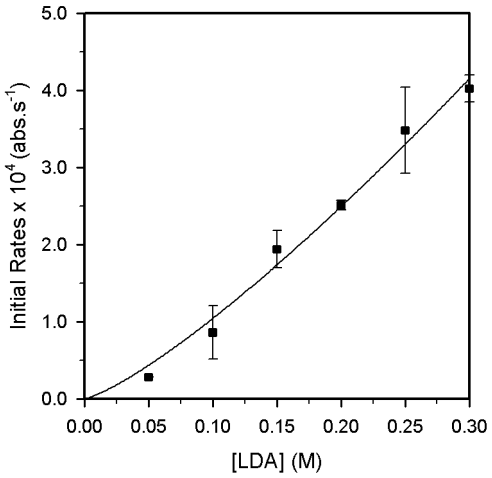

Figure AIII.31. Plot of initial rates vs [LDA] in THF (12.20 M) for the ortholithiation of **2** (0.10 M) at -78 °C. The curve depicts an unweighted least-squares fit to $y = k[\text{LDA}]^n$ ($k = (1.8 \pm 0.2) \times 10^{-3}$, $n = 1.25 \pm 0.09$).

[LDA] (M)	$y_1 \times 10^4$ (abs.s^{-1})	$y_2 \times 10^4$ (abs.s^{-1})	$y_3 \times 10^4$ (abs.s^{-1})
0.05	0.283 ± 1E-3	0.278 ± 1E-3	0.281 ± 1E-3
0.10	0.975 ± 4E-3	0.473 ± 2E-3	1.121 ± 9E-3
0.15	2.13 ± 2E-2	2.02 ± 2E-2	1.67 ± 1E-2
0.20	2.56 ± 3E-2	2.51 ± 3E-2	2.45 ± 3E-2
0.25	3.08 ± 4E-2	3.88 ± 6E-2	—
0.35	4.15 ± 6E-2	4.10 ± 7E-2	3.82 ± 6E-2

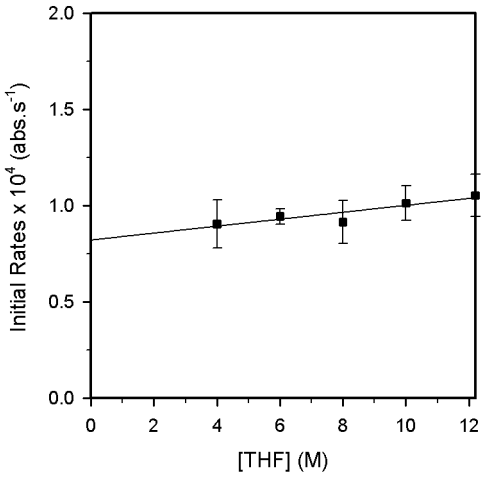

Figure AIII.32. Plot of initial rates vs [THF] in hexanes cosolvent for the ortholithiation of **2** (0.10 M) with LDA (0.10 M) at -78 °C. The curve depicts an unweighted least-squares fit to $y = -k[THF] + k'$ ($k = (1.8 \pm 0.9) \times 10^{-6}$, $k' = (8.2 \pm 0.8) \times 10^{-5}$).

[THF] (M)	$y_1 \times 10^4$ (abs.s^{-1})	$y_2 \times 10^4$ (abs.s^{-1})
4.0	0.99 ± 1E-2	0.81 ± 1E-2
6.0	0.97 ± 2E-2	0.91 ± 1E-2
8.0	0.90 ± 1E-2	0.83 ± 1E-2
10.0	0.95 ± 1E-2	1.08 ± 1E-2
12.20	0.975 ± 5E-3	1.131 ± 9E-3

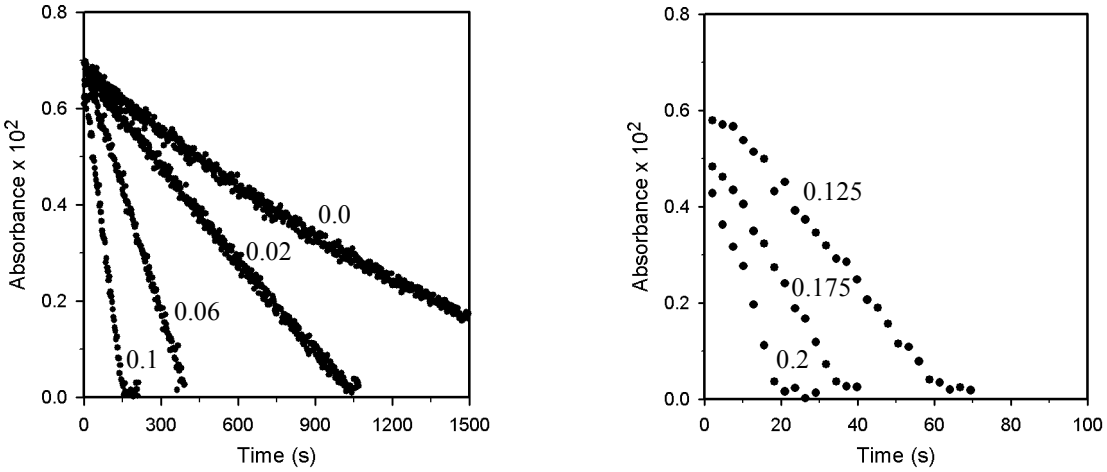

Figure AIII.33. Plot of IR absorbances vs time for the ortholithiation of **2** (0.005 M) with LDA (0.10 M) in THF (12.20 M) at -78 °C in the presence of varying mol percentages of LiCl.

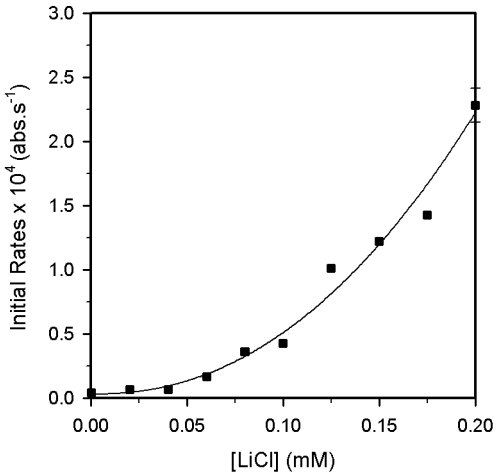

Figure AIII.34. Plot of initial rates vs [LiCl] for the ortholithiation of **2** (0.004 M) with LDA (0.10 M) in THF (12.20 M) at -78 °C. The curve depicts an unweighted least-squares fit to $y = k[LiCl]^n + k'$ ($k = (7 \pm 3) \times 10^{-3}$, $n = 2.2 \pm 0.3$, $k' = (3 \pm 7) \times 10^{-6}$).

[LiCl] (mM)	$y_1 \times 10^4$ ($M.s^{-1}$)
0.0	0.0399 ± 3E-4
0.02	0.0646 ± 2E-4
0.04	0.0662 ± 2E-4
0.06	0.1707 ± 8E-4
0.08	0.359 ± 3E-3
0.10	0.424 ± 5E-3
0.125	1.01 ± 2E-2
0.15	1.22 ± 3E-2
0.175	1.42 ± 3E-2
0.2	2.19 ± 9E-2

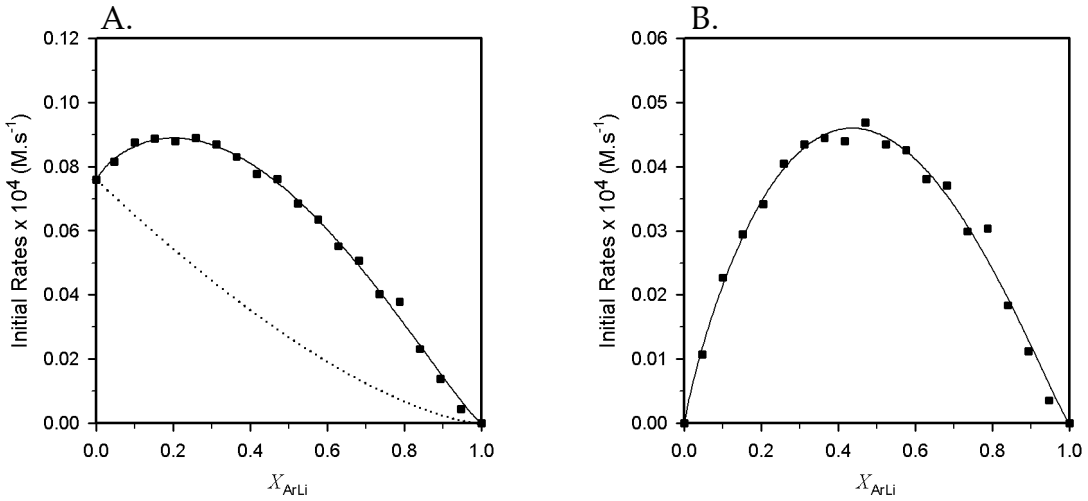

Figure AIII.35. Plot of initial rates versus mole fraction of 2,6-difluoro-3-lithiopyridine **4** (X_{ArLi}) for the serial injection of 0.0053 M aliquots of **2** to 0.10 M LDA in 12.20 M THF at -78 °C. The solid line depicts an unweighted least-squares fit to $-d[\mathbf{2}]/dt = k(X_{ArLi})^n(1-X_{ArLi})^m$ (see page 32 for derivation), $n = 0.87 \pm 0.04$, $m = 1.13 \pm 0.05$, $k = (1.8 \pm 0.1) \times 10^{-5}$). In figure B, the contribution of the uncatalyzed pathway (dotted line in figure A) is subtracted.

X_{ArLi}	y x 10^4 ($M.s^{-1}$)	X_{ArLi}	y x 10^4 ($M.s^{-1}$)=
0.0000	0.0759 ± 6E-4	0.5556	0.0685 ± 7E-4
0.0556	0.0815 ± 9E-4	0.6111	0.0635 ± 9E-4
0.1111	0.087 ± 1E-3	0.6667	0.0552 ± 6E-4
0.1667	0.089 ± 1E-3	0.7222	0.0507 ± 9E-4
0.2222	0.088 ± 1E-3	0.7778	0.0403 ± 6E-4
0.2778	0.081 ± 6E-3	0.8333	0.0378 ± 9E-4
0.3333	0.087 ± 1E-3	0.8889	0.0232 ± 3E-4
0.3889	0.0830 ± 8E-4	0.9444	0.0138 ± 3E-4
0.4444	0.0777 ± 8E-4	1.0000	0.0045 ± 1E
0.5000	0.0762 ± 9E-4		

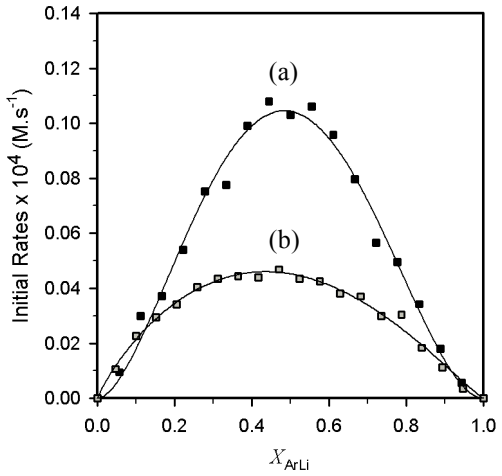

Figure AIII.36. Comparison of the plots of initial rates versus mole fractions of 3-lithiofluoropyridines **3** and **4** (X_{ArLi}) for the serial injection of 0.005 M aliquots of pyridines **1** and **2** to 0.10 M LDA in 12.20 M THF at -78 °C: (a) pyridine **1**. The solid line depicts an unweighted least-squares fit to $-d[\mathbf{1}]/dt = k(X_{ArLi})^n(1-X_{ArLi})^m$ (see page 32 for derivation), $n = 1.8 \pm 0.1$, $m = 1.9 \pm 0.1$, $k = (1.3 \pm 0.2) \times 10^{-5}$; (b) pyridine **2**. The solid line depicts an unweighted least-squares fit to $-d[\mathbf{2}]/dt = k(X_{ArLi})^n(1-X_{ArLi})^m$ ($n = 0.87 \pm 0.04$, $m = 1.13 \pm 0.05$, $k = (1.8 \pm 0.1) \times 10^{-5}$). The contribution of the uncatalyzed pathway (assuming an LDA order of 1.5) is subtracted from both the plots.

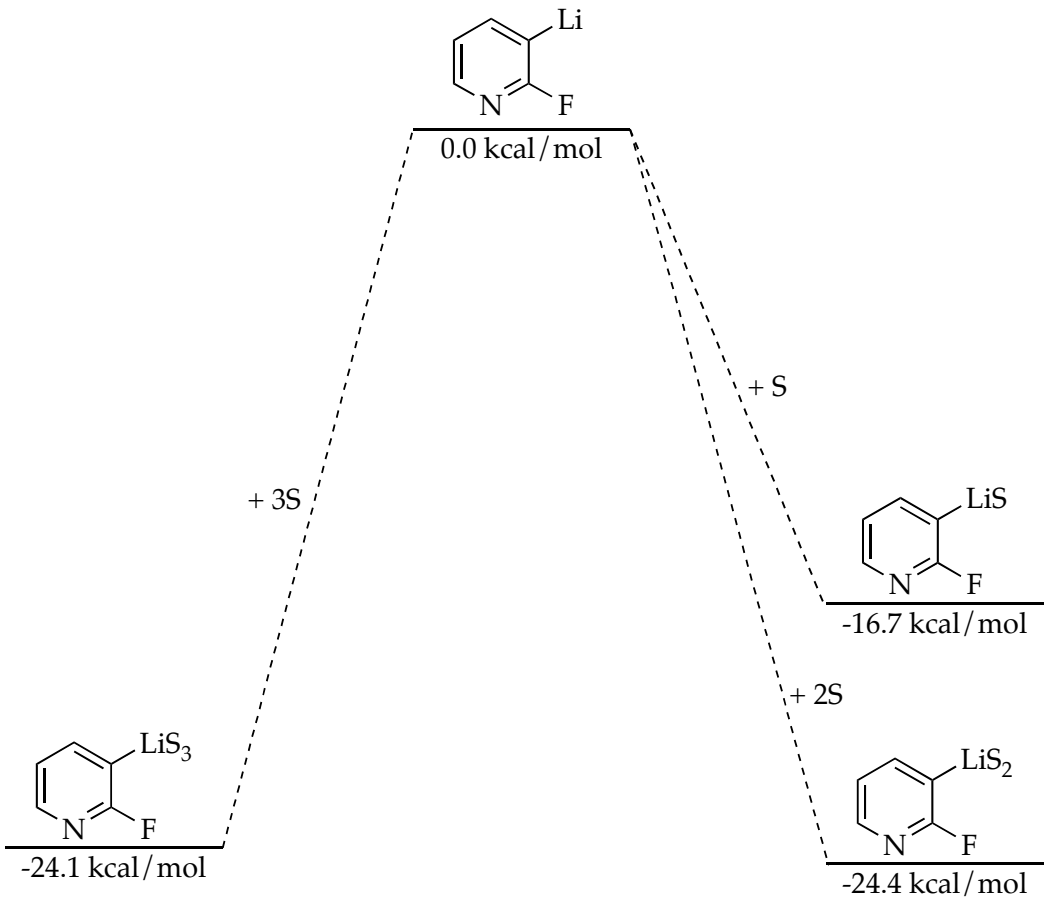

Figure AIII.37. Relative free energies for the solvation (ΔG, kcal/mol) of 2-fluoro-3-lithiopyridine (**3**) at -78 °C (S = THF) calculated using B3LYP level of theory with 6-31G(d) basis set.

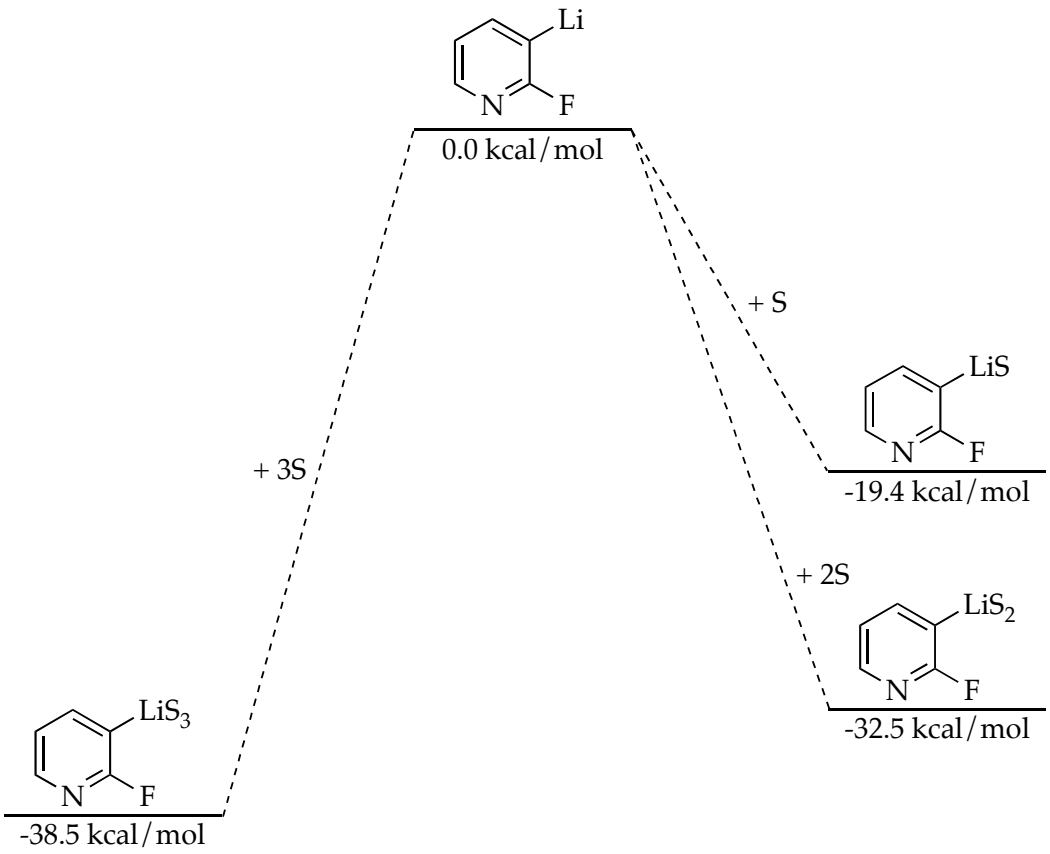

Figure AIII.38. Relative free energies for the solvation (ΔG, kcal/mol) of **3** at -78 °C (S = THF) calculated using single point MP2 corrections to B3LYP/6-31G(d) optimized structures.

Table AIII.1. Optimized geometries at B3LYP level of theory with 6-31G(d) basis set for the serial solvation of 2-fluoro-3-lithiopyridine (**3**) at -78 °C with free energies (Hartrees) and cartesian coordinates (X, Y, Z). (Note: G_{MP2} includes single point MP2 corrections to B3LYP/6-31G(d) optimized structures)

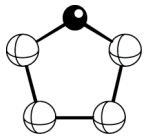

G = -232.349202
G_{MP2} = -231.569352

Atom	X	Y	Z	Atom	X	Y	Z
C	-0.77676	0.78926	-0.12614	H	1.31917	-0.90803	1.14900
C	-1.13241	-0.69941	0.08086	H	1.16400	1.14893	-1.08517
O	-0.00028	-1.43271	-0.37154	H	1.20108	1.42138	0.65905
C	1.13192	-0.69999	0.08156	H	-1.16426	1.15158	-1.08311
C	0.77743	0.78860	-0.12707	H	-1.19880	1.42112	0.66158
H	-1.99954	-1.03544	-0.49441				
H	-1.32099	-0.90818	1.14790				
H	1.99943	-1.03711	-0.49250				

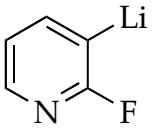

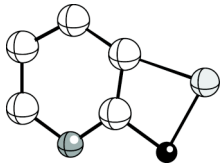

G = -354.394923
G_{MP2} = -353.331677

Atom	X	Y	Z	Atom	X	Y	Z
C	0.86201	0.97288	-0.00006	C	-1.41854	0.07596	0.00005
C	1.14630	-0.38236	-0.00012	C	-0.53093	1.16338	0.00005
Li	2.83029	1.20280	-0.00015	H	-0.94421	2.17226	0.00008
F	2.58112	-0.65448	0.00014	H	-2.49487	0.22687	0.00010
N	0.42332	-1.46768	-0.00007	H	-1.55223	-2.09092	0.00001
C	-0.90225	-1.21871	-0.00002				

Table AIII.1 (Continued).

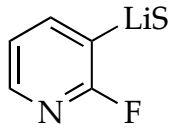

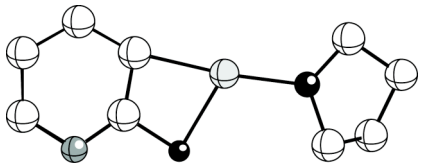

G = -586.770686
G_{MP2} = -584.9319088
S = THF

Atom	X	Y	Z	Atom	X	Y	Z
C	-2.50499	1.17711	-0.24166	N	3.48701	-1.39756	-0.03019
O	-1.54999	0.14705	-0.61792	H	-4.31203	0.97174	0.98209
C	-2.09542	-1.17105	-0.33443	H	-4.44709	0.28896	-0.64680
C	-3.21235	-0.92142	0.67415	H	-3.96072	-1.71886	0.67231
C	-3.76863	0.43181	0.20174	H	-2.80029	-0.83941	1.68640
Li	0.32708	0.33538	-0.70371	H	-1.27700	-1.79302	0.03530
F	1.25006	-1.38176	-0.53787	H	-2.47775	-1.59937	-1.26932
C	2.45357	-0.63118	-0.26527	H	5.50599	-1.30065	0.42391
C	2.26029	0.74138	-0.31003	H	5.58997	1.20021	0.43479
C	3.47387	1.39778	-0.03913	H	3.51499	2.48794	-0.03171
C	4.65480	0.68598	0.22681	H	-2.66371	1.83101	-1.10404
C	4.61691	-0.70636	0.22228	H	-2.06457	1.76430	0.57232

Table AIII.1 (Continued).

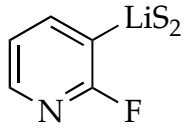

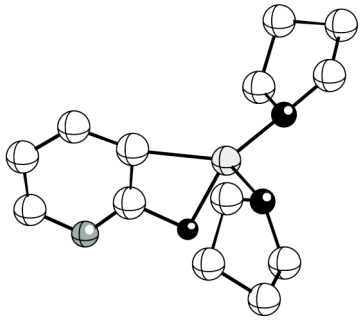

G = -819.132244
G_{MP2} = -816.522168
S = THF

Atom	X	Y	Z	Atom	X	Y	Z
C	1.40459	2.07056	1.21795	H	3.23764	1.57287	0.18733
O	0.45881	1.89993	0.13075	H	2.94610	3.37960	-1.45434
C	0.94235	2.58396	-1.05842	H	1.99303	4.33584	-0.30633
C	2.22195	3.31593	-0.63711	H	1.13873	1.82428	-1.82202
C	2.71589	2.46717	0.54568	H	0.15456	3.25583	-1.41338
Li	-0.16396	0.05942	-0.12065	H	1.32843	-2.60428	2.36280
C	1.00190	-1.53788	0.50199	H	3.05159	-4.14427	1.45065
C	1.51990	-1.61548	-0.78548	H	3.71685	-3.94505	-0.95438
F	0.95433	-0.66227	-1.69046	H	-1.72780	-2.09112	-0.58226
N	2.42166	-2.37850	-1.35508	H	-2.80322	-1.45403	-1.85996
C	2.96315	-3.28931	-0.52186	H	-4.47504	-2.31546	-0.30523
C	2.58837	-3.39309	0.81496	H	-3.46442	-1.91551	1.09745
C	1.61164	-2.51390	1.31197	H	-4.99031	0.01605	1.02136
O	-2.06466	-0.05639	-0.51137	H	-4.91755	0.06087	-0.74952
C	-3.07181	0.69648	0.20431	H	-3.17904	1.67235	-0.27836
C	-4.34189	-0.15747	0.15753	H	-2.72630	0.84980	1.23494
C	-3.77018	-1.58290	0.09877	H	1.45105	1.12178	1.75826
C	-2.54530	-1.39778	-0.79506	H	1.03411	2.85992	1.88606
H	3.38482	3.01204	1.21851				

Table AIII.1 (Continued).

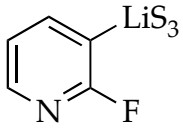

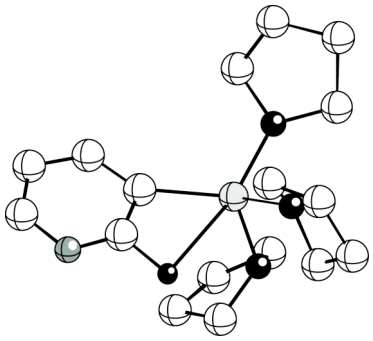

G = -1051.480867
G_{MP2} = -1048.101158
S = THF

Atom	X	Y	Z	Atom	X	Y	Z
Li	0.06194	-0.11884	-0.08758	H	1.85625	-3.66780	-1.27766
O	0.40437	-0.97447	-1.90448	H	1.76400	-3.60893	-3.03959
C	1.65876	-0.63887	-2.53298	H	3.43541	-1.89452	-2.82226
C	2.59143	-1.78179	-2.13499	H	2.98149	-1.58909	-1.13169
C	1.65161	-3.01205	-2.12864	H	1.51372	-0.59012	-3.62335
C	0.23159	-2.39808	-2.05292	H	1.95753	0.33921	-2.15642
C	1.78887	0.23325	1.07632	H	2.10639	-1.19343	2.68239
C	2.48387	1.33542	0.57308	H	4.23710	-0.21336	3.47798
F	1.90354	1.97237	-0.53432	H	5.15925	1.80190	2.30626
N	3.61148	1.91286	0.93498	H	-0.07697	2.92002	0.47066
C	4.22553	1.34049	1.98706	H	-1.45238	2.22488	1.36771
C	3.70829	0.22440	2.63412	H	-3.02704	3.62642	0.19223
C	2.49748	-0.31223	2.16556	H	-1.61936	4.65746	-0.07539
O	-1.16585	1.46243	-0.51721	H	-1.71624	4.07773	-2.39669
C	-1.13506	2.04370	-1.83312	H	-3.07898	3.00812	-2.05186
C	-2.06105	3.26876	-1.74603	H	-0.10428	2.33686	-2.06812
C	-2.02227	3.65398	-0.24028	H	-1.46053	1.27642	-2.53807
C	-1.11500	2.58129	0.39184	H	-0.18778	-1.29280	2.43579
O	-1.31639	-1.38221	0.72964	H	-1.03532	-2.84808	2.18674
C	-2.73373	-1.28198	0.44690	H	-2.54814	-1.75260	3.78038
C	-3.46379	-1.51690	1.78194	H	-2.27605	-0.17042	3.02440
C	-2.36886	-1.24498	2.82778	H	-4.33741	-0.86795	1.89437
C	-1.12148	-1.75407	2.11105	H	-3.80792	-2.55478	1.85627
H	-0.35287	-2.73463	-1.19464	H	-2.99829	-2.02674	-0.31282
H	-0.33775	-2.59331	-2.97232	H	-2.90910	-0.28297	0.03795

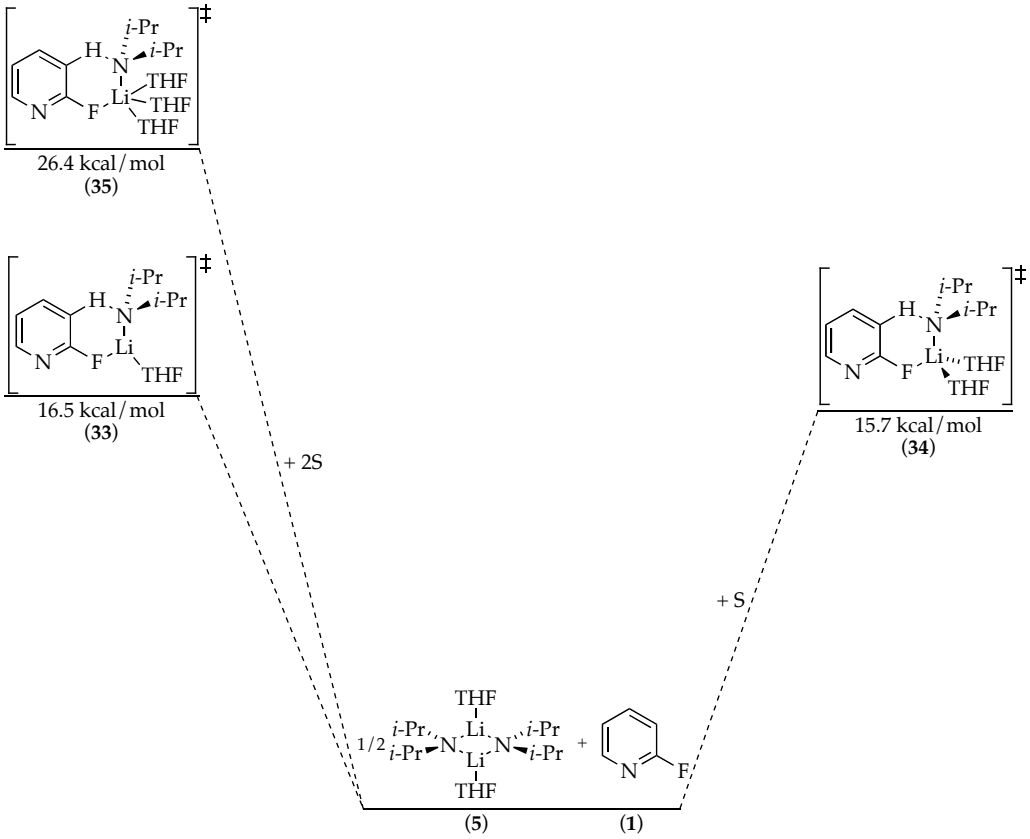

Figure AIII.39. Free energies of activation ($\Delta G^{\ddagger}$) for monomer-based transition structures for the ortholithiation of **1** at -78 °C calculated using B3LYP level of theory with 6-31G(d) basis set.

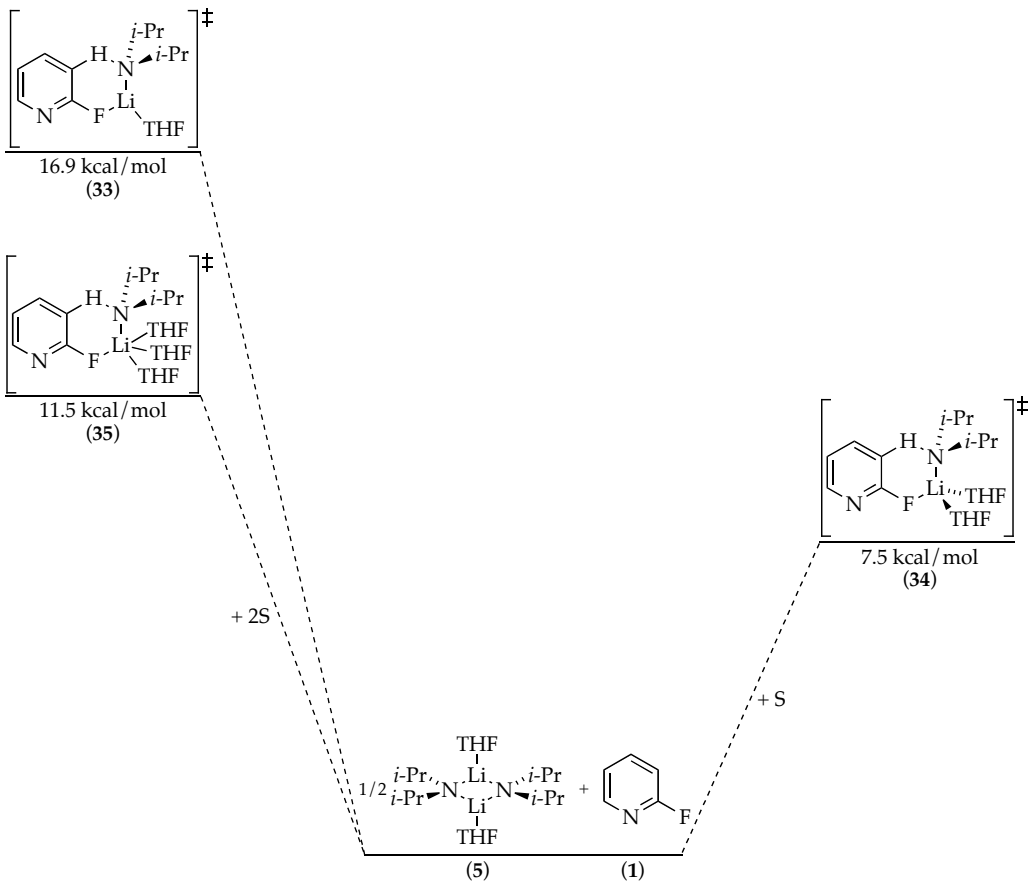

Figure AIII.40. Free energies of activation ($\Delta G^{\ddagger}$) for monomer-based transition structures for the ortholithiation of **1** at -78 °C calculated using single point MP2 corrections to B3LYP/6-31G(d) optimized structures.

Table AIII.2. Optimized geometries of reactants and monomer-based transition structures at B3LYP level of theory with 6-31G(d) basis set for the ortholithiation of **1** at -78 °C with free energies (Hartrees), and cartesian coordinates (X,Y,Z). (Note: G_{MP2} includes single point MP2 corrections to B3LYP/6-31G(d) optimized structures)

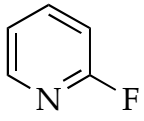

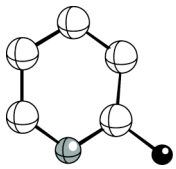

G = -347.462128
G_{MP2} = -346.4450685

Atom	X	Y	Z	Atom	X	Y	Z
C	-0.75185	1.04361	-0.00000	F	-2.74537	-0.19710	0.00001
C	0.63880	1.01860	0.00000	H	1.20092	1.94828	0.00000
C	1.29814	-0.21475	0.00000	H	2.38156	-0.27571	0.00000
C	0.52570	-1.37331	0.00000	H	0.99462	-2.35470	0.00000
N	-0.81720	-1.36891	-0.00000	H	-1.32306	1.96509	0.00000
C	-1.40228	-0.19110	-0.00001				

Table AIII.2 (Continued).

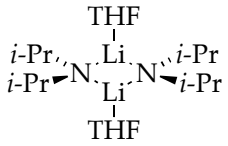

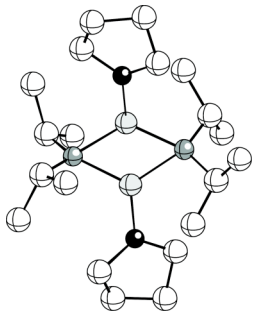

G = -1063.135543
G_{MP2} = -1059.34387
S = THF

Atom	X	Y	Z	Atom	X	Y	Z
Li	-1.19464	-0.00774	0.01421	H	1.83816	-3.21720	1.36630
O	-3.18299	0.01572	-0.13583	H	-2.15959	-1.60468	1.84082
C	-3.98409	-1.09503	-0.60154	H	-1.26327	-2.26497	3.22164
C	-5.41144	-0.77445	-0.16155	H	-0.80287	-0.70251	2.54173
C	-5.43839	0.75767	-0.27769	H	-0.65863	-3.39245	1.09537
C	-4.03238	1.14387	0.19102	H	-1.65573	-2.60864	-2.05785
N	-0.01403	-1.64369	0.06875	H	-0.68498	-4.07367	-2.32132
C	-0.19692	-2.41025	1.31036	H	-1.50052	-3.82045	-0.77116
C	-1.16039	-1.70758	2.28179	H	1.87669	-1.33857	-1.92728
C	1.13099	-2.71953	2.04026	H	1.14764	-2.49745	-3.05209
Li	1.19465	0.00783	0.01436	H	0.26500	-1.03245	-2.60504
N	0.01400	1.64376	0.06872	H	1.00263	-3.33501	-0.73003
C	0.19652	2.41040	1.31033	H	3.90323	1.15737	-1.69393
C	1.15952	1.70771	2.28220	H	3.57283	2.00952	-0.16815
C	-1.13164	2.71990	2.03968	H	6.16235	1.26993	-0.78433
C	-0.27768	2.55391	-1.04433	H	5.57076	1.08298	0.87817
C	-0.93195	1.81412	-2.22127	H	5.59112	-1.05745	-1.32156
C	0.96199	3.31164	-1.57823	H	6.21990	-1.22706	0.32667
O	3.18302	-0.01557	-0.13517	H	3.99129	-1.30081	1.27554
C	4.03229	-1.14374	0.19184	H	3.63030	-2.03115	-0.30431
C	5.43806	-0.75816	-0.27799	H	-1.87605	1.33861	-1.92791
C	5.41178	0.77396	-0.16178	H	-1.14658	2.49738	-3.05257
C	3.98424	1.09517	-0.60075	H	-0.26417	1.03236	-2.60515
C	0.27810	-2.55390	-1.04412	H	1.65649	2.60840	-2.05742
C	0.93270	-1.81416	-2.22091	H	0.68595	4.07349	-2.32131
C	-0.96133	-3.31179	-1.57838	H	1.50097	3.82031	-0.77087
H	2.15887	1.60463	1.84163	H	-1.00225	3.33509	-0.73054
H	1.26211	2.26520	3.22203	H	-3.99064	1.30159	1.27458
H	0.80177	0.70272	2.54212	H	-3.63100	2.03110	-0.30596
H	-1.59922	1.79146	2.39591	H	-6.21992	1.22625	0.32760
H	-0.98370	3.37716	2.90874	H	-5.59242	1.05690	-1.32113
H	-1.83853	3.21752	1.36538	H	-5.56953	-1.08360	0.87850
H	0.65842	3.39254	1.09542	H	-6.16225	-1.27067	-0.78359
H	1.59838	-1.79101	2.39653	H	-3.90377	-1.15665	-1.69482
H	0.98277	-3.37667	2.90936	H	-3.57208	-2.00943	-0.16966

Table AIII.2 (Continued).

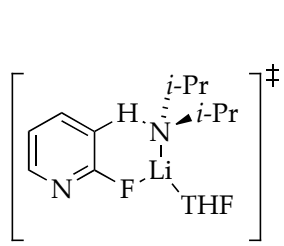

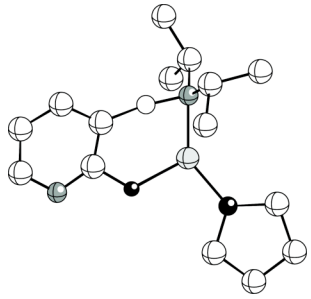

33
G = -879.003664
G_{MP2} = -876.0900414
S = THF
$\Delta G^{‡}$ = 16.5 kcal/mol
$\Delta G_{MP2}^{‡}$ = 16.9 kcal/mol

Atom	X	Y	Z	Atom	X	Y	Z
C	-2.70101	-2.39998	0.43881	H	1.49653	0.32213	2.44204
O	-2.30634	-1.00305	0.40443	H	1.00356	1.73846	3.38547
C	-3.46316	-0.16106	0.15594	H	-0.22666	0.74136	2.59959
C	-4.67147	-1.10415	0.14037	H	0.13297	2.82603	1.32382
C	-4.04512	-2.44289	-0.28206	H	-0.35698	3.82471	-0.54298
Li	-0.48372	-0.42637	0.32530	H	-0.65573	3.47306	-2.24793
F	0.43357	-2.06971	0.38427	H	-1.57094	2.61377	-0.98870
C	1.83831	-2.08227	0.08968	H	-0.81749	0.43525	-2.19966
C	2.40807	-0.84408	-0.14640	H	0.17784	1.36319	-3.33115
C	3.77891	-0.97360	-0.41976	H	0.91978	0.08245	-2.35276
C	4.40933	-2.22667	-0.43253	H	1.44191	2.38124	-1.49598
C	3.64561	-3.36040	-0.16777	H	4.08525	-4.35554	-0.16670
N	2.32697	-3.29537	0.10089	H	5.47099	-2.32514	-0.64395
N	0.57301	1.19096	0.04556	H	4.37488	-0.08404	-0.62797
C	0.47680	1.90674	-1.23413	H	-3.89485	-2.47483	-1.36744
C	0.17656	0.88651	-2.34370	H	-4.64584	-3.31030	0.00611
C	-0.58444	3.02058	-1.25063	H	-5.10681	-1.18776	1.14265
C	0.88453	2.02577	1.21871	H	-5.45480	-0.75827	-0.53996
C	0.78540	1.15599	2.48253	H	-3.51296	0.59994	0.94016
C	2.26773	2.70726	1.15620	H	-3.31668	0.33734	-0.80896
H	2.35824	3.35759	0.27920	H	-1.90709	-2.97940	-0.03556
H	2.43947	3.32779	2.04492	H	-2.79284	-2.71371	1.48655
H	3.06686	1.95850	1.10339	H	1.54186	0.30198	-0.06989

Table AIII.2 (Continued).

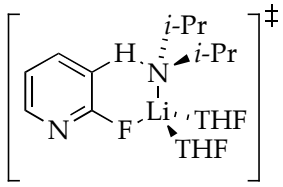

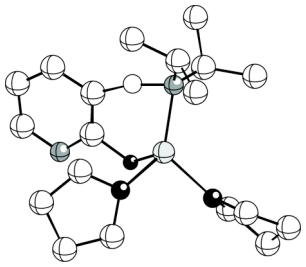

34
G = -1111.354111
G_{MP2} = -1107.674425
S = THF
$\Delta G^{‡}$ = 15.7 kcal/mol
$\Delta G_{MP2}^{‡}$ = 7.5 kcal/mol

Atom	X	Y	Z	Atom	X	Y	Z
C	0.57461	2.43920	-0.86232	H	1.73554	-1.86654	-2.48853
N	0.02440	1.65041	0.25363	H	2.44763	-0.23580	-2.46219
C	0.05268	2.32047	1.56380	H	-2.04946	-0.70887	1.64108
C	0.97333	1.58871	2.56060	H	-1.33811	-1.65757	2.97723
C	-1.35747	2.47348	2.16677	H	-3.14313	-3.15192	2.30465
Li	0.35400	-0.31242	-0.01467	H	-2.98161	-2.67724	0.60070
F	-0.67052	-0.84928	-1.66168	H	-1.69130	-4.76785	0.64737
C	-2.02195	-0.42762	-1.61812	H	-1.00811	-4.36825	2.23457
C	-2.27793	0.69480	-0.84596	H	0.76996	-3.50032	0.85132
C	-3.63987	1.02658	-0.86584	H	-0.35724	-3.08265	-0.46532
C	-4.56700	0.26956	-1.59832	H	-1.19035	1.29422	-0.19113
C	-4.10911	-0.83764	-2.30712	H	-3.99396	1.89011	-0.30078
N	-2.81248	-1.20520	-2.31915	H	-5.62262	0.52834	-1.61787
O	2.09269	-1.09498	-0.60424	H	-4.78741	-1.46154	-2.88573
C	3.25151	-1.23114	0.24983	H	1.99531	1.52985	2.16786
C	4.46286	-1.20284	-0.68563	H	1.01189	2.09656	3.53451
C	3.88778	-1.80742	-1.97641	H	0.61980	0.56289	2.73254
C	2.47287	-1.22849	-1.99585	H	-1.82931	1.49461	2.31784
O	-0.35605	-1.78496	1.14937	H	-1.32297	2.97861	3.14089
C	-1.58608	-1.66085	1.90765	H	-2.00556	3.05511	1.50230
C	-2.42726	-2.87727	1.52419	H	0.45679	3.34013	1.46352
C	-1.34969	-3.94515	1.28232	H	2.62703	1.72877	-0.66251
C	-0.23420	-3.13144	0.62174	H	2.47539	3.20033	-1.65161
C	-0.16557	3.76873	-1.13200	H	2.34283	3.29865	0.10934
C	2.09286	2.68099	-0.76248	H	-0.04649	4.47923	-0.30486
H	3.23772	-0.41504	0.97777	H	0.21929	4.25610	-2.03737
H	3.17678	-2.18522	0.78795	H	-1.23605	3.58673	-1.27298
H	4.78707	-0.17046	-0.85983	H	0.41046	1.81816	-1.75927
H	5.31234	-1.76307	-0.28402	H	-3.96159	-1.72769	-0.47756
H	3.85468	-2.90121	-1.90686	H	-2.89614	-1.09771	-1.76135
H	4.45875	-1.54107	-2.87066				

Table AIII.2 (Continued).

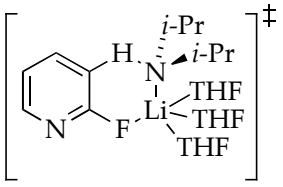

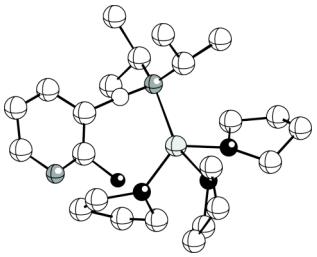

35
G = -1343.686183
G_{MP2} = -1339.237299
S = THF
$\Delta G^{‡}$ = 26.4 kcal/mol
$\Delta G_{MP2}{}^{‡}$ = 11.5 kcal/mol

Atom	X	Y	Z	Atom	X	Y	Z
Li	-0.48170	-0.31703	-0.04953	H	-0.25633	-3.15937	-0.19657
N	0.37396	1.56629	-0.22056	H	-1.47875	-3.53375	-1.44261
C	0.18519	1.98853	-1.62856	H	6.36400	-1.27536	0.12002
C	-1.11042	2.77854	-1.88929	H	6.29222	1.20118	0.48111
C	1.38587	2.70434	-2.29752	H	4.08517	2.36122	0.41368
C	0.12398	2.58789	0.81024	H	-1.20510	-3.28941	2.15424
C	0.26531	1.94090	2.19773	H	-2.27191	-1.86814	1.99368
C	1.01637	3.85162	0.76635	H	-1.57579	-1.01267	4.15564
C	2.93689	0.56884	0.03547	H	-1.37696	-2.73610	4.49595
C	3.18986	-0.78750	-0.14033	H	1.00778	-2.48870	4.44696
F	2.07927	-1.59879	-0.36468	H	0.73044	-0.74684	4.39748
N	4.31738	-1.46885	-0.12160	H	1.59373	-0.85142	2.15759
C	5.42080	-0.73127	0.10250	H	1.39120	-2.61545	2.11922
C	5.37512	0.64476	0.30257	H	1.29471	1.60008	2.35826
C	4.12447	1.27992	0.26397	H	0.01987	2.65804	2.99095
O	-0.50226	-1.71321	-1.64896	H	-0.39672	1.07471	2.30143
C	0.26472	-1.53318	-2.86910	H	0.83248	4.45573	-0.12628
C	0.50203	-2.93791	-3.42442	H	0.81799	4.49034	1.63760
C	0.58053	-3.77636	-2.14041	H	2.07864	3.58200	0.77884
C	-0.48010	-3.11049	-1.26341	H	-0.91763	2.95300	0.73513
O	-2.60074	-0.24678	0.07638	H	-1.08423	3.77601	-1.43528
C	-3.30028	0.75872	0.84991	H	-1.26377	2.91665	-2.96724
C	-4.71485	0.86544	0.25249	H	-1.98204	2.24875	-1.48728
C	-4.54404	0.26068	-1.15155	H	2.31303	2.15402	-2.11462
C	-3.49791	-0.82054	-0.89501	H	1.23084	2.76137	-3.38407
O	-0.29170	-1.48818	1.66374	H	1.52427	3.72715	-1.93398
C	0.92458	-1.66933	2.42037	H	0.07586	1.05079	-2.19467
C	0.49241	-1.69203	3.90218	H	1.60259	1.12465	-0.08465
C	-1.04306	-1.91861	3.84973	H	-2.73551	1.69035	0.76286
C	-1.30716	-2.21321	2.36746	H	-3.31126	0.45453	1.90303
H	-0.31266	-0.88990	-3.53979	H	-5.42687	0.27098	0.83651
H	1.20554	-1.03853	-2.61313	H	-5.07749	1.89720	0.23488
H	-0.34373	-3.25777	-4.04558	H	-4.15082	1.00729	-1.85041
H	1.41062	-2.99218	-4.03111	H	-5.47519	-0.14026	-1.56353
H	1.56573	-3.66816	-1.67863	H	-3.96159	-1.72769	-0.47756
H	0.37928	-4.83975	-2.30289	H	-2.89614	-1.09771	-1.76135

Table AIII.3. Optimized geometries from the IRC calculations on disolvated monomeric transition structure (**34**) at B3LYP level of theory with 6-31G(d) basis set, for the ortholithiation of **1** at -78 °C with free energies (Hartrees), and cartesian coordinates (X,Y,Z).

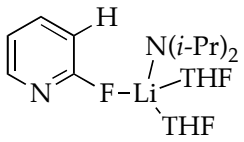

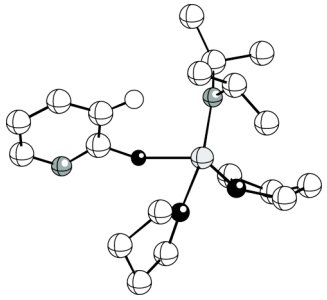

36
G = -1111.365230
S = THF

Atom	X	Y	Z	Atom	X	Y	Z
C	1.13362	2.19613	-0.91468	H	3.96840	-2.14491	-3.02789
N	0.63915	1.51690	0.27990	H	1.25176	-2.29265	-2.55887
C	0.84694	2.24930	1.52331	H	2.07939	-0.71825	-2.45259
C	-0.44589	2.90694	2.06764	H	-1.95872	-0.12897	1.97016
C	1.44235	1.33883	2.61736	H	-1.30007	-1.26523	3.17271
Li	0.38032	-0.35930	0.08669	H	-3.53236	-2.21069	2.86050
F	-0.93889	-0.73772	-1.67126	H	-3.52912	-1.79652	1.13359
C	-2.20044	-0.19966	-1.65629	H	-2.81976	-4.15005	1.06873
C	-2.36933	1.01378	-0.99691	H	-1.82416	-3.93821	2.51919
C	-3.66603	1.52159	-1.00832	H	-0.10059	-3.54612	0.88531
C	-4.68113	0.80856	-1.65774	H	-1.26101	-2.91588	-0.30635
C	-4.35736	-0.39985	-2.26817	H	-3.88112	2.46565	-0.51488
N	-3.11327	-0.91358	-2.26766	H	-5.70071	1.17985	-1.68762
O	1.71950	-1.67968	-0.64406	H	-5.11401	-0.99109	-2.77903
C	2.91221	-1.88236	0.15377	H	2.42935	0.97028	2.31232
C	4.08306	-1.90383	-0.83339	H	1.55139	1.85461	3.58217
C	3.41716	-2.41273	-2.12157	H	0.79518	0.46516	2.78091
C	2.04686	-1.73946	-2.05258	H	-1.19944	2.13724	2.28696
O	-0.73709	-1.59583	1.19690	H	-0.26993	3.47593	2.99299
C	-1.72623	-1.17825	2.16412	H	-0.87677	3.58989	1.32765
C	-2.90331	-2.13161	1.96881	H	1.57325	3.07324	1.39332
C	-2.18534	-3.44244	1.61045	H	3.11148	1.26639	-0.93974
C	-1.00936	-2.95082	0.75854	H	3.01660	2.72649	-1.95525
C	0.54911	3.60749	-1.18265	H	3.10184	2.86960	-0.19245
C	2.68087	2.27252	-1.01130	H	0.84568	4.31825	-0.40154
H	2.97487	-1.07171	0.88547	H	0.89849	4.01266	-2.14253
H	2.80906	-2.83723	0.68510	H	-0.54652	3.57860	-1.20801
H	4.47391	-0.89112	-0.98254	H	0.81277	1.57732	-1.77410
H	4.90499	-2.53852	-0.48893	H	-1.51204	1.47491	-0.48963
H	3.31043	-3.50382	-2.09602				

Table AIII.3 (Continued).

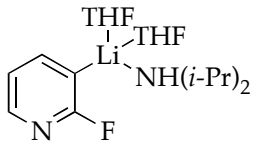

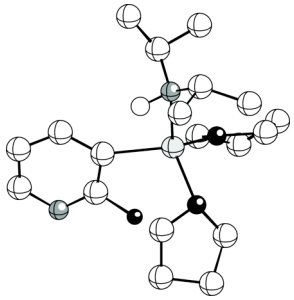

37
G = -1111.363605
S = THF

Atom	X	Y	Z	Atom	X	Y	Z
C	-2.10275	-1.59267	-1.06251	H	0.91858	3.36318	-3.87527
N	-1.59419	-1.16472	0.26961	H	1.76954	1.34705	-2.16953
C	-2.60255	-0.96808	1.34773	H	0.33064	1.10254	-3.19398
C	-2.80054	0.52535	1.63816	H	1.71502	-1.10127	2.00786
C	-2.17456	-1.71889	2.61373	H	1.11056	-0.36139	3.52360
Li	0.23436	0.01903	-0.02895	H	3.48426	0.16702	3.70513
C	1.58727	-1.46626	-0.74097	H	3.62716	0.36329	1.94106
C	1.59477	-2.82449	-1.11765	H	3.37121	2.69389	2.67051
C	2.76011	-3.50057	-1.51552	H	2.16290	2.23354	3.88452
C	3.95515	-2.79103	-1.53629	H	0.65599	2.79430	2.09152
N	4.02810	-1.49173	-1.19269	H	1.83787	2.30509	0.84561
C	2.88166	-0.95008	-0.83429	H	0.66179	-3.39602	-1.11012
F	3.02840	0.40071	-0.49029	H	2.74138	-4.54986	-1.80181
O	-0.03740	1.63578	-1.21826	H	4.89122	-3.26099	-1.83540
C	-0.79380	2.84987	-1.03190	H	-3.11927	1.06271	0.73930
C	-0.63912	3.64421	-2.33110	H	-3.56600	0.67501	2.40985
C	0.75700	3.21041	-2.80413	H	-1.86045	0.96694	1.98672
C	0.78104	1.73225	-2.41692	H	-1.19757	-1.36310	2.96323
O	0.84388	0.75408	1.78850	H	-2.89560	-1.56169	3.42344
C	1.63567	-0.17178	2.57669	H	-2.10180	-2.79781	2.43163
C	2.97582	0.52388	2.80436	H	-3.56835	-1.38428	1.02752
C	2.55447	1.99891	2.88724	H	-2.47782	0.43335	-1.74883
C	1.44066	2.07289	1.83865	H	-3.27865	-0.82453	-2.71084
C	-3.00151	-0.52568	-1.69364	H	-3.93158	-0.38506	-1.12972
C	-2.78280	-2.97341	-1.05463	H	-3.71178	-2.97547	-0.47145
H	-1.82957	2.58197	-0.80300	H	-3.03655	-3.27978	-2.07630
H	-0.37924	3.39822	-0.17582	H	-2.11651	-3.73694	-0.63536
H	-1.40047	3.34012	-3.05926	H	-1.19913	-1.67307	-1.67897
H	-0.73257	4.72297	-2.17353	H	-0.93834	-1.88939	0.56383
H	1.53398	3.76154	-2.26109				

REFERENCES III

1. (a) Schlosser, M. *Angew. Chem., Int. Ed.* **2005**, *44*, 376. (b) Schlosser, M.; Rausis, T. *Eur. J. Org. Chem.* **2004**, 1018. (c) Kuethe, J. T. *et al.* Tetrahedron **2009**, *65*, 5013. (d) Güngör, T.; Marsais, F.; Queguiner, G. *J. Organomet. Chem.* **1981**, *215*, 139.

2. (a) Queguiner, G.; Marsais, F.; Snieckus, Epsztajn, J. *Adv. Heterocycl. Chem.* **1991**, *52*, 187. (b) Mongin, F.; Queguiner, G. *Tetrahedron* **2001**, *57*, 5897. (c) Mongin, F.; Queguiner, G. *Tetrahedron* **2001**, *57*, 4059. (d) Merino, P. *Progr Heterocycl. Chem.* **1999**, *11*, 21. (e) Clayden, J. In *The Chemistry of Organolithium Compounds*; Rappoport, Z.; Marek, I., Eds.; Wiley: New York, 2004, Vol. 1, p 495. (f) Caubere, P. In *Reviews of Heteroatom Chemistry*; MYU: Tokyo, *vol. 4*, (1991); pp. 78-139. (g) Caubere, P. *Chem. Rev.* **1993**, *93*, 2317. (h) Marsais, F.; Queguiner, G. *Tetrahedron* **1983**, *39*, 2009. (i) Collins, I. *Perkin 1* **2000**, 2845. (i) Schlosser, M.; Mongin, F. *Chem. Soc. Rev.* **2007**, *36*, 1161. (j) Hartung, C. G.; Snieckus, V. In *Modern Arene Chemistry*, Astruc, D. (Ed.), Wiley-VCH: Weinheim, 2002; Chapter 10. (k) Snieckus, V. *Chem. Rev.* **1990**, *90*, 879. (l) Taylor, C. M.; Watson, A. J. *Curr. Org. Chem.* **2004**, *8*, 623. (m) Bakker, W. I. I.; Wong, P. L.; Snieckus, V. Lithium Diisopropylamide. In *e-EROS*; Paquette, L. A., Ed.; John Wiley: New York, 2001.

3. (a) Fort, Y. *2-Fluoropyridine* In *e-EROS Encyclopedia of Reagents for Organic Synthesis*; John Wiley & Sons, NewYork; 2001. (b) Bhardwaj, P.; Forgione, P. *2,6-Difluoropyridine.* In *e-EROS Encyclopedia of Reagents for Organic Synthesis*; John Wiley & Sons, NewYork; 2001.

4. (a) Eames, J. Product Subclass 6: Lithium Amides. In *Science of Synthesis*; Snieckus, V., Ed.; Thieme; New York, 2006; Vol. 8a, p 173. (b) Clayden, J. *Organolithiums: Selectivity for Synthesis*; Pergamon: New York, 2002.

5. (a) Singh, K. J.; Hoepker, A. C.; Collum, D. B. *J. Am. Chem. Soc.* **2008**, *130*, 18008. (b) Ma, Y.; Hoepker, A. C.; Gupta, L.; Faggin, M. F.; Collum, D. B., unpublished. (c) Hoepker, A. C.; Gupta, L.; Ma, Y.; Faggin, M. F.; Collum, D. B., unpublished

6. For examples of reactions that are fast relative to the rates of aggregate-aggregate exchanges see: (a) McGarrity, J. F.; Ogle, C. A. *J. Am. Chem. Soc.* **1985**, *107*, 1810. (b) Jones, A. C.; Sanders, A. W.; Bevan, M. J.; Reich, H. J. *J. Am. Chem. Soc.* **2007**, *129*, 3492. (c) Thompson, A.; Corley, E. G.; Huntington, M. F.; Grabowski, E. J. J.; Remenar, J. F.; Collum, D. B. *J. Am. Chem. Soc.* **1998**, *120*, 2028. (d) Jones, A. C.; Sanders, A. W.; Sikorski, W. H.; Jansen, K. L.; Reich, H. J.

J. Am. Chem. Soc., **2008**, *130*, 6060. (e) Reich, H. J.; Sikorski, W. H.; Sanders, A. W.; Jones, A. C.; Plessel, K. N. *J. Org. Chem.* **2009**, *74*, 719. (f) See ref 5.

7. Collum, D. B.; McNeil, A. J.; Ramirez, A. *Angew. Chem., Int. Ed.* **2007**, *46*, 3002.

8. Liao, S.; Collum, D. B. *J. Am. Chem. Soc.* **2003**, *125*, 15114.

9. (a) Espenson, J. H. *Chemical Kinetics and Reaction Mechanisms*, 2nd ed.; McGraw-Hill: New York, 1995; Chapter 2, p 44. Atkins, P. W.; Jones, L. L. *Chemical Principles: the Quest for Insight*, 2nd ed.; W H. Freeman: New York, 2002.

10. (a) Besson, C.; Finney, E. E.; Finke, R. G. *J. Am. Chem. Soc.* **2005,** *127,* 8179. (b) Besson, C.; Finney, E. E.; Finke, R. G. *Chem. Mater.* **2005,** *17,* 4925. (c) Huang, K. T.; Keszler, A.; Patel, N.; Patel, R. P.; Gladwin, M. T.; Kim-Shapiro, D. B.; Hogg, N. *J. Biol. Chem.* **2005**, *280*, 31126. (d) Huang, Z.; Shiva, S.; Kim-Shapiro, D. B.; Patel, R. P.; Ringwood, L. A.; Irby, C. E.; Huang, K. T.; Ho, C.; Hogg, N.; Schechter, A. N.; Gladwin, M. T. *J. Clin. Invest.* **2005**, *115*, 2099. (e) Tanj, S; Ohno, A; Sato, I; Soai, K *Org. Lett.* **2001**, *3*, 287. (f) Barrios-Kabderism, F.; Carrow, B. P.; Hartwig, J. F. *J. Am. Chem. Soc.* **2008**, *130*, 5842.

11. Gupta, L.; Hoepker, A. C.; Singh, K. J.; Collum, D. B. *J. Org. Chem.* **2009**, *74*, 2231.

12. Hoepker, A. C.; Collum, D. B., unpublished.

13. (a) Gregory, K.; Schleyer, P. v. R.; Snaith, R. *Adv. Inorg. Chem.* **1991**, *37*, 47. (b) Mulvey, R. E. *Chem. Soc. Rev.* **1991**, *20*, 167. (c) Rutherford, J. L.; Collum, D. B. *J. Am. Chem. Soc.* **1999**, *121*, 10198. (d) Beswick, M. A.; Wright, D. S. In *Comprehensive Organometallic Chemistry II*; Abels, E. W., Stone, F. G. A., Wilkinson, G., Eds.; Pergamon: New York, 1995; Vol. 1, Chapter 1. (e) Mulvey, R. E. *Chem. Soc. Rev*. **1998**, *27,* 339.

14. Review of ^{6}Li NMR spectroscopy: Günther, H. *J. Brazil. Chem.* **1999**, *10*, 241.

15. (a) Collum, D. B. *Acc. Chem. Res.* **1993**, *26*, 227. (b) Lucht, B. L.; Collum, D. B. *Acc. Chem. Res.* **1999**, *32*, 1035.

16. Kim, Y.-J.; Bernstein, M. P.; Galiano-Roth, A. S.; Romesberg, F. E.; Fuller, D. J.; Harrison, A. T.; Collum, D. B.; Williard, P. G. *J. Org. Chem.* **1991**, *56*, 4435.

17. Warming pyridyllithium **4** causes reversible protonation by *i*-Pr_2NH and subsequent 1,2-addition to form the corresponding 2-aminopyridine: Viciu, M.; Gupta, L.; Collum, D. B. *J. Am. Chem. Soc.* **2010**, *132*, 6361.

18. Similar $^2J_{C\text{-}F}$ values have been observed for related 2-fluorophenyllithiums: (a) Singh, K. J.; Collum, D. B. *J. Am. Chem. Soc.* **2006**, *128*, 13753. (b) Menzel, K.; Fisher, E. L.; DiMichele, L.; Frantz, D. E.; Nelson, T. D.; Kress, M. H. *J. Org. Chem.* **2006**, *71*, 2188. (c) See ref 46a,b.

19. $^2J_{C\text{-}F}$ values have been correlated with π-bond orders and total electronic charge at the ^{13}C atom: (a) Doddrell, D.; Jordan, D.; Riggs, N. V. *J. Chem. Soc., Chem. Commun.* **1972**, 1158. (b) Doddrell, D.; Barfield, M.; Adcock, W.; Aurangzeb, M.; Jordan, D. *J. Chem. Soc., Perkin Trans. 2* **1976**, 402.

20. For a review of structural studies using ^{19}F NMR spectroscopy, see: (a) Gakh, Y. G.; Gakh, A. A.; Gronenborn, A. M. *Magn. Reson. Chem.* **2000**, *38*, 551. (b) McGill, C. A.; Nordon, A.; Littlejohn, D. *J. Process Analyt. Chem.* **2001**, *6*, 36. (c) Espinet, P.; Albeniz, A. C.; Casares, J. A.; Martinez-Ilarduya, J. M. *Coor. Chem. Rev.* **2008**, *252*, 2180.

21. Gaussian 03, Revision B.04, Frisch, M. J.; Trucks, G. W.; Schlegel, H. B.; Scuseria, G. E.; Robb, M. A.; Cheeseman, J. R.; Montgomery, Jr., J. A.; Vreven, T.; Kudin, K. N.; Burant, J. C.; Millam, J. M.; Iyengar, S. S.; Tomasi, J.; Barone, V.; Mennucci, B.; Cossi, M.; Scalmani, G.; Rega, N.; Petersson, G. A.; Nakatsuji, H.; Hada, M.; Ehara, M.; Toyota, K.; Fukuda, R.; Hasegawa, J.; Ishida, M.; Nakajima, T.; Honda, Y.; Kitao, O.; Nakai, H.; Klene, M.; Li, X.; Knox, J. E.; Hratchian, H. P.; Cross, J. B.; Bakken, V.; Adamo, C.; Jaramillo, J.; Gomperts, R.; Stratmann, R. E.; Yazyev, O.; Austin, A. J.; Cammi, R.; Pomelli, C.; Ochterski, J. W.; Ayala, P. Y.; Morokuma, K.; Voth, G. A.; Salvador, P.; Dannenberg, J. J.; Zakrzewski, V. G.; Dapprich, S.; Daniels, A. D.; Strain, M. C.; Farkas, O.; Malick, D. K.; Rabuck, A. D.; Raghavachari, K.; Foresman, J. B.; Ortiz, J. V.; Cui, Q.; Baboul, A. G.; Clifford, S.; Cioslowski, J.; Stefanov, B. B.; Liu, G.; Liashenko, A.; Piskorz, P.; Komaromi, I.; Martin, R. L.; Fox, D. J.; Keith, T.; Al-Laham, M. A.; Peng, C. Y.; Nanayakkara, A.; Challacombe, M.; Gill, P. M. W.; Johnson, B.; Chen, W.; Wong, M. W.; Gonzalez, C.; and Pople, J. A.; Gaussian, Inc., Wallingford CT, 2004.

22. Derivations and experimental details are included in supporting information.

23. (a) Kottke, T.; Sung, K.; Lagow, R. J. *Angew. Chem., Int. Ed. Engl.* **1995**, *34*, 1517. (b) Reich, H. J.; Green, D. P.; Medina, M. A.; Goldenberg, W. S.; Gudmundsson, B. Ö.; Dykstra, R. R.; Phillips, N. H. *J. Am. Chem. Soc.* **1998**, *120*, 7201. (c) Bonasia, P. J.; Arnold, J. *J. Organometal. Chem.* **1993**, *449*, 147.

24. (a) Reich, H. J.; Borst, J. P.; Dykstra, R. R.; Green, D. P. *J. Am. Chem. Soc.* **1993**, *115*, 8728. (b) Wong, M. K.; Popov, A. I. *J. Inorg. Nucl. Chem.* **1972**, *34*, 3615. (c) Yakimansky, A. V.; Müller, A. H.; Beylen, M. V. *Macromolecules* **2000**, *33*, 5686. (d) Goralski, P.; Chabanel, M. *Inorg. Chem.* **1987**, *26*, 2169 and references cited therein.

25. (a) Kottke, T.; Stalke, D. *Angew. Chem., Int. Ed. Engl.* **1993**, *32*, 580. (b) Rennels, R. A.; Maliakal, A. J.; Collum, D. B. *J. Am. Chem. Soc.* **1998**, *120*, 421.

26. A. Evans, *Potentiometry and Ion-Selective Electrodes*. New York: Wiley, 1987.

27. Fuji, T. *Anal. Chem.* **1992**, *64*, 775.

28. (a) Marck, W.; Huisgen, R. *Chem. Ber.* **1960**, *93*, 608. (b) Gaudemar-Bardone, F.; Gaudemar M. *Synthesis* **1979**, 463. (c) Reetz, M. T.; Maier, W. F. *Liebigs Ann. Chem.* **1980**, 1471. (d) Williard, P. G.; Carpenter, G. B. *J. Am. Chem. Soc.* **1986**, *108*, 462. Williard, P. G.; Salvino, J. M. *J. Org. Chem.* **1993**, *58*, 1. (e) Morrison, R. C.; Hall, R. W.; Rathman, T. L. Stable Lithium Diisopropylamide and Method of Preparation. U.S. Patent 4,595,779, June 17, 1986.

29. Traces of oxygen, air, water, and joint greases failed to elicit unusual rate effects.

30. Snaith and coworkers underscored the merits of R_3NHX salts as precursors to anhydrous LiX salts: Barr, D.; Snaith, R.; Wright, D. S.; Mulvey, R. E.; Wade, K. *J. Am. Chem. Soc.* **1987**, *109*, 7891. Also, see: Hall, P. L.; Gilchrist, J. H.; Harrison, A. T.; Fuller, D. J.; Collum, D. B. *J. Am. Chem. Soc.* **1991**, *113*, 9575.

31. Zhao, P.; Collum, D. B. *J. Am. Chem. Soc.* **2003**, *125*, 14411 and references cited therein.

32. Rein, A. J.; Donahue, S. M.; Pavlosky, M. A. *Curr. Opin. Drug Discovery Dev.* **2000**, *3*, 734.

33. (a) Espenson, J. H. *Chemical Kinetics and Reaction Mechanisms*, 2nd ed.; McGraw-Hill: New York, 1995. (b) Rae, M.; Berberan-Santos, M. N. *J. Chem. Educ.*, **2004**, *81*, 436.

34. Determining initial rates (slopes) of a curved decay can be strongly dependent on the percent conversion, requiring a compromise between adequate sample size and loss of linearity. This problem is avoided by fitting a significant part of the decay—a portion that includes some curvature—to a third-order polynomial (at^2+bt+c). Be sure not to include too much curvature or the function will no longer fit well. The parameter b represents the rate at time=zero (one may verify this by taking the first derivative with respect to t and setting t=0. Initial rate=$f'(0)=b$). Prior to this analysis, be sure to convert your experimental observable (NMR intensity, IR absorbance etc.) to concentration to ensure a valid comparison between initial rates of varying concentrations and/or experimental conditions.

35. The concentration of LDA, although expressed in units of molarity, refers to the concentration of the monomer unit (normality). The concentration of THF is expressed as total concentration of free (uncoordinated) ligand.

36. Superposition of autocatalysis on a first-order decay can produce a perfectly linear decay (ref 5a).

37. (a) Ma, Y.; Collum, D. B. *J. Am. Chem. Soc.* **2007**, *129*, 14818. (b) Depue, J. S.; Collum, D. B. *J. Am. Chem. Soc.* **1988**, *110*, 5524. (c) Galiano-Roth, A. S.; Collum, D. B. *J. Am. Chem. Soc.* **1989**, *111*, 6772.

38. (a) Lucht, B. L.; Collum, D. B. *J. Am. Chem. Soc.* **1994**, *116*, 6009. (b) Remenar, J. F.; Lucht, B. L.; Collum, D. B. *J. Am. Chem. Soc.* **1997**, *119*, 5567.

39. For leading references to spectroscopic, crystallographic, and kinetic evidence of open dimers, see: Ramirez, A.; Sun, X.; Collum, D. B. *J. Am. Chem. Soc.* **2006**, *128*, 10326.

40. Cyclic tetramers of lithium 2,2,6,6-tetramethylpiperidide were shown to react by dissociation to dimers: Wiedemann, S. H.; Ramírez, A.; Collum, D. B. *J. Am. Chem. Soc.* **2003**, *125*, 15893.
41. Lithium amide tetramers: (a) Cyclic: Lucht, B. L.; Collum, D. B. *J. Am. Chem. Soc.* **1994**, *116*, 7949. (b) Ladders: Armstrong, D. R.; Barr, D.; Clegg, W.; Mulvey, R. E.; Reed, D.; Snaith, R.; Wade, K. *J. Chem. Soc., Chem. Commun.* **1986**, 869. (c) Ladders: Gardiner, M. G.; Raston, C. L. *Inorg. Chem.* **1996**, *35*, 4047. (d) Ladders: Vestergren, M.; Eriksson, J.; Hilmersson, G.; Hakansson, M.

J. Organomet. Chem. **2003**, *682*, 172. (e) Ladders: Boche, G.; Langlotz, I.; Marsch, M.; Harms, K.; Nudelman, N. E. S. *Angew. Chem.* **1992**, *104*, 1239. (f) Cubic: Gardiner, M. G.; Raston, C. L. *Inorg. Chem.* **1995**, *34*, 4206.

42. (a) Ma, Y.; Ramirez, A.; Singh, K. J.; Keresztes, I.; Collum, D. B. *J. Am. Chem.* Soc. **2006**, *128*, 15399. (b) Ramirez, A.; Lobkovsky, E.; Collum, D. B. *J. Am. Chem. Soc.* **2003**, *125*, 15376. (c) Bernstein, M. P.; Collum, D. B. *J. Am. Chem. Soc.* **1993**, *115*, 789. (d) Ramirez, A.; Collum, D. B. *J. Am. Chem. Soc.* **1999**, *121*, 11114. (e) Remenar, J. F.; Collum, D. B. *J. Am. Chem. Soc.* **1998**, *120*, 4081.

43. (a) Hindermann, D. K.; Cornwell, C. D. *J. Chem. Phys.* **1968**, *48*, 4148. (b) Forsyth, D. A.; Yang, J.-R. *J. Am. Chem. Soc.* **1986**, *108,* 2157. (c) Lambert, J. B.; Greifenstein, L. G. *J. Am. Chem. Soc.* **1973**, *95*, 6150.

44. Competitive and intramolecular isotope effects can be used to examine post-rate-limiting proton transfer. They differ in that the intramolecular isotope effect demands a symmetry-equivalent choice of H versus D within the same molecule whereas the competitive isotope effect requires an exchange mechanism to establish the choice of H versus D.

45. (a) Carpenter, B. K., *Determination of Organic Reaction Mechanisms*; Wiley: New York, 1984. (b) Whisler, M. C.; MacNeil, S.; Snieckus, V.; Beak, P. *Angew. Chem., Int. Ed.* **2004**, *43*, 2206.

46. (a) Chadwick, S. T.; Rennels, R. A.; Rutherford, J. L.; Collum, D. B. *J. Am. Chem. Soc.* **2000**, *122*, 8640. (b) Riggs, J. C.; Ramirez, A.; Cremeens, M. E.; Bashore, C. G.; Candler, J.; Wirtz, M. C.; Coe, J. W.; Collum, D. B. *J. Am. Chem. Soc.* **2008**, *130*, 3406. (c) Riggs, J. C.; Ramirez, A.; Cremeens, M. E.; Bashore, C. G.; Candler, J.; Wirtz, M. C.; Coe, J. W.; Collum, D. B. *J. Am. Chem. Soc.* **2008**, *130*, 3406. (d) Ma, Y.; Breslin, S.; Keresztes, I.; Lobkovsky, E.; Collum, D. B. *J. Org. Chem.* **2008**, *73*, 9610.

47. Selected examples of fully-characterized through-space Li-F interactions: (a) Armstrong, D. R.; Khandelwal, A. H.; Kerr, L. C.; Peasey, S.; Raithby, P. R.; Shields, G. P.; Snaith, R.; Wright, D. S. *Chem. Commun.* **1998**, 1011. (b) Plenio, H.; Diodone, R. *J. Am. Chem. Soc.* **1996**, *118*, 356. (c) Henderson, K. W.; Dorigo, A. E.; Liu, Q.-Y.; Williard, P. G. *J. Am. Chem. Soc.* **1997**, *119*, 11855. (d) Kessar, S. V.; Singh, P.; Singh. K. N.; Bharatam, P. V.; Sharma, A. K.; Lata, S.; Kaur, A. *Angew. Chem., Int. Ed.* **2008**, *47*, 4703. (e) Lee, W.-Y.; Liang, L.-C. *Inorg. Chem.* **2008**, *47*, 3298. (f) Stalke, D.; Klingebiel, U.; Sheldrick, G. M. *Chem. Ber.* **1988**, *121*, 1457. (g) Sini, G.; Tessier, A.; Pytkowicz, J.; Brigaud, T. *Chem. Eur. J.* **2008**, *14*, 3363 and references cited therein.

48. (a) Huang, C. Y. *Method Enzymol.* **1982**, *87*, 509. (b) Hirose, K. *J. Incl. Phenom.* **2001**, *39*, 193. (c) Likussar, W.; Boltz, D. F. *Anal. Chem.* **1971**, *43*, 1265.

49. Job, P. *Ann. Chim.* **1928**, *9*, 113.

50. Liou, L. R.; McNeil, A. J.; Ramirez, A.; Toombes, G. E. S.; Gruver, J. M.; Collum, D. B. *J. Am. Chem. Soc.* **2008**, *130*, 4859.

51. More precisely, introducing catalysis would elevate the rate constant for conversion of SM to I according to $k_{obsd} = k_1 + k_{cat}$.

52. The principle of microscopic reversibility seems to have been the source of frequent controversies and must be applied with caution. It is not obvious to us, for example, that following authors, all warning of the risks, would agree with each other's assertions: (a) Blackmond, D. G. *Angew. Chem., Int. Ed.* **2009**, *48*, 2648. (b) Krupka, R. M.; Kaplan, H.; Laidler, K. J. *J. Chem. Soc., Faraday Trans. 62*, **1966**, 2754. (c) Chandrasekhar, S. *Res. Chem. Intermed.* **1992**, *17*, 173. (d) Burwell, R. L.; Pearson, R. G. *J. Phys. Chem.* **1966**, *70*, 300.

53. (a) Chadwick, S. T.; Rennels, R. A.; Rutherford, J. L.; Collum, D. B. *J. Am. Chem. Soc.* **2000,** *122,* 8640. (b) Anderson, D. R.; Faibish, N. C.; Beak, P. *J. Am. Chem. Soc.* **1999,** *121,* 7553. (c) Singh, K. J.; Collum, D. B. *J. Am. Chem. Soc.* **2006**, *128*, 13753. (d) Meyers, A. I.; Mihelich, E. D. *J. Org. Chem.* **1975**, *40*, 3158. (e) Ramirez, A.; Sun, X.; Collum, D. B. *J. Am. Chem. Soc.* **2006**, *128*, 10326. (f) Sun, X.; Collum, D. B. *J. Am. Chem. Soc.* **2000**, *122*, 2452.

54. The metalations of carbamate **6** (eq 2) showed an approximate first-order dependence on **6** affiliated with a standard isotope effect that was small (k_H/k_D = 3-4) when compared with some LDA-mediated metalations but still reasonable for a rate-limiting proton transfer. Prompted by the substrate orders and isotope effects described herein, we have reinvestigated the metalation of **6** by monitoring the *competitive* isotope effect and found a large KIE ($k_H/k_D > 30$) and clear biphasic kinetics. We conclude, therefore, that the proton transfer is only partially rate limiting for **6-*d*$_1$**.

55. For crystallographically characterized examples of lithium amide ladder structures showing open-dimer-like subunits, see Armstrong, D. R.; Barr, D.; Clegg, W.; Hodgson, S. M.; Mulvey, R. E.; Reed, D.; Snaith, R.; Wright, D. S. *J. Am. Chem. Soc.* **1989**, *111*, 4719.

56. A four-rung LDA/LiX ladder has been characterized: Williard, P. G.; Hintze, M. J. *J. Am. Chem. Soc.* **1987**, *109*, 5539.

57. (a) Evans, W. J.; Broomhall-Dillard, R. N. R.; Ziller, J. W. *J. Organomet. Chem.* **1998**, *569*, 89. (b) Klingebiel, U.; Tecklenburg, B.; Noltemeyer, M.; Schmidt-Baese, D.; Herbst-Irmer, R. *Z. Naturforsch., B: Chem. Sci.* **1998**, *53*, 355.

58. Romesberg, F. E.; Collum, D. B. *J. Am. Chem. Soc.* **1994**, *116*, 9198.

59. Examples and leading references to complex ion pairs: Kolonko, K. J.; Biddle, M. M.; Guzei, I. A.; Reich, H. J. *J. Am. Chem. Soc.* **2009**, *131*, 11525.

60. Y-intercepts derived from plots of initial rates versus arene concentration using 0.10 M LDA in neat THF ($M \cdot s^{-1}$) are as follows: **1**, 1.0×10^{-6}; **1-*d*$_1$**, 0.5×10^{-6}; **2**, 3.0×10^{-6}; **2-*d*$_2$**, 0.8×10^{-6}.

61. A survey of approximately 500 total syntheses revealed LDA to be the most commonly used reagent. Reich, H. J., unpublished.

62. Kofron, W. G.; Baclawski, L. M. *J. Org. Chem.* **1976**, *41*, 1879.

63. Krasovskiy, A.; Knochel, P. *Angew. Chem., Int. Ed.* **2004**, *43*, 3333.

64. 2-fluoro-5-(trimethylsilyl)pyridine: synthesized using commercially available 2-fluoro-5-iodopyridine; 2-fluoro-6-(trimethylsilyl)pyridine: synthesized using commercially available 2-bromo-6-fluoropyridine; 2,6-difluoro-4-(trimethylsilyl)pyridine: synthesized using 2,6-difluoro-4-iodopyridine. For the synthesis of the iodo-derivative, see ref 1b.

CHAPTER IV

Reaction of Lithium Diethylamide with an Alkyl Bromide and an Alkyl Benzenesulfonate: Origins of Alkylation, Elimination, and Sulfonation

Reaction of Lithium Diethylamide with an Alkyl Bromide and Alkyl Benzenesulfonate: Origins of Alkylation, Elimination, and Sulfonation

Abstract

A combination of NMR, kinetic, and computational methods are used to examine reactions of lithium diethylamide in tetrahydrofuran (THF) with *n*-dodecyl bromide and *n*-octyl benzenesulfonate. The alkyl bromide undergoes competitive S_N2 substitution and E2 elimination in proportions independent of all concentrations except for a minor medium effect. Rate studies show that both reactions occur via trisolvated-monomer-based transition structures. The alkyl benzenesulfonate undergoes competitive S_N2 substitution (minor) and N-sulfonation (major) with N-sulfonation favored at low THF concentrations. The S_N2 substitution is shown to proceed via a disolvated monomer suggested computationally to involve a cyclic transition structure. The dominant N-sulfonation follows a disolvated-dimer-based transition structure suggested computationally to be a bicyclo[3.1.1] form. The differing THF and lithium diethylamide orders for the two reactions explain the observed concentration-dependent chemoselectivities.

Introduction

Many may remember being confounded by the substitution-elimination dichotomy presented in our first course on organic chemistry (eq 1).[1] It was difficult to grasp why a given electrophile-nucleophile-solvent combination causes the prevalence of substitution over elimination (or vice versa), despite support from an enormous body of empirical observations. In

our opinion, the confusion stems from the incomplete picture of how solvation and aggregation influence nucleophilicity and basicity. The nomenclature based on "ion pairing" prevalent in the older literature is too inflexible to describe underlying aggregation effects. Similarly, using terms such as "polarity" to explain solvent-dependent reactivities and selectivities is inadequate to describe inherently molecular solvation events. Amid the few studies designed to untangle the coordination chemistry underlying substitutions and eliminations,[2] the efforts of Streitwieser and coworkers are prominent.[3]

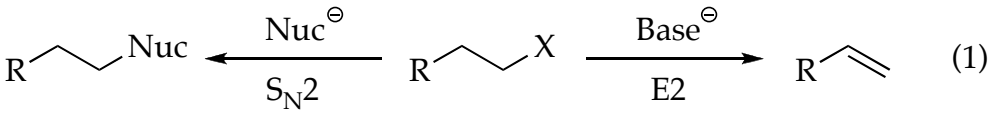

(1)

Understanding the S_N2-E2 dichotomy is more than an aging academic problem. One is struck, for example, by the profound importance of C-N bond formation in pharmaceutical syntheses and the role played by S_N2 substitutions.[4] Given the scope of the applications and their scales,[5] even incremental improvements in simple N-alkylations of mono- and dialkylamines could prove significant.

We describe herein reactions of lithium diethylamide (Et_2NLi) in tetrahydrofuran (THF) with an *n*-alkyl bromide (eq 2) and an *n*-alkyl sulfonate (eq 3). The competing N-substitution, elimination, and N-sulfonation (O-desulfonation) pathways are traced to specific solvation and aggregation events.[6]

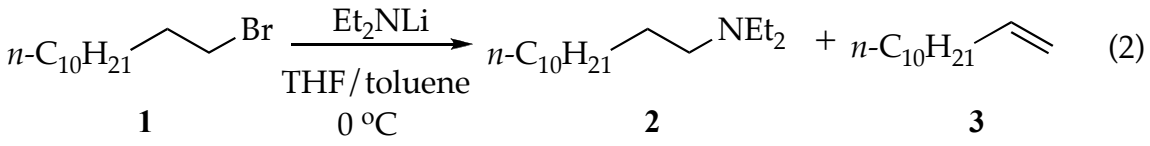

1 **2** **3** (2)

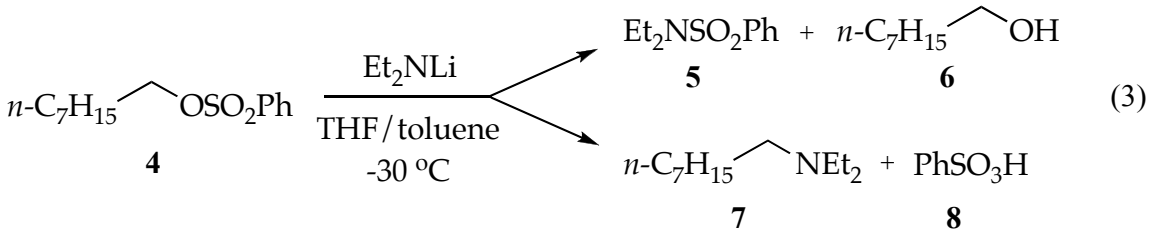

4 **5** **6** **7** **8** (3)

Results

Concentration-Dependent Selectivities. Using protocols and conditions described below, the selectivities of N-alkylation, elimination, and N-sulfonation versus Et_2NLi and THF concentrations were measured and are depicted graphically in Figures IV.1-4. The notable feature is that *n*-alkyl bromide **1** affords ratios of **2** and **3** displaying a minor THF dependence (Figures IV.1 and IV.2), whereas the relative proportions of N-sulfonation (**5**) and N-alkylation (**7**) show both a dependence on the Et_2NLi concentration and a striking THF concentration dependence (Figures IV.3 and IV.4). The product ratios allow us to deconvolute the mechanistic contributions to each pathway.

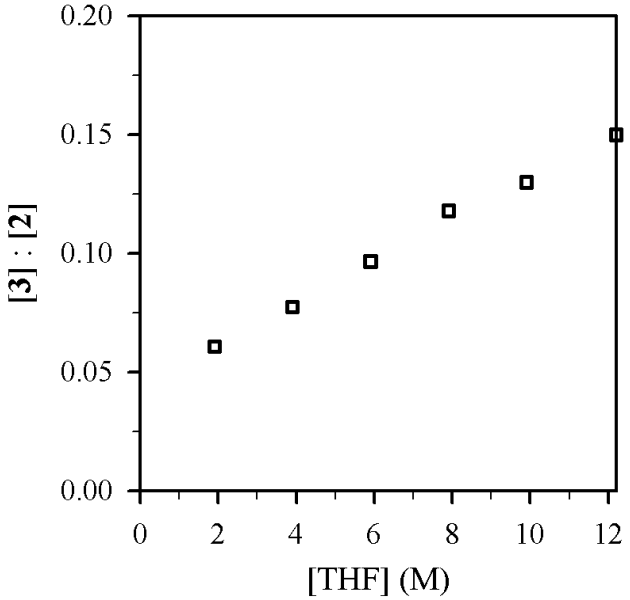

Figure IV.1. Plot of [**3**]:[**2**] vs [THF] in toluene cosolvent for the reaction of 0.004 M 1-bromododecane (**1**) with Et_2NLi (0.10 M) at 0 °C.

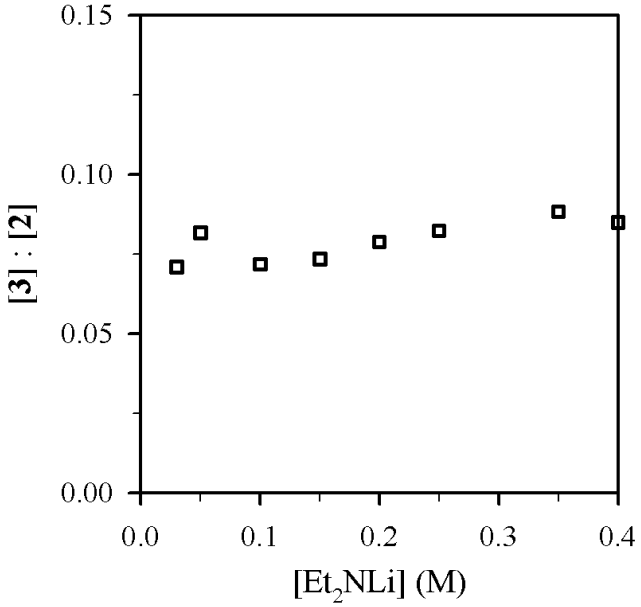

Figure IV.2. Plot of [**3**]:[**2**] vs [Et_2NLi] in THF (3.9 M) and toluene cosolvent for the reaction of 0.004 M 1-bromododecane (**1**) with Et_2NLi at 0 °C.

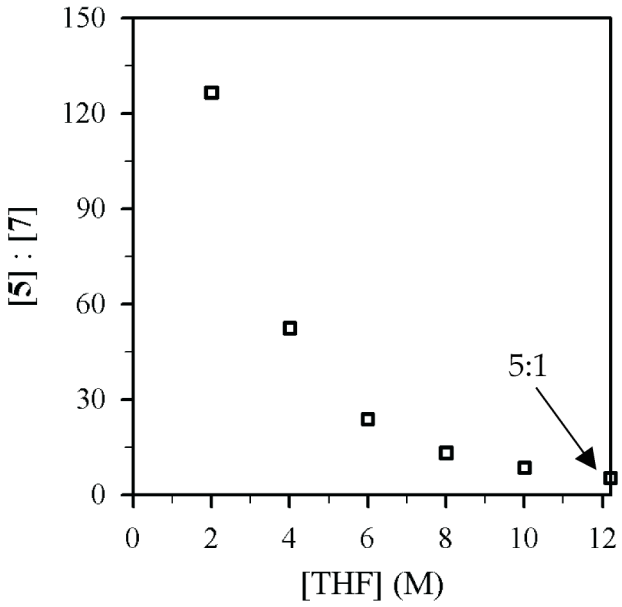

Figure IV.3. Plot of [**5**]:[**7**] vs [THF] in toluene cosolvent for the reaction of 0.004 M 1-octyl benzenesulfonate (**4**) with Et_2NLi (0.10 M) at -30 °C.

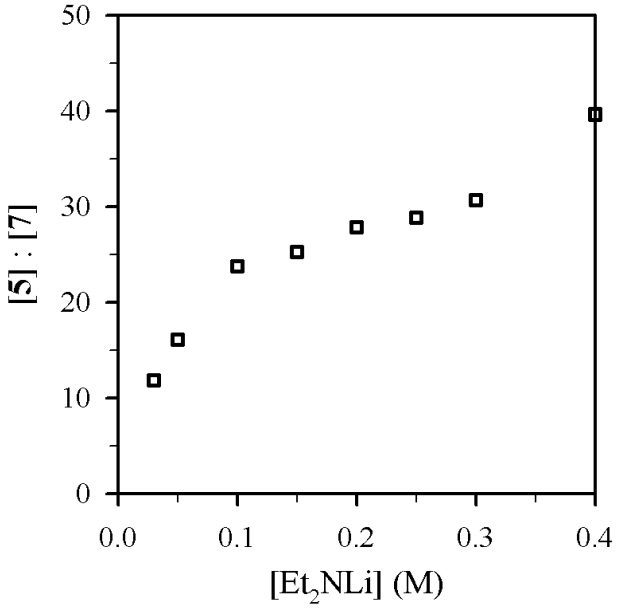

Figure IV.4. Plot of [**5**]:[**7**] vs [Et_2NLi] in THF (6.0 M) and toluene cosolvent for the reaction of 0.004 M 1-octyl benzenesulfonate (**4**) with Et_2NLi at -30 °C.

Structure of Lithium Diethylamide. Previous ^{6}Li and ^{15}N NMR spectroscopic investigations have shown that [^{6}Li,^{15}N]Et_2NLi is a dimer in THF (**9**).[7] Computational studies suggest that dimer **9** is disolvated (see Supporting Information). At low THF concentrations (<2.0 M), minor amounts of 3- and 4-rung ladders are observed.[7,8]

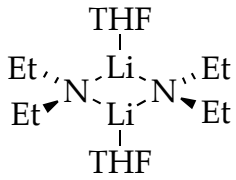

9

General Protocols. Pseudo-first-order rate constants (k_{obsd}) were determined using excess Et_2NLi (0.030-0.40 M) and limiting substrate concentrations (0.004 M). THF was restricted to >2.0 M to avoid the larger aggregates observed at low THF concentrations.[7,8] The disappearance of the substrate (**1** or **4**) and the formation of products were monitored relative to an internal *n*-decane standard using gas chromatographic (GC) analysis of quenched aliquots; they displayed clean first-order decays. Measured values of k_{obsd} were independent of the initial concentrations of the substrate ($\pm$10%), consistent with first-order dependencies on the substrates. The product ratios allow k_{obsd} to be partitioned into the rate constants for the parallel pathways as described below. Results from the rate studies are summarized in Table 1. Additional data are archived in Supporting Information.

N-Alkylation and Elimination of 1-Bromododecane. Reaction of Et_2NLi with 1-bromododecane (**1**) in THF/toluene yields *N,N*-diethyldodecylamine (**2**)[9] and 1-dodecene (**3**) as shown in eq 2 and Figure IV.5.

n-Dodecane that resulted from reduction[10] was also detected, but the concentrations were erratic and very low (<2%).[11] Plots of k_{obsd} versus THF concentration (Figure IV.6) and k_{obsd} versus Et_2NLi concentration (Figure IV.7) furnish orders of 2.0 ± 0.1 and 0.54 ± 0.03, respectively. Replacing toluene cosolvent with 2,2,4,4-tetramethyltetrahydrofuran revealed no measurable cosolvent dependence, arguing against long-range medium effects as the source of second-order THF dependence.[6b,12]

Table IV.I. Summary of Rate Studies for the Et_2NLi-Mediated Reactions (eqs 2 and 3)

Entry	Substrate	Product(s)	THF order	Et_2NLi order	k_H/k_D[d]	k_H/k_D[e]
1	**1**	**2**+**3**	2.0 ± 0.1[a]	0.54 ± 0.03[b]	1.1 ± 0.1	1.22 ± 0.05
2		**2**	2.0 ± 0.1[a]	0.52 ± 0.03[b]	1.1 ± 0.1	1.12 ± 0.05
3		**3**	2.5 ± 0.1[a]	0.57 ± 0.03[b]	1.1 ± 0.1	3.02 ± 0.04
4	**4**	**5**+**7**	0[a]	0.98 ± 0.05[c]		
5		**5**	0[a]	0.99 ± 0.04[c]		
6		**7**	1.29 ± 0.05[a]	0.59 ± 0.04[c]		

[a][Et_2NLi] = 0.10 M. [b][THF] = 3.9 M in toluene cosolvent. [c][THF] = 6.0 M in toluene cosolvent. [d]Measured using **1** and 1,1-**1**-d_2. [e]Measured using **1** and 2,2-**1**-d_2.

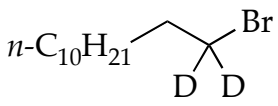

1,1-**1**-d_2

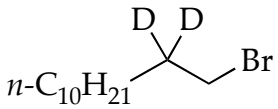

2,2-**1**-d_2

To separate contributions from the two pathways one simply notes that $k_{obsd} = k_{alk} + k_{elim}$ and $[\mathbf{2}]/[\mathbf{3}] = k_{alk}/k_{elim}$ such that k_{alk} and k_{elim} correspond to the pseudo-first-order rate constants for N-alkylation and elimination, respectively. The task was simple because the product ratios were nearly independent of all concentrations (see Figures IV.1 and IV.2); the rate laws for

substitution and elimination are identical. (A slight preference for the formation of **3** at elevated THF concentrations is reflected by the slightly higher order; Table 1, entry 3.) Thus, the idealized rate law[13] is described by eq 4. The product ratios are sensitive to isotopic substitution. The measured isotope effects using 1,1-**1**-d_2 and 2,2-**1**-d_2 (Table 1) are consistent with an S_N2 substitution[14] and E2 elimination.[15] GC-MS analyses also confirmed β- rather than α-eliminations.[16] The stereochemistries of N-alkylation and elimination were *not* addressed experimentally.[17]

$$-d[\mathbf{1}]/dt = (k_{alk} + k_{elim})[Et_2NLi]^{1/2}[THF]^2[\mathbf{1}] \quad (4)$$

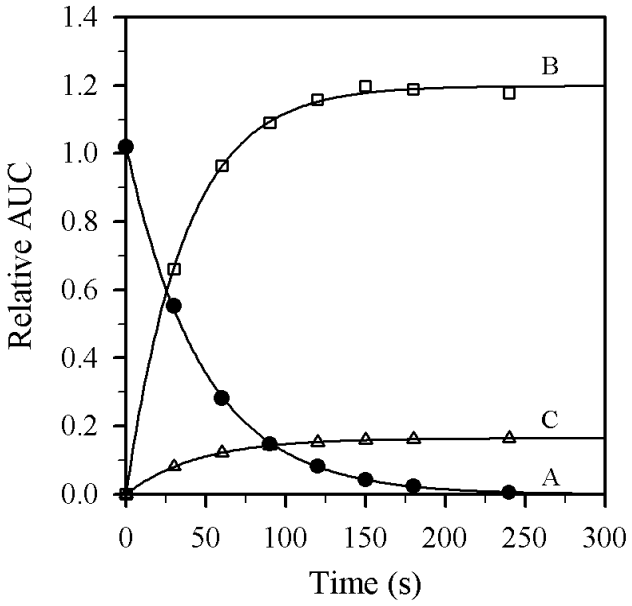

Figure IV.5. Representative plot of the time-dependent decay of **1** (curve A) and formation of **2** (curve B) and **3** (curve C) relative to an *n*-decane internal standard (relative area under the curve, AUC) for sequentially quenched samples of a reaction mixture containing Et_2NLi (0.10 M), THF (9.90 M), **1** (0.004 M), and toluene cosolvent at 0 °C. The curves depict least squares fit to: (A) $y = ae^{-bx}$ ($a = 1.022 \pm 0.005$, $b = k_{obsd} = (2.11 \pm 0.02) \times 10^{-2}$); (B) $y = \{a(1\text{-}e^{-bx})\}$ ($a = 1.199 \pm 0.006$, $b = k_{alk} = (2.71 \pm 0.06) \times 10^{-2}$); (C) $y = \{a(1\text{-}e^{-bx})\}$ ($a = 1.648 \pm 0.003$) $\times 10^{-1}$, $b = k_{elim} = (2.25 \pm 0.02) \times 10^{-2}$).

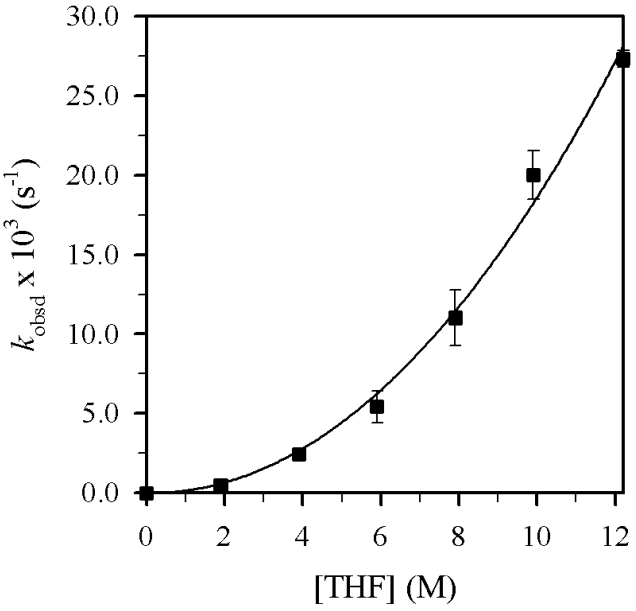

Figure IV.6. Plot of k_{obsd} vs [THF] in toluene cosolvent for the reaction of **1** (0.004 M) with Et_2NLi (0.10 M) at 0 °C. The curve depicts an unweighted least-squares fit to $k_{obsd} = k[THF]^n$ ($k = (1.6 \pm 0.4) \times 10^{-4}$, $n = 2.0 \pm 0.1$).

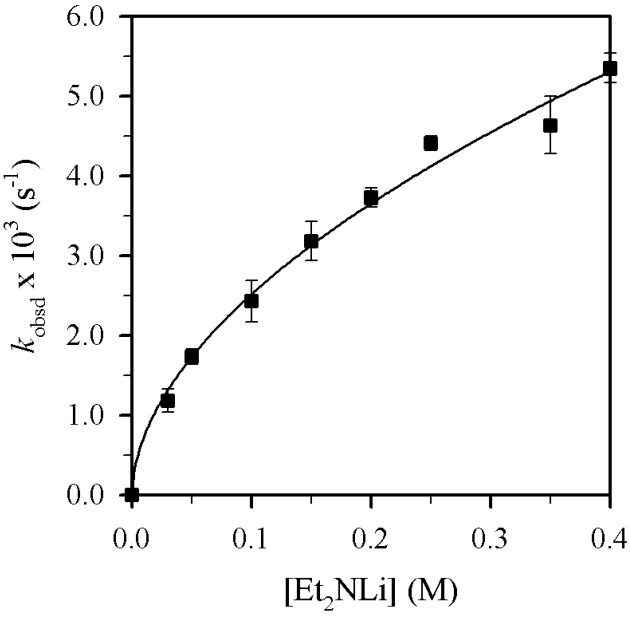

Figure IV.7. Plot of k_{obsd} vs [Et_2NLi] in THF (3.9 M) and toluene cosolvent for the reaction of **1** (0.004 M) with Et_2NLi at 0 °C. The curve depicts an unweighted least-squares fit to $k_{obsd} = k[Et_2NLi]^n$ ($k = (8.7 \pm 0.4) \times 10^{-3}$, $n = 0.54 \pm 0.03$).

A variety of seemingly plausible transition structures for substitution and elimination are shown in Chart IV.1. Density functional theory (DFT) calculations using the SVP basis set for Br and 6-31G* for the rest of the atoms[18] afforded enthalpies of activation ($\Delta H^{\ddagger}$, kcal/mol) that include thermal corrections at 298.15 K. 1-Bromododecane, Et_2NLi, and THF were modeled using EtBr, Me_2NLi and Me_2O, respectively, to restrict the number of conformers. Calculated free energies were ridiculously high (even with single-point MP2 corrections). Enthalpies are reported according to eq 5. Although absolute energies are not terribly informative, the relative values and calculated geometries are.

Chart IV.1

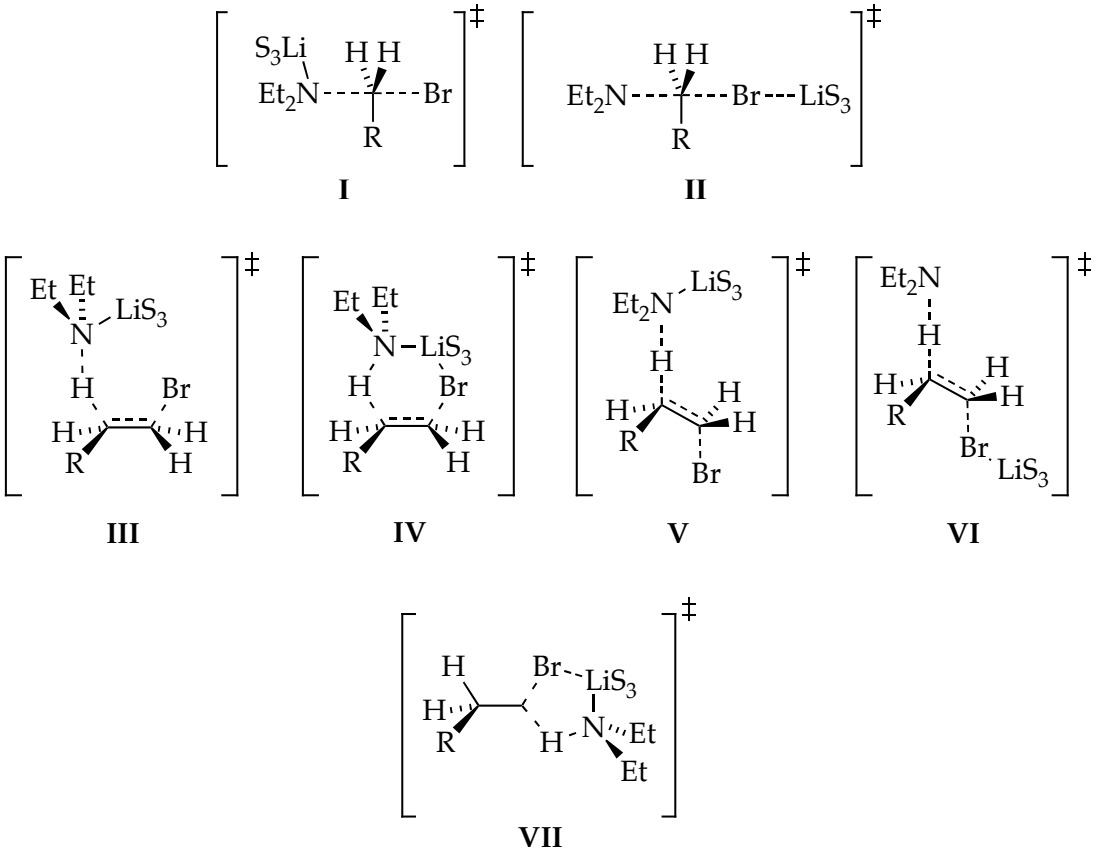

The results of the DFT computations are illustrated in Chart IV.2. Optimization of isomer **I** resulted in legitimate transition structure **10** displaying an N-Li interaction and a highly bent N-C-Br bond angle (155°).[19] In contrast, we failed to locate structures akin to **II**.[20] Optimizations of β-eliminations **III-VI** afforded only **11** and **12** (types **III** and **V**), both containing N-Li contacts. No structures of type **IV** or **VI** displaying Br-Li contacts could be found. Efforts to find structure **VII** corresponding to a hypothetical (unobserved) α-elimination failed, possibly because the trisolvation implicated by the rate studies precludes a Br-Li interaction.[21] The relative enthalpies of transition structures **10**, **11** and **12** indicate that the nucleophilic substitution (**10**) is enthalpically favored.

$$1/2\ (Et_2NLi)_2(S)_2 + RX + 2S \xrightarrow[(S=Me_2O)]{\Delta H^{\ddagger}} [(Et_2NLi)(S)_3(RX)]^{\ddagger} \qquad (5)$$

Chart IV.2

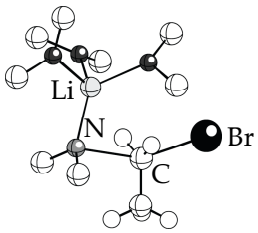

10
$\Delta H^{\ddagger}$ = 13.0 kcal/mol

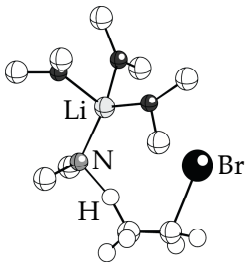

11
$\Delta H^{\ddagger}$ = 16.8 kcal/mol

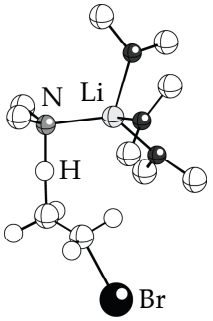

12
$\Delta H^{\ddagger}$ = 18.9 kcal/mol

N-Alkylation and N-Sulfonation of *n*-Octyl benzenesulfonate. The reaction of 1-octyl benzenesulfonate (**4**) with 0.10 M Et_2NLi in THF/toluene mixtures at -30 °C affords products derived from N-sulfonation (**5** and **6**) and N-alkylation (**7** and **8**) to the exclusion of 1-octene expected from elimination

(eq 3). Figure IV.3 shows the THF dependence on the ratio of substitution and elimination (**5**/**7**). In contrast to the reaction of 1-bromododecane, the selectivity is highly sensitive to the proportion of THF. By monitoring the **5**/**7** ratio (vide supra), k_{obsd} can be deconvoluted to give the rate constants for the N-sulfonation (k_{sulf}) and N-alkylation (k_{alk}).

Plots of k_{alk} and k_{sulf} versus THF concentration (Figures IV.8 and IV.9) reveal first- and zeroth-order dependencies, respectively. The linear and slightly downward THF concentration dependence observed for k_{sulf} is consistent with secondary shell (medium) effects accompanying the increasing THF concentration.[6b,12] Figures IV.10 and IV.11 illustrate the dependence of k_{alk} and k_{sulf} on the Et_2NLi concentration (0.03-0.40 M) in 6.0 M THF. The fractional order ($k_{alk} \propto [Et_2NLi]^{0.59 \pm 0.04}$) and first order ($k_{sulf} \propto [Et_2NLi]^{0.99 \pm 0.04}$) are consistent with monomer- and dimer-based pathways, respectively. The data support the idealized rate law in eq 6 and the generic mechanisms in eqs 7 and 8.

$$d[\mathbf{4}]/dt = k_{alk}[Et_2NLi]^{1/2}[THF]^{1}[\mathbf{4}] + k_{sulf}[Et_2NLi]^{1}[THF]^{0}[\mathbf{4}] \quad (6)$$

$$1/2\ \underset{(\mathbf{9})}{(Et_2NLi)_2(THF)_2} + \mathbf{4} \xrightarrow{k_{alk}[THF]} [(Et_2NLi)(THF)_2(\mathbf{4})]^{\ddagger} \quad (7)$$

$$\underset{(\mathbf{9})}{(Et_2NLi)_2(THF)_2} + \mathbf{4} \xrightarrow{k_{sulf}} [(Et_2NLi)_2(THF)_2(\mathbf{4})]^{\ddagger} \quad (8)$$

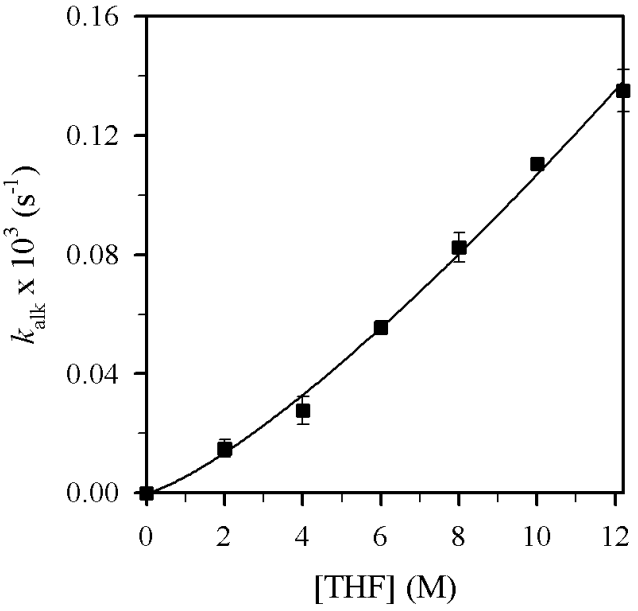

Figure IV.8. Plot of k_{alk} vs [THF] in toluene cosolvent for the N-alkylation of **4** (0.004 M) with Et_2NLi (0.10 M) at -30 °C. The curve depicts an unweighted least-squares fit to $k_{alk} = k[THF]^n$ ($k = (5.5 \pm 0.7) \times 10^{-6}$, $n = 1.29 \pm 0.05$).

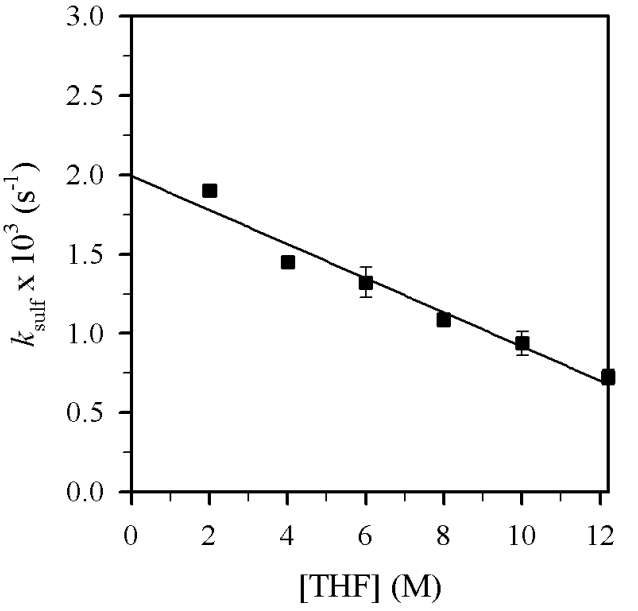

Figure IV.9. Plot of k_{sulf} vs [THF] in toluene cosolvent for the N-sulfonation of **4** (0.004 M) with Et_2NLi (0.10 M) at -30 °C. The curve depicts an unweighted least-squares fit to $k_{sulf} = c[THF] + k'$ ($c = (-1.07 \pm 0.08) \times 10^{-4}$, $k' = (1.99 \pm 0.06) \times 10^{-3}$).

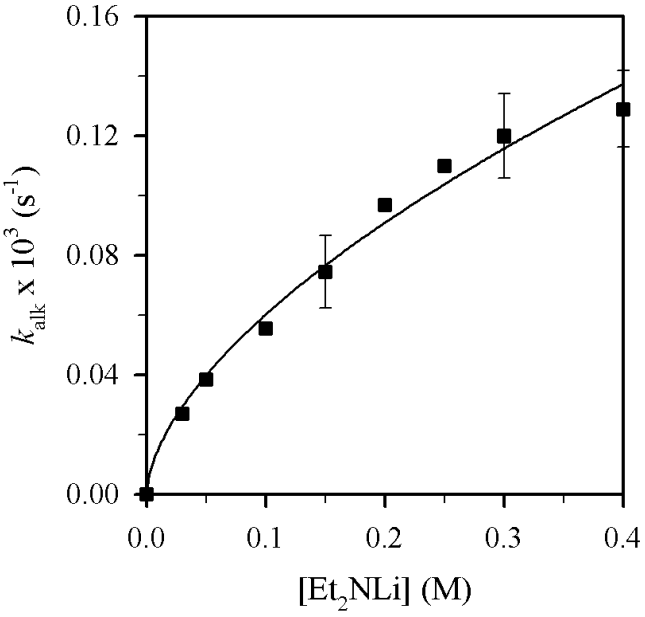

Figure IV.10. Plot of k_{alk} vs [Et_2NLi] in THF (6.0 M) and toluene cosolvent for the N-alkylation of **4** (0.004 M) with Et_2NLi at -30 °C. The curve depicts an unweighted least-squares fit to $k_{alk} = k[Et_2NLi]^n$ ($k = (2.4 \pm 0.1) \times 10^{-4}$, $n = 0.59 \pm 0.04$).

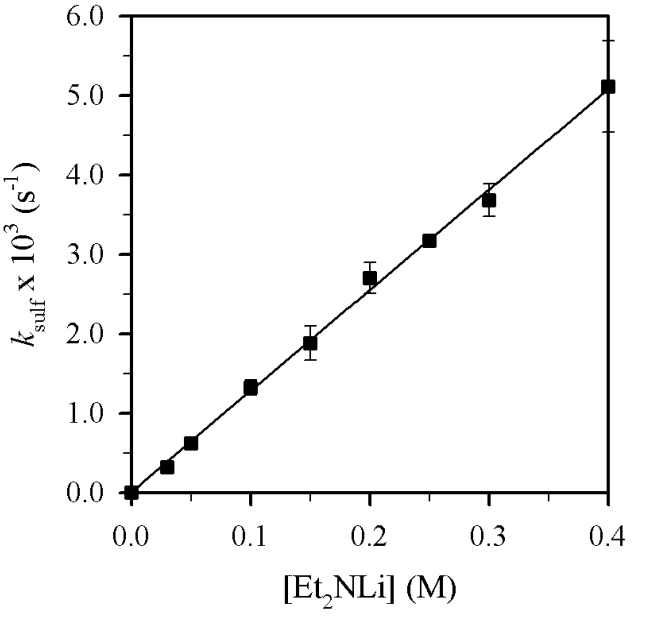

Figure IV.11. Plot of k_{sulf} vs [Et_2NLi] in THF (6.0 M) and toluene cosolvent for the N-sulfonation of **4** (0.004 M) with Et_2NLi at -30 °C. The curve depicts an unweighted least-squares fit to $k_{sulf} = k[Et_2NLi]^n$ ($k = (1.26 \pm 0.07) \times 10^{-2}$, $n = 0.99 \pm 0.04$).

Rate data indicate that N-alkylation occurs via disolvated Et_2NLi monomer, possibly with a minor contribution from trisolvated monomer, whereas N-sulfonation takes place via disolvated Et_2NLi dimer. The generic transition structures in Chart IV.3 seem plausible, yet a much smaller subset proved computationally viable (Chart IV.4). Attempts to optimize parent geometries **VIII** and **IX** for the nucleophilic substitution (using $PhSO_2OEt$ as a model) converged on hybrid isomer **13**, which displays a 6-membered ring and a tetracoordinate lithium[22] that interacts with the sulfonyl leaving group.[23] Transition structure **13** corresponds to a 6-*endo*-*tet* closure, which is considered to be geometrically implausible in many settings.[24] Transition structure **14**, a trisolvated analog of **13**, lacks an S=O-Li contact.

Searches for disolvated-dimer-based transition structures for N-sulfonation afforded only structure **15** (type **XII**), solvated at the external and internal Li atoms. (Optimization of proximally solvated forms (types **X** and **XI**) led to desolvation.[25,26]) Transition structure **15** displays a bicyclo[3.1.1] ring system with coordination of each S=O moiety to one lithium atom of the Me_2NLi dimer. The sulfur atom adopts trigonal bipyramidal hybridization with the attacking nitrogen and the leaving RO group in apical positions. IRC calculations support a stepwise addition-elimination.[27] The computations qualitatively support a preference for N-sulfonation over N-alkylation.

Cursory searches of hypothetical (unobserved) monomer-based β-eliminations afford **16** and **17**. Activation enthalpies (and free energies) suggest that eliminations will not compete with alkylation and sulfonation.

Chart IV.3

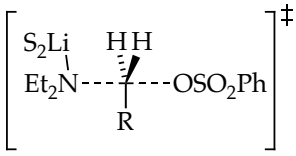

VIII

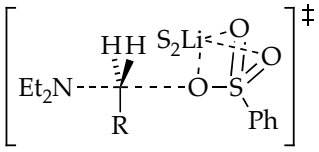

IX

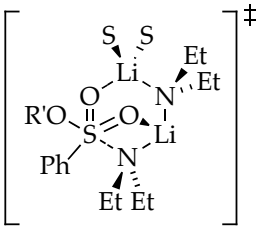

X

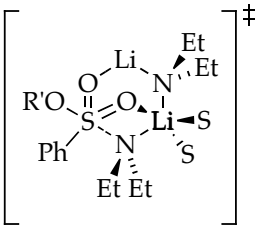

XI

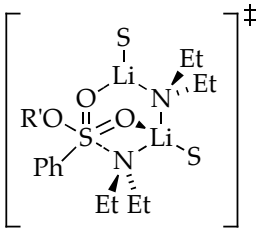

XII

Chart IV.4

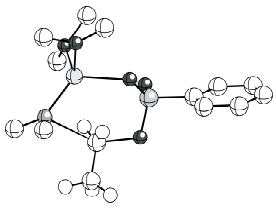

13
$\Delta H^{\ddagger}$ = 15.5 kcal/mol

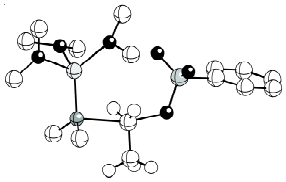

14
$\Delta H^{\ddagger}$ = 12.3 kcal/mol

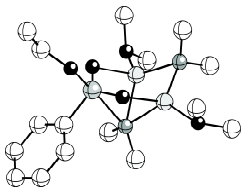

15
$\Delta H^{\ddagger}$ = 3.1 kcal/mol

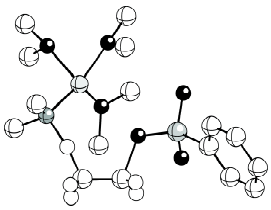

16
$\Delta H^{\ddagger}$ = 16.8 kcal/mol

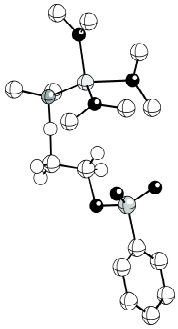

17
$\Delta H^{\ddagger}$ = 17.9 kcal/mol

Discussion

We introduced this paper with the assertion that nucleophilic substitutions and eliminations can be confounding because of a limited understanding of how aggregation and solvation—two inherently molecular phenomena—influence the mechanisms. A combination of kinetic and computational methods was used to study reactions of Et_2NLi in THF with *n*-alkyl bromide **1** and *n*-alkyl benzenesulfonate **4** (eqs 2 and 3). The resulting mechanistic scenario summarized in Scheme IV.1 is discussed in the context of several longstanding issues.

Scheme IV.1

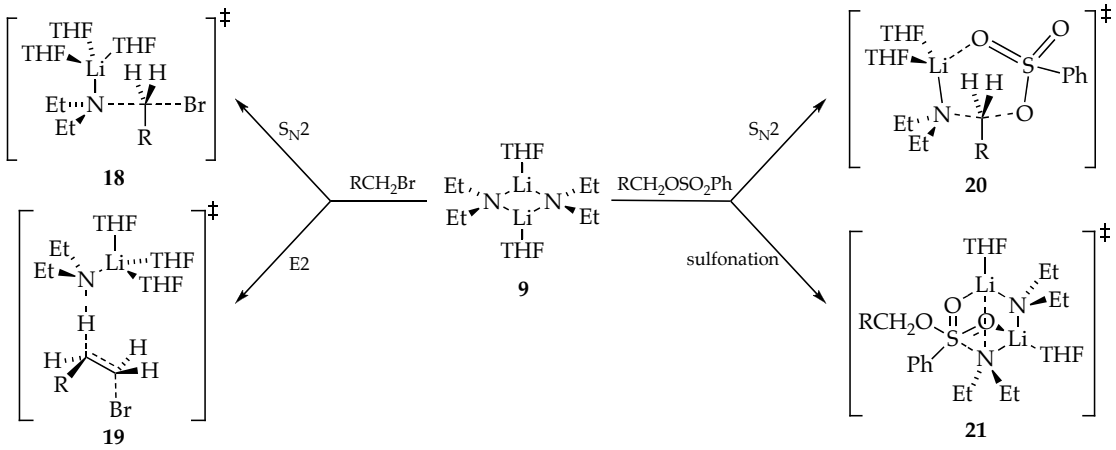

S_N2-E2 Dichotomy. We intended to study the mechanistic basis underlying competing substitutions and eliminations. Such an analysis of sulfonate **4** was precluded by its failure to undergo detectable elimination that is somewhat surprising given the pronounced Brönsted basicity of Et_2NLi.[29] Focussing on *n*-alkyl bromide **1**, we found that both substitution and elimination proceed via isomeric trisolvated-monomer-based pathways. One of the most obvious and practical consequences is that concentration changes

provide no means of controlling selectivity (Figures IV.1 and IV.2). The drifting selectivity with increasing THF concentration shown in Figure IV.1 derives from secondary shell solvation effects; vide infra.

S_N2 Substitutions: RBr versus $ROSO_2Ph$. Inspection of transition structure **18** (or the structurally simpler computed analog, **10**) reveals pronounced steric interactions between the CH_2-Br moiety and the THF ligands. Now imagine an analogous substitution of a secondary alkyl bromide via transition structure **22**. The vast literature suggests that it would be markedly slower (possibly orders of magnitude). It appears, however, that solvent-substrate interactions are pronounced and that focusing on Et_2N-RBr interactions may be misleading. The literature also suggests that highly ionizing conditions can markedly promote the S_N2 substitution,[28c,30] which would logically stem from both the increasing charge on the nucleophile as well as removal of the lithium cation and, with it, the solvent-substrate contacts. This scenario is very unlikely to occur, however, for Et_2NLi even under highly ionizing conditions. The conclusion is a recurring theme: steric demands of solvation are an important determinant of aggregate structure and reactivity.[31]

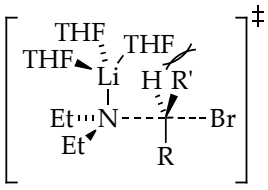

22

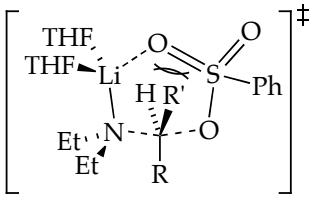

23

Comparing the mechanism for S_N2 substitutions of *n*-alkyl bromide **1** and benzenesulfonate **4** reveals that the sulfonate ester undergoes substitution via a disolvated rather than a trisolvated monomer. Computational studies

show that transition structure **20** (Scheme IV.1), in which a THF ligand has been replaced by chelation of the sulfonate, is quite plausible with a 25° distortion of the N-C-O angle from the optimal 180°, a distortion comparable to that observed for the alkyl bromide.[32] Those who use Baldwin's ring closure rules categorically may find transition structure **20** disquieting. Let us return to the hypothetical displacements and consider the displacement of a secondary alkyl sulfonate ester. The additional alkyl moiety (R') in cyclic transition structure **23** would likely render the reaction untenable because of acute interactions between the sulfonyl moiety and the alkyl group of the sulfonate ester. The reaction would be forced to proceed through a noncyclic form, which is suggested by the rate studies to be less viable. The interactions *within the sulfonate ester moiety* are quite prominent whereas those with the Et_2N moiety almost seem to be of secondary importance. Although this description is certainly an oversimplification, most conventional discussions of S_N2 displacements of sulfonate esters do not consider interactions between the sulfonyl moiety and the alkyl substituents as potentially dominant.[33]

S_N2 Substitution versus N-Sulfonation. The reaction of Et_2NLi with sulfonate **4** in THF affords products of substitution and N-sulfonation. The name N-sulfonation, however, is a lithium amide-centric view. It would be equally valid to call it O-desulfonation. Such desulfonations are consequential side reactions during displacements of tosylates and related aryl sulfonate esters.[34] In contrast to the substitution-elimination selectivity observed for *n*-alkyl bromide **1**, the alkylation-sulfonation selectivity is sensitive to both THF and Et_2NLi concentrations (Figures IV.3 and IV.4). The dominant sulfonation (120:1) becomes less so (<5:1) at low Et_2NLi and high THF concentrations. The concentration dependencies derive from differential solvation and aggregation

numbers in transition structures **20** and **21**. The sulfonation appears to benefit from multidentate contacts with lithium as well as from conservation of the Et_2NLi dimer structure. IRC calculations revealed a two-step (addition-elimination) mechanism.

Primary Shell versus Secondary Shell Solvation. Both N-alkylation and β-elimination of 1-bromododecane show approximate second-order THF dependencies, which we attribute to monomer-based pathways in THF/toluene mixtures. The THF order for the elimination pathway is actually 2.5 ± 0.1 (Table 1, entry 3). One consequence is that the selectivity shows a preference for elimination at elevated THF concentrations (Figure IV.1). By using 2,2,5,5-tetrahydrofuran, a cosolvent with a polarity akin to that of THF but no capacity to coordinate competitively to lithium, the THF order for the β-elimination drops to 2.1 ± 0.1.[35] Thus, there is a medium effect of marginal practical consequence. The N-sulfonation using sulfonate **4** shows an analogous medium effect, except that a slight rate reduction occurs at elevated THF concentrations. Similar secondary shell effects contributing to solvent-dependent rates have been documented previously.[6,36] Moreover, they are known to cause both modest accelerations and decelerations, depending on the specific reaction. Although it may be tempting to focus on how and why the medium influences reaction rates, we find that the medium effects are surprisingly minor given that lithium amides are often viewed as highly polar species. The chemistry of lithium amides in particular, and probably organolithium reagents in general, is dominated by ligands in the primary coordination shell.

Conclusion

Reaction of Et_2NLi with an *n*-alkyl bromide reveals competing S_N2 substitution and E2 elimination via trisolvated lithium amide monomers in both instances. Within this sliver of the enormous field of substitution and elimination, the relative reaction rates and, consequently, the chemoselectivity are insensitive to solvent and lithium amide concentrations. Analogous reaction of Et_2NLi with an *n*-alkyl arylsulfonate affords low levels of substitution and substantial N-sulfonation to the exclusion of elimination. Because the N-alkylation proceeds via disolvated monomers and the N-sulfonation via disolvated dimers, the selectivity is controllable by adjusting concentrations, although the N-sulfonation remains dominant under all conditions. Whereas primary shell solvation is of profound importance, secondary-shell solvation (medium effects) has marginally detectable influence on rates and selectivities. We are reminded that to understand organolithium reaction mechanism is to understand the coordination chemistry of lithium, not vague notions of polarity and ionicity.

Experimental Section

Reagents and Solvents. THF and toluene were distilled from blue or purple solutions containing sodium benzophenone ketyl. The toluene still contained 1% tetraglyme to dissolve the ketyl. [^{6}Li]Et_2NLi and [^{6}Li,^{15}N]Et_2NLi were prepared as insoluble white solids by metalating Et_2NH and [^{15}N]Et_2NH (respectively) with [^{6}Li]*n*-BuLi in pentane.[37] Recrystallization from hexane/diethyl ether as the etherate and subsequent evacuation afforded solvent-free Et_2NLi.[7] Air- and moisture-sensitive materials were manipulated under argon or nitrogen using standard glove box, vacuum line, and syringe

techniques. Solutions of *n*-BuLi and Et_2NLi were titrated for active base using a literature method.[38]

Kinetics. For a kinetic run corresponding to a single rate constant, a stock solution of Et_2NLi (0.03-0.4 M) in a THF-toluene solution was prepared. A series of oven-dried, nitrogen-flushed 5 mL serum vials (10 per rate constant) fitted with stir bars were charged with the Et_2NLi stock solution and brought to the desired temperature ($\pm$ 0.2 °C) using a constant-temperature bath fitted with a thermometer. The substrate (**1** or **4**) was added as a 0.08 M stock solution in hexane containing decane (0.08 M) as a GC standard. The vessels were periodically quenched with 1:1 H_2O-THF at intervals chosen to ensure an adequate sampling of each of the first three half-lives. The quenched aliquots were extracted into Et_2O and the extracts analyzed using GC. The reactions were monitored by following the decrease of substrates **1** or **4** and the formation of products **2** and **3** or **5** and **7** (eqs 2 and 3) relative to the internal decane standard. Following the formation of the corresponding products afforded equivalent rate constants within $\pm$ 10%. Rate constants were determined using non-linear least-squares fits. The reported errors correspond to one standard deviation. The observed rate constants were shown to be reproducible within $\pm$ 10%.

APPENDIX IV

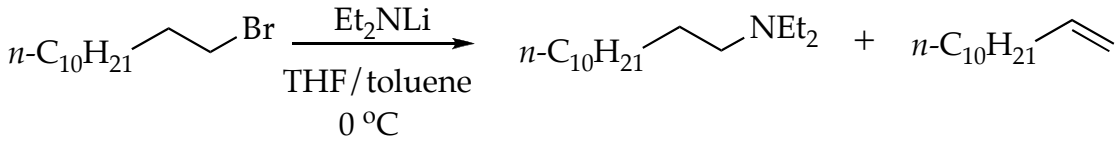

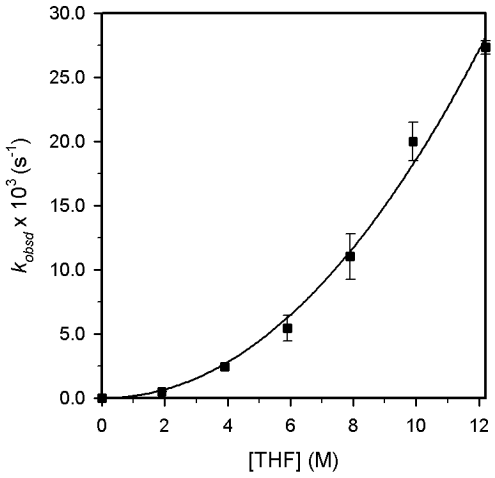

Figure AIV.1. Plot of k_{obsd} vs [THF] in toluene cosolvent for the reaction of **1** (0.004 M) with Et_2NLi (0.10 M) at 0 °C. The curve depicts an unweighted least-squares fit to $k_{obsd} = k[THF]^n$ ($k = (1.6 \pm 0.4) \times 10^{-4}$, $n = 2.0 \pm 0.1$).

[THF] (M)	$k_{obsd}1 \times 10^3$ (s^{-1})	$k_{obsd}2 \times 10^3$ (s^{-1})	$k_{obsd}avg \times 10^3$ (s^{-1})
1.9	0.466 ± 8E-3	0.47 ± 1E-2	0.468 ± 3E-3
3.9	2.24 ± 2E-2	2.61 ± 2E-2	2.4 ± 3E-1
5.9	4.7 ± 6E-1	6.1 ± 3E-1	5.4 ± 9E-1
7.9	9.77 ± 7E-2	12.3 ± 3E-1	11 ± 2
9.9	18.9 ± 9E-1	21.1 ± 3E-1	20 ± 2
12.2	26.9 ± 1E-1	27.7 ± 4E-1	27.3 ± 5E-1

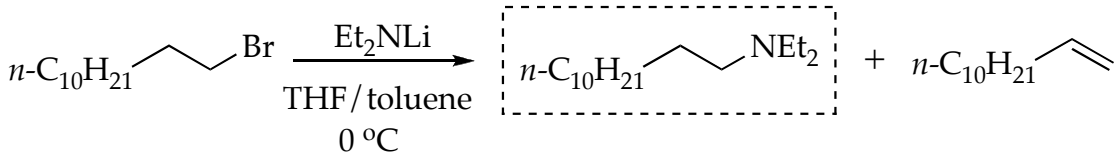

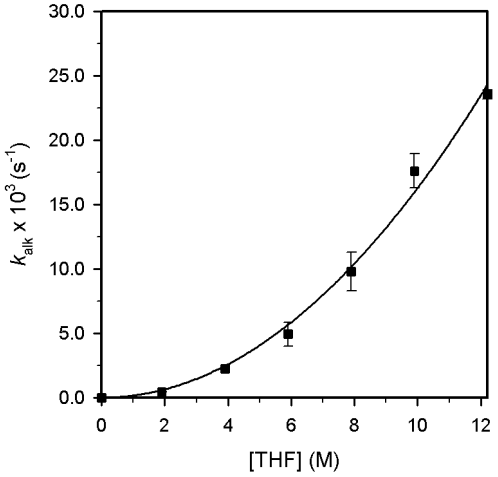

Figure AIV.2. Plot of k_{alk} vs [THF] in toluene cosolvent for the N-alkylation of **1** (0.004 M) with Et_2NLi (0.10 M) at 0 °C. The curve depicts an unweighted least-squares fit to $k_{alk} = k[THF]^n$ ($k = (1.6 \pm 0.4) \times 10^{-4}$, $n = 2.0 \pm 0.1$).

[THF] (M)	$k_{alk}1 \times 10^3$ (s^{-1})	$k_{alk}2 \times 10^3$ (s^{-1})	k_{alk}avg $\times 10^3$ (s^{-1})
1.9	0.430 ± 4E-3	0.441 ± 4E-3	0.435 ± 8E-3
3.9	2.062 ± 4E-3	2.41 ± 2E-2	2.2 ± 2E-1
5.9	4.274 ± 9E-3	5.56 ± 4E-2	4.9 ± 9E-1
7.9	8.72 ± 1E-2	10.87 ± 5E-2	10 ± 2
9.9	16.67 ± 5E-2	18.54 ± 8E-2	18 ± 1
12.2	23.3 ± 4E-1	23.8 ± 8E-1	23.5 ± 4E-1

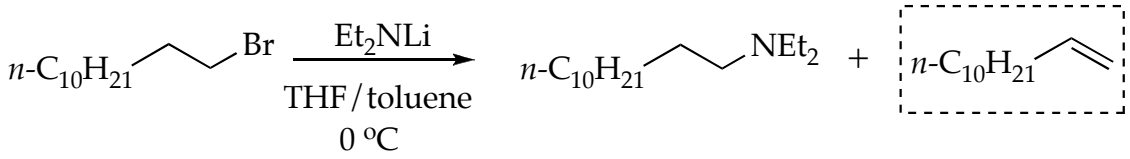

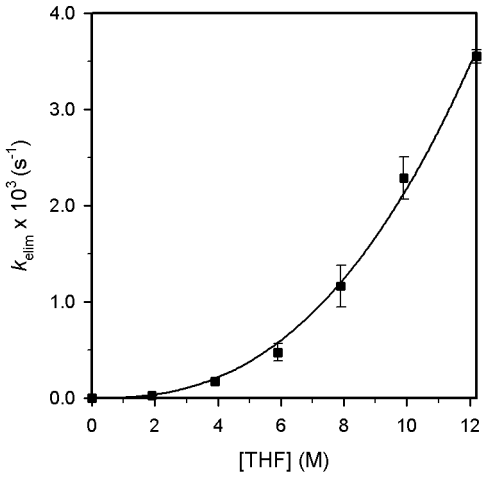

Figure AIV.3. Plot of k_{elim} vs [THF] in toluene cosolvent for the elimination of **1** (0.004 M) with Et_2NLi (0.10 M) at 0 °C. The curve depicts an unweighted least-squares fit to $k_{elim} = k[THF]^n$ ($k = (6 \pm 2) \times 10^{-6}$, $n = 2.5 \pm 0.1$).

[THF] (M)	$k_{elim}1 \times 10^3$ (s^{-1})	$k_{elim}2 \times 10^3$ (s^{-1})	k_{elim}avg $\times 10^3$ (s^{-1})
1.9	0.026 ± 1E-3	0.027 ± 1E-3	0.0265 ± 7E-4
3.9	0.162 ± 8E-3	0.184 ± 9E-3	0.17 ± 2E-2
5.9	0.41 ± 1E-2	0.54 ± 3E-2	0.47 ± 9E-2
7.9	1.01 ± 1E-2	1.313 ± 5E-3	1.2 ± 2E-1
9.9	2.13 ± 8E-2	2.44 ± 9E-2	2.3 ± 2E-1
12.2	3.6 ± 3E-1	3.5 ± 2E-1	3.55 ± 7E-2

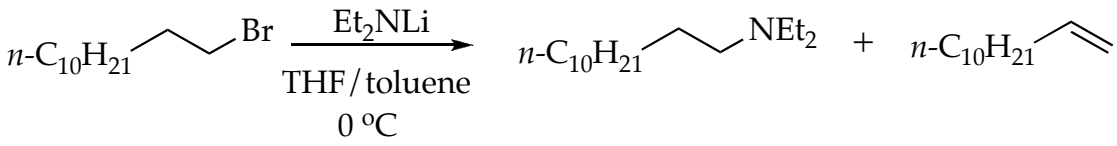

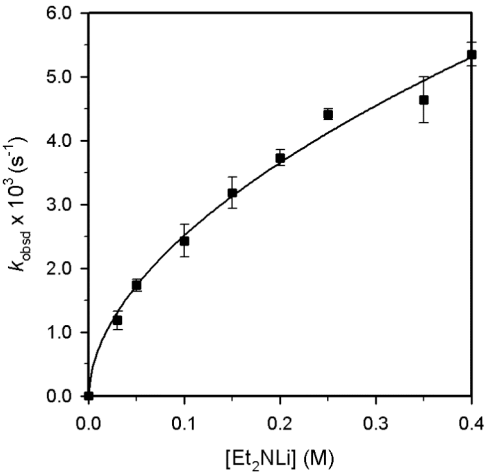

Figure AIV.4. Plot of k_{obsd} vs [Et_2NLi] in THF (3.9 M) and toluene cosolvent for the reaction of **1** (0.004 M) with Et_2NLi at 0 °C. The curve depicts an unweighted least-squares fit to $k_{obsd} = k[Et_2NLi]^n$ ($k = (8.7 \pm 0.4) \times 10^{-3}$, $n = 0.54 \pm 0.03$).

[Et_2NLi] (M)	$k_{obsd}1 \times 10^3$ (s^{-1})	$k_{obsd}2 \times 10^3$ (s^{-1})	$k_{obsd}avg \times 10^3$ (s^{-1})
0.03	1.28 ± 6E-2	1.08 ± 5E-2	1.2 ± 1E-1
0.05	1.67 ± 3E-2	1.80 ± 1E-2	1.74 ± 9E-2
0.10	2.24 ± 2E-2	2.61 ± 2E-2	2.4 ± 3E-1
0.15	3.36 ± 6E-2	3.01 ± 7E-2	3.2 ± 2E-1
0.20	3.83 ± 8E-2	3.64 ± 8E-2	3.7 ± 1E-1
0.25	4.35 ± 7E-2	4.47 ± 8E-2	4.41 ± 8E-2
0.35	4.4 ± 3E-1	4.9 ± 1E-1	4.6 ± 3E-1
0.40	5.2 ± 1E-1	5.5 ± 2E-1	5.3 ± 2E-1

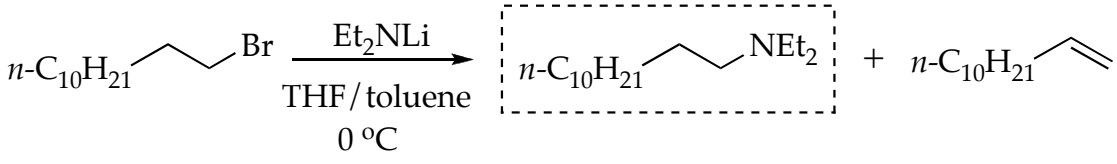

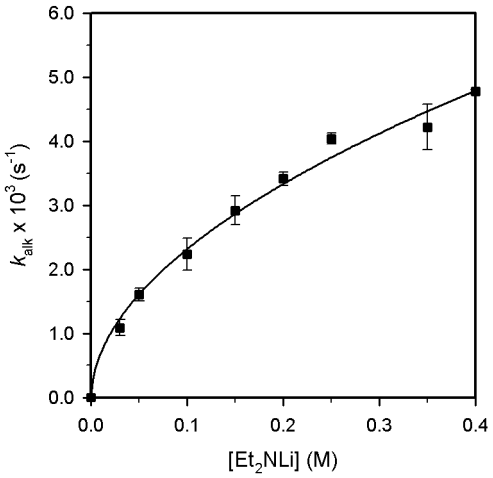

Figure AIV.5. Plot of k_{alk} vs [Et_2NLi] in THF (3.9 M) and toluene cosolvent for the N-alkylation of **1** (0.004 M) with Et_2NLi at 0 °C. The curve depicts an unweighted least-squares fit to $k_{alk} = k[Et_2NLi]^n$ ($k = (7.7 \pm 0.3) \times 10^{-3}$, $n = 0.52 \pm 0.03$).

[Et_2NLi] (M)	$k_{alk}1 \times 10^3$ (s^{-1})	$k_{alk}2 \times 10^3$ (s^{-1})	$k_{alk}avg \times 10^3$ (s^{-1})
0.03	1.177 ± 5E-3	0.999 ± 5E-3	1.1 ± 1E-1
0.05	1.536 ± 8E-3	1.680 ± 9E-3	1.6 ± 1E-1
0.10	2.062 ± 4E-3	2.41 ± 2E-2	2.2 ± 2E-1
0.15	3.08± 2E-2	2.76 ± 3E-2	2.9 ± 2E-1
0.20	3.49 ± 2E-2	3.34 ± 1E-2	3.4 ± 1E-1
0.25	3.98 ± 2E-2	4.10 ± 2E-2	4.04 ± 8E-2
0.35	3.97 ± 3E-2	4.47 ± 2E-2	4.2 ± 4E-1
0.40	4.75 ± 3E-2	4.8 ± 4E-1	4.77 ± 4E-2

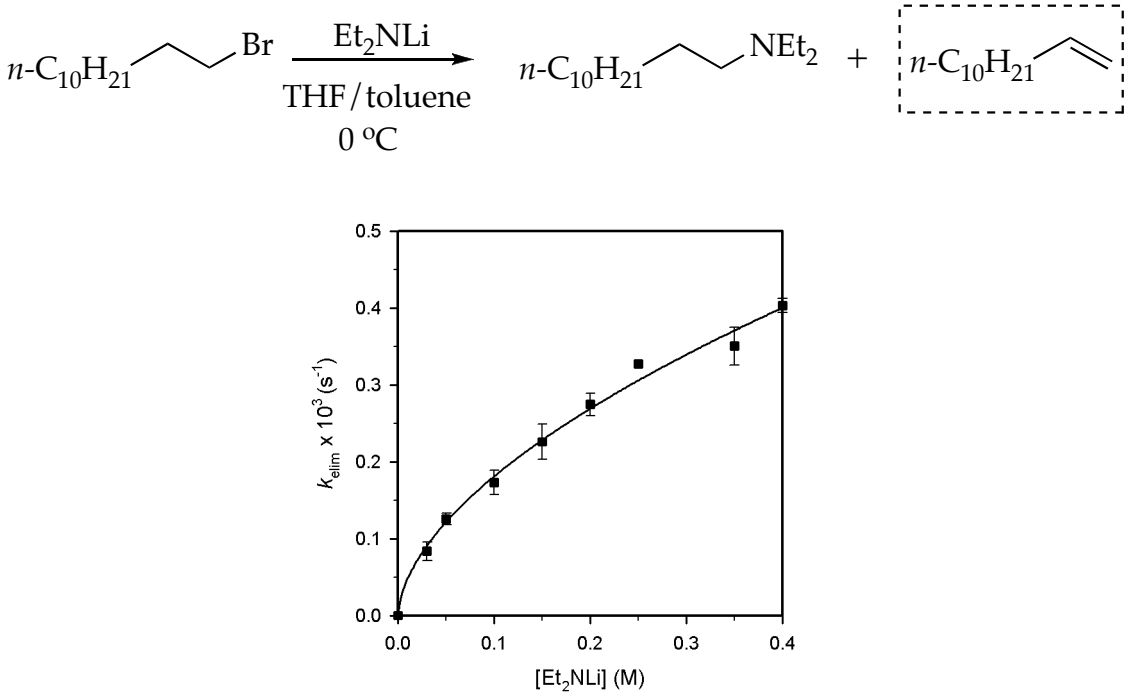

Figure AIV.6. Plot of k_{elim} vs [Et_2NLi] in THF (3.9 M) and toluene cosolvent for the elimination of **1** with Et_2NLi (0.004 M) at 0 °C. The curve depicts an unweighted least-squares fit to $k_{elim} = k[Et_2NLi]^n$ ($k = (6.8 \pm 0.3) \times 10^{-4}$, $n = 0.57 \pm 0.03$).

[Et_2NLi] (M)	$k_{elim}1 \times 10^3$ (s^{-1})	$k_{elim}2 \times 10^3$ (s^{-1})	k_{elim}avg $\times 10^3$ (s^{-1})
0.03	0.092 ± 2E-3	0.075 ± 4E-3	0.08 ± 1E-2
0.05	0.120 ± 1E-3	0.131 ± 2E-3	0.125 ± 8E-3
0.10	0.162 ± 8E-3	0.184 ± 9E-3	0.17 ± 2E-2
0.15	0.242 ± 8E-3	0.21 ± 1E-2	0.23 ± 2E-2
0.20	0.285 ± 1E-3	0.264 ± 6E-3	0.27 ± 1E-2
0.25	0.325 ± 3E-3	0.33 ± 1E-2	0.327 ± 3E-3
0.35	0.333 ± 4E-3	0.368 ± 4E-3	0.35 ± 2E-2
0.40	0.397 ± 2E-3	0.41 ± 4E-2	0.403 ± 9E-3

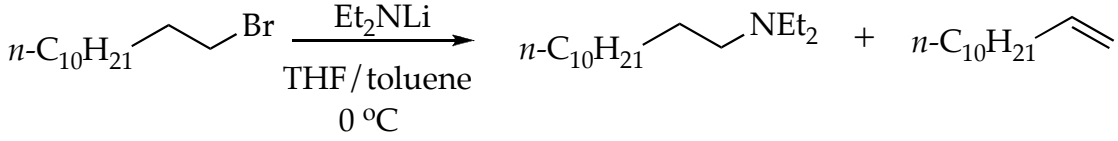

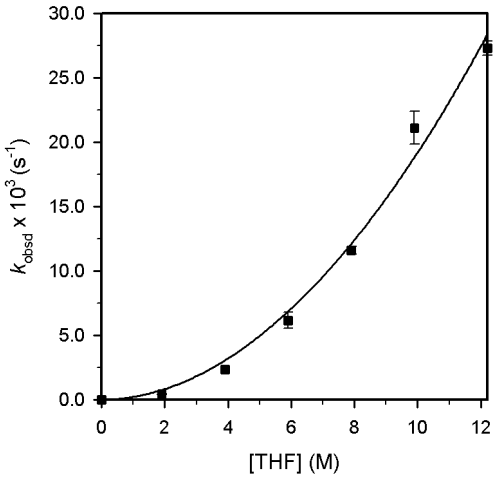

Figure AIV.7. Plot of k_{obsd} vs [THF] in 2,2,5,5-Me_4THF cosolvent for the reaction of **1** (0.004 M) with Et_2NLi (0.10 M) at 0 °C. The curve depicts an unweighted least-squares fit to $k_{obsd} = k[THF]^n$ ($k = (2.1 \pm 0.6) \times 10^{-4}$, $n = 1.9 \pm 0.1$).

[THF] (M)	$k_{obsd}1 \times 10^3$ (s^{-1})	$k_{obsd}2 \times 10^3$ (s^{-1})	k_{obsd}avg $\times 10^3$ (s^{-1})
1.9	0.39 ± 2E-2	0.44 ± 3E-2	0.41 ± 4E-2
3.9	2.4 ± 1E-1	2.3 ± 2E-1	2.35 ± 7E-2
5.9	5.7 ± 2E-1	6.6 ± 2E-1	6.1 ± 6E-1
7.9	11.8 ± 5E-1	11.4 ± 4E-1	11.6 ± 3E-1
9.9	22 ± 2	20.2 ± 4E-1	21 ± 1
12.2	26.9 ± 1E-1	27.7 ± 4E-1	27.3 ± 5E-1

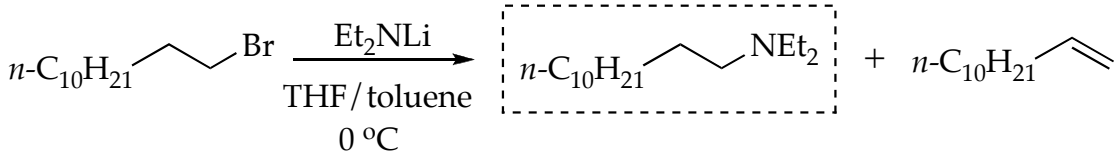

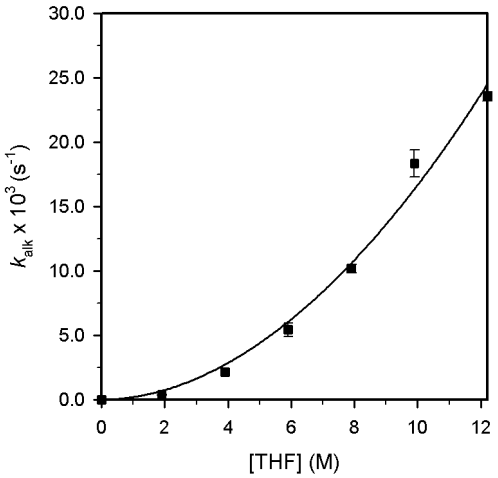

Figure AIV.8. Plot of k_{alk} vs [THF] in 2,2,5,5-tetramethyltetrahydrofuran cosolvent for the N-alkylation of **1** (0.004 M) with Et_2NLi (0.10 M) at 0 °C. The curve depicts an unweighted least-squares fit to $k_{alk} = k[THF]^n$ ($k = (2.0 \pm 0.5) \times 10^{-4}$, $n = 1.9 \pm 0.1$).

[THF] (M)	$k_{alk}1 \times 10^3$ (s^{-1})	$k_{alk}2 \times 10^3$ (s^{-1})	$k_{alk}avg \times 10^3$ (s^{-1})
1.9	0.356 ± 6E-3	0.395 ± 5E-3	0.38 ± 3E-2
3.9	2.18 ± 5E-2	2.10 ± 1E-2	2.14 ± 6E-2
5.9	5.05 ± 8E-2	5.81 ± 5E-2	5.4 ± 5E-1
7.9	10.4 ± 1E-1	9.93 ± 4E-2	10.2 ± 3E-1
9.9	19.1 ± 3E-1	17.6 ± 1E-1	18 ± 1
12.2	23.3 ± 4E-1	23.8 ± 8E-1	23.5 ± 4E-1

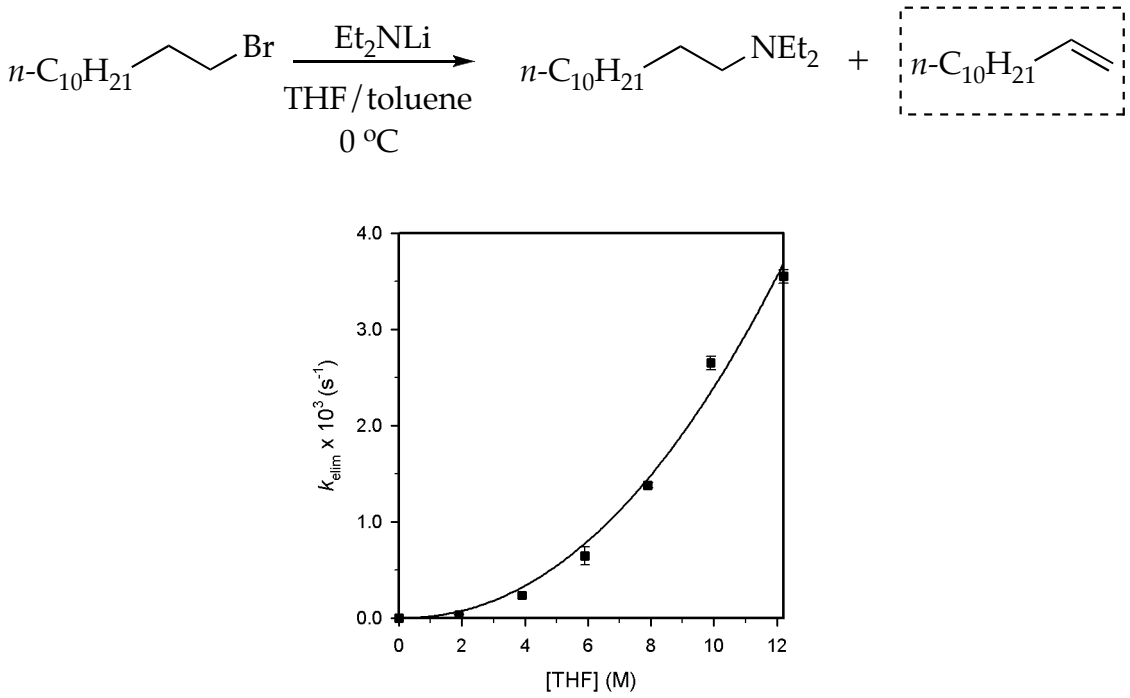

Figure AIV.9. Plot of k_{elim} vs [THF] in 2,2,5,5-tetramethyltetrahydrofuran cosolvent for the elimination of **1** (0.004 M) with Et_2NLi (0.10 M) at 0 °C. The curve depicts an unweighted least-squares fit to $k_{elim} = k[THF]^n$ ($k = (1.7 \pm 0.5) \times 10^{-5}$, $n = 2.1 \pm 0.1$).

[THF] (M)	$k_{elim}1 \times 10^3$ (s^{-1})	$k_{elim}2 \times 10^3$ (s^{-1})	$k_{elim}avg \times 10^3$ (s^{-1})
1.9	0.033 ± 4E-3	0.036 ± 4E-3	0.034 ± 2E-3
3.9	0.23 ± 3E-2	0.24 ± 1E-2	0.235 ± 7E-3
5.9	0.58 ± 8E-2	0.71 ± 5E-2	0.64 ± 9E-2
7.9	1.4 ± 1E-1	1.36 ± 5E-2	1.38 ± 3E-2
9.9	2.7 ± 3E-1	2.6 ± 1E-1	2.65 ± 7E-2
12.2	3.6 ± 3E-1	3.5 ± 2E-1	3.55 ± 7E-2

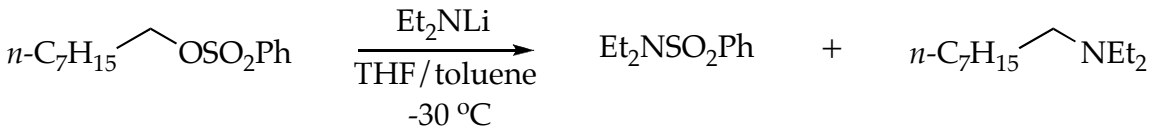

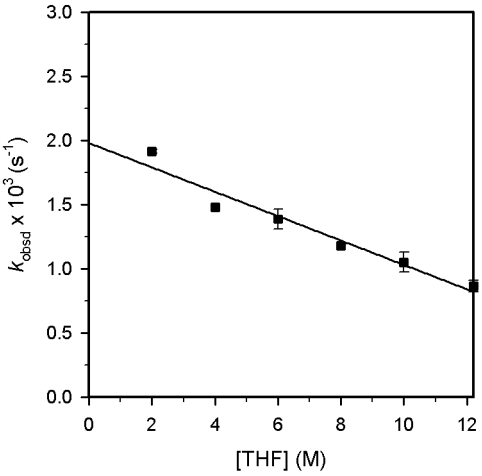

Figure AIV.10. Plot of k_{obsd} vs [THF] in toluene cosolvent for the reaction of **4** (0.004 M) with Et_2NLi (0.10 M) at -30 °C. The curve depicts an unweighted least-squares fit to $k_{obsd} = c[THF] + k'$ ($c = (-9.5 \pm 0.8) \times 10^{-5}$, $k' = (1.98 \pm 0.06) \times 10^{-3}$).

[THF] (M)	$k_{obsd}1 \times 10^3$ (s^{-1})	$k_{obsd}2 \times 10^3$ (s^{-1})	$k_{obsd}avg \times 10^3$ (s^{-1})
2.0	1.90 ± 2E-2	1.93 ± 5E-2	1.92 ± 2E-2
4.0	1.5 ± 2E-1	1.47 ± 2E-2	1.49 ± 2E-2
6.0	1.44 ± 4E-2	1.31 ± 5E-2	1.38 ± 9E-2
8.0	1.17 ± 4E-2	1.18 ± 3E-2	1.175 ± 7E-3
10.0	1.10 ± 2E-2	0.99 ± 2E-2	1.05 ± 8E-2
12.2	0.90 ± 3E-2	0.83 ± 2E-2	0.87 ± 5E-2

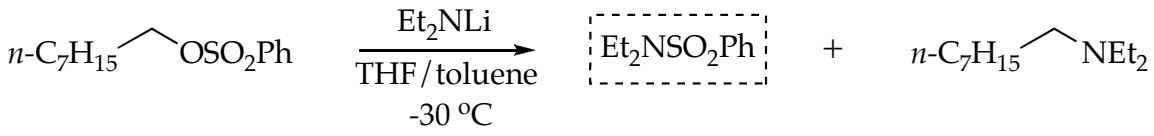

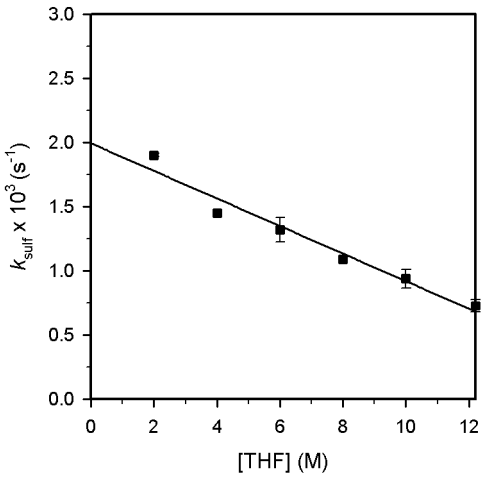

Figure AIV.11. Plot of k_{sulf} vs [THF] in toluene cosolvent for the N-sulfonation of **4** (0.004 M) with Et_2NLi (0.10 M) at -30 °C. The curve depicts an unweighted least-squares fit to $k_{obsd} = c[THF] + k'$ (c = (-1.07 ± 0.08) x 10^{-4}, k' = (1.99 ± 0.06) x 10^{-3}).

[THF] (M)	$k_{sulf}1$ x 10^3 (s^{-1})	$k_{sulf}2$ x 10^3 (s^{-1})	k_{sulf}avg x 10^3 (s^{-1})
2.0	1.892 ± 1E-3	1.9093 ± 8E-4	1.90 ± 1E-2
4.0	1.458 ± 1E-3	1.442 ± 2E-3	1.455 ± 4E-3
6.0	1.388 ± 4E-3	1.253 ± 3E-3	1.32 ± 9E-2
8.0	1.095 ± 8E-3	1.08 ± 4E-2	1.09 ± 1E-2
10.0	0.99 ± 1E-2	0.886 ± 8E-3	0.94 ± 7E-2
12.2	0.76 ± 1E-2	0.69 ± 1E-2	0.73 ± 5E-2

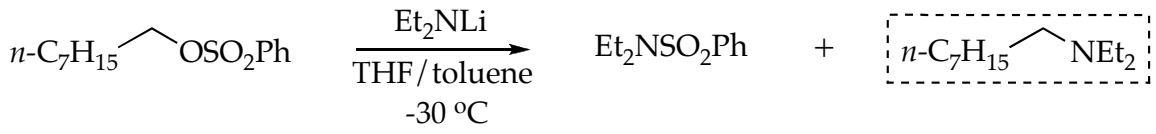

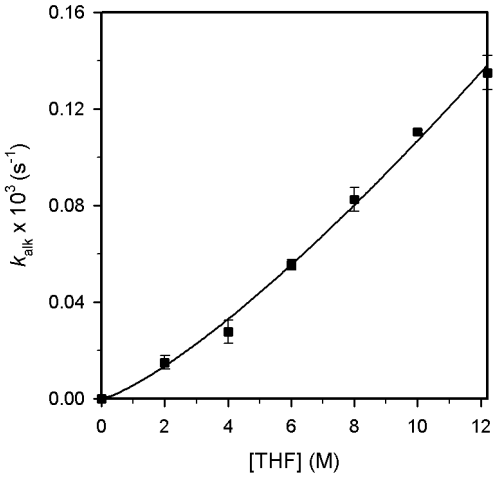

Figure AIV.12. Plot of k_{alk} vs [THF] in toluene cosolvent for the N-alkylation of **4** (0.004 M) with Et_2NLi (0.10 M) at -30 °C. The curve depicts an unweighted least-squares fit to $k_{alk} = k[THF]^n$ ($k = (5.5 \pm 0.7) \times 10^{-6}$, $n = 1.29 \pm 0.05$).

[THF] (M)	$k_{alk}1 \times 10^3$ (s^{-1})	$k_{alk}2 \times 10^3$ (s^{-1})	$k_{alk}avg \times 10^3$ (s^{-1})
2.0	0.013 ± 1E-3	0.017 ± 1E-3	0.015 ± 3E-3
4.0	0.0243 ± 7E-4	0.031 ± 3E-3	0.028 ± 5E-3
6.0	0.054 ± 4E-3	0.057 ± 3E-3	0.055 ± 2E-3
8.0	0.079 ± 8E-3	0.086 ± 5E-3	0.083 ± 5E-3
10.0	0.11 ± 1E-2	0.111 ± 8E-3	0.1105 ± 7E-4
12.2	0.13 ± 1E-2	0.14 ± 1E-2	0.135 ± 7E-3

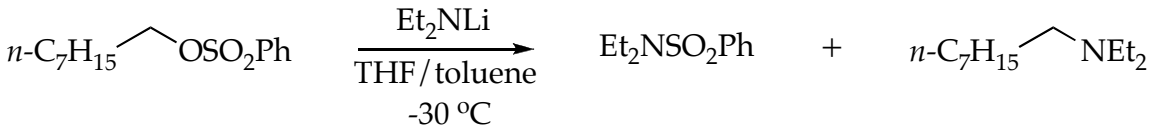

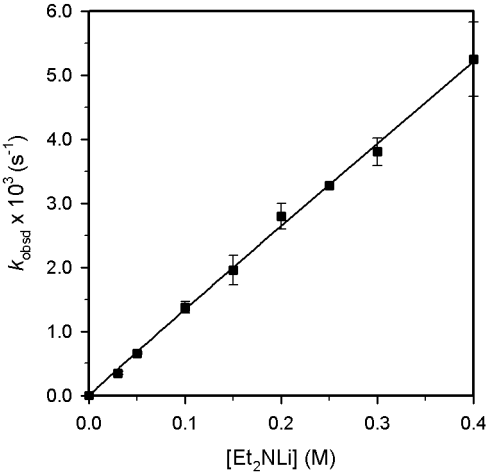

Figure AIV.13. Plot of k_{obsd} vs [Et_2NLi] in THF (6.0 M) and toluene cosolvent for the reaction of **4** (0.004 M) with Et_2NLi at -30 °C. The curve depicts an unweighted least-squares fit to $k_{obsd} = k[Et_2NLi]^n$ ($k = (1.28 \pm 0.07) \times 10^{-2}$, $n = 0.98 \pm 0.04$).

[Et_2NLi] (M)	$k_{obsd}1 \times 10^3$ (s^{-1})	$k_{obsd}2 \times 10^3$ (s^{-1})	$k_{obsd}avg \times 10^3$ (s^{-1})
0.03	0.329 ± 6E-3	0.364 ± 7E-3	0.35 ± 2E-2
0.05	0.667 ± 9E-3	0.65 ± 2E-2	0.66 ± 1E-2
0.10	1.44 ± 4E-2	1.31 ± 5E-2	1.38 ± 9E-2
0.15	2.12 ± 6E-2	1.79 ± 7E-2	2.0 ± 2E-1
0.20	2.94 ± 6E-2	2.66 ± 3E-2	2.8 ± 2E-1
0.25	3.27 ± 6E-2	3.29 ± 7E-2	3.28 ± 1E-2
0.35	3.95 ± 5E-2	3.7 ± 1E-1	3.8 ± 2E-1
0.40	5.7 ± 1E-1	4.84 ± 9E-2	5.3 ± 6E-1

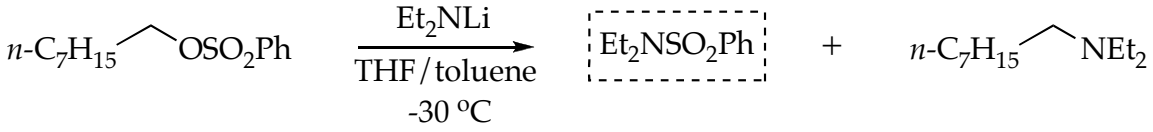

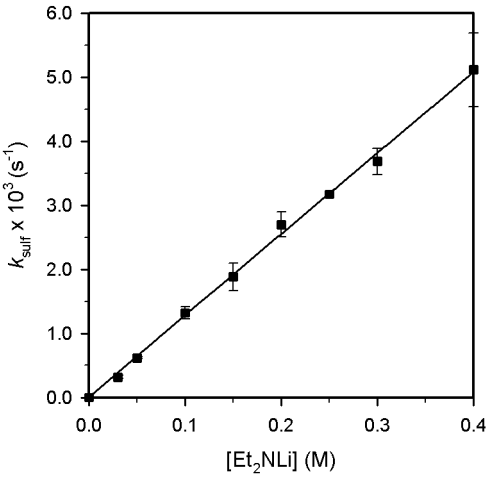

Figure AIV.14. Plot of k_{sulf} vs [Et_2NLi] in THF (6.0 M) and toluene cosolvent for the N-sulfonation of **4** (0.004 M) with Et_2NLi at -30 °C. The curve depicts an unweighted least-squares fit to $k_{sulf} = k[Et_2NLi]^n$ ($k = (1.26 \pm 0.07) \times 10^{-2}$, $n = 0.99 \pm 0.04$).

[Et_2NLi] (M)	$k_{sulf}1 \times 10^3$ (s^{-1})	$k_{sulf}2 \times 10^3$ (s^{-1})	$k_{sulf}avg \times 10^3$ (s^{-1})
0.03	0.303 ± 6E-3	0.336 ± 2E-3	0.32 ± 2E-2
0.05	0.628 ± 2E-3	0.610 ± 3E-3	0.62 ± 1E-2
0.10	1.388 ± 4E-3	1.253 ± 3E-3	1.3 ± 1E-1
0.15	1.728 ± 3E-3	2.036 ± 6E-3	1.9 ± 2E-1
0.20	2.838 ± 7E-3	2.561 ± 9E-3	2.7 ± 2E-1
0.25	3.163 ± 7E-3	3.18 ± 1E-2	3.17 ± 1E-2
0.35	3.83 ± 1E-2	3.54 ± 2E-2	3.7 ± 2E-1
0.40	5.521 ± 5E-3	4.71 ± 1E-2	5.1 ± 6E-1

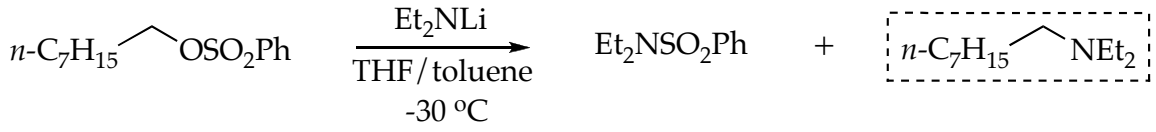

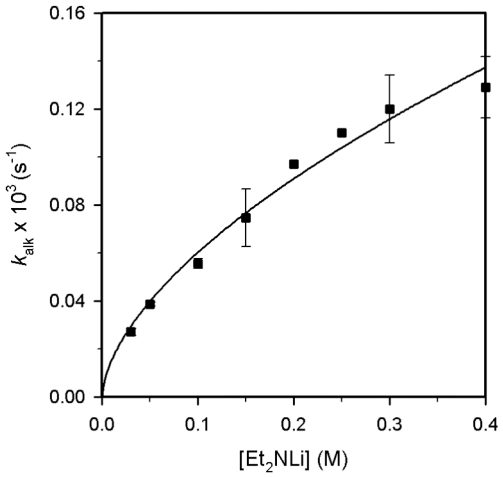

Figure AIV.15. Plot of k_{alk} vs [Et_2NLi] in THF (6.0 M) and toluene cosolvent for the N-alkylation of **4** (0.004 M) with Et_2NLi at -30 °C. The curve depicts an unweighted least-squares fit to $k_{alk} = k[Et_2NLi]^n$ ($k = (2.4 \pm 0.1) \times 10^{-4}$, $n = 0.59 \pm 0.04$).

[Et_2NLi] (M)	$k_{alk}1 \times 10^3$ (s^{-1})	$k_{alk}2 \times 10^3$ (s^{-1})	k_{alk}avg $\times 10^3$ (s^{-1})
0.03	0.026 ± 2E-3	0.028 ± 2E-3	0.027 ± 1E-3
0.05	0.039 ± 2E-3	0.038 ± 3E-3	0.0385 ± 7E-4
0.10	0.054 ± 4E-3	0.057 ± 3E-3	0.055 ± 2E-3
0.15	0.083 ± 6E-3	0.066 ± 3E-3	0.07 ± 1E-2
0.20	0.098 ± 7E-3	0.096 ± 8E-3	0.097 ± 1E-3
0.25	0.110 ± 7E-3	0.11 ± 1E-2	0.11 ± 0
0.35	0.13 ± 1E-2	0.11 ± 2E-2	0.12 ± 1E-2
0.40	0.138 ± 5E-3	0.12 ± 1E-2	0.13 ± 1E-20.40

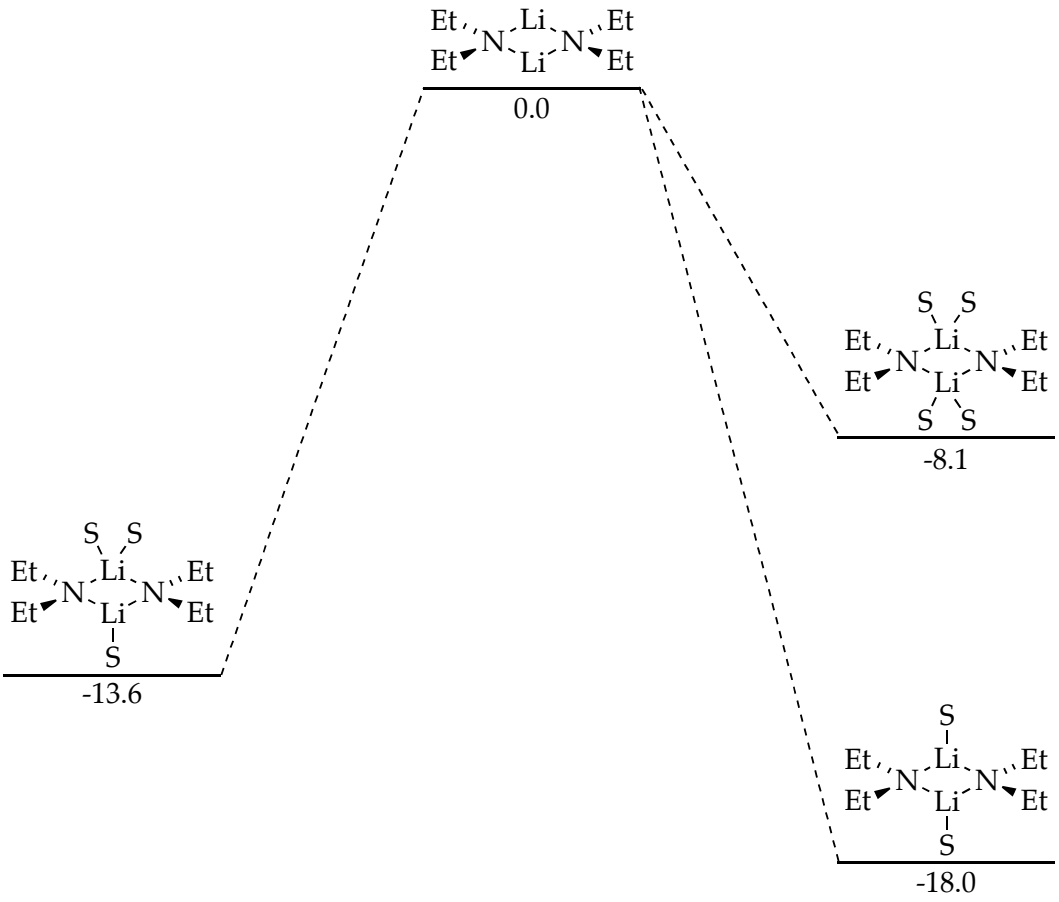

Figure AIV.16. Relative free energies for the solvation (ΔG, kcal/mol) of Et_2NLi with THF (S = THF) calculated using B3LYP level of theory with 6-31G(d) basis set at -90 °C.

Table AIV.1. Optimized geometries at B3LYP level of theory with 6-31G(d) basis set for the serial solvation of Et_2NLi with THF with free energies (*G*, Hartrees) and cartesian coordinates (X, Y, Z) at -90 °C.

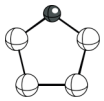

G = -232.347930
(-90 °C)

Atom	X	Y	Z	Atom	X	Y	Z
C	1.13237	-0.69946	0.08092	H	-1.16402	1.14915	-1.08500
O	0.00023	-1.43271	-0.37154	H	-1.20089	1.42136	0.65927
C	-1.13196	-0.69994	0.08150	H	-1.99944	-1.03696	-0.49266
C	-0.77738	0.78865	-0.12699	H	-1.31932	-0.90804	1.14890
C	0.77682	0.78920	-0.12622	H	1.32083	-0.90816	1.14799
H	1.19899	1.42114	0.66137	H	1.99953	-1.03559	-0.49425
H	1.16423	1.15136	-1.08328				

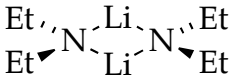

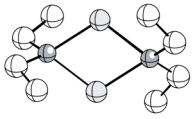

G = -441.267084
(-90 °C)
S = THF

Atom	X	Y	Z	Atom	X	Y	Z
N	-1.61287	0.00001	-0.00000	H	3.02647	1.56976	0.33251
C	-2.46755	1.07535	0.48941	H	0.90588	-2.60145	0.63673
C	-1.69571	2.15553	1.25365	H	2.35926	-2.96537	1.57759
Li	0.00000	0.00004	1.12061	H	1.22889	-1.75324	2.16919
Li	-0.00000	-0.00005	-1.12062	H	3.02634	-1.56989	-0.33256
N	1.61287	-0.00001	-0.00000	H	3.25304	-0.68494	1.16895
C	2.46753	-1.07538	0.48941	H	-0.90596	2.60150	0.63662
C	1.69568	-2.15550	1.25371	H	-2.35931	2.96537	1.57755
C	2.46757	1.07532	-0.48944	H	-1.22885	1.75331	2.16911
C	1.69574	2.15552	-1.25364	H	-3.25302	0.68491	1.16900
C	-2.46754	-1.07536	-0.48940	H	-3.02641	1.56983	-0.33255
C	-1.69571	-2.15549	-1.25370	H	-0.90591	-2.60145	-0.63672
H	0.90603	2.60152	-0.63657	H	-2.35930	-2.96536	-1.57756
H	2.35936	2.96534	-1.57756	H	-1.22893	-1.75325	-2.16919
H	1.22882	1.75333	-2.16909	H	-3.02635	-1.56986	0.33258
H	3.25301	0.68486	-1.16906	H	-3.25306	-0.68492	-1.16894

Table AIV.1 (Continued).

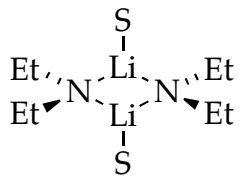

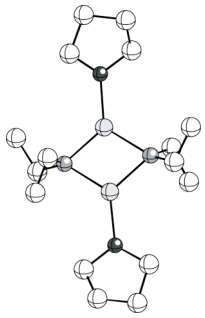

G = -905.991622
(-90 °C)
S = THF

Atom	X	Y	Z	Atom	X	Y	Z
Li	-1.18777	0.06068	0.28533	H	-4.31804	-1.26059	1.37174
O	-3.13515	0.09835	0.32686	H	1.63650	-2.33786	2.35094
C	-3.93036	-1.10699	0.35496	H	0.70633	-3.78915	2.78884
C	-5.05997	-0.85054	-0.63873	H	1.52137	-3.69860	1.21942
C	-5.33666	0.64549	-0.41423	H	-0.79856	-1.90558	2.14451
C	-3.93586	1.21372	-0.14016	H	-0.99553	-3.29638	1.09158
N	-0.05931	-1.57116	0.21754	H	-1.71750	-2.10320	-2.01764
C	-0.29581	-2.47179	1.34046	H	-0.72328	-3.43569	-2.64814
C	0.96399	-3.11338	1.96112	H	-1.54100	-3.60366	-1.08680
Li	1.18894	-0.02177	0.30402	H	0.95375	-3.11012	-0.88752
N	0.06100	1.60870	0.21578	H	0.69058	-1.59355	-1.73619
C	-0.18840	2.34544	-1.01760	H	1.75857	2.14874	-1.98835
C	1.05745	2.94511	-1.70510	H	0.79061	3.50229	-2.61432
C	0.27921	2.49471	1.35429	H	1.58572	3.63743	-1.03801
C	-0.99155	3.12866	1.96027	H	-0.91802	3.17120	-0.88589
O	3.13588	-0.09082	0.36686	H	-0.65885	1.66261	-1.74909
C	3.89889	-1.24096	-0.08044	H	-1.67167	2.34810	2.32621
C	5.30425	-0.71593	-0.41239	H	-0.74959	3.79271	2.80212
C	5.05788	0.77933	-0.67445	H	-1.53460	3.72410	1.21608
C	3.96288	1.09306	0.34106	H	0.76763	1.91822	2.16005
C	0.21684	-2.29063	-1.02016	H	0.98351	3.32171	1.12792
C	-1.01112	-2.89521	-1.73530	H	4.38168	1.26361	1.34272
H	-3.92719	1.99626	0.62396	H	3.31840	1.93291	0.07409
H	-3.46236	1.60756	-1.04637	H	4.68567	0.93890	-1.69333
H	-5.98500	0.78352	0.45872	H	5.95164	1.39484	-0.53534
H	-5.81829	1.12910	-1.26910	H	5.97518	-0.84401	0.44487
H	-4.71156	-1.03135	-1.66249	H	5.74816	-1.23679	-1.26577
H	-5.93376	-1.48331	-0.45681	H	3.39120	-1.65621	-0.95786
H	-3.27104	-1.93688	0.09340	H	3.89409	-1.99491	0.71188

Table AIV.1 (Continued).

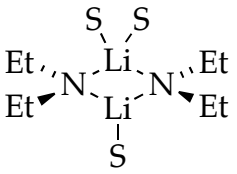

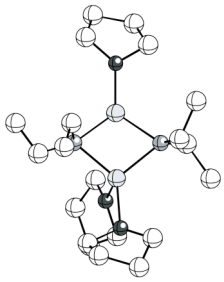

G = -1138.332641
(-90 °C)
S = THF

Atom	X	Y	Z	Atom	X	Y	Z
Li	-0.94920	-0.00381	-0.07959	H	-0.49163	-2.73601	-0.57884
N	0.27495	-0.98090	-1.39758	H	-0.78821	-2.61715	-2.30553
Li	1.37298	-0.54130	0.18531	H	1.87701	1.88838	2.49866
N	0.12940	-0.18560	1.66686	H	1.00022	2.24242	4.00533
C	0.37453	-1.46238	2.33171	H	1.79118	0.67317	3.78720
C	-0.86781	-2.18048	2.90219	H	-0.73663	0.60003	3.46325
C	-0.06307	0.88775	2.62904	H	-0.57707	1.72279	2.12749
C	1.22354	1.45633	3.26931	H	-1.56954	-2.42586	2.09554
O	3.32654	-0.45501	0.14205	H	-0.59457	-3.11439	3.41367
C	4.12112	-0.69095	-1.03189	H	-1.39329	-1.54797	3.62800
C	5.28241	0.30647	-0.91374	H	0.83139	-2.16738	1.60961
C	5.44457	0.50359	0.61987	H	1.11435	-1.38508	3.15656
C	4.25315	-0.27002	1.22485	H	4.56691	-1.25458	1.59989
C	-0.02991	-2.40140	-1.52332	H	3.72304	0.25949	2.01769
C	1.16969	-3.33821	-1.79342	H	5.40131	1.56407	0.88408
C	0.62749	-0.37252	-2.67061	H	6.39626	0.11091	0.99003
C	-0.52171	-0.19770	-3.68871	H	6.19210	-0.06949	-1.39113
O	-1.07618	2.03525	-0.49963	H	5.01933	1.25232	-1.39716
C	0.03218	2.94259	-0.49555	H	3.47540	-0.54530	-1.89872
C	-0.58786	4.34308	-0.31080	H	4.47962	-1.73070	-1.02373
C	-2.06273	4.15787	-0.76749	H	-3.04801	2.17224	-1.00884
C	-2.11547	2.69192	-1.23268	H	-1.91147	2.60964	-2.31116
O	-2.97519	-0.32433	-0.08058	H	-2.34729	4.84723	-1.56822
C	-3.59671	-1.33301	-0.91264	H	-2.74807	4.32028	0.06991
C	-4.92108	-1.68235	-0.22649	H	-0.54249	4.65395	0.73685
C	-4.59822	-1.42133	1.25322	H	-0.05752	5.09514	-0.90288
C	-3.69310	-0.19216	1.16746	H	0.56719	2.86732	-1.45403
H	-0.16985	0.29024	-4.60898	H	0.70060	2.63599	0.31095
H	-0.95794	-1.16142	-3.97658	H	-2.92457	-2.19602	-0.97161
H	-1.32388	0.41500	-3.25814	H	-3.71961	-0.92119	-1.91870
H	1.03444	0.63333	-2.46775	H	-5.72054	-1.01286	-0.56648
H	1.44391	-0.90812	-3.20473	H	-5.23404	-2.71138	-0.42743
H	1.90804	-3.26430	-0.98321	H	-4.04804	-2.26728	1.68076
H	0.84968	-4.38728	-1.86544	H	-5.48654	-1.24580	1.86771
H	1.67899	-3.08610	-2.73139	H	-4.28077	0.73645	1.14157
H	-2.95372	-0.12612	1.96877				

Table AIV.1 (Continued).

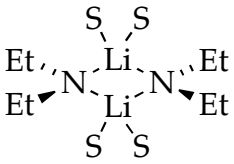

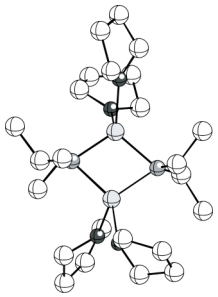

G = -1370.6717
(-90 °C)
S = THF

Table AIV.1 (Continued).

Atom	X	Y	Z	Atom	X	Y	Z
Li	-1.359791	-0.098372	0.191622	Li	1.138431	-0.194024	-0.042566
O	-3.217047	-1.210572	0.397360	N	0.037107	-0.170738	1.688633
C	-4.337971	-0.927040	-0.450352	C	-0.088212	-1.387553	2.476318
C	-4.434289	-2.127537	-1.401245	C	-1.246273	-1.439331	3.499506
C	-3.845975	-3.297413	-0.567524	H	-2.204576	-1.220749	3.012929
C	-3.301297	-2.611138	0.704314	H	-1.312779	-2.429280	3.972422
H	-3.983589	-2.752383	1.555471	H	-1.109531	-0.704846	4.302132
H	-2.304016	-2.940680	0.998088	H	-0.225856	-2.228521	1.774791
H	-3.044598	-3.797741	-1.116797	H	0.833746	-1.646670	3.045906
H	-4.600503	-4.049148	-0.315258	C	0.255029	0.999827	2.523543
H	-3.823416	-1.947162	-2.289408	C	1.504786	0.983202	3.434584
H	-5.463073	-2.311336	-1.726521	H	2.410430	0.763711	2.855003
H	-4.139309	0.026560	-0.940928	H	1.640298	1.950404	3.939317
H	-5.246707	-0.833579	0.166461	H	1.425212	0.219102	4.216693
O	-2.434710	1.706636	0.182689	H	-0.603112	1.236852	3.192893
C	-3.114418	2.082125	1.390392	H	0.339906	1.875191	1.856919
C	-3.922970	3.324036	0.997058	O	2.290044	1.575799	-0.527879
C	-3.034344	3.998238	-0.082291	C	2.469544	2.110300	-1.854368
C	-1.963875	2.927875	-0.406336	C	3.810777	2.841882	-1.819539
H	-0.992205	3.191025	0.034471	C	3.815250	3.405044	-0.390124
H	-1.826840	2.741067	-1.472752	C	3.133601	2.284795	0.407258
H	-2.567482	4.916054	0.288465	H	2.514708	2.654083	1.228943
H	-3.619406	4.263335	-0.967757	H	3.861345	1.573815	0.817222
H	-4.887028	3.027767	0.570869	H	3.221214	4.325566	-0.345579
H	-4.121705	3.976694	1.852548	H	4.816952	3.634131	-0.014057
H	-3.712401	1.225919	1.706508	H	4.638886	2.135838	-1.959276
H	-2.377138	2.309426	2.172402	H	3.889903	3.613324	-2.591678
N	-0.275394	-0.576863	-1.474904	H	2.423642	1.279050	-2.561099
C	-0.370517	-2.002519	-1.756768	H	1.648435	2.803244	-2.083596
C	0.767824	-2.623767	-2.598026	O	2.914938	-1.363211	0.099491
H	1.736406	-2.444717	-2.116599	C	2.995366	-2.591651	0.836347
H	0.630858	-3.708692	-2.711096	C	4.479383	-2.730050	1.225181
H	0.812280	-2.194049	-3.605935	C	5.221562	-1.871666	0.162513
H	-0.384637	-2.535881	-0.790636	C	4.084236	-1.327604	-0.723580
H	-1.321498	-2.293238	-2.256459	H	4.221114	-0.296003	-1.051552
C	-0.377995	0.232500	-2.676346	H	3.931947	-1.964057	-1.608263
C	-1.725832	0.196124	-3.434224	H	5.767863	-1.052265	0.639909
H	-2.550328	0.491711	-2.772104	H	5.942054	-2.452686	-0.421341
H	-1.715138	0.878509	-4.296330	H	4.652969	-2.335304	2.230564
H	-1.952085	-0.805765	-3.818208	H	4.800894	-3.775956	1.219784
H	0.408233	0.008787	-3.432593	H	2.674566	-3.422808	0.190486
H	-0.200494	1.281030	-2.390470	H	2.311550	-2.509559	1.680801

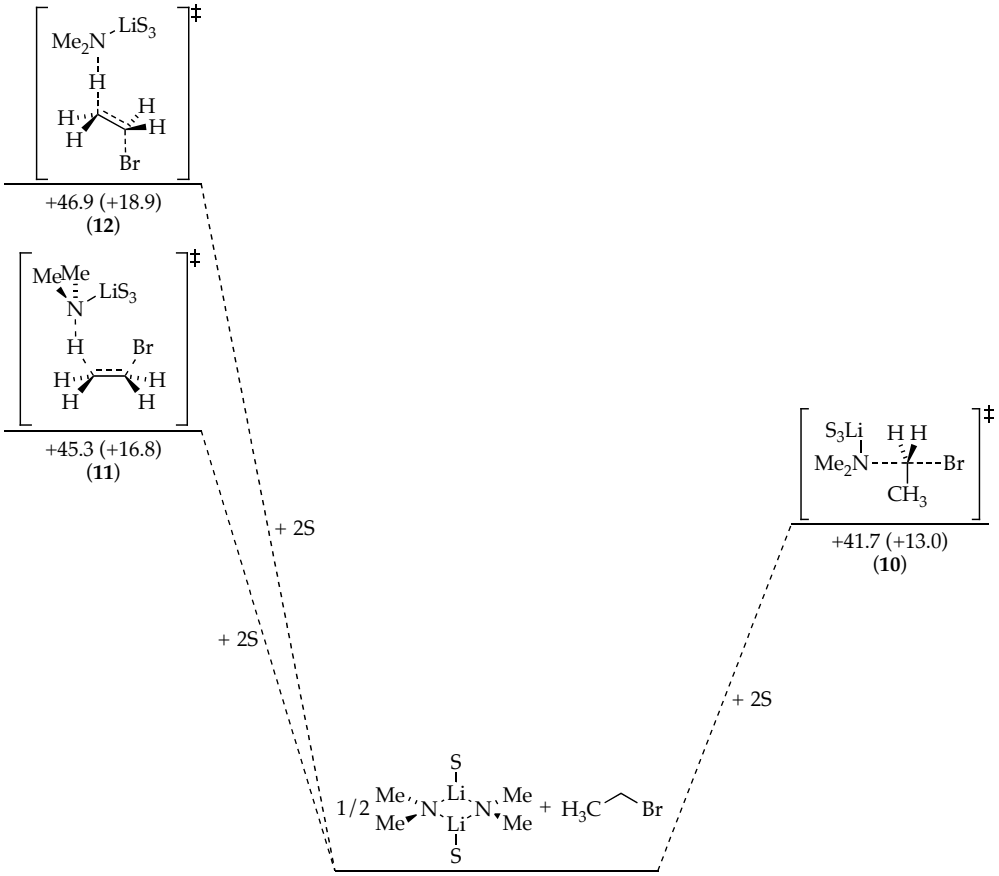

Figure AIV.17. Free energies of activation ($\Delta G^{\ddagger}$, kcal/mol) for the reaction of EtBr with Me_2NLi calculated using B3LYP level of theory with SVP basis set for Br and 6-31G(d) basis set for the rest of atoms at 25 °C (S = Me_2O). Values in parentheses correspond to the enthalpies of activation ($\Delta H^{\ddagger}$, kcal/mol).

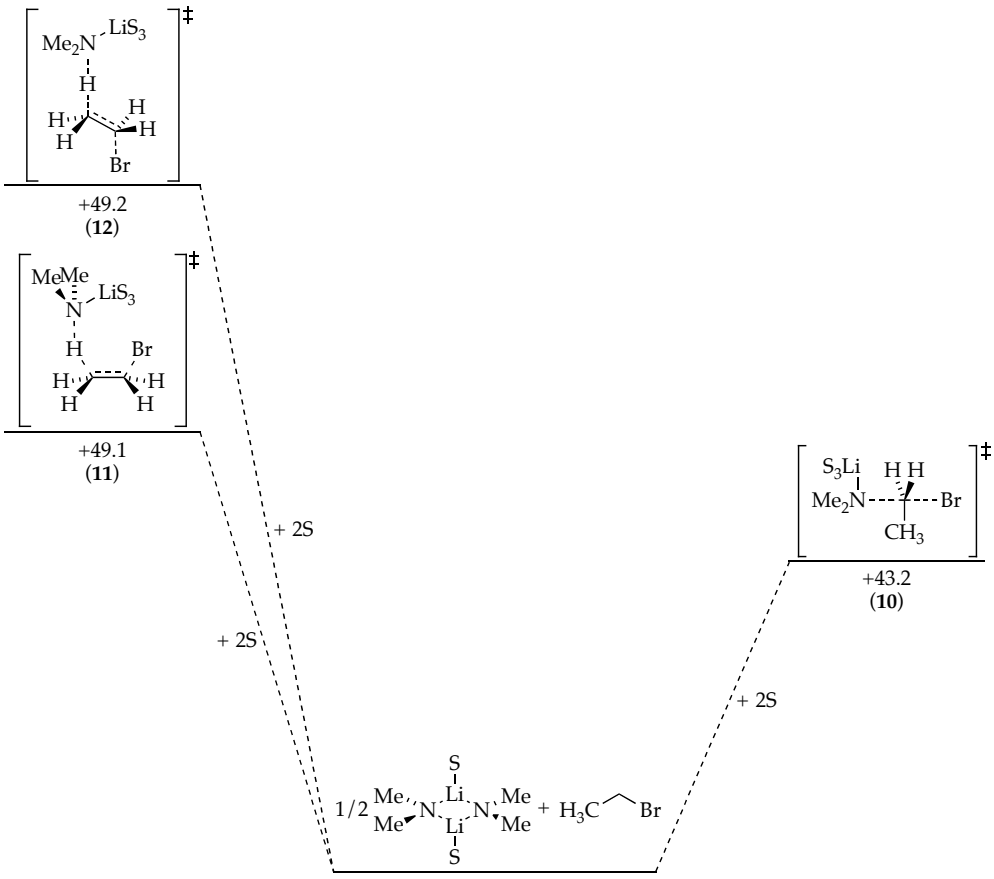

Figure AIV.18. Free energies of activation ($\Delta G^{\ddagger}$, kcal/mol) for the reaction of EtBr with Me_2NLi calculated using single point MP2 corrections to B3LYP/6-31G(d)-SVP optimized structures at 25 °C (S = Me_2O).

Table AIV.2. Optimized geometries of reactants and transition structures calculated at B3LYP level of theory using SVP basis set for Br and 6-31G(d) basis set for the rest of atoms, for the reaction of EtBr with Me_2NLi, with free energies (*G*, Hartrees), enthalpies (*H*, Hartrees), and cartesian coordinates (X,Y,Z) at 25 °C. (Note: G_{MP2} includes single point MP2 corrections to B3LYP/6-31G(d)-SVP optimized structures)

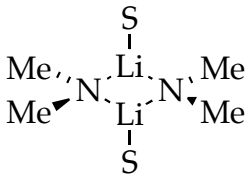

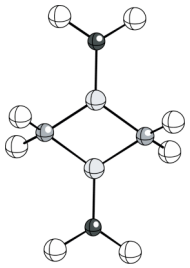

G = -594.095723
H = -594.012498
G_{MP2} = -591.9718824
S = Me_2O

Atom	X	Y	Z	Atom	X	Y	Z
N	-0.00029	1.58912	0.00241	H	0.24405	-1.82190	2.08420
C	-0.13735	2.43163	-1.16832	H	-1.02167	3.10935	-1.13224
C	0.13657	2.43144	1.17332	H	0.73155	3.10793	-1.33862
Li	1.17676	0.00019	-0.09846	H	-0.24444	1.82175	-2.07925
Li	-1.17703	-0.00005	0.10335	H	-0.73258	3.10736	1.34387
N	0.00008	-1.58897	0.00255	H	0.24401	1.82140	2.08410
C	0.13711	-2.43165	1.17317	H	1.02063	3.10949	1.13727
C	-0.13646	-2.43113	-1.16851	H	-3.18143	-2.02649	0.06426
O	-3.11150	-0.00013	0.08916	H	-4.59271	-1.25114	0.85061
C	-3.88399	-1.19293	0.01302	H	-4.44014	-1.23550	-0.93378
C	-3.88449	1.19232	0.01288	H	-4.44076	1.23448	-0.93387
O	3.11106	0.00022	-0.08852	H	-4.59315	1.25039	0.85053
C	3.88437	1.19281	-0.01786	H	-3.18228	2.02618	0.06390
C	3.88421	-1.19250	-0.01816	H	3.18163	2.02652	-0.06389
H	-0.24374	-1.82097	-2.07923	H	4.44743	1.23510	0.92485
H	0.73278	-3.10696	-1.33897	H	4.58697	1.25099	-0.86060
H	-1.02046	-3.10927	-1.13278	H	4.58696	-1.25046	-0.86079
H	-0.73173	-3.10807	1.34328	H	4.44710	-1.23520	0.92464
H	1.02152	-3.10925	1.13707	H	3.18138	-2.02610	-0.06461

Table AIV.2 (Continued).

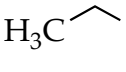

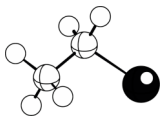

G = -2653.059326
H = -2653.026798
G_{MP2} = -2651.202161

Atom	X	Y	Z
C	-0.55881	-0.59674	0.00000
C	0.61513	0.36648	0.00000
Br	0.01565	2.25184	0.00000
H	1.23836	0.26391	0.88902
H	1.23836	0.26391	-0.88902
H	-0.18075	-1.62781	0.00000
H	-1.18397	-0.46079	0.88731
H	-1.18397	-0.46079	-0.88731

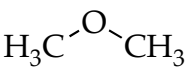

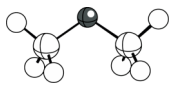

G = -154.970104
H = -154.939502
G_{MP2} = -154.4483767

Atom	X	Y	Z
C	-1.17099	0.04651	0.00000
O	-0.00000	0.83197	0.00000
C	1.17099	0.04651	0.00000
H	1.23209	-0.59788	-0.89294
H	2.02183	0.73315	-0.00008
H	1.23216	-0.59777	0.89301
H	-1.23215	-0.59779	-0.89300
H	-1.23211	-0.59786	0.89295
H	-2.02183	0.73315	0.00005

Table AIV.2 (Continued).

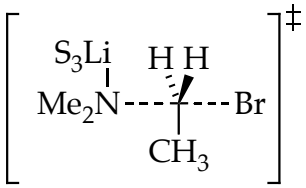

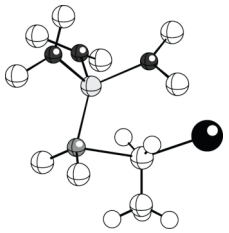

G = -3259.980987
H = -3259.891266
G_{MP2} = -3256.016051
S = Me_2O

Atom	X	Y	Z	Atom	X	Y	Z
C	2.36876	0.93362	-0.08970	H	0.06630	1.91528	1.97005
C	3.11661	2.23184	-0.13929	H	-3.91919	-1.88989	-0.48309
Br	4.11544	-0.69227	-0.03162	H	-3.33549	-1.39662	-2.09959
N	0.07956	1.67173	-0.11763	H	-2.29683	-2.40264	-1.05203
C	-0.07895	2.48106	-1.30253	H	-2.61720	1.51845	-0.11374
C	-0.08496	2.50281	1.05215	H	-3.51823	0.95023	-1.54906
Li	-0.42315	-0.22576	-0.04232	H	-4.12813	0.56266	0.08832
O	0.33446	-1.71090	-1.23875	H	1.76881	-1.39813	1.84265
C	0.88406	-1.40245	-2.51957	H	1.13690	-0.46555	3.23118
C	0.90109	-2.90925	-0.70089	H	0.88764	-2.23494	3.15622
O	-0.26279	-1.11766	1.82804	H	-1.51445	-1.92292	3.28426
C	0.94932	-1.31424	2.55943	H	-1.29100	-0.14929	3.36289
C	-1.39282	-1.00885	2.68581	H	-2.26535	-0.87035	2.04601
O	-2.40459	-0.45764	-0.49115	H	1.97330	-1.28731	-2.45445
C	-3.22300	0.70812	-0.51888	H	0.64399	-2.19752	-3.23983
C	-3.03166	-1.59674	-1.06231	H	0.42940	-0.46606	-2.85085
H	1.98180	0.57889	0.84609	H	0.40301	-3.09194	0.25242
H	1.98123	0.50149	-0.99117	H	0.71570	-3.75321	-1.38053
H	0.07991	1.88079	-2.21132	H	1.97931	-2.78408	-0.54372
H	-1.08914	2.93864	-1.39372	H	2.41784	3.07872	-0.15478
H	0.62844	3.33736	-1.35610	H	3.76491	2.34149	0.73427
H	0.62320	3.35931	1.09560	H	3.74131	2.28873	-1.03477
H	-1.09537	2.96498	1.12800				

Table AIV.2 (Continued).

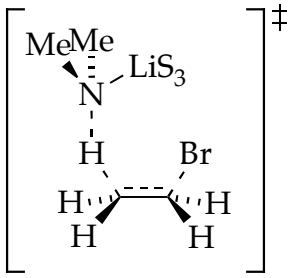

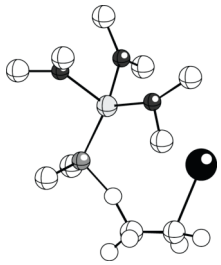

G = -3259.975168
H = -3259.885193
G_{MP2} = -3256.006667
S = Me_2O

Atom	X	Y	Z	Atom	X	Y	Z
C	-2.95558	2.03235	0.19069	H	-1.25948	-2.01674	-1.76822
C	-4.00431	1.05187	0.19925	H	2.65677	-2.06682	-0.69371
Br	-3.27444	-1.18026	-0.11134	H	1.93255	-3.61514	-1.23390
N	-0.44847	1.38780	-0.74507	H	2.30156	-2.33738	-2.42651
C	-0.78096	1.38058	-2.16137	H	3.27830	1.92910	-0.22501
C	0.12528	2.67551	-0.39460	H	4.11371	0.43916	-0.76105
Li	0.35318	-0.26904	-0.00833	H	2.54272	0.90922	-1.48887
O	-0.06512	-0.93827	1.86341	H	2.36389	-0.45574	2.31711
C	-0.89388	-0.07796	2.64621	H	4.00849	-0.38225	1.60178
C	-0.37827	-2.31498	2.07312	H	0.27135	-2.89246	1.41287
O	0.68779	-1.94847	-1.16670	H	3.16075	1.12495	2.05560
C	-0.30914	-2.47610	-2.04415	H	-0.18557	-2.59414	3.11922
C	1.96325	-2.52796	-1.39731	H	-1.42597	-2.51014	1.81880
O	2.39890	0.14157	0.38459	H	-1.94764	-0.23325	2.39132
C	3.13174	0.89713	-0.57048	H	-0.73044	-0.26520	3.71749
C	3.02538	0.10831	1.65917	H	-0.60880	0.94772	2.40457
H	-1.82828	1.57418	-0.16745	H	-1.25507	0.42996	-2.43218
H	-4.47862	0.77653	1.13459	H	-1.48879	2.18789	-2.44342
H	-4.67055	0.98889	-0.65433	H	0.10760	1.51738	-2.80938
H	-3.10218	2.80663	-0.57109	H	1.01909	2.92763	-0.99681
H	-2.75667	2.47215	1.17312	H	-0.58208	3.51905	-0.53901
H	-0.06111	-2.24476	-3.08957	H	0.42951	2.68794	0.66209
H	-0.38044	-3.56643	-1.92513				

Table AIV.2 (Continued).

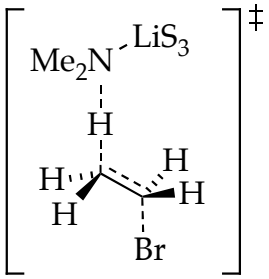

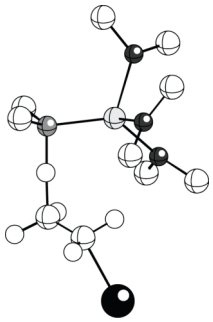

G = -3259.972702
H = -3259.881948
G_{MP2} = -3256.006477
S = Me_2O

Atom	X	Y	Z	Atom	X	Y	Z
H	-1.26487	1.86225	-0.08054	H	-0.00248	3.70262	1.06152
N	0.10572	1.87050	-0.04567	H	0.00029	3.56407	-1.35695
C	0.48195	2.57114	-1.26613	H	1.57091	2.74635	-1.34445
C	0.44206	2.68945	1.11005	H	0.18224	1.98667	-2.14753
Li	0.40905	-0.10492	-0.01562	H	4.19514	-0.19097	-0.34097
O	-0.80100	-1.43187	-1.01668	H	3.49074	0.81418	-1.64453
C	-1.44360	-1.07031	-2.24375	H	2.97201	1.06510	0.04426
C	-1.42090	-2.57258	-0.41746	H	2.24645	-1.95260	1.39492
O	0.52940	-0.96860	1.83991	H	2.22615	-1.21510	3.02407
C	-0.33956	-0.60979	2.91229	H	1.28748	-2.70408	2.70927
C	1.63166	-1.75530	2.27382	H	-2.48735	-2.38389	-0.23957
O	2.21007	-0.60747	-0.81841	H	-1.31131	-3.45206	-1.06765
C	3.28440	0.31840	-0.68684	H	-0.90923	-2.74989	0.52976
C	2.45405	-1.60603	-1.80128	H	-2.50841	-0.87106	-2.07577
C	-2.62478	1.77557	-0.31555	H	-0.95329	-0.16670	-2.61058
C	-3.09561	0.71813	0.53670	H	-1.33114	-1.87641	-2.98263
Br	-5.00135	-0.35372	-0.06897	H	1.56129	-2.23101	-1.84286
H	-3.14353	2.72983	-0.19116	H	2.62979	-1.15030	-2.78567
H	-2.57929	1.51081	-1.37732	H	3.32763	-2.21632	-1.53100
H	-3.40384	0.99994	1.54215	H	-0.76613	-1.50754	3.38034
H	-2.51534	-0.19939	0.53030	H	0.20151	-0.02899	3.67127
H	0.07145	2.21876	2.03040	H	-1.14086	-0.00227	2.49114
H	1.53244	2.83540	1.23337				

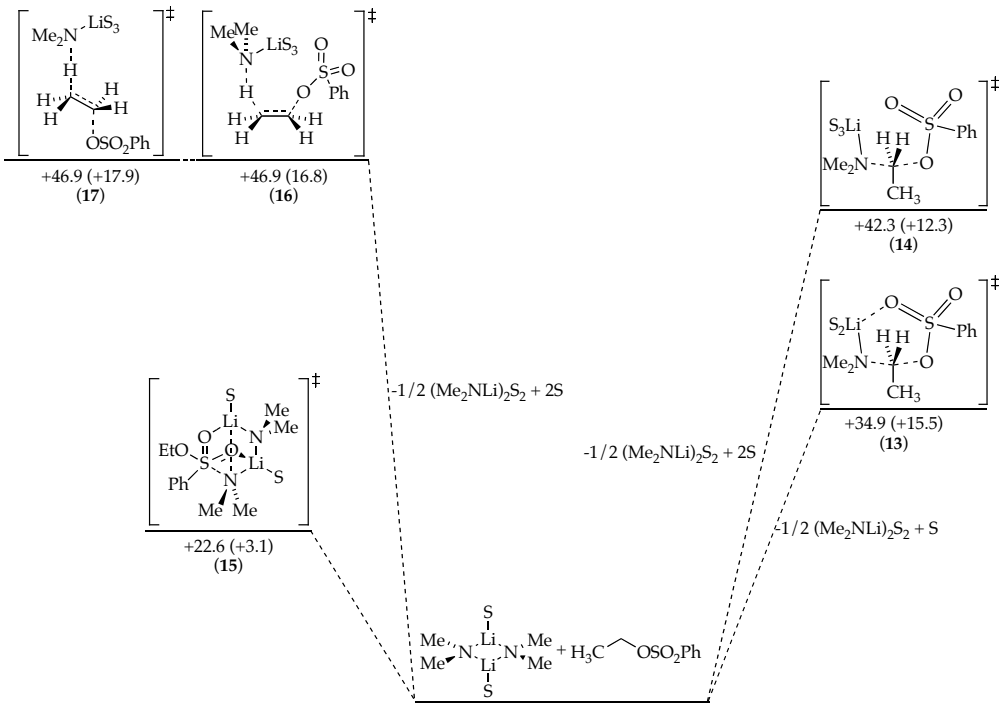

Figure AIV.19. Free energies of activation ($\Delta G^{\ddagger}$, kcal/mol) for the reaction of $EtOSO_2Ph$ with Me_2NLi calculated using B3LYP level of theory with SVP basis set for S and 6-31G(d) basis set for the rest of atoms at 25 °C (S = Me_2O). Values in parentheses correspond to the enthalpies of activation ($\Delta H^{\ddagger}$, kcal/mol).

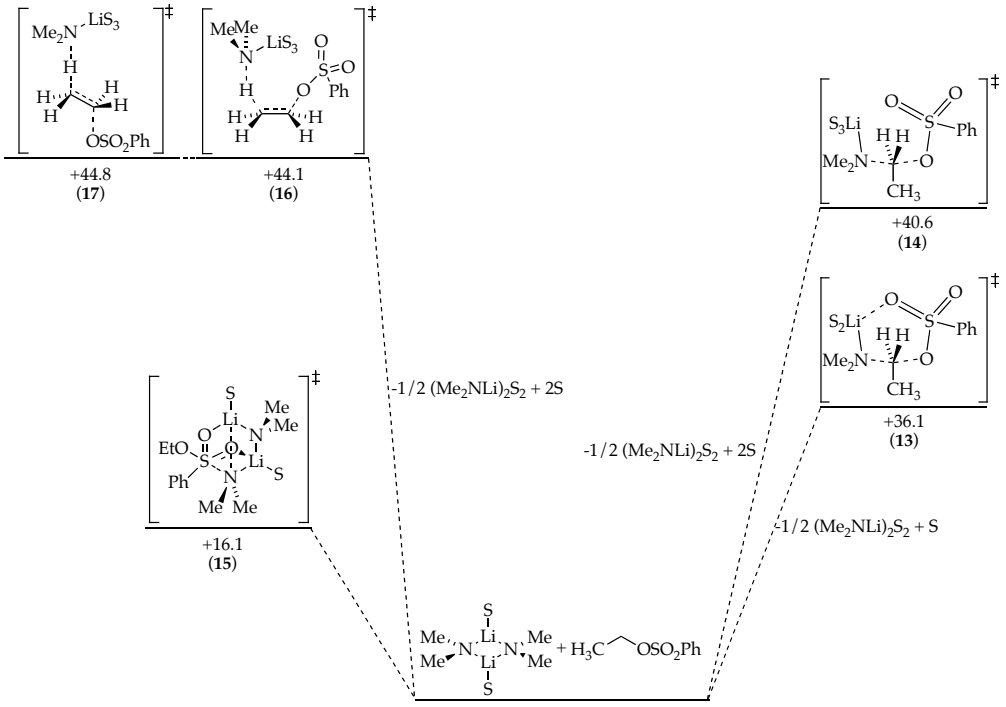

Figure AIV.20. Free energies of activation ($\Delta G^{\ddagger}$, kcal/mol) for the reaction of $EtOSO_2Ph$ with Me_2NLi calculated using single point MP2 corrections to B3LYP/6-31G(d)-SVP optimized structures at 25 °C (S = Me_2O).

Table AIV.3. Optimized geometries of reactant and transition structure calculated at B3LYP level of theory using SVP basis set for S and 6-31G(d) basis set for the rest of atoms, for the reaction of $EtOSO_2Ph$ with Me_2NLi, with free energies (*G*, Hartrees), enthalpies (*H*, Hartrees) and cartesian coordinates (X,Y,Z) at 25 °C. (Note: G_{MP2} includes single point MP2 corrections to B3LYP/6-31G(d)-SVP optimized structures)

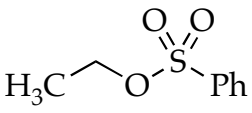

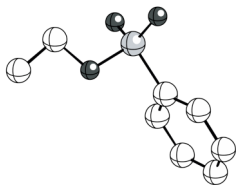

G = -934.410892
H = -934.357927
G_{MP2} = -932.2256042

Atom	X	Y	Z	Atom	X	Y	Z
S	0.65338	-1.30081	0.00085	C	-1.63851	-0.40605	1.22145
O	0.92232	-1.97919	-1.27244	H	-1.12143	-0.62872	-2.14838
O	0.92252	-1.97701	1.27525	H	-3.44530	0.29557	-2.15334
O	1.44650	0.14611	-0.00044	H	-4.59316	0.75574	-0.00047
C	2.89826	0.04184	-0.00085	H	-3.44525	0.29847	2.15299
C	3.44324	1.45792	-0.00027	H	-1.12137	-0.62581	2.14922
C	-1.00885	-0.64928	0.00043	H	3.11006	2.00240	0.88867
C	-1.63854	-0.40770	-1.22089	H	4.53859	1.43018	-0.00069
C	-2.93651	0.10295	-1.21331	H	3.10941	2.00338	-0.88838
C	-3.58126	0.36004	-0.00022	H	3.21094	-0.51189	-0.89257
C	-2.93648	0.10458	1.21320	H	3.21141	-0.51273	0.89019

Table AIV.3 (Continued).

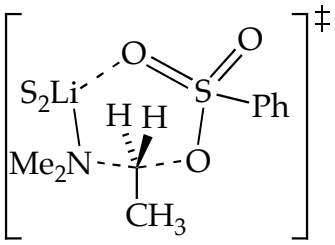

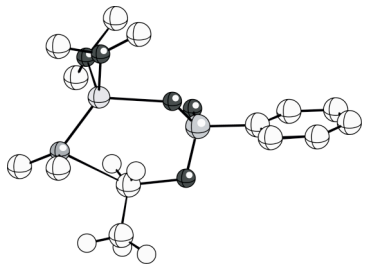

(**13**)
G = -1386.373193
H = -1386.279001
G_{MP2} = -1382.602451
S = Me_2O

Atom	X	Y	Z	Atom	X	Y	Z
C	-0.23702	2.12260	-0.05938	H	-0.73343	-2.74064	-2.74818
C	-0.34392	3.59030	-0.32214	H	0.27067	-2.56286	-1.27636
N	-2.44877	1.12868	-0.47219	H	-3.62733	-1.52759	-0.96871
C	-3.45228	1.86994	0.24830	H	-3.08567	-2.16522	-2.54728
C	-2.66987	1.29736	-1.88885	H	-3.32216	-3.28740	-1.17090
Li	-1.36632	-0.43346	0.12635	H	-0.78385	-2.92473	1.44865
O	0.78601	-0.47341	0.05847	H	0.28082	-1.99011	2.54400
S	1.74760	0.42521	0.78606	H	-1.17780	-2.81753	3.18895
O	1.50878	1.90469	0.35870	H	-2.01960	-0.70729	4.00905
O	1.79224	0.25216	2.25157	H	-0.58333	0.14925	3.35720
C	3.38180	0.08626	0.13273	H	-2.23398	0.60805	2.82218
C	3.58338	0.09402	-1.24992	H	-3.46795	2.95735	-0.00137
C	4.85757	-0.17277	-1.74677	H	-4.49065	1.51899	0.05759
C	5.91220	-0.44133	-0.86773	H	-3.29315	1.79903	1.33478
C	5.69506	-0.44411	0.51117	H	-1.89492	0.77272	-2.47037
C	4.42237	-0.17846	1.02164	H	-3.64970	0.90296	-2.23908
O	-1.54535	-1.13284	2.02728	H	-2.65552	2.36235	-2.21817
C	-1.58932	-0.22001	3.12260	H	-1.37091	3.82014	-0.63330
C	-0.75385	-2.28025	2.32858	H	-0.11592	4.17359	0.57446
O	-1.66685	-2.03063	-1.02910	H	0.33428	3.89601	-1.12422
C	-3.00107	-2.27563	-1.45742	H	4.22668	-0.17563	2.08832
C	-0.70545	-2.86683	-1.65627	H	2.75669	0.30445	-1.92074
H	-0.62952	1.75379	0.87127	H	6.51507	-0.65268	1.19253
H	-0.19867	1.45445	-0.89668	H	5.02927	-0.17065	-2.81952
H	-0.89028	-3.92445	-1.41707	H	6.90395	-0.64782	-1.26073

Table AIV.3 (Continued).

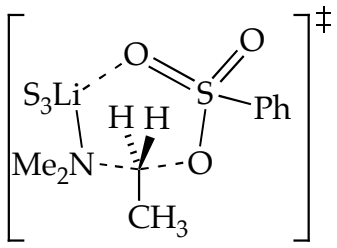

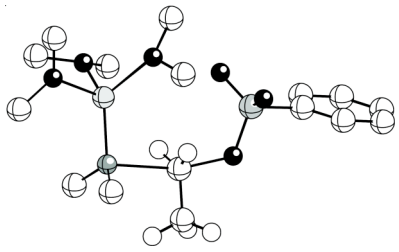

(14)
G = -1541.331460
H = -1541.223547
G_{MP2} = -1537.043616
S = Me_2O

Atom	X	Y	Z	Atom	X	Y	Z
Li	-1.96456	-0.24647	-0.03571	H	-1.62490	3.48323	-1.28006
N	-1.67834	1.70847	-0.06715	H	-0.60811	-0.12361	3.19618
C	-2.10733	2.43630	1.10484	H	-0.52871	-1.90858	3.26677
C	-2.05115	2.45610	-1.24693	H	0.24388	-1.03950	1.90968
C	0.73524	1.70806	-0.00705	H	-3.82321	-1.26472	1.95797
C	0.97286	3.18879	-0.03956	H	-2.93540	-2.08626	3.27845
O	2.51299	1.24192	0.06705	H	-3.05992	-0.30159	3.25861
S	2.78967	-0.25459	-0.25062	H	-4.51318	1.13484	-0.00295
O	2.20104	-1.14563	0.78369	H	-5.28071	0.52169	-1.49457
O	2.47087	-0.58218	-1.66179	H	-5.80350	-0.10864	0.09613
C	4.57604	-0.32649	-0.06875	H	-5.13630	-2.41774	-0.60828
C	5.12486	-0.61721	1.18071	H	-4.69155	-1.72302	-2.19473
C	6.51287	-0.65051	1.31910	H	-3.45819	-2.57761	-1.22502
C	7.33402	-0.39616	0.21729	H	0.38820	-0.97790	-2.61863
C	6.77003	-0.11200	-1.02932	H	-0.93586	-1.99133	-3.28846
C	5.38323	-0.07638	-1.17911	H	-1.25643	-0.29415	-2.82874
O	-1.80351	-1.13213	1.81635	H	-0.56671	-3.57937	-1.47414
C	-0.60656	-1.04300	2.59390	H	0.71424	-2.53834	-0.76082
C	-2.96681	-1.19886	2.63025	H	-0.73422	-2.95709	0.19664
O	-3.91671	-0.72862	-0.53721	H	0.47350	1.22799	0.91973
C	-4.94242	0.25573	-0.48350	H	0.51259	1.17863	-0.91752
C	-4.33195	-1.92748	-1.17611	H	0.03125	3.74338	0.00384
O	-1.06718	-1.57110	-1.25258	H	1.58779	3.48954	0.81368
C	-0.68488	-1.19070	-2.57714	H	1.49939	3.47014	-0.95559
C	-0.36128	-2.73178	-0.80385	H	4.92307	0.12733	-2.14017
H	-1.66933	3.45660	1.18708	H	7.41015	0.07753	-1.88672
H	-3.20840	2.60262	1.15183	H	8.41469	-0.42476	0.32908
H	-1.82886	1.89586	2.02196	H	6.95339	-0.87940	2.28575
H	-1.70881	1.94355	-2.15848	H	4.46820	-0.82632	2.01852
H	-3.14905	2.60298	-1.35375				

Table AIV.3 (Continued).

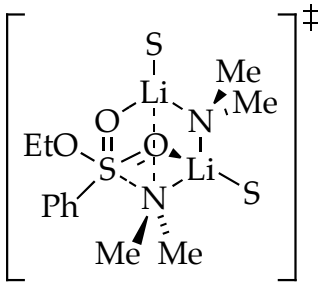

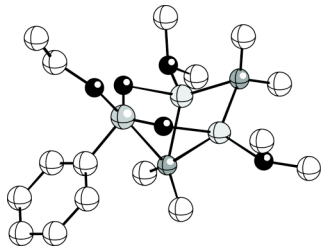

(**15**)
G = -1528.470612
H = -1528.365538
G_{MP2} = -1524.171891
S = Me_2O

Atom	X	Y	Z	Atom	X	Y	Z
S	1.25159	0.09864	0.72457	H	2.07021	-1.86879	2.69432
O	0.49808	1.35929	0.92243	H	-2.80902	-3.35349	1.01822
Li	-1.24846	1.26416	-0.06143	H	-1.88138	-4.80975	0.52167
Li	-1.10902	-1.14041	-0.27174	H	-1.04977	-3.44299	1.32286
O	0.63322	-1.25395	0.75897	H	-2.17015	-2.91220	-2.54233
N	0.07709	0.18212	-1.47781	H	-2.53553	-4.49586	-1.80149
C	0.26320	1.42787	-2.20156	H	-3.49521	-3.04995	-1.34766
C	0.38727	-0.90439	-2.38975	H	0.08420	2.29942	-1.55847
N	-2.57207	-0.07541	0.50761	H	1.28890	1.54249	-2.60898
C	-2.85450	-0.14968	1.92515	H	-0.41979	1.51681	-3.06985
C	-3.81872	-0.13909	-0.22134	H	-0.29404	-0.92969	-3.26445
O	-1.54089	-3.10195	-0.61910	H	1.41248	-0.84029	-2.80960
C	-1.84829	-3.71676	0.63107	H	0.31405	-1.88040	-1.89119
C	-2.49692	-3.41137	-1.62746	H	-1.92469	-0.10187	2.50969
O	-1.79258	3.21948	-0.02319	H	-3.51055	0.67320	2.29303
C	-1.56989	3.85648	1.23321	H	-3.37839	-1.08652	2.22829
C	-3.06138	3.54338	-0.58105	H	-3.64268	-0.08279	-1.30811
C	2.65327	0.23560	-0.35634	H	-4.39973	-1.07496	-0.03994
C	3.19530	1.50426	-0.59374	H	-4.53097	0.68201	0.02816
C	4.34982	1.60886	-1.36699	H	-1.58145	4.94898	1.11521
C	4.96274	0.46534	-1.88671	H	-2.33829	3.56117	1.96091
C	4.41088	-0.79290	-1.63850	H	-0.59010	3.53092	1.58417
C	3.25282	-0.91973	-0.87017	H	-3.13400	3.02813	-1.54108
O	2.07740	0.14588	2.18604	H	-3.87565	3.20614	0.07358
C	2.77620	-1.03587	2.62120	H	-3.14488	4.62715	-0.74373
C	3.39568	-0.71066	3.97039	H	2.81598	-1.89273	-0.67549
H	2.62124	-0.43789	4.69395	H	4.88138	-1.68509	-2.04237
H	3.93716	-1.58385	4.35183	H	5.86465	0.55571	-2.48522
H	4.09831	0.12412	3.88487	H	4.77445	2.59032	-1.55903
H	3.55280	-1.30085	1.89090	H	2.71863	2.38420	-0.17644

Table AIV.3 (Continued).

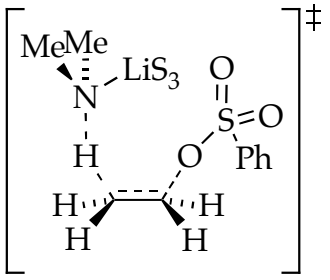

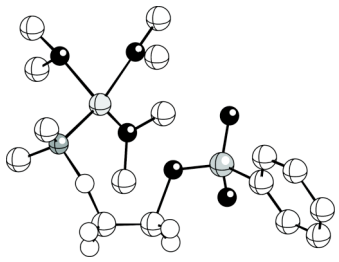

(**16**)
G = -1541.324155
H = -1541.216364
G_{MP2} = -1537.038062
S = Me_2O

Atom	X	Y	Z	Atom	X	Y	Z
S	2.27268	-0.37844	0.95502	H	0.21254	3.61978	0.23807
O	1.75804	-1.76051	0.86493	H	0.69235	3.40532	-1.48434
O	2.35911	0.25025	2.29209	H	2.08666	2.33248	0.93983
O	1.43862	0.50772	-0.04656	H	2.59969	2.15547	-0.78322
C	1.76128	2.20307	-0.09016	H	0.92653	-2.32306	-1.35634
C	0.57564	2.91335	-0.51460	H	-0.23823	-2.71564	-2.67088
N	-1.69901	1.47515	-1.04182	H	0.12698	-1.01007	-2.25912
Li	-1.63075	-0.22177	0.00658	H	-2.11896	-3.10411	0.39195
O	-1.29750	-0.04489	2.02602	H	-1.43383	-4.01311	-0.98364
C	-0.86700	1.21045	2.55937	H	-0.35829	-3.45786	0.33938
C	-0.97717	-1.12640	2.89894	H	-4.91804	0.52761	0.91335
O	-1.07107	-1.96432	-0.92054	H	-5.26356	-1.12681	1.50329
C	0.00385	-2.01540	-1.85786	H	-3.84345	-0.22595	2.12659
C	-1.24626	-3.21057	-0.25501	H	-3.55497	-1.58721	-1.67413
O	-3.60935	-0.95317	0.25059	H	-5.10474	-1.91370	-0.83565
C	-4.29116	-1.18695	-0.97615	H	-4.70800	-0.25302	-1.37702
C	-4.46427	-0.41479	1.25043	H	-0.79012	0.81598	-2.82298
C	-1.63502	1.43460	-2.49434	H	-2.55014	1.01507	-2.95393
C	-2.74429	2.40627	-0.64752	H	-1.49214	2.43711	-2.94782
C	3.94152	-0.37547	0.27283	H	-2.55944	3.44158	-1.00210
C	4.17270	-0.95853	-0.97602	H	-3.74042	2.12366	-1.04055
C	5.46542	-0.95655	-1.49719	H	-2.83204	2.45149	0.44701
C	6.51415	-0.38146	-0.77213	H	-1.36230	-2.03814	2.43945
C	6.27116	0.19336	0.47630	H	0.10648	-1.21220	3.02721
C	4.97861	0.19975	1.00639	H	-1.45802	-0.98251	3.87780
H	4.76616	0.63648	1.97606	H	-1.07196	1.96645	1.80147
H	7.08647	0.63685	1.04113	H	-1.42658	1.44186	3.47782
H	7.52058	-0.38435	-1.18185	H	0.20587	1.18531	2.77328
H	5.65645	-1.40588	-2.46783	H	-0.49434	2.12304	-0.71393
H	3.35291	-1.40669	-1.52793				

Table AIV.3 (Continued).

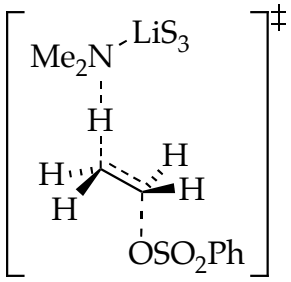

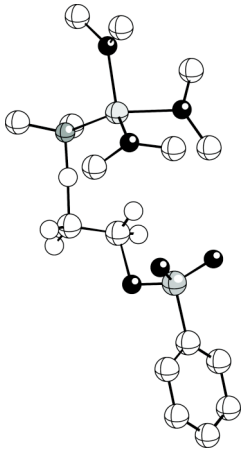

(**17**)
G = -1541.324279
H = -1541.214592
G_{MP2} = -1541.214592
S = Me_2O

Atom	X	Y	Z	Atom	X	Y	Z
C	1.12543	1.30889	0.22198	H	0.80325	3.37801	-0.23926
C	0.50188	2.36758	-0.52937	H	0.57014	2.23802	-1.61509
O	2.75403	1.08227	-0.09701	H	0.73796	0.31798	-0.01120
S	3.20034	-0.43287	-0.05207	H	1.17980	1.46457	1.29897
O	2.75802	-1.07127	1.20998	H	-5.50932	0.13686	-1.46262
O	2.84313	-1.12563	-1.31321	H	-5.96782	-0.61363	0.09611
C	-0.43866	-0.75375	-2.43653	H	-4.88367	0.81644	0.06530
O	-0.94453	-1.25296	-1.19289	H	-3.24872	-2.67119	-1.19147
C	-0.33046	-2.49316	-0.82652	H	-4.95116	-2.76141	-0.63949
Li	-2.14398	-0.14481	-0.02432	H	-4.55148	-1.97992	-2.19832
N	-2.17961	1.86532	-0.12011	H	-0.51008	-0.06636	3.16017
C	-2.79672	2.53358	-1.25960	H	-0.52570	-1.85349	3.22898
C	-2.51607	2.57661	1.10753	H	0.24309	-1.02228	1.85119
O	-3.99312	-0.91647	-0.49633	H	-3.82867	-1.09921	2.06497
C	-4.20614	-2.15041	-1.16892	H	-2.89991	-1.92772	3.34864
C	-5.16031	-0.10390	-0.44928	H	-2.98631	-0.14070	3.32167
O	-1.81361	-1.00891	1.82984	H	-2.52684	2.01927	-2.19234
C	-0.58348	-0.98365	2.56061	H	-3.89978	2.55235	-1.20373
C	-2.94146	-1.04366	2.69694	H	-2.47114	3.58678	-1.36252
C	4.98358	-0.25378	-0.00860	H	-2.22756	3.64522	1.07649
C	5.69281	-0.19847	-1.20900	H	-3.59788	2.55219	1.33683
C	7.07749	-0.03241	-1.16721	H	-1.99010	2.12372	1.95921
C	7.73483	0.07310	0.06146	H	-0.71134	-1.43448	-3.25568
C	7.01078	0.00924	1.25522	H	-0.89923	0.22198	-2.60073
C	5.62576	-0.15500	1.22637	H	0.65065	-0.65122	-2.39043
H	5.04436	-0.21998	2.13994	H	-0.54920	-3.26286	-1.58104
H	7.52520	0.08393	2.20939	H	0.75387	-2.37122	-0.73431
H	8.81369	0.20091	0.08898	H	-0.76185	-2.78788	0.13183
H	7.64338	0.01052	-2.09377	H	-0.89021	2.11572	-0.27532
H	5.16267	-0.29642	-2.15028				

REFERENCES IV

1. (a) Smith, M.; March, J. *March's Advanced Organic Chemistry: Reactions, Mechanisms, and Structure*, 6th ed.; Wiley-Interscience, 2007; Chapters 10,17. (b) Carey, F. A.; Sundberg, R. J. Advanced Organic Chemistry, 5th ed.; Springer, 2007; Chapters 4,5. (c) Saunders, W. H., Jr.; Cockerill, A. F. *Mechanisms of Elimination Reactions*; John Wiley & Sons: New York, 1973; Vol. II, pp 60-68. (d) Baciocchi, E. In *The Chemistry of Halides, Pseudo Halides and Azides, Supplement D*; Patai, S., Rappoport, Z., Eds.; Wiley: Chichester, U. K., 1983.

2. (a) Reichardt, C. *Solvents and Solvent Effects in Organic Chemistry*, 3rd ed.; VCH; Weinheim, 2003; Chapter 5. (b) Hiraoka, M. *Crown Compounds: Their Characteristics and Application*; Elsevier; Amsterdam, 1982. (c) Atwood, J. L.; Steed, J. W., Eds. *Encyclopedia of Supramolecular Chemistry*; CRC Press, 2004; pp 940-949.

3. (a) Wang, D. Z.; Streitwieser, A. *J. Org. Chem.* **2003**, *68*, 8936. (b) Harder, S.; Streitwieser, A.; Petty, J. T.; Schleyer, P. v. R. *J. Am. Chem. Soc.* **1995,** *117,* 3253. (c) Streitwieser, A.; Choy, G. S. C.; Abu-Hasanayn, F. *J. Am. Chem. Soc.* **1997,** *119,* 5013. (d) Streitwieser, A., Jr. *Proc. Natl. Acad. Sci.* **1985**, *82*, 8288-8290. See also ref 19. (e) Streitwieser, A.; Jayasree, E. G. *J. Org. Chem.* **2007**, *72*, 1785.

4. (i) For a survey of chemical syntheses within the process chemistry R&D departments of GlaxoSmithKline, AstraZeneca and Pfizer, see: (a) Carey, J. S.; Laffan, D.; Thomson, C.; Williams, M. T. *Org. Biomol. Chem.* **2006**, *4*, 2337. (b) Dugger, R. W.; Ragan, J. A.; Ripin, D. H. B. *Org. Process Res. Dev.* **2005**, *9*, 253. (ii) For examples of N-alkylation of lithium dialkylamides, see: (c) Smith, J. K.; Bergbreiter, D. E.; Newcomb, M. *J. Org. Chem.* **1985**, *50*, 4549. (d) Sard, H.; Duffley, R. P.; Razdan, R. K. *Synth. Comm.* **1983**, *13*, 813. (iii) For representative reactions of lithium dialkylamides with sulfonates, see: (e) Evans, D. A.; Wood, M. R.; Trotter, B. W.; Richardson, T. I.; Barrow, J. C.; Katz, J. L. *Angew. Chem. Int. Ed*. **1998**, *37*, 2700. (f) Andersen, K. K.; Gowda, G.; Jewell, L.; McGraw, P.; Phillips, B. T. *J. Org. Chem.* **1982**, *47*, 1884.

5. Butters, M.; Catterick, D.; Craig, A.; Curzons, A.; Dale, D.; Gillmore, A.; Green, S. P.; Marziano, I.; Sherlock, J.-P.; White, W. *Chem. Rev.* **2006**, *106*, 3002.

6. (a) DePue, J. S.; Collum, D. B. *J. Am. Chem. Soc.* **1988**, *110*, 5518. (b) DePue, J. S.; Collum, D. B. *J. Am. Chem. Soc.* **1988**, *110*, 5524.

7. Rutherford, J. L.; Collum, D. B. *J. Am. Chem. Soc.* **1999**, *121*, 10198.

8. (a) Gardiner, M. G.; Raston, C. L. *Inorg. Chem.* **1996**, *35*, 4162. (b) Gardiner, M. G.; Raston, C. L. *Inorg. Chem.* **1996**, *35*, 4047. (c) Gardiner, M. G.; Raston, C. L. *Inorg. Chem.* **1995**, *34*, 4206. (d) Boche, G.; Langlotz, I.; Marsch, M.; Harms, K.; Nudelman, N. E. S. *Angew. Chem., Int. Ed. Engl.* **1992**, *31*, 1205. (e) Barr, D.; Clegg, W.; Hodgson, S. M.; Lamming, G. R.; Mulvey, R. E.; Scott, A. J.; Snaith, R.; Wright, D. S. *Angew. Chem., Int. Ed. Engl.* **1989**, *28*, 1241. (f) Armstrong, D. R.; Barr, D.; Clegg, W.; Hodgson, S. M.; Mulvey, R. E.; Reed, D.; Snaith, R.; Wright, D. S. *J. Am. Chem. Soc.* **1989**, *111*, 4719.

9. Ceruti, M.; Balliano, G.; Viola, F.; Cattel, L.; Gerst, N.; Shuber, F. *Eur. J. Med. Chem.* **1987**, *22*, 199.

10. (a) Majewski, M.; Gleave, D. M. *J. Organomet. Chem.* **1994**, *470*, 1. (b) Newcomb, M.; Reeder, R. A. *J. Org. Chem.* **1980,** *45***,** 1489. (c) Newcomb, M.; Burchill, M. T. *J. Am. Chem. Soc.* **1984,** *106*, 8276. (d) Newcomb, M.; Burchill, M. T. *J. Am. Chem. Soc.* **1984,** *106*, 2450.

11. We do note, however, that the highest levels of *n*-dodecane loosely correlated with higher THF concentrations.

12. Galiano-Roth, A. S.; Collum, D. B. *J. Am. Chem. Soc.* **1989**, *111*, 6772.

13. We define the idealized rate law as that obtained by rounding the observed reaction orders to the nearest rational order.

14. (a) Anslyn, E. V.; Dougherty, D. A. *Modern Physical Organic Chemistry*; University Science, 2006; Chapter 11. (b) Fang, Y.-R.; Westaway, K. C. *Can. J. Chem.* **1991**, *69*, 1017. (c) Westaway, K. C.; Lai, Z.-G. *Can. J. Chem.* **1989**, *67*, 345.

15. (a) Remenar, J. F.; Collum, D. B. *J. Am. Chem. Soc.* **1998**, *120*, 4081. (b) Remenar, J. F.; Collum, D. B. *J. Am. Chem. Soc.* **1997**, *119*, 5573.

16. Dehydrobrominations of 2,2-**1**-d_2-dodecane afforded exclusively **1**-d_1-dodecene, whereas dehydrobrominations of 1,1-**1**-d_2-dodecane yielded **1**-d_2-dodecene .

17. (a) Bock, P. L.; Whitesides, G. M. *J. Am. Chem. Soc.* **1974**, *96*, 2826. (b) Whitesides, G. M.; Fischer, W. F., Jr.; San Filippo, J., Jr.; Bashe, R. W.; House, H. O. *J. Am. Chem. Soc.* **1969**, *91*, 4871.

18. All calculations were performed with Gaussian 03, Revision B.04, Frisch, M. J.; Trucks, G. W.; Schlegel, H. B.; Scuseria, G. E.; Robb, M. A.; Cheeseman, J. R.; Montgomery, Jr., J. A.; Vreven, T.; Kudin, K. N.; Burant, J. C.; Millam, J. M.; Iyengar, S. S.; Tomasi, J.; Barone, V.; Mennucci, B.; Cossi, M.; Scalmani, G.; Rega, N.; Petersson, G. A.; Nakatsuji, H.; Hada, M.; Ehara, M.; Toyota, K.; Fukuda, R.; Hasegawa, J.; Ishida, M.; Nakajima, T.; Honda, Y.; Kitao, O.; Nakai, H.; Klene, M.; Li, X.; Knox, J. E.; Hratchian, H. P.; Cross, J. B.; Bakken, V.; Adamo, C.; Jaramillo, J.; Gomperts, R.; Stratmann, R. E.; Yazyev, O.; Austin, A. J.; Cammi, R.; Pomelli, C.; Ochterski, J. W.; Ayala, P. Y.; Morokuma, K.; Voth, G. A.; Salvador, P.; Dannenberg, J. J.; Zakrzewski, V. G.; Dapprich, S.; Daniels, A. D.; Strain, M. C.; Farkas, O.; Malick, D. K.; Rabuck, A. D.; Raghavachari, K.; Foresman, J. B.; Ortiz, J. V.; Cui, Q.; Baboul, A. G.; Clifford, S.; Cioslowski, J.; Stefanov, B. B.; Liu, G.; Liashenko, A.; Piskorz, P.; Komaromi, I.; Martin, R. L.; Fox, D. J.; Keith, T.; Al-Laham, M. A.; Peng, C. Y.; Nanayakkara, A.; Challacombe, M.; Gill, P. M. W.; Johnson, B.; Chen, W.; Wong, M. W.; Gonzalez, C.; and Pople, J. A.; Gaussian, Inc., Wallingford CT, 2004.The combination of the Ahlrichs all-electron SVP basis set for second-row atoms and 6-31G* for the rest is denoted as 631A and has been previously applied to mechanistic studies on organolithium-mediated reactions: Nakamura,E.; Yamanaka, M.; Yoshikai, N.; Mori, S. *Angew. Chem., Int. Ed.* **2001**, *40*, 1935. Mori, J.; Nakamura, E.; Morokuma, K. *J. Am. Chem. Soc.* **2000**, *122*, 7294 and references therein.

19. Recent theoretical studies on S_N2 reactions involving lithium-containing species: (i) No solvent: (a) Ren, Y.; Gai, J.-G.; Xiong,Y.; Lee, K.-H.; Chu, S.-Y. *J. Phys. Chem. A* **2007,** *111,* 6615. (b) Streitwieser, A.; Jayasree, E. G.; Leung, S. S.-H; Choy, G. S.-C. *J. Org. Chem.* **2005**, *70*, 8486. (c) Pratt, L. M.; Nguyen, N. V.; Ramachandran, B. *J. Org. Chem.* **2005**, *70*, 4279. (d) Pomelli, C. S.; Bianucci, A. M.; Crotti, P.; Favero, L. *J. Org. Chem.* **2004**, *69*, 150. (e) Ren, Y.; Chu, S. Y. *J. Comput. Chem.* **2004**, *25*, 461. (f) Xiong, Y.; Zhu, H.; Ren, Y. *J. Mol. Struct.* **2003**, *664-665*, 279. (g) Leung, S. S.-H.; Streitwieser, A. *J. Comput. Chem.* **1998**, *19*, 1325. (ii) Dielectric solvation models: (f) Streitwieser, A.; Jayasree, E. G.; Hasanayn, F.; Leung, S. S.-H. *J. Org. Chem.* **2008**, *73*, 9426. (g) Ren, Y.; Li, M.; Wong, N.-B.; Chu, S.-Y. *J. Mol. Model.* **2006**, *12*, 182. (h) Ren, Y.; Chu, S. Y. *J. Phys. Chem. A* **2004**, *108*, 7079. (i) Zhu, H.; Ren, Y.; Ren, J. *J. Mol. Struct.* **2004**, *686*, 65. (iii) Microsolvation models: (j) Streitwieser, A.; Jayasree, E. G. *J. Org. Chem.* **2007**, *72*, 1785. (k) Ando, K. *J. Org. Chem.* **2006**, *71*, 1837. (l) Ando, K. *J. Am. Chem. Soc.* **2005**, *127*, 3964. See also reference 20a.

20. RBr-Li interactions do not appear to be stabilizing: (a) Zuend, S. J.; Ramirez, A.; Lobkovsky, E.; Collum, D. B. *J. Am. Chem. Soc.* **2006**, *128*, 5939. (b) Ikuta, Y.; Tomoda, S. *Org. Lett.* **2004**, *6*, 189.

21. (i) Basic nucleophiles tend to generate Nuc-Ha complexes upon unrestricted geometry optimizations: (a) Yi, R.; Basch, H.; Hoz, S. *J. Org. Chem.*

2002, *67*, 5891. (b) Buhl, M.; Schaefer, H. F. *J. Am. Chem. Soc.* **1993,** *115*, 9143. (ii) Nu-CR_3-X angle restriction to collinearity is a common technique to circumvent this limitation in the study of S_N2 reactions: (c) Hoz, S.; Basch, H.; Wolk, J. L.; Hoz, T.; Rozental, E. *J. Am. Chem. Soc.* **1999,** *121*, 7724.

22. Schlosser, M. In *Organometallics in Synthesis: A Manual*; Schlosser, M., Ed.; 2nd Edition; John Wiley & Sons: Chichester, 2002; Chapter 1.

23. (i) For reports on R_2SO_2-Li complexation: (a) Linnert, M.; Bruhn, C.; Wagner, C.; Steinborn, D. *J. Organomet. Chem.* **2006**, *689*, 2358. (b) Rhodes, C. P.; Frech, R. *Macromolecules* **2001**, *34*, 2660. (c) Pregel, M. J.; Dunn, E. J.; Buncel, E. *J. Am. Chem. Soc.* **1991**, *113*, 3545. (d) Eisch, J. J.; Galle, J. E. *J. Org. Chem.* **1980**, *45*, 4536. (ii) The nucleophilic substitutions of arylsulfonates with lithium halides occur with inversion of configuration: Braddock, D. C.; Pouwer, R. H.; Burton, J. W.; Broadwith, P. *J. Org. Chem.* **2009**, *74*, 6042.

24. (a) Beak, P. *Acc. Chem. Res.* **1992**, *25*, 215. (b) Baldwin, J. E. *J. Chem. Soc., Chem. Commun.* **1976**, 734. (c) Baldwin, J. E. *Further Perspectives in Organic Chemistry; A Ciba Foundation Symposium;* Elsevier: Amsterdam, 1978, 736. (d) Johnson, C. D. *Acc. Chem. Res.* **1993**, *26*, 476.

25. (a) Fressigné, C.; Lautrette, A.; Maddaluno, J. *J. Org. Chem.* **2005**, *70*, 7816. (b) Pomelli, C. S.; Bianucci, A. M.; Crotti, P.; Favero, L. *J. Org. Chem.* **2004**, *69*, 150. (c) Gillies, M. B.; Tønder, J. E.; Tanner, D.; Norrby, P. *J. Org. Chem.* **2002**, *67*, 7378. (d) Fressigné, C.; Maddaluno, J.; Marquez, A.; Giessner-Prettre, C. *J. Org. Chem.* **2000**, *65*, 8899.

26. (a) Ramirez, A.; Sun, X.; Collum, D. B. *J. Am. Chem. Soc.* **2006**, *128*, 10326. (b) Romesberg, F. E.; Collum, D. B. *J. Am. Chem. Soc.* **1995**, *117*, 2166. Searches for structures disolvated at the external Li led to severe transannular interactions involving the solvent and the S=O-Li bridge.

27. For discussions of S_N2 mechanism versus that with a discrete tetrahedral intermediate, see: (a) Erdik, E.; Eroglu, F. *Cent. Eur. J. Chem.* **2008**, *6*, 237. (b) Fox, J. M.; Dmitrenko, O.; Liao, L.; Bach, R. D. *J. Org. Chem.* **2004**, *69*, 7317. (c) Weiner, H.; Sneen, R. A. *J. Am. Chem. Soc.* **1965**, *87*, 292. (d) Chang, F. C. *Tetrahedron Lett.* **1964**, *6*, 305.

28. (i) For additional examples showing that Br leaving groups do not require metal assistance during the alkylation of lithium-based nucleophiles, see: (a) Zuend, S. J.; Ramirez, A.; Lobkovsky, E.; Collum, D. B. *J. Am. Chem. Soc.* **2006**,

128, 5939. (b) Ikuta, Y.; Tomoda, S. *Org. Lett.* **2004**, *6*, 189. (ii) For a general discussion of lithium-assisted departure of the leaving group, see: (c) Reich, H. J.; Sanders, A. W.; Fiedler, A. T.; Bevan, M. J. *J. Am. Chem. Soc.* **2002**, *124*, 13386.

29. (i) For studies on the acidity of Et_2NH in THF, see: (a) Furlong, J. J. P.; Lewkowicz, E. S.; Nudelman, N. S. *J. Chem. Soc., Perkin Trans. 2*, **1990**, 1461. (ii) For selective substitutions of sulfonates with organolithiums, see: (b) Nelson, T. D.; Rosen, J. D.; Smitrovich, J. H.; Payack, J.; Craig, B.; Matty, L.; Huffman, M. A.; McNamara, J. *Org. Lett.* **2005**, *7*, 55. (c) Kusumoto, T.; Ichikawa, S.; Asaka, K.; Sato, K.-I.; Hiyama, T. *Tetrahedron Lett.* **1995**, *36*, 1071. (iii) For a recent discussion on b-eliminations of benzenesulfonates, see: (d) Mohrig, J. R.; Alberg, D. G.; Cartwright, C. H.; Pflum, M. K. H.; Aldrich, J. S.; Anderson, J. K.; Anderson, S. R.; Fimmen, R. L.; Snover, A. K. *Org. Biomol. Chem.* **2008**, *6*, 1641.

30. (a) Humeres, E.; Nunes, R. J.; Machado, V. G.; Gasques, M. D. G.; Machado, C. *J. Org. Chem.* **2001**, *66*, 1163. (b) Westaway, K. C.; Lai, Z. *Can. J. Chem.* **1988**, *66*, 1263. (c) Reichardt, C. *Solvents and Solvent Effects in Organic Chemistry*, 2nd ed.; VCH: Weinheim, 1988; Chapter 7. (d) Arnett, E. M.; Maroldo, S. G.; Schriver, G. W.; Schilling, S. L.; Troughton, E. B. *J. Am. Chem. Soc.* **1985**, *107*, 2091. (e) Doolitle, R. E. *Org. Prep. Proced. Int.* **1980**, *12*, 1. (f) Parker, A. J.; Mayer, U.; Schmid, R.; Gutmann, V. *J. Org. Chem.* **1978**, *43*, 1843. (g) Sam, D. J.; Simmons, H. E. *J. Am. Chem. Soc.* **1974**, *96*, 2252.

31. Collum, D. B.; McNeil, A. J.; Ramirez, A. *Angew. Chem., Int. Ed. Engl.* **2007**, *46*, 3002.

32. For challenges to the reputed linear trajectory of ideal S_N2 reactions, see: Sato, M.; Yamataka, H.; Komeiji, Y.; Mochizuki, Y.; Ishikawa, T.; Nakano, T. *J. Am. Chem. Soc.* **2008**, *130*, 2396 and references cited therein.

33. (a) Bentley, T. W.; Bowen, C. T.; Morten, D. H.; Schleyer, P. v. R. *J. Am. Chem. Soc.* **1981**, *103*, 5466. (b) Bentley, T. W.; Bowen, C. T.; Parker, W.; Watt, C. I. F. *J. Am. Chem. Soc.* **1979**, *101*, 2486. (c) Bentley, T. W.; Bowen, C. T. *J. Chem. Soc., Perkin Trans. 2* **1978**, 557. (d) Mori, A.; Nagayama, M.; Mandai, H. *Bull. Chem. Soc. Jpn* **1971**, *44*, 1669.

34. Studies on nucleophilic displacements at sulfonate sulfur: (a) Holterman, H. A. J.; Engberts, B. F. N. *J. Org. Chem.* **1977**, *42*, 2792. (b) Van de Langkruis, G. B.; Engberts, J. B. F. N. *J. Org. Chem.* **1984**, *49*, 4152. (c) Mori, A.; Nagayama, M.; Mandai, H. *Bull. Chem. Soc. Jpn*. **1971**, *44*, 1669. (d) Weiner, H.; Sneen, R. A. *Tetrahedron Lett.* **1963**, 1309.

35. The dielectric constants of substituted THF are only slightly lower than THF. Harada, Y.; Salomon, M.; Petrucci. S. *J. Phys. Chem.* **1985**, *89*, 2006. Carvajal, C.; Tolle, K. J.; Smid, J.; Szwarc, M. *J. Am. Chem. Soc.* **1965**, *87*, 5548.

36. Related secondary shell effects: (a) Ma, Y.; Collum, D. B. *J. Am. Chem. Soc.* **2007**, *129*, 14818. (b) Ma, Y.; Ramirez, A.; Singh, K. J.; Keresztes, I.; Collum, D. B. *J. Am. Chem. Soc.* **2006**, *128*, 15399. (c) Bordwell, F. G.; Hughes, D. L. *J. Am. Chem. Soc.* **1986**, *108*, 7300.

37. (a) Rennels, R. A.; Maliakal, A. J.; Collum, D. B. *J. Am. Chem. Soc.* **1998**, *120*, 421. (b) Kottke, T.; Stalke, D. *Angew. Chem., Int. Ed. Engl.* **1993**, *32*, 580.

38. Kofron, W. G.; Baclawski, L. M. *J. Org. Chem.* **1976**, *41*, 1879.